Nadja Schmidt

Genesis and distribution of lithium enriched pore brines at the Salar de Uyuni, Bolivia

156 pages, 66 figures, 28 tables, 186 references

Table of contents

I Acknowledgements

II Abstract

With a size of ~10,000 km² the Salar de Uyuni is the largest salt lake in the world. It is located at a height of 3,653 m a.s.l. in the southern part of the Bolivian Altiplano, an endorheic high plateau separating the Eastern and Western cordillera of the Andes. The salt flat is characterized by an alternating sequence of evaporate layers mainly consisting of halite and lacustrine mud layers up to a depth of at least 220 m, whereby the stratification is ascribed to the alternation of dry and humid climatic phases during the Quaternary. With estimated 7 Mio tonnes in brine, the salt lake is considered the world's largest Li deposit. Knowledge about genesis and distribution of Li is essential for the possible extraction of Li and other valuable elements from the brine in a commercial scale, which is the driving force for the investigation of hydrochemical properties of the Salar de Uyuni.

Practical work comprised the sampling of brines from drilled wells and along transects, salts from the surface, sampling of streams, rocks and sediments in the catchment, as well as chemical and isotopical analyses. The surface catchment, delineated with ArcGIS, has a size of 63,000 km² and is mainly characterized by volcanic deposits as ignimbrites, and unconsolidated sediments, salt deposits and lacustrine material in widespread flood plains. The pores of the upper salt crust, which shows a varying thickness of 2-11 m, are filled with a saturated NaCl brine rich in Mg, K, Li and B. The distribution of Li along the salt lake is inhomogeneous, with two regions of significantly higher concentrations up to 1.5 g/L in the southern part near the delta of the main inflow Río Grande and in the northern part, compared to an average of 0.3-0.4 g/L in brine.

The age of brines from the upper salt crust was determined to 6,200 - 13,340 years, corresponding in age to the surrounding evaporates and showing a stable stratification with depth. However, a local mixing of the brine with freshwater feeding from groundwater aquifers especially near the shore of the salar was observed by the analysis of δ^2H and δ^{18}O in the brines. The distribution of stable isotopes also shows the strong influence of evaporation, even smaller tributaries feeding the Río Grande are enriched in heavy isotopes of H and O. Element to bromine ratios in the brine showed that Li, K and Mg are not removed from solution by the formation of precipitates, but are rather released from clay minerals by ion exchange leading to their enrichment in the pore brine.

Analyzed rocks, mostly of rhyolitic and dacitic type, show moderate lithium concentrations in the range of 4 to 37 mg/kg. Different types of digestion revealed that rock types occurring in the Salar de Uyuni catchment are a substantial supplier of lithium by the intensive physical and chemical weathering due to the specific environmental conditions. Increased lithium concentrations in rock and sediment samples from the volcano flanks south of the salar

indicate, that the southern catchment is the main supplier of lithium to the salt lake. The enrichment of lithium could also be observed by the analysis of superficial salts from the upper crust. Salt efflorescences are significantly enriched regarding Li, K, Mg and other ions compared to the surface within the polygons. The enrichment of Li in brine occurs all-season along shrinkage cracks at polygon borders, where brine rises up, water evaporates and NaCl precipitates, leaving a solution even more concentrated in Li and other solutes as Br, B, K and Mg.

In conclusion, the accumulation of lithium in the brine of the Salar de Uyuni results from the combination of various site-specific circumstances, which are analyzed and discussed in the present thesis.

III Zusammenfassung

Mit einer Größe von ~10.000 km² ist der Salar de Uyuni der größte Salzsee der Welt. Er befindet sich auf einer Höhe von 3.653 m im Süden des bolivianischen Altiplano, einer abflusslosen Hochebene zwischen der Ost- und Westkordillere der Anden. Der Salzsee besteht bis zu einer Tiefe von mind. 220 m aus einer Wechselfolge evaporitischer Schichten (hauptsächlich halitisch) und lakustrinen Tonschichten, wobei die Schichtung auf den Wechsel von trockenen und feuchten klimatischen Phasen während des Quartärs zurückzuführen ist. Mit einer geschätzten Menge von 7 Mio. t gilt der Salzsee als die gegenwärtig größte Li-Ressource der Welt. Das Wissen über Genese und Verteilung von Li ist grundlegend für eine mögliche Gewinnung von Li und anderen Elementen in kommerziellem Maßstab, worin sich die Motivation für die Untersuchung hydrochemischer Eigenschaften des Salar de Uyuni begründet.

Praktische Tätigkeiten umfassten die Probenahme von Solen aus eigens gebohrten Brunnen und entlang von Transekten, die Entnahme von Oberflächensalzen, die Beprobung von Zuflüssen, Gesteinen und Sedimenten im Einzugsgebiet, sowie deren chemische und isotopische Analytik. Das oberflächliche, mittels ArcGIS ermittelte Einzugsgebiet, weist eine Größe von 63.000 km² auf und besteht hauptsächlich aus vulkanischen Gesteinen wie Ignimbriten und unverfestigten Ablagerungen, Salzausblühungen und lakustrinen Sedimenten in ausgeprägten Überschwemmungsebenen. Die Poren der obersten, zwischen 2 und 11 m mächtigen Salzschicht, sind mit einer an NaCl gesättigten Salzlösung, die reich an Mg, K, Li und B ist, gefüllt. Die inhomogene Verteilung von Li im Salzsee weist zwei Bereiche signifikant erhöhter Konzentrationen von bis zu 1,5 g/L auf, und zwar im südlichen Einmündungsbereich des Hauptzuflusses Río Grande und im Nordosten etwa 20 km von der Küste entfernt, verglichen mit einem durchschnittlichen Gehalt von 0,3-0,4 g/L in der Sole.

Das Alter der Solen der obersten Salzkruste wurde auf 6.200 – 13.340 Jahre bestimmt, was dem Alter der umgebenden Evaporite entspricht und eine stabile Schichtung aufweist. Allerdings weist die Analytik von δ^2H und $\delta^{18}O$ auch auf eine lokale Vermischung der Sole mit Frischwasser aus ufernahen Aquiferen hin. Die Verteilung der stabilen Isotope δ^2H und $\delta^{18}O$ deutet auf einen signifikanten Einfluss der Verdunstung auf die Entwicklung der Porenlösung hin, denn auch kleinere Zuflüsse zum Salar sind angereichert an ^2H und ^{18}O. Das Verhältnis verschiedener Elemente zu Brom zeigt, dass Li, K und Mg weniger durch die Ausfällung von Salzen aus der Lösung entfernt, sondern eher durch Ionenaustausch aus Tonmineralen freigesetzt und folglich in der Sole angereichert werden.

Die analysierten Gesteine, hauptsächlich rhyolitischen und dazitischen Typs, weisen moderate Lithiumkonzentrationen von 4 – 37 mg/kg auf. Die Anwendung verschiedener Aufschlüsse

zeigte, dass die im Einzugsgebiet des Salar de Uyuni vorkommenden Gesteinstypen aufgrund der intensiven physikalischen und chemischen Verwitterung unter den spezifischen Umweltbedingungen eine wesentliche Quelle des Lithiums im Salzsee sind. Erhöhte Li-Konzentrationen in Gesteinen und Sedimenten der vulkanischen Flanken südlich des Salars deuten auf das südliche Einzugsgebiet als hauptsächlichen Zulieferer für Li hin. Die Anreicherung von Li wurde auch mittels der Untersuchung der Salze der obersten Kruste bestätigt. Im Vergleich zur Oberfläche innerhalb der Polygone sind die Salzausblühungen entlang der Polygonränder signifikant an Li, K, Mg und anderen Ionen angereichert. Die Anreicherung von Li geschieht ganzjährig entlang der Schrumpfungsrisse an Polygonrändern, indem die Sole durch kapillare Kräfte aufsteigt, Wasser verdunstet und NaCl ausfällt. Schließlich bleibt eine an Li und anderen Ionen wie Br, B, K und Mg noch stärker aufkonzentrierte Lösung zurück.

Schlussfolgernd resultiert die Akkumulation von Lithium in der Porenlösung aus der Kombination zahlreicher standortspezifischer Faktoren, welche innerhalb der vorliegenden Arbeit untersucht und bewertet wurden.

IV Resumen

El Salar de Uyuni, con una superficie de ~10.000 km² es el lago salado más grande del mundo y se encuentra a una altitud de 3.653 m en el sur del Altiplano Boliviano, una cuenca endorreica entre las cordilleras oriental y occidental de los Andes. Hasta una profundidad de al menos 220 m, el salar consta de una alternancia de estratos evaporíticos (principalmente halítico) y capas de arcilla lacustre. La estratificación deriva de la alternancia de fases climáticas secas y húmedas durante el Cuaterna. Con una cantidad estimada de 7 millones de toneladas, el salar está actualmente considerado el recurso de litio (Li) más grande del mundo. El conocimiento de la génesis y distribución del Li es fundamental para su extracción y la de otros elementos de valor a escala comercial. Este es el objectivo que se persigue al realizar esta investigación sobre las características hidroquímicas del Salar de Uyuni.

El trabajo práctico comprendia el muestreo de salmueras de pozos (perforado y construido por sí mismo) y a lo largo de transectos, la toma de sales de la superficie, el muestreo de afluentes, rocas y sedimentos en la cuenca, así como el análisis químico e isotópico. La cuenca superficial, determinada mediante ArcGIS, tiene una tamaño de 63.000 km² y principalmente consiste en rocas volcánicas como ignimbritas, sedimentos sueltos, depósitos salados y material lacustre en llanuras inundables extensas. Los poros de la capa de sal superior con un grosor de 2 y 11 m están llenos de una salmuera saturada, rica en Mg, K, Li y B. La distribución de Li heterogénea en el salar promedio es de 0.3-0.4 g/L en la salmuera. Muestra dos regiónes de concentraciónes muy elevadas de hasta 1.5 g/L, en el sur del delta del afluente principal Río Grande y en el nordeste a una distancia de 20 km de la orilla.

Las salmueras de la capa de sal superior tienen una edad entre 6.200 y 13.340 años, que corresponde a la edad de las evaporitas circundantes y tienen una estratificación estable. Sin embargo, el análisis de δ2H y δ18O indica la mezcla local de la salmuera con aguas dulces de acuíferos ribereños. La distribución de isótopos estables indica una importante influencia de la evaporación en el desarrollo de la salmuera, ya que los afluentes pequeños están enriquecidos con los isótopos pesados de H y O. La relación de elementos diferentes a bromo muestra que Li, K y Mg no son eliminados de la solución por precipitación de sales, sino que se liberan por intercambio iónico con arcilla y, por lo tanto, se enriquecen en la salmuera.
Las rocas analizadas, principalmente de tipo riolítico y dacítico, tienen concentraciones moderadas de litio de 4 a 37 mg/kg. El uso de diferentes disgregaciones mostró que los tipos de roca presentes en la cuenca del Salar de Uyuni son una fuente importante de litio en el lago salado, debido al intenso desgaste físico y químico bajo las condiciones ambientales específicas de la zona. En las rocas y sedimentos de los flancos volcánicos al sur del salar hay un aumento de las concentraciónes de Li que indica la cuenca sur es el proveedor principal de Li. La acumulación de Li también se ha confirmado mediante la investigación de

sales superficiales de la capa superior. En comparación con la superficie dentro de los polígonos de fisuras, las eflorescencias salinas se enriquecen significativamente en Li, K, Mg y otros iones. La acumulación de Li ocurre durante todo el año a lo largo de las grietas de desecación en los bordes de los polígonos. Allí, la salmuera aumenta por fuerzas capilares, el agua se evapora y el NaCl precipita. Finalmente, queda una solución aún más concentrada de Li y otros iones como Br, B, K y Mg.

En conclusión, la acumulación de litio en la solución de poros resulta de la combinación de numerosos factores específicos del lugar, que han sido investigados y evaluados en el presente trabajo.

V List of figures

XIII

VI List of tables

VII Abbreviations

a.s.l.	above sea level
AMS	Accelerator mass spectrometer
ASTER	Advanced Spaceborne Thermal Emission and Reflection Radiometer
BGR	Federal Institute of Geosciences and Natural Resources
COMIBOL	Corporación Minera de Bolivia (Bolivian Mining Company)
CRDS	Cavity ring-down spectroscopy
DEM	Digital elevation model
DF	Dilution factor
DI	Deionized water
DL	Detection limit
GMWL	Global meteoric water line
EC	Electric conductivity (calculated for 25°C)
E_H	Redox potential (with reference to hydrogen)
EMF	Electromotive force (field readings with oxygen-reduction-potential probe)
ENSO	El Niño–Southern Oscillation
GEOBOL	Servicio Geológico de Bolivia (Geological Service of Bolivia)
IC	Ion chromatography
IR	Insoluble rest
IRMS	Isotope ratio mass spectrometer
ITCZ	Inter-Tropical Convergence Zone
LEL	Local evaporation line
LMWL	Local meteoric water line
ICP-MS	Inductively coupled plasma mass spectrometry
n.e.	No equilibrium
n.d.	Not determined
ORSTOM	Office de la recherche scientifique et technique outre-mer
PE	Polyethylene
pmC	Percent modern carbon
PP	Polypropylene
PVC	Polyvinylchloride
QAPF	Quarz, Alkali feldspar, Plagioclase, Foid (Streckeisen diagram)
SACZ	South Atlantic Convergence Zone
Senamhi	Servicio nacional de meteorología e hidrología

SRTM	Shuttle Radar Topography Mission
TDS	Total dissolved solids
TIC	Total inorganic carbon
TUBAF	TU Bergakademie Freiberg
UATF	Universidad Autónoma Tomás Frías
UFZ	Helmholtz Centre for Environmental Research
UNEP	United Nations Environment Programme
USGS	United States Geological Service
UTM	Universal Transverse Mercator (coordinate system)
VCDT	Vienna-Canyon Diablo Troilite
VSMOW	Vienna Standard Mean Ocean Water
WGS 84	World Geodetic System 1984
yr B.P.	Years before present

1   Introduction

Salt lakes all over the world have long attracted people for their unique striking appearance, encouraging to wonder and think about the nature's ability of forming such impressive phenomena. For mankind, they serve as an archive of climatic history, as a place of recreation and, with increasing importance, as a resource of a growing number of present and future strategic elements. Salt lakes occur in a large variety of appearances, exhibiting a wide range of hydrological, geochemical and hydrochemical characteristics. Williams (1996) defined salt lakes as endorheic lakes containing salt accumulations or waters with at least 3‰ salinity. Salt pans, or salt flats, form from salt lakes by the complete evaporation of the superficial water. Depending on the location, salt lakes are named Sabhka (Arabian Peninsula), Chott (Northern Africa), playa (Southern USA) or Salar (South America). Regardless their significant differences, salt lakes exhibit two equal features: they form the deepest part of endorheic basins, and they usually occur under semiarid to arid climatic conditions, where evaporation exceeds precipitation. Depending on the climate, geological and hydrological conditions, salt lakes can be (seasonally) flooded or all-the-year dry, covered by a few mm or several m thick evaporate crust, very small or up to 10,000 m² in size, filled with varying layers of impermeable clayey sediments or porous salt aggregations. Salt lakes mainly contain NaCl, but also other salts and elements, which are transported by inflows in dissolved form or as suspended matter over large time spans. The general characteristics of salt lakes are responsible for a certain feature of some of them: the occurrence of elements, e.g. lithium, bromine and boron, in a highly concentrated form, strongly enriched compared to the element concentration in the inflow. The following thesis deals with the largest of all salt pans on earth and its giant lithium accumulations, the Salar de Uyuni in Bolivia: The salt lake, which has attracted scientists and tourists in equal measure for a long time. The salt lake, that Neil Armstrong thought to be a giant glacier after seeing it from space. Today this lake is focal point of an entire nation for a wealthy future.

1.1   Lithium market and availability

In view of the depletion of fossil fuels and the increasing threat of climate change, the focus is intensively put on electric mobility and replacing fossil fuels by alternative energy which requires storage systems for electricity. Among numerous energy storage systems, lithium batteries have turned out to be the most promising tool for an effective value chain from resource extraction over efficient energy use to recycling processes. In 2009, the German government defined an ambitious goal by bringing one million electric cars onto German roads

until 2020[1]. Although the amount of 35,000 electric cars in Germany (Jan. 2017) was far away from that goal, the worldwide number has rapidly risen in the last years. The high demand for lithium as a resource has increased the lithium price on the global market by a multiple from 1,500 US$ per metric ton in 2005 to 9,000 US$ in 2017[2], whereat a strong further rise is to be expected in the next years. Besides its use in batteries, lithium is required in several other industrial branches. Amongst others, it is needed for the production of glass and ceramics, lubricating greases, aluminium alloys and pharmaceuticals (Angerer et al. 2009). Thereby, the demand for lithium in the various industrial fields has increased by 400% between 1995 and 2015 (Martin et al. 2017).

In nature, lithium deposits of three types occur: brines, pegmatites and sedimentary rocks. Deposits of lithium salts do not occur naturally caused by the high tendency of the element to stay in solution. The distribution of lithium resources according to the source type is shown in Fig. 1. Pegmatites, intrusive igneous rocks, occur in the proximity of large magmatic intrusions and were formed by the crystallization of post magmatic fluids (Evans 2008). Spodumene, lepidolite and petalite are the main lithium containing minerals, recoverable amounts are for example exploited in the mining areas Greenbushes, Australia, and King's Mountain, USA. The process chain of flotation, grinding, leaching and precipitation of lithium carbonate is energy and cost intensive and adherent to a high consumption of concentrated chemicals (Grosjean et al. 2012). Sedimentary rocks as lacustrine evaporates and clay can also host considerable amounts of lithium (Gruber et al. 2011). The element is incorporated in the structures of clay minerals as smectite and illite, from where it must be separated by chemical treatment. Hectorite, a magnesium lithium smectite, is formed by the alteration of volcanic ash and tuff with a high silica content in combination with hot spring activity (Mineralogy Database[3]). Bearable amounts can be found in Hector, California, and Kings Valley, Nevada. A recently recognized deposit of jadarite, a silicate mineral containing lithium and boron, was found in lacustrine evaporite layers in the Jadar Valley, Serbia (Stanley et al. 2007, Kesler et al. 2012). The by far largest amounts of profitably recoverable lithium are contained in natural brines (Garrett 2004). According to the origin, two types of lithium bearing brines must be differentiated. Formation brines develop from the evaporation of saline fluids and their trapping into the pores of evaporates. Thereby, lithium is enriched in the pore brine, as it is not incorporated in mineral phases under saline formation conditions. In the course of the sediment sinking the pore brine is transported to deeper lying strata, where it is diagenetically altered under the influence of high temperatures and pressure (Müller & Papendieck 1975). These

---

[1] According to "Nationaler Entwicklungsplan Elektromobilität", published by the Federal Government (2009)

[2] Level as per Dec. 2017, www.metalary.com

[3] Access on homepage: http://webmineral.com/

brines are usually accessed in the course of geothermal exploration (geothermal water) as well as oil and gas production (oilfield brines). Brines in deep aquifers of the Rotliegend and Buntsandstein in the North German basin show lithium concentrations up to 360 ppm (Lüders et al. 2010). Lithium enriched formation brines with contents up to 1,500 mg/L occur worldwide, amongst others, in the Smackover Formation in USA (Collins 1978), the Chinese Qaidam Basin (Tan et al. 2011), the Mexican Activo Luna Oilfield (Birkle et al. 2002) and the Russian Siberian Platform (Shouakar-Stash et al. 2007). Due to comparably low Li concentrations, the exploitation of the element Li is nowadays only profitable in combination with the extraction of other value components, and is currently performed only in few locations (e.g. Salton Sea, USA).
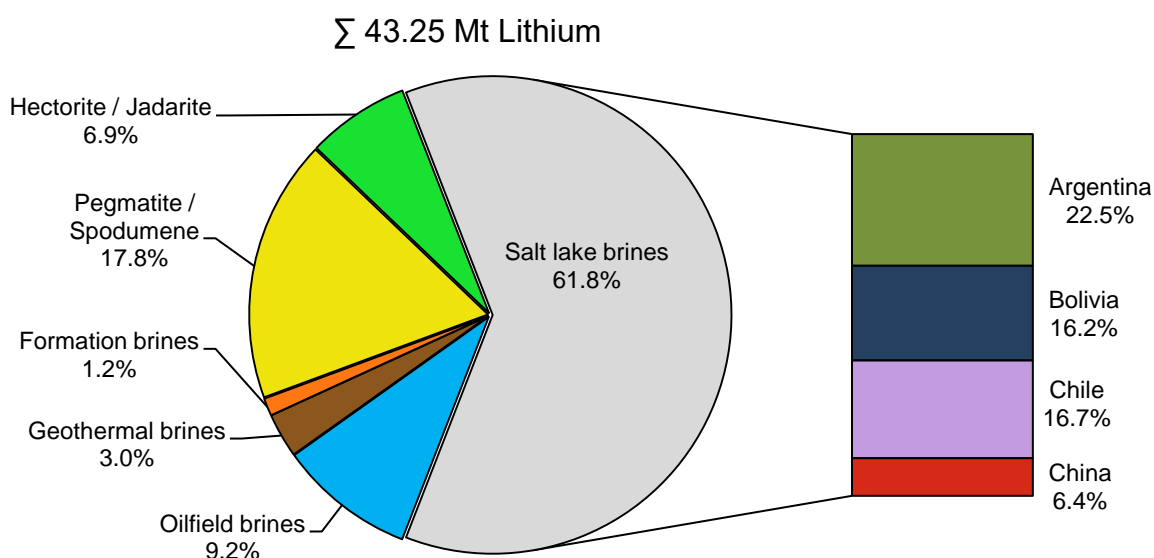
∑ 43.25 Mt Lithium

Fig. 1:   *Estimated global distribution of lithium resources (∑ = 43.25 Mt Lithium) according to source type, and shares of different countries on resources in salt lake brines (numbers and data sources are collected in Table A - 1)*

The second type of lithium bearing brines are the pore brines of salt lakes and salt pans. The majority of lithium-enriched lacustrine evaporate basins occur in the so-called lithium triangle consisting of northern Chile, western Bolivia and north-western Argentina (Fig. 2). Hundreds of salt pans of varying sizes exist in that area, many of them containing lithium-enriched brines. Different conceptions exist about the increased occurrence of lithium brines in that region. These include the frequency of closed basins, high intensity of weathering processes due to specific climatic conditions and high altitude, volcanic activity and the occurrence of lithium-containing source rocks. Differing regional tectonic and climatic conditions lead to strong variations in structure and stratification, the chemical composition of sediments and brine, and the hydrogeological situation.

For the sake of completeness regarding lithium resources, it should be mentioned, that Japanese scientists put strong efforts in the developments of methods for the extraction of lithium from seawater, as there is a huge total reserve base worldwide (Wang et al. 2008). However, at the current state of technology and the current Li-price it is not possible to handle the low lithium concentrations cost efficiently. Most recent estimates of total lithium resources worldwide from all source types amount to roughly 43 million tonnes, whereby values vary largely according to different sources and correctness of data. When discussing the supply of any value element it must be distinguished between resources and reserves. While resources describe the physical amount of an element in a geologic deposit with a current or near-future economic extraction feasibility, reserves name the part of
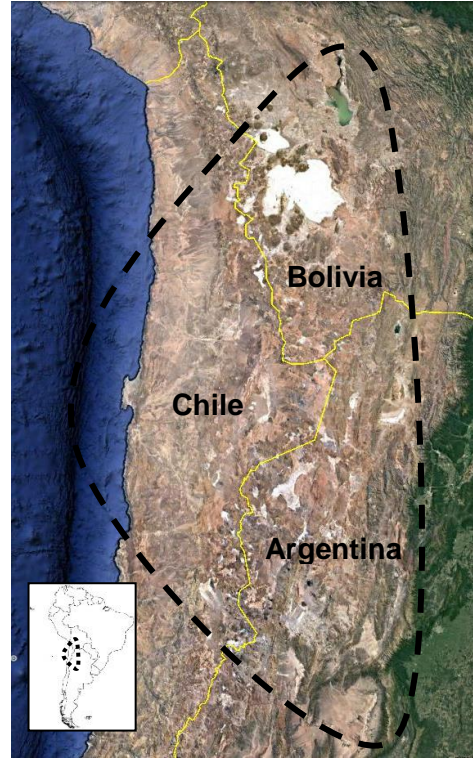
Fig. 2: *Location of the lithium triangle in South America*

resources that are assumed to be extracted in the future (Mohr et al. 2012). Hence, the global reserve estimate for lithium is much lower with 14,000 Mt or 74,500 Mt Li_2CO_3. In 2016, approximately 35,000 t of metallic Li were mined worldwide, mainly produced by Australia (41%), Chile (34%), Argentina (16%), and China (6%) (U.S. Geological Survey 2017). The largest known deposits are contained in the pore brine of the Salar de Uyuni in Bolivia, the largest salt flat on earth. Different studies amount the lithium resources in the range of 5 to 10 million tonnes (Ballivian & Risacher 1981, Gruber et al. 2011, Risacher & Fritz 1991b, Sieland 2014). The large range is due to different assumptions of porosity, concentrations and depth of the evaporate layers.

To date, a large-scale industrial production of lithium carbonate from the Salar de Uyuni does not exist. In the past years, the Bolivian government in form of the national mining corporation COMIBOL put strong efforts and large financial means in the development of an extraction technology and the build-up of a pilot plant near the shore of the salar. It was planned to win potassium chloride, lithium and other by-products with the help of giant evaporation ponds similar to the large facilities run by the company SQM in the Salar de Atacama. However, the natural conditions at Uyuni like the annual flooding of the salt lake and its southern vicinity during the rainy season, the high magnesium concentrations in the brine requiring costly separation techniques, and the position in an extreme remote area lacking infrastructure and large water reservoirs, makes the mining of lithium challenging.

1.2   Contribution of TU Bergakademie Freiberg

Research at the Salar de Uyuni under participation of workers from TU Bergakademie Freiberg dates back to the 1980's, back then mainly under the aspect of a general geological and geochemical characterisation (Wolf 1988). Since then, joint research was performed in cooperation with the Universidad Autónoma Tómas Frías (UATF) in Potosí, Bolivia. The focus was mainly set on the utilization of the salar as a lithium resource by the use of innovative and regionally adapted extraction methods in cooperation with local authorities and including the resident population (Voigt et al. 2010a, b; Voigt 2014). Parallel to that goal, research was expanded to geological and hydrogeological aspects, because the knowledge of enrichment processes and the exact characterization of the hydrochemical and hydraulic properties is a mandatory requirement for a successful mining in combination with minimizing environmental impacts (Fig. 3). In 2014, Sieland published an extensive work dealing with the hydraulic conditions at the Salar de Uyuni (Sieland 2014). Pumping tests, porosity determinations and long-term brine level measurements served for the investigation of the hydraulic properties of the uppermost salt crust. Based on the gained information, detailed lithium resource estimations for the upper salt layer could be established.
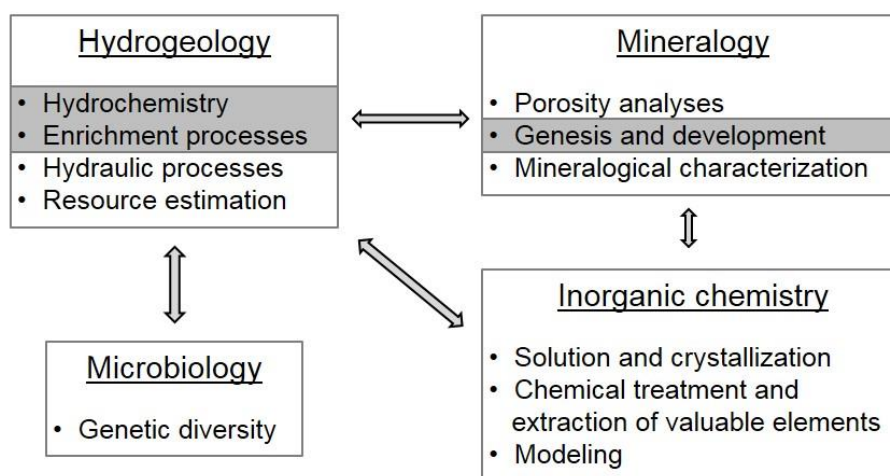
Fig. 3:   Participation of institutes and departments of the TU Bergakademie Freiberg in the research of the Salar de Uyuni, shaded fields are part of the work

1.3 Aim of work

Brines, contained in the pores of salt deposits all over the world, show a wide range of element compositions. Accordingly, also lithium occurs in concentrations of below detection limit to highly economically exploitable values of several grams per litre. This work aims to examine the (hydro)-geological, hydrochemical and hydrological circumstances that led to the specific distribution of lithium and other solutes as bromine, potassium and boron in the pore brine of the Salar de Uyuni. This includes the identification of the sources / origin of the elements, their mobilization, transport mechanisms and the study of the final deposition, influenced by several processes of enrichment. In concrete, the work should help solving the following questions:

1. What are the sources of the lithium detected in the brines of the Salar de Uyuni?
2. What specific geological, hydrogeological and hydrochemical conditions must be present and interact leading to the formation of highly lithium-enriched pore brines, especially for the Salar de Uyuni?
3. What enrichment mechanisms provide the accumulation of lithium and other solutes in the pore brine of the Salar de Uyuni?
4. How can the heterogeneous distribution of lithium and other elements in the pore brine be explained, especially regarding an anomaly in the northeastern part of the Salar de Uyuni?
5. Did a superficial connection to the Salar de Coipasa exist in the past and is it still active in recent times?
6. Does the composition of the uppermost salt crust give hints to the underlying brine composition?
7. How does wind influence the distribution of solutes in the pore brine?
8. What is the recent influx of lithium and other solutes to the salar, especially in proportion to the withdrawal planned for the industrial extraction of the brine?
9. Why do some saltpans accumulate large amounts of lithium, but others, existing under similar environmental conditions, are unremarkable regarding that feature?

This work aims to close the gap between the fragmentary comprehension of complex and interconnected processes of salt lake development and the economical need of understanding the hydrogeological system for the estimation of the region's mining potential. It will provide help for companies interested in the exploitation of the world's largest known lithium resource, researchers in deepening the understanding of salt lake characteristics, and locals helping to realize the impressive miracle of nature at their front door. It was not aim of this work to investigate environmental problems including availability of water for the processing of the brine.

2   Region of interest

The investigations were concentrated on the Salar de Uyuni including its vicinity and catchment. With a size of roughly 10,000 m² the Salar is considered as the largest salt flat on earth, situated at an altitude of 3,650 m. It forms the central trough and largest depression in the southern part of the Bolivian Altiplano. Scientific research at the Salar and its vicinity goes back to the 1980s and was strongly intensified after the first descriptions of high lithium appearances in the pore brine. Between 1965 and 1985 the Mining Academy Freiberg intensively investigated the salars of the Altiplano regarding geological, geochemical and hydrological aspects, putting a special emphasis on the Salar de Uyuni (Wolf 1988, Wolf 2010). The U.S. Geological Service first published data on lithium-enriched brines in the Salar de Uyuni and other salars in the central Andes (Ericksen et al. 1976, Ericksen et al. 1977, Ericksen et al. 1978). At the same time, field partys lead by the ORSTOM[4] investigated cross-sections in the delta region of the Río Grande (Risacher & Miranda 1977, Rettig et al. 1980). First analyses of surrounding rhyolites as a possible source of lithium were done by the GEOBOL-ORSTOM-USGS cooperation in 1978 (Davis et al. 1982). From the 1990s, several papers concerning the geochemistry, source and enrichment of solutes in the salars were published (Risacher & Fritz 1991a, Risacher & Fritz 1991b, Risacher & Fritz 1992, Schuler et al. 1995, Risacher & Fritz 2009), whereby also the behaviour of bromide was in the focus of attention (Risacher & Fritz 2000, Risacher et al. 2006). Superficial features in form of parabolic halite dunes were described in Svendsen (2003). The Salar de Uyuni was also target to several remote sensing studies, either as a reference for several elevation detection satellite missions (Fricker et al. 2005, Borsa et al. 2008b), the correlation of topography to the local equipotential surface (Borsa et al. 2008a), or high-accuracy bathymetrical measurements (Bills et al. 2007). Further research, supported by remote sensing techniques and field investigations, focused on the morphology in the course and the terminus of the Uyuni contributing river systems (Hosseini Aria et al. 2012, Donselaar et al. 2013, Li 2014, Li et al. 2014). Recently, the focus of research was put on the extraction of lithium from the Uyuni pore brine.

2.1   Geographical and hydrological situation

The Altiplano (Spanish meaning high plateau) is a large interior drainage basin extending on an area of roughly 200,000 m² between the eastern and western cordilleras of the Andes, encompassing parts of Chile, Peru and Bolivia (Fig. 4). With a length of 1000 km and a width

---

[4] Office de la recherche scientifique et technique outre-mer

of 200 km it forms a large and narrow depression (Guyot et al. 1990). From north to south the precipitation decreases significantly leading to a N-S transition from drained freshwater lakes over desiccating brackish water bodies to the poorly drained intra-volcanic basins occupying temporarily flooded salt pans and playas. The Altiplano can be divided into four separate sub basins (Risacher et al. 2006). Lake Titicaca, situated at an elevation of 3810 m, forms the northernmost drainage system, having a size of approximate 7000 km² and depths up to 300 m. It is considered oligosaline and mesotrophic (Fritz et al. 2007). The annual water input to the lake amounts to nearly equal parts from riverine input and direct precipitation on the lake surface (Roche et al. 1992). The Río Desaguadero to the south of lake Titicaca is the only outflow, thus the river accounts for less than 10% of water loss from the lake.
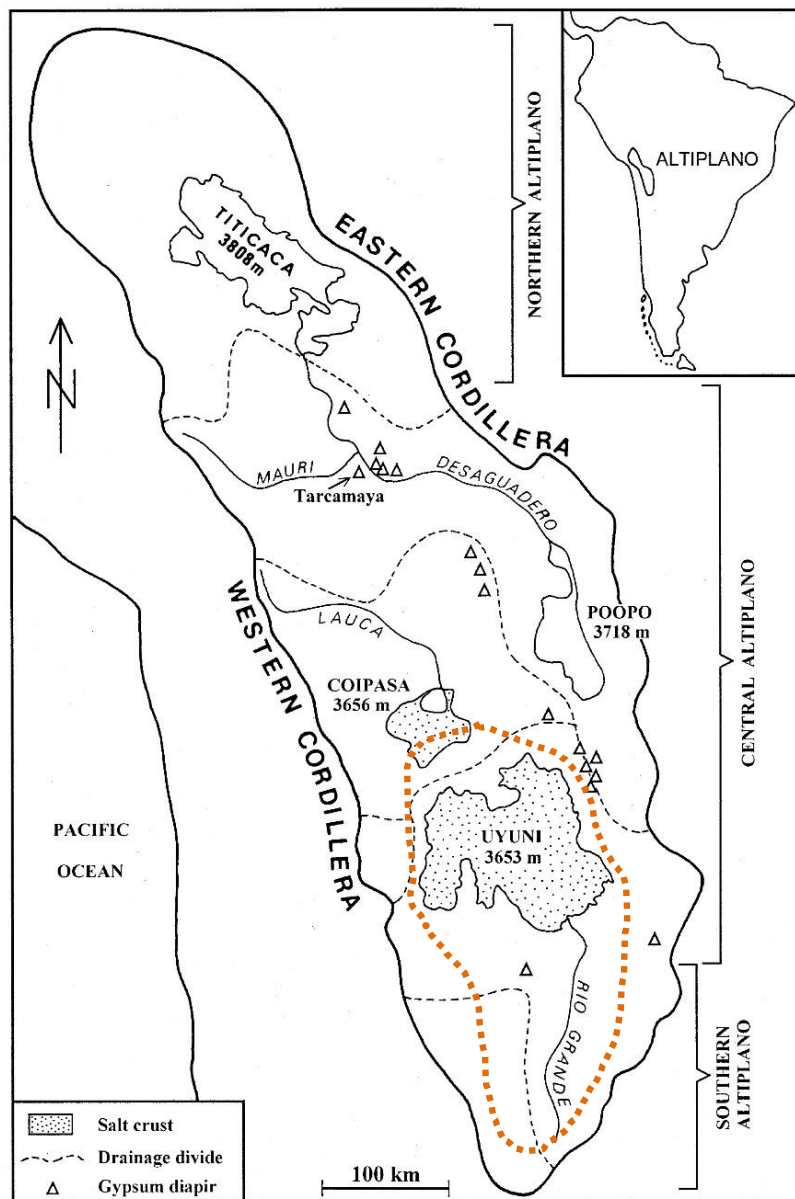
Fig. 4: *Hydrological systems and drainage basins of the Altiplano (after Risacher & Fritz 2000) with the outline of the investigation area (orange dotted line)*

More than 90% of the water loss results from evaporation on the lake surface (Fontes et al. 1979). The river serves as overflow to Lake Poopó, a very shallow salty lake with a depth of less than 2 m and a size of maximum 2,000 km² (Bengtsson 2012). Depending on the season, its size varies strongly and due to a lacking outflow it can be considered a terminal lake. To the southwest follows the third sub basin, the Salar de Coipasa (2,500 km²; 3,656 m). An insuperable watershed between Río Marques flowing towards Lake Poopó and Río Lacajahuira flowing to Coipasa impedes a superficial hydraulic connection between the two lakes (Wolf 1988, Wolf 2010). Especially during the rainy season the Salar receives large water masses from several perennial streams including Río Lauca and Lacajahuira, enriched with sediments and dissolved salts from the Altiplano. To the south the fourth and largest sub basin of the Altiplano, the Salar de Uyuni, adjoins. With N-S and W-E extensions of max. 140 km and 110 km, respectively, and located at a height of 3,653 m, it forms the deepest part of the depression. To the north the Salar is bordered by the Serrania Intersalar with Mt. Tunupa directly adjoining to the lake shore (Fig. 5). The Salar de Uyuni receives year-round inflows only from the southeastern side by means of the Río Grande de Lípez and the Río Colorado (locally called Río Pucumayu).

Fig. 5:   View of Mt. Tunupa at the northern shore from the center of the Salar de Uyuni

The southwestern part of the Bolivian Altiplano, located at heights of 4,100 to 4,600 m in a region of high volcanic activity, is characterized by large endorheic basins which are in different stadiums of salt pan formation (Wolf 1988). Basins are delineated by volcanoes reaching up to 6,000 m in height, lava flows and ignimbrites (Risacher & Fritz 1991a). The mountain range of the Serrania Khenval forms the drainage divide to the eastern located Río Grande river system (Fig. 4).

2.2 Geological situation and evolution from paleolakes

The eastern cordillera of the Andes is predominantly characterized by palaeozoic sediments (sandstones, shales, quartzites). In the Altiplano, where they constitute the basement, they are covered by a ~15,000 m thick continental sedimentary sequence of Cretaceous, Tertiary and Quaternary age (sandstones, claystones, mudstones, shales and evaporates) (Risacher 1991b, Lebrun et al. 2002). Gypsum diapirs of cretaceous and tertiary age crop out in northern and central-eastern parts of the basin. The origin of the Cordillera Occidental (Western cordillera) is mostly volcanic, whereby tertiary formations are overlaid by strato-volcanoes, ignimbrites and lava flows. Volcanoes reach up to 6,000 m along the north-south striking chain and range from andesites to rhyodacites (Fernández et al. 1973).

The Altiplano basin was formed during the uplift of the Andes, which began 25 Ma ago in the early Tertiary. The uplifting was the result of crustal thickening caused by horizontal shortening of a thermally softened lithosphere supported by magmatic processes and upper mantle hydration (Allmendinger et al. 1997). Coincident with the Andean orogeny, the volcanic activity on the Altiplano began in early Miocene times. Large volumes of ignimbrite erupting from caldera-shield complexes in the southern Altiplano were followed by the built of stratovolcanoes during late Miocene to Holocene time along the Andean arc. Major volcanoes, as Mt. Sajama at the Chilean border and Mt. Tunupa at the northern shore of the Salar de Uyuni, are composed of andesitic to dacitic lava flows, pyroclastic rocks and flow breccias and distinctly underlie hydrothermal alteration effects (U.S. Geological Survey 1975).

In the past, the Altiplano was covered by numerous paleolakes which repeatingly were subject to flooding and desiccation, according to the prevailing climatic conditions (Fornari et al. 2001). Thereby, the water balance in the high plateau is linked to climatic changes in the Amazon basin, which is the main source of humidity in the northern Altiplano (Chepstow-Lusty et al. 2005). In a phase of increased effective moisture during the early Pleistocene, two large lakes were present, Lake Ballivian in the north, which left Lake Titicaca as remnant and Pre-Minchin in the south (Ahlfeld & Branisa 1960). In the late Pleistocene Pre-Minchin was followed by Lake Minchin (>32,200 yr. B.P.) which covered the salars of Uyuni, Coipasa and lake Poopó in the southern Altiplano (Fig. 6). During its maximum size, large amounts of $CaCO_3$ were deposited in the lake (Ericksen et al. 1978), leading to the enrichment of more soluble components as chloride and sulphate in the lake water. Radiocarbon dating of shells in lacustrine outcrops from the central Altiplano showed that the most recent lacustrine phase occurred from about 25,000 yr. B.P. to about 12,000 yr. B.P., named as Lake Tauca (Servant & Fontes 1978). Investigations on carbonate algal reefs (bioherms) marking ancient shorelines showed that paleolake Tauca covered an area of 60,000 km² and reached depths of >100 m (Sylvestre et al. 1999). The modeling of surface energies and water budgets lead Hastenrath & Kutzbach

(1985) to the conclusion, that a precipitation increase of 50 – 75% was needed to form the extensions of paleolake Tauca.
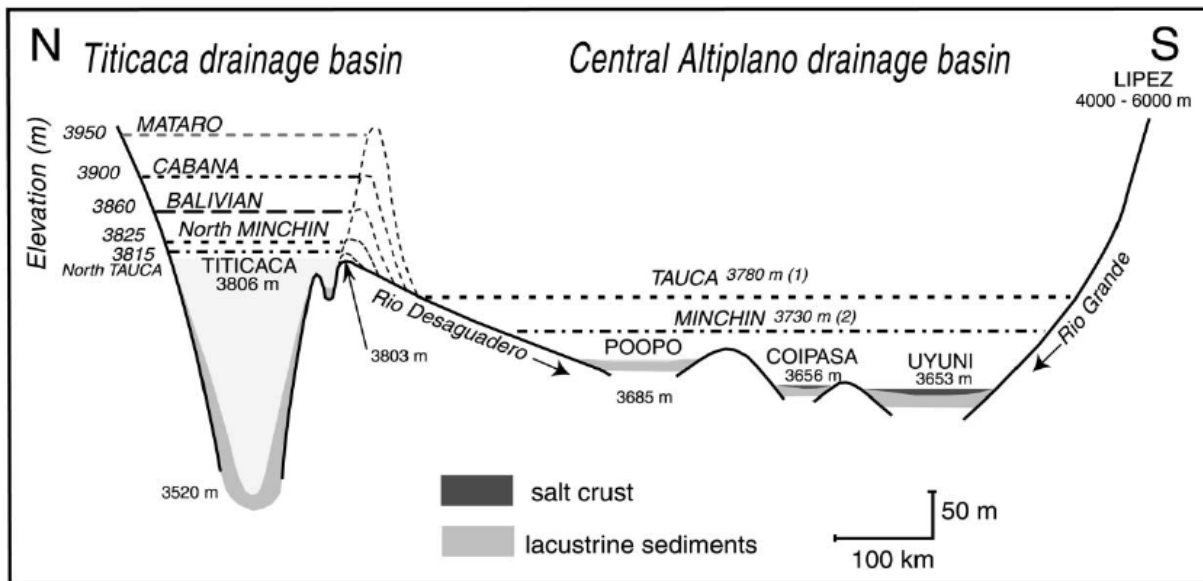
Fig. 6: *Reconstruction of paleolake levels in a N-S profile along the northern and central drainage basins of the Altiplano (Fornari et al. 2001). The dotted line represents the overflow level for the older paleolakes*

In 1995 the U.S. Geological Service published a detailed digital geological map of the Altiplano and the western cordillera of the Andes, containing major and minor volcanic centers. The map was digitized from 15 field compilation maps produced by the Servicio Geológico de Bolivia over the last decades, and verified by field studies (Marsh et al. 1995). The southeastern part of the Salar de Uyuni catchment is mainly characterized by surficial deposits and sediments dating back to Holocene and Pleistocene, including unconsolidated alluvial, eolian and colluvial material, locally supplemented by shallow lacustrine and salt deposits (Fig. 7). The region west of the salar mostly consists of stratovolcano deposits with lava flows and flow breccias of andesitic to dacitic composition, complemented by extensive outflow sheets of ignimbrites and ash-flow tuffs (Fig. 7). Tributaries to the Río Grande and Río Colorado have their source in springs and thermal springs located in elevated mountain regions and volcanic flanks, which are rich in ignimbrites and pyroclastic rocks of volcanic origin. The main course of the rivers and their tributaries is characterized by unconsolidated surficial deposits resulting from the alternating processes of weathering, associated mineral dissolution, and the deposition of silts in the extended floodplains. The dominance of these deposits is reflected in Fig. 36, which illustrates the distribution of geological units in the catchment of the Salar de Uyuni. The evaluation of Skylab and Landsat images by Francis & Baker (1978) showed that ignimbrite shields in the Southern Bolivian Altiplano have their source in large calderas which erupted during the Miocene and Pliocene.

Fig. 7: *Geological map of the southern Altiplano including the estimated drainage line for the Salar de Uyuni catchment (Marsh et al. 1995; for description of geological units see Table A - 14)*

2.3 Climate

The climate of the Altiplano is arid according to the definition of the UNEP (Barrow 1992). Depending on the prevailing circulation, the Altiplano receives influences from the dry and stable conditions of the Southeast Pacific Anticyclone across the western cordillera of the Andes and from moist and warm conditions of the lower troposphere across the eastern cordillera (Vuille 1999). The majority of precipitation occurs during the Austral summer from December to March, where between 70% (Titicaca) and 90% (Uyuni) of the rain falls (Fig. 8). Intensity and timing of rainfall in the Altiplano is controlled by several major circulation systems as the Inter-Tropical Convergence Zone (ITCZ), the El Niño-Southern Oscillation (ENSO), the Bolivian High and the South Atlantic Convergence Zone (SACZ) (Garreaud et al. 2003). A pluviometric gradient exists from north to south, leading to a variation in mean annual precipitation between 700 mm at lake Titicaca and less than 100 mm at the southern border of the Altiplano (Fig. 8). The southward shift of the ITCZ in austral summer goes along with easterly winds and high temperatures, leading to the incursion of humid air from the Amazonian basin. With further distance from the northern parts of the basin this influence becomes rare, explaining the N-S increase in aridity.
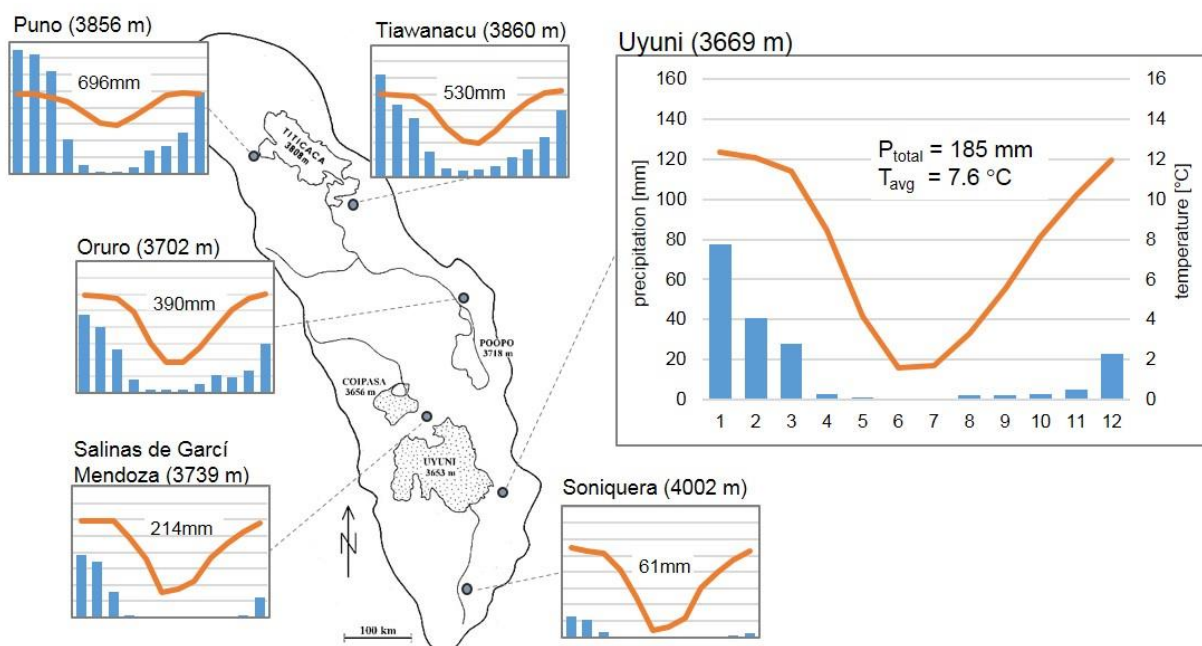
Fig. 8:   Climate at different stations on the Altiplano (climate data stem from the SisMet database of the Bolivian Senamhi – Servicio Nacional de Meteorología e Hidrología); numbers in the diagrams show the annual precipitation, T_{avg} is the average temperature (map adapted from Risacher & Fritz 2000)

According to the Köppen climate classification the salar and its catchment are located in the Bwk belt, named as cold-arid dry winter desert (Warren 2016). The mean evaporation rate of

more than 1,500 mm/a strongly exceeds the annual precipitation of 180 mm, which results in the Salar de Uyuni being a saltpan (Argollo & Morguiart 2000). The Altiplano experiences large variations in the amount of precipitation on the interannual timescale. For example, the austral summer of 1983/1984 with a total rainfall of 420 mm was extremely wet, compared to the very dry rainy season with 60 mm the year before[5]. This difference can to a significant fraction be explained by the El Niño phenomenon, which describes unusual anticyclic currents in the ENSO system. Generally, El Niño years are associated with dry conditions on the Altiplano, whereas La Niña occasions lead to high rainfalls.

2.4 Geochemistry and hydrochemistry

The stratigraphy of the Salar de Uyuni sediments is characterized by the alternation of evaporites and lacustrine layers, which were formed according to the prevailing climatic conditions. The thickness of the uppermost salt crust varies between 0.5 m near the south-western shore and 11 m in the eastern part. A few drillings for scientific purpose have been performed on the Salar in the past, whereby the focus was mainly set on the research of climatology on quaternary time scales and associated vegetation changes and paleolimnological conditions. In 1986 a first drilling in the center of the Salar de Uyuni was performed by a cooperation of the French scientific institute ORSTOM and the Bolivian Ministry of Mines (Fornari et al. 2001). The 121 m deep drilling revealed 12 hard salt crusts separated by 11 soft mud layers reflecting the alteration of desiccation stages during dry climatic periods and lacustrine phases during humid climatic periods (Fig. 10). Geochemical analyses showed that salt layers are mainly composed of NaCl with minor amounts of gypsum. Mud layers are composed of calcite, volcanic detritus, gypsum and organic matter. By radiocarbon dating of the sediment cores the two upper major mud layers could be assigned to the corresponding paleolakes Tauca and Minchin, lasting from 16,000 to 12,000 yr. BP. and 70,000 to 30,000 yr. BP, respectively (Fornari et al. 2001). In 1999 another drilling to a depth of 220 m was performed by researchers from Duke University, USA.

Fig. 9:   *Polygon structures with salt efflorescences in detail (pictures by Wolfram Canzler, August 2015)*

[5] Data from Senamhi (Servicio Nacional de Meteorología e Hidrología); meteorological station: Uyuni

The measurement of natural γ-radiation in the upper 188 m of the cased borehole revealed a decreasing persistence and thickness of the mud layers until a depth of 140 m, beyond that a continuous salt layer follows until the final depth of 220 m (Baker et al. 2001, Fritz et al. 2004). Hence, the duration of paleolakes increased significantly during the Pleistocene. Model calculations showed that a temperature lowering of 5°C together with a 30% increased precipitation compared to the modern time must have prevailed in order to preserve the large paleolakes of the Altiplano against desiccation by evaporation (Blodgett et al. 1997). The total depth of the evaporite filled basin is not known so far. The upper salt crust is characterized by an average porosity of 30-40% (Risacher 1991b). The pores are filled with an interstitial brine, the brine table is localized in a depth of 10-40 cm. First investigations on brine chemistry were done in the 1970s by the U.S. Geological Survey (Ericksen et al. 1977, Ericksen et al. 1978, Rettig et al. 1980), who as first researcher constituted the Salar de Uyuni as a potential major deposit for lithium. The saturated brine is of Na-Cl type, with high concentrations of potassium (up to 20 g/L) and boron (up to 1 g/L). Lithium concentrations are about 500 ppm in average, showing a high range between 100-1,500 mg/L, depending on the location on the salar. Risacher et al. (1991b) collected brine samples from a marshy area at the southern shore in the delta region of the Río Grande, and measured lithium concentrations as much as 4 mg/L.

Fig. 10: Depth profile of the Salar de Uyuni (modified from Fornari et al. 2001)

Large parts of the salar surface are characterized by smooth, polygonal structures with diameters up to one meter, which are formed as a result of the drying of the superficial water layer at the end of the rainy season, similar to shrinkage cracks in clayey sediments (Fig. 9). Evaporation of surface water due to strong solar insolation and very low humidity associated with the precipitation of salts conducted the formation of a very hard, dense, cemented crust. During the dry season, evaporation is limited to the polygon margins, where brine rises due to capillary forces. As a consequence, salt efflorescences are formed on these cracks, reaching heights of few cm.

During austral summer between December and March, the salar is completely covered with a water layer up to a level of about 50 cm, brought by precipitation on the lake surface and from the main tributaries and ephemeral streams transporting the rainfall from the catchment. An extensive study of the geological, hydrological and geochemical characteristics of the Salar de Uyuni and its surrounding was done in the 1980s by Wolf. He divided the geochemical cycle of the year at the salars of Uyuni and Coipasa into four different stages (Wolf 2010):

1. Stage of desert soil weathering: dissolved solutes resulting from intensive physical and chemical weathering at the end of the rainy season attain the surface by capillary rise, where they precipitate as salt efflorescences due to evaporation of the solvent

2. Stage of salt solution and transport: during heavy rainfalls at the beginning of the austral summer, superficial salt crusts from stage 1 are dissolved and transported together with detritus along the drainage system to the salar basin; meanwhile, aquifers are filled up, which enhances the solution weathering of subsurface sedimentary structures

3. Stage of extensive flooding and pre-concentration: at the end of the rainy season extended floodplains at the southern shore of the salar exist, which serve for the slowdown of water masses and the sedimentation of detrital material in the delta areas of the tributaries

4. Stage of major concentration and salt precipitation: with the beginning dry season and the corresponding higher solar insolation the flooding concentrates on the salar itself, where the uppermost crust is dissolved until the point of saturation; after exceeding the solubility product with further evaporation, halite precipitates and forms a new crust

3   Fundamentals

The following section describes general characteristics of the element lithium and its geochemical behaviour in different compartments of the sedimentary cycle. Principal sources of lithium and mechanisms of enrichment are explained and its use as a tracer in genetic studies is presented.

3.1   Lithium geochemistry

Lithium (from *lithos*, the Greek word for stone) occurs in the earth's crust with a concentration of about 20 ppm (Vine 1980), whereby literature values range from as low as 7 ppm (Bach et al. 1967) up to 60 ppm (Deberitz 1993). It thus belongs to the upper third of the most abundant minerals (Wietelmann & Steinbild 2000). Lithium, the third element in the periodic table, represents the lightest element (after H and He) in the periodic system with a density of 0.534 g/cm³ at 20°C (Table 1), which is solid at room temperature and by this as well the lightest metal. On the other hand, it shows the highest energy density of all metals. As the other alkali elements, the lithium metal is very reactive to water and oxygen, which is increased in the presence of sodium, even at low concentrations of 0.5 – 1%. Its melting point is the highest of all alkali metals. With a value of -3.04 V lithium has the lowest standard electrochemical potential of all elements. This property together with its high electrochemical equivalent and the good electrical conductivity account for the advantages of lithium for its use as anode material in battery cells, as the high power output, very good storage properties and a small power loss (Wietelmann & Steinbild 2000).

Table 1:   Chemical and geochemical characteristics of lithium (values for average abundance are from Vine et al. (1980))

Atomic number	3	Stable isotope ratio	^{6}Li: 7.59%, ^{7}Li: 92.41%
Atomic weight	6.941 g/mol	Oxidation potential	Li $\rightarrow$ Li$^+$; E = 3.045 V
Atomic radius	0.68 Å	Geochemical classification	Lithophile
Density	0.534 g/cm³	Behaviour	High reactivity with oxygen, high solubility
Melting point	180.5°C	Average abundance [ppm]	57 - Pelagic clay, 40 – granite, 17 – basalt, 15 - sandstones, 5 - carbonates, 0.17 - seawater
Mohs hardness	0.6		

The geochemical character according to the Goldschmidt classification is lithophile, which is responsible for its high affinity to oxygen and the strong association with silica, leading to the formation of low-density minerals enriching in the earth's crust rather than sinking to the core. Due to the small ionic radius, the substitution of lithium to sodium and potassium in common rock minerals like quartz and feldspar is rather low. The high solubility of the element in both liquid magma and water leads to its concentration in the residual fraction of magmatic melts and in residual brines during evaporative concentration (Vine et al. 1980). About 150 naturally occurring minerals with lithium as a major component are known, as Spodumene ($LiAl(SiO_3)_2$), Amblygonite ($(Li,Na)Al(PO_4)(F,OH)$), Petalite ($LiAlSi_4O_{10}$), Lepidolite ($K(Li,Al)_3(Al,Si)_4O_{10}(F,OH)_2$) or Zinnwaldite ($KLiFe^{2+}Al(AlSi_3)O_{10}(F,OH)_2$). Most of these minerals are typical for the latest crystallization stage of igneous rocks, forming residual fluids of magmatic melts. Lithium has (as other alkali elements) in natural aqueous systems more or less no limiting mineral. Thus, Li behaves extremely conservative and stays in solution if dissolved. Lithium has two stable isotopes ^7Li and ^6Li, with a distribution of 92.58% and 7.42%, respectively, and a number of radioactive isotopes with very low half-lifes. The diagonal relationship between lithium and magnesium in the periodic system leads to similar chemical properties as the comparable atomic radius. This makes the separation of the two elements in the course of an industrial lithium extraction challenging, especially at high Mg/Li ratios.

3.1.1   Lithium in the sedimentary cycle

Generally, the lithium content increases from ultrabasic to acid igneous rocks, due to the elements' tendency to accumulate in residual melts (Ronov et al. 1970). In contrast to ancient rocks, where the distribution of lithium and lithium-bearing minerals usually depends on geochemical processes occurring at higher temperatures and pressures, the content of lithium in sediments is a function of weathering, diagenesis and sedimentation processes taking place at low temperatures (Vine 1980). The release of lithium from rock-forming minerals can be attributed to weathering processes. A part of the lithium is incorporated into new minerals, and thus, enriched in the products of weathering, as it retains and concentrates in the clay mineral fraction (Horstman 1957). Thus, the element is mainly associated with the clay fraction of sedimentary rocks (Vine 1975). Shales for example show much higher lithium concentrations (20-100 ppm) than sandstones and limestones, where values are usually less than 20 ppm (Vine 1980). Another part of the lithium is transported in dissolved form by streams and rivers towards the terminal lake. Although evaporite sequences in closed basins should provide the best possibility to show high lithium concentrations, most evaporites a very low in lithium, due to the elements' high solubility and its small size, which inhibits its substitution for other alkalis

in sulfates, halides and carbonates. Thus, it rather concentrates in residual brines trapped in the pore volume of evaporites in the shallow subsurface (Bradley et al. 2013).

3.1.2 Lithium in salt lake brines

Average lithium concentrations in salt lake brines vary from less than 50 ppm to 1,400 ppm in the Salar de Atacama (Fig. 11). Besides showing impressive maximum values of lithium in brine, the Atacama salt pan is also the largest producing lithium deposit at the time being; 65,000 Mt Li_2CO_3 were produced from different operating mining companies in 2008 (Gruber et al. 2011). The Salar de Uyuni exhibits a rather large range of Li concentrations, which cannot be explained by evaporative concentration of the brine itself. Hence, the existence of enrichment processes leading to the heterogeneous distribution of the element in the pore brine must be considered. As indicated in Fig. 11, most lithium enriched salt lake brines occur within the lithium triangle. The 400,000 km² large region encompassing parts of the Bolivian Altiplano, eastern Chile and the Argentinian Puna contains about 130 salars with sizes from 0.03 to 10,000 km² (Risacher & Fritz 2009). The morphology is widespread, ranging from permanent saline lakes with depths up to 10 m, over playas with seasonally drying shallow pools on the top of a confined aquifer, to salt crusts filled with interstitial brine and underlain by impermeable sediments.
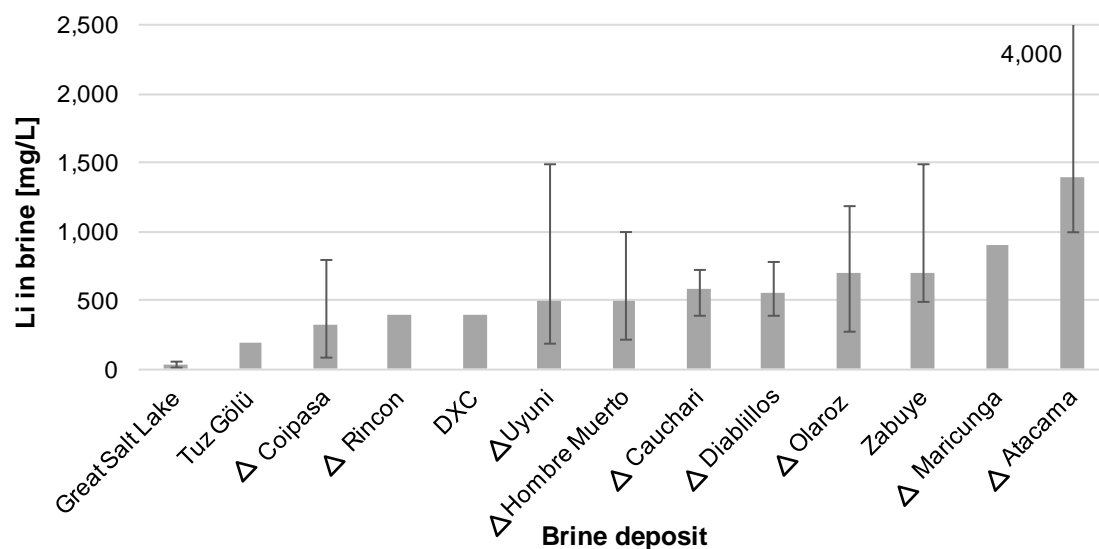
Fig. 11:   *Average lithium concentrations and min-max range of salt lake brines worldwide; triangle indicates location in the Lithium Triangle (references are shown in Table A - 1)*

The development of strongly enriched lithium brines in porous evaporate crusts is bound to the synchronous existence of specific circumstances and regional features during large geological timescales. Noticeably, all closed-basin brines containing lithium deposits of economic interest

are of Quaternary age (Bradley et al. 2013). Generally, these continental brines share the following features (Bradley et al. 2013, Ericksen et al. 1976, Munk et al. 2016):

1. Location in closed-basin environments undergoing tectonically driven subsidence: Only where outflow from the basin is absent or negligible, a significant accumulation of solutes can occur

2. Semi-arid to arid climate: Only where evaporation exceeds precipitation, an enrichment of solutes in a residual brine is possible, and the removal of dissolved lithium from the basin by overflow along the drainage divide is impeded

3. The existence of lithium-rich host rocks and other lithium sources: Easily leachable volcanic rocks such as tuffs and rhyolite sheets, magmatic fluids, ancient evaporate deposits and clay lenses are supposable sources of lithium; the coeval existence of multiple sources increases the final concentration of lithium in the salar brine

4. Time for brine generation: The transformation of dilute waters to strongly enriched brines by leaching, transportation and concentration processes is time consuming; during that time, geologic, climatic and environmental conditions must remain unchanged

5. Volcanic and hydrothermal activity: By providing hot water for the leaching of host rocks and/or serving as a lithium source from magmatic brines itself, hydrothermal activities in the subsurface are a significant contributor of lithium to the salar brines; further, hydrothermal flows enhance the formation of hectorite, which in turn can serve as a source of lithium by leaching of the clay sediments

6. Large ratio of catchment size to salar size: A large drainage area results in a higher amount of weathered material, which is transported by rivers and streams to the salars

Additionally, characteristics exist, that are not common in all salt lake lithium brines, but which lead to the further enrichment of the brine, making the difference of several magnitudes of lithium concentration in the brine. Summarizing, the best chances to find lithium enriched brines are closed desert basins in volcanic terrain in combination with the occurrence of lithium-rich rock and water sources.

3.2   Mineral sources

Usually, the exceptionally high accumulation of lithium in deposits is the result of the combination of more than one source. Mostly, a main source is amended by one or more minor contributors. Following, potential sources of lithium in salt lakes will be described.

3.2.1   Leaching of volcanic rocks

Volcanic activity plays a major role in the accumulation of lithium in brines. On the one hand, it serves as a primary lithium source due to the occurrence of volcanic rocks, on the other hand, it provides the heat for the convective circulation of groundwater as a requirement for the leaching of solutes from subsurface rocks (Vine et al. 1975). Generally, the leaching of lithium from the crystal lattice of all kind of rocks and minerals is very low at ambient temperatures. Though, long-term experiments have shown that the leaching of lithium from granitic rocks is strongly enhanced at temperatures of 275°C and pressures of 500 bar (Dibble & Dickson 1976). The occurrence of water-soluble salts in rhyolitic volcanic rocks of the central Andes and the possible leaching by circulating groundwater has been known since long (Ericksen 1961). Possibly, igneous intrusions provide the heat to power a convective circulation of meteoric waters in permeable rocks, leading to the leaching of lithium, which is then concentrated in adjacent closed basins (Vine 1975).

Rock decomposition due to weathering leads to the release of B and Li, which are then easily sorbed to clay minerals and transported as suspended matter in streams towards the deepest part of the basin (Tan et al. 2012). The cycle of desert soil weathering, transport by run-offs, accumulation in the floodplains and precipitation of minerals, described in chapter 2.4, could play a major role in delivering lithium from the source rock to the brine. The composition of source rocks, weathered material, fluviatile sediments and the mud layers of salt lakes should give hints for the verification of these processes at the Salar de Uyuni.

3.2.2   Hydrothermal and magmatic fluids

Magmatic fluids associated to residual melts during differentiation, are enriched in elements as lithium and boron, which are incompatible or moderately imcompatible in magmatic systems. With 6-50 ppm Li in average, geothermal waters are generally elevated in lithium (Campbell 2009, Garrett 2004). Investigations in the Dead Sea, Tibetian salt lakes and the Qaidam basin showed, that hot spring waters from geothermal fields significantly contribute to the regional rivers' high lithium and boron contents (Grimaud et al. 1985, Mianping 1997, Vengosh et al. 1991). Dischargings in springs and flowing as small streams towards larger

tributaries, hydrothermal waters can contribute to the elevated lithium content in rivers. If faults, which are frequently occurring in active tectonic zones of volcanic regions, are cutting through the river catchment, they serve as conduits for geothermal waters to the tributaries (Tan et al. 2012). Hydrothermal systems, in combination with the occurrence of lithium rich rhyolitic rocks of Quaternary age, are suggested to play a major role in delivering lithium by thermal springs to the salt lake brines of the Andean salars (Ericksen 1978, Shcherbakov & Dvorov 1970, Tan et al. 2012).

3.2.3   Ancient evaporites

The huge amounts of halite in evaporate basins as the Salar de Uyuni cannot only be the results of leaching processes in volcanic rocks and the evaporative concentration from inflowing streams and precipitation. A possible source of sodium chloride and sulphate could be the recycling of ancient, buried evaporites (Risacher 1991a, Risacher 1991b). Gypsum diapirs are known from several regions of the Altiplano, also in the catchments of the salars of Uyuni and Coipasa (Fig. 4). The re-solution of older paleolake sediments by groundwaters provides large masses of salt for the accumulation in recent salt pan environments. Also, quaternary salars and associated brines covered by lava deposits and ignimbrites could be a possible source of solutes (Risacher 1991a). The ratio of Na/Cl in streams and brines may act as an indicator for the sources of halite.

3.2.4   Atmospheric contribution

A minor portion of mineral input can be related to precipitation and windblown dust. The mineralization of rainfall waters is generally low, but precipitation rates during the austral summer can be comprehensive. A significant higher grade of mineralization has snow, but due to the sparsity of snowfall events in the Bolivian Altiplano this aspect is probably negligible. The atmospheric input of dust particles is considerably higher. Especially during the dry season, wind speed can reach high values, and storm events are often. Due to the sparse vegetation cover and the flat morphology, salt and fine-grained sediment particles deposited at the end of the rainy season in the large flooding plains around the salar, are easily lifted and transported by wind. A significant part accumulates on the salar, leading to the coverage of the bright salt crust with a fine dust layer. Salt efflourescents at polygon borders then retain the particles blown along the salt surface and support the enrichment of fine-grained material. Due to the complete drying-up of the waters covering the flooding plains at the end of the austral summer, it should be assumed that lithium containing salts precipitate, leading to elevated concentrations in superficial salts and adhered to sediment particles.

3.3   Processes of enrichment

Considering the amounts of lithium added by each of the previously introduced possible sources, magnitudes are too low in order to produce brines with several grams of lithium per litre. Hence, enrichment mechanisms must be present for the concentration of the element over geological time spans. Further, the inhomogeneous distribution of lithium along the salt lake shows, that selected enrichment mechanisms are limited to certain regions and do not take place ubiquitously. Following, the most important processes of brine and solute, especially lithium, concentration are presented.

3.3.1   Evaporative concentration

An important component of the hydrological cycle is the loss of water from sediments, soils and water surfaces. Studies on evaporation from different types of halite crust at the Salar de Atacama showed very low evaporation rates of about 2 mm per year (Kampf et al. 2005, Mardones 1998). However, the Salar de Atacama crust is characterized by a densely cemented crust without visible openings in the surface structure. Thorburn et al. (1992) report evaporation rates in the range of 230 mm/year for salt crusts and found a logarithmic trend of increasing evaporation rate with decreasing depth of the brine table. Beside that, evaporation on a salt crust is controlled by a variety of factors as air humidity and temperature, morphology of the crust, and intensity of solar radiation. At the Salar de Uyuni, the evaporation of water from the brine table during the dry season is impeded by the formation of a densely cemented salt crust. At that time, evaporation is limited to superficial openings as shrinkage cracks and holes in the crust. Large parts of the Salar de Uyuni are covered by polygonal structures, whereby the margins of the polygons are characterized by the formation of efflorescences resulting from evaporation along those structures.

Due to its high solubility, lithium concentrates in the residual fraction during evaporation, whereas other alkalis as sodium, potassium or calcium as earth alkali element are removed from solution to a large extent by forming evaporate minerals.

3.3.2   Sorption on clay minerals

Sorption of lithium to clay minerals and ion exchange reactions have been investigated for long. Extensive studies in the field of lithium sorption have been done with tuff from the Yucca Mountain in Nevada (Anghel et al. 2002, Newman et al. 1991). Research was done in the background of a possible utilization of the mountain complex as a nuclear waste repository, and lithium served as a reactive tracer. Anghel et al. (2002) showed correlation between lithium

sorption and Li-specific ion exchange on smectite in the tuff rock, and Newman et al. (1991) verified the reversibility of lithium sorption up to solution concentrations of 150 mg/L Li^+. The cation selectivity in ion exchange reactions depends on the valence, hydration energies, hydration radii and polarizability of the exchanged cation (Anderson et al. 1989). The order of replaceability is reflected by the Hofmeister or lyotropic series (Carroll 1959):

$$Li^+ < Na^+ < K^+ < Rb^+ < Cs^+ \quad \text{and} \quad Mg^{2+} < Ca^{2+} < Sr^{2+} < Ba^{2+}$$
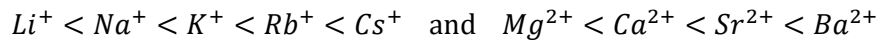
Lithium, with a valence of 1, a high hydration energy, very low polarizability and a large hydrated radius should be the least preferred cation for exchange. On the other side, it should be the ion being most easily replaced to other ions in clay minerals. Lithium shows the tendency to become dispersed in the clay-mineral fraction of rocks during weathering processes and the deposition of fresh- and brackish-water river and stream sediments (Horstman 1957, Tardy et al. 1972). Glanzman et al. (1978) found high concentrations of lithium in fluviatile lacustrine sediments of the McDermitt caldera, USA. He suggested that the element origins from volcanic material and was incorporated into the clay layers during alteration processes. Indeed, Starkey (1982) proposed that the occurrence of lithium in clay minerals results from the inclusion of the element along with Mg^{2+} during clay formation by precipitation due to weathering, or its addition to the clay mineral structure during hydrothermal alteration. Vine (1980) states, that hydrothermal lithium-clays such as hectorite are often located in basins that are coevally containing lithium brines, suggesting a strong connection. The amount of lithium incorporated in clay minerals depends on several conditions, as the concentration of lithium in solution, the content of other ions, pH, temperature, and crystal structure of the involved clay minerals.

4 Methods

The intensive study of the geochemical characteristics of the Salar de Uyuni required the sampling of large amounts of fluid and solid material, a broad range of analytical approaches and the support of field and laboratory methods by the use of modeling software and remote sensing techniques. Between 2009 and 2014, altogether six drilling and sampling campaigns took place on and in the vicinity of the Uyuni and Coipasa salt lakes (Fig. 12).
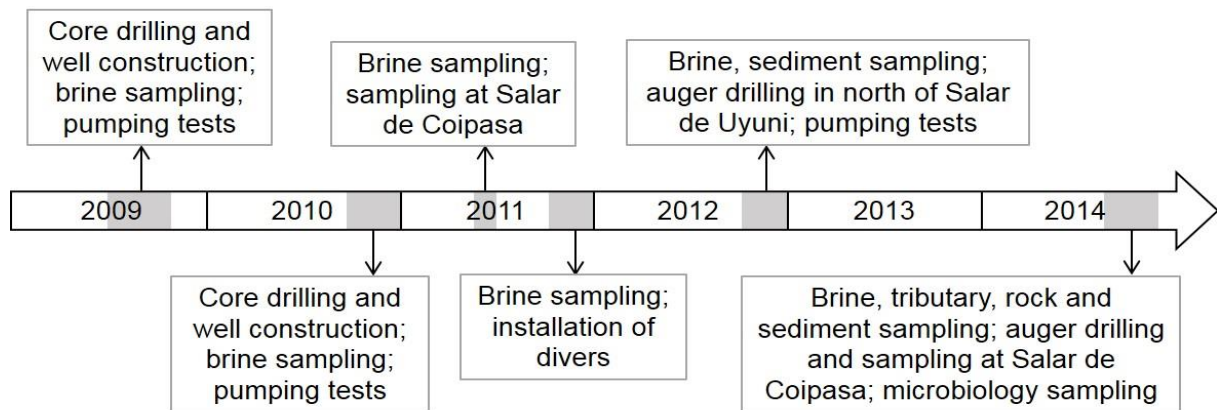
Fig. 12:   Time line of field campaigns at the Salar de Uyuni organized by TUBAF and UATF

Drillings in 2009 and 2010 served for the installation of wells on the Salar de Uyuni, which were used for the sampling campaigns in the following years. Hundreds of brine, sediment and rock samples could be gained throughout the fieldwork in cooperation between the TUBAF and the UATF.

4.1   Field works / methods

On-site activities comprised preparative works as the realization of drillings with different drilling machines, well completion, measurement of on-site parameters, and finally sampling of brines, streams, rocks and sediments. Below, these steps are described in detail.

4.1.1   Drilling procedure and well installation

Core drillings at 11 locations on the Salar de Uyuni were performed using a rotary hand drill DK32S from DIAMASA (Handbohrtechnik GmbH & Co. KG., Grimma, Germany) customized for the local operating conditions (Fig. 13). Using a 64 mm plate drill bit with core retainer salt cores of 62 mm diameter could be gained. The electricity for the drilling machine was

produced by a 5.5 kW gasoline driven generator (HONDA). An elaborate description of the drilling machines' technical characteristics can be found in Sieland (2014). The interstitial brine served as drilling fluid and was pumped from a nearby shallow basin which was excavated for that purpose. The maximum drilling depth was limited to 12-13 m, caused by the difficulties arising from the increasing weight of the bore rods with depth together with the challenge of drilling in muddy sediments. Drilled core pieces were spread on plastic tarps, measured and documented and dried several days in the sun, before they were packed in plastic sheets and PVC tubes for the transport to Germany. For the stabilization of the borehole and depth dependent brine sampling boreholes were completed to wells. Due to time and money restrictions this was performed by inserting PVC casings (waste-water tubes) and self-made screens (by slotting tubes with a disk grinder) at the lowermost meter. When the drilling ended in a mud layer, the screen was arranged for 1 m in the salt crust above the mud

Fig. 13: Core drilling with a hand drill using the pore brine as drilling fluid

zone. The slots had a width of 1 mm. The annulus between the screens and casings and the borehole wall was filled up with filter gravel and salt grit, respectively. For that purpose, gravel from a nearby desiccated stream bed was sieved to a size of 2-4 mm. The zones of clayey lacustrine deposits were filled up with clay provided from a nearby clay pit. The original chunks of clay were crushed, sieved and mixed with fresh water to prepare a clay mud. An exact description of the well casing can be looked up in Schmidt (2010), an illustration is found in the appendix (Fig. B - 2).

Altogether 11 drilling locations are scattered over the Salar de Uyuni in order to gain information from the whole salt lake (Fig. 15). At each location, either one (single well) or 4 - 5 boreholes (multiple wells, denoted as A...E) were drilled and completed to wells as described above. The distance between the wells at a multiple wells field was between 2 and 5 m, depending on the need for the likewise performed pumping tests. The distribution of wells for brine sampling at SLT-10-PES is shown in Fig. 14.

Fig. 14: Drilling site SLT-10-PES with wells
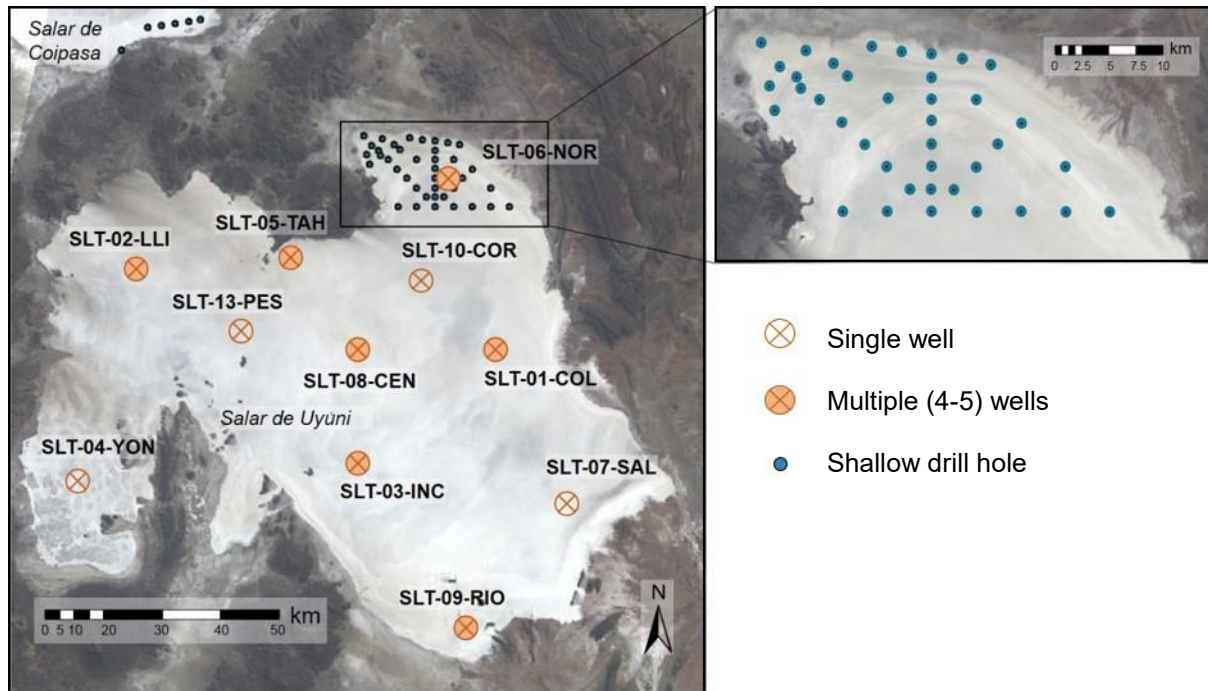
Fig. 15:   Distribution of drilling locations in the investigation area with single and multiple sampling wells, and shallow drillings along transects

The filter depth of wells in multiple well fields varied in order to enable a depth dependent brine sampling, however, screens were always arranged in a salt layer. Table 2 shows the geographic coordinates of drilling locations, together with the salt aquifer zone and screening (=sampling) depth of each well. The arrangement and specifications of drill holes at all drilling sites and the exact characteristics of the wells can be found in Sieland (2014).

Table 2:   Overview of drilling locations on the Salar de Uyuni with geographic position and screened depth of the wells

Name	Coordinates (UTM, WGS 84)		Brine sampling depth [m]				
	longitude	latitude	A	B	C	D	E
SLT-01-COL	679816	7774574		4.5 – 5.5	7.0 – 8.0	6.4 – 7.4	2.0 – 3.0
SLT-02-LLI	601596	7791495	0.3 – 1.1	8.0 – 9.0	2.8 – 3.8	0.8 – 1.8	
SLT-03-INC	649792	7749641	2.5 – 3.5	3.5 - 4.5	4.3 - 5.3		1.5 - 2.5
SLT-04-YON	590267	7745962	6.9 - 7.9				
SLT-05-TAH	635275	7797122	0.0 - 0.7	0.0 – 0.7	0.0 - 0.6	2.8 - 3.6	
SLT-06-NOR	669422	7811071	0.2 - 0.9	2.8 - 3.8	1.8 - 2.8	0.8 - 1.8	
SLT-07-SAL	694556	7742079	7.1 - 8.1				
SLT-08-CEN	649590	7774480	7.5 - 9.5	3.8 – 4.8	1.8 - 2.8	4.5 – 5.5	
SLT-09-RÍO	666568	7720469	2.0 - 3.0	1.5 - 2.5	2.8 - 3.8	0.7 - 1.7	
SLT-10-PES	625383	7777770	5.0 - 6.0				
SLT-13-COR	663551	7788958	5.1 - 6.1				

27

Auger drillings to depths of 0.5 m were performed with a Bosch drill hammer (GBH 2-26 DRE) using a 45 cm long drill bit with a diameter of 25 mm (Fig. 16, left) to tap brine samples from the uppermost brine level. No flushing with a drilling fluid was needed. In cases of a densely cemented salt surface or where the brine table was more than 0.5 m below the surface, a small hole was dug with a pickaxe in order to continue the auger drilling in the hole. In preparation of brine sampling procedure, drill holes were cleaned from drill sludge by air lift with the help of a bellows foot pump. For that purpose, a short hose was connected to the pump and inserted into the bore hole (Fig. 16, right). Applying this procedure, the largest part of mud and salt detritus could be removed. The sampling pattern of auger drills is shown in Fig. 15. Points were arranged along transects and complemented by points close to the shore. The distance between points ranged from 1 to 2.5 km. Several planned spots could not be sampled due to a thin upper salt crust, underlying soft mud and year-round moisture, which impeded the access by car. The same applied for the Salar de Coipasa, which was only partly traversable because of the decreasing thickness of salt cover. That's why, sampling was limited to 5 points along a transect, with a distance of 2 km between the single points.

Fig. 16:   Auger drillings with a Bosch drill hammer (left) and using air lift for cleaning the bore hole from drill sludge

4.1.2 Sampling and field measurements

Sampling took place at various locations on the Salar de Uyuni and its surrounding, and comprises brines, water from tributaries, springs and wells, inner lake salt crusts and lacustrine sediments, as well as rocks and sediments from the salt lakes' catchment. An overview of sampling sites including coordinates is found in Table A - 3.

Brines

Brine from the installed wells was sampled by means of a submersible pump (*Comet Geo-Duplo Plus*) run by means of a commercial car battery. For ensuring representative samples, the pumped brine was discarded until the fluid was clear. Additionally, the volume of the screen was pumped off several times and until a constant flow was maintained. Hydraulic short-circuit was avoided by heading the extracted brine with a hose to a distance of a least 5 m from the sampling well. Brines from the auger drills were taken by means of a 100 mL PP-syringe (*Omnifix*) connected to a thin hose. The parameters pH, electric conductivity (EC), redox potential, oxygen content and water temperature were determined after obtaining stability of these values. For these measurements, the brine was pumped directly into a small plastic vessel; the continuous overflow guaranteed flow-through conditions and prevented contamination with ambient air. The parameters pH, EC and oxygen content were obtained with the portable multimeter device *HQ40d* from *HACH*. For dissolved oxygen, the luminescent probe *IntelliCAL LDO101* was used, where a calibration is not necessary. The optional salinity correction was set off, due to the exceedance of the salinity range. Thus, obtained values were corrected manually afterwards, using TDS and temperature specific correction factors (see chapter 5.4.3). An *IntelliCAL PHC301* glass electrode served for pH measurement, whereby a daily calibration was done with buffer solutions of pH 4 and pH 7. Electric conductivity was obtained by an *IntelliCAL CDC401* standard conductivity probe, using 3 molar KCl for calibration. Temperature correction was done internally by the *HACH* device. The electromotive force (EMF) was measured with the device *WinLab Data Line pH-Meter* (*Windaus Labortechnik*) connected to an Ag/AgCl electrode containing 3 molar KCl. A daily calibration with a redox buffer was performed. The EMF value was converted to the redox potential E_H by the following steps:

1. Calculation of EMF_{corr} by correction according to the value of the reference standard solution

2. Calculation of $E_{0(25°C)}$ by referring the EMF_{corr} to standard temperature of 25°C

3. Calculation of E_H by referring to the standard hydrogen electrode

Temperature was measured from each of the probes, except redox. Brine temperature was then calculated as the mean from these values.

Samples were taken directly from the flow-through container after flushing the vessels with sampling fluid. Samples for IC and TIC were stored untreated, whereas samples for ICP-MS (a few mL were sufficient) were filtrated with syringe filter holders (cellulose-acetate, pore size 0.2 µm) and acidified to a pH < 2 with 65% HNO_3 suprapur. All brine samples were kept in PE bottles at ambient temperature, due to lacking cooling capabilities and the unlikelihood of microbial influence on the chemical composition of the highly saline brines.

Streams and thermal springs

Several streams and small inlets to the Salar de Uyuni were sampled during the 2014 field campaign. Further, the main tributaries Río Grande de Lipez and Río Colorado were sampled in different years to gain knowledge about the seasonal change in chemical composition. In addition, different thermal springs were sampled. Waters were measured for field parameters and samples were treated as described for the brines.

Rocks

Rock sampling took place in the catchment of the Salar de Uyuni in order to investigate host rocks as sources for the leaching of lithium. The volcanoes Irruputuncu, Olca and Uturuncu in the vicinity of the Salar de Uyuni were subject to sampling procedure (Fig. 17). Rock samples were stored and transported in plastic zipper bags. Coordinates of sampling sites are given in Table A - 15.

Uturuncu (6,008 m a.s.l.)

The dormant stratovolcano Uturuncu (22°15'S; 67°11'W) is located in the Cordillera de Lipez, about 150 km south of the Salar de Uyuni. It is composed of porphyritic dacite lava flows and domes and was active during Pleistocene times. Today, fumarolic activity occurs. Dacite lavas and andesite inclusions show a high content of incompatible trace elements, which could be a hint for a potential lithium source. Large-scale magma intrusions into the Altiplano-Puna crustal magma body lead to a huge deformation field underneath the volcanic complex with a central uplift rate of 1-2 cm/a at recent times (Sparks et al. 2006). The Río Grande de Lipez flows along the western side of Uturuncu and receives inflows from smaller streams at the western flank of the volcano.

Irruputuncu (5,165 m a.s.l.)

The stratovolcano Irruputuncu (20°45'S; 68°34'W) at the Bolivian-Chilean border is part of the Andean Central Volcanic Zone. It is a composite type and the volcanic complex is located on

top of ignimbrite layers of the Ujina and Pastillos formations (Rodríguez et al. 2015). Volcanic activity producing andesitic to trachy-andesitic magmas dates back to Pleistocene and Holocene times and active fumaroles exist until today, leaving sulphur deposits in the crater. Geothermal activities with temperatures up to 220°C in deep reservoirs at the base of the volcano were detected during geothermal prospections (Aravena et al. 2016).

Fig. 17: Locations of rock sampling: north-western side of volcano Uturuncu, crater of volcano Irruputuncu, and south-eastern side of Irruputuncu (from left to right; photographer: Wolfram Canzler)

Olca (5,407 m a.s.l.)

The stratovolcano Olca (20°56'S; 68°29'W) is as well located at the Bolivian-Chilean border, in the western part of a 15 km long E-W lineament of stratovolcanoes. It is mainly composed of andesitic to dacitic lava flows with volcanic debris and shows fumarolic activity at the crater. Drillings at the base of the volcano revealed a zone of smectite and illite clays and the existence of hot water aquifers up to 70°C (Reyes et al. 2011). A hydrothermal spring exists at the base of the volcano, which was also sampled.

Sediments

Fluvial and lacustrine sediments play a significant role in the enrichment of lithium in pore brines, as they serve as carrier, repository and source of lithium during its way from the source bedrock over streams to the final place of deposition. Therefore, various sediment samples were gained at the main tributaries Río Grande and Río Colorado (Fig. 18). Lacustrine mud layers were sampled from different depths at various spots of the salt flats of Uyuni and Coipasa. Further, sediment from the gas emanation spot "Ojos del Salar" (Eyes of the Salar) was taken. In addition to rock sampling, sediment samples were taken from the catchment, at the base and the flanks of the described volcanoes.
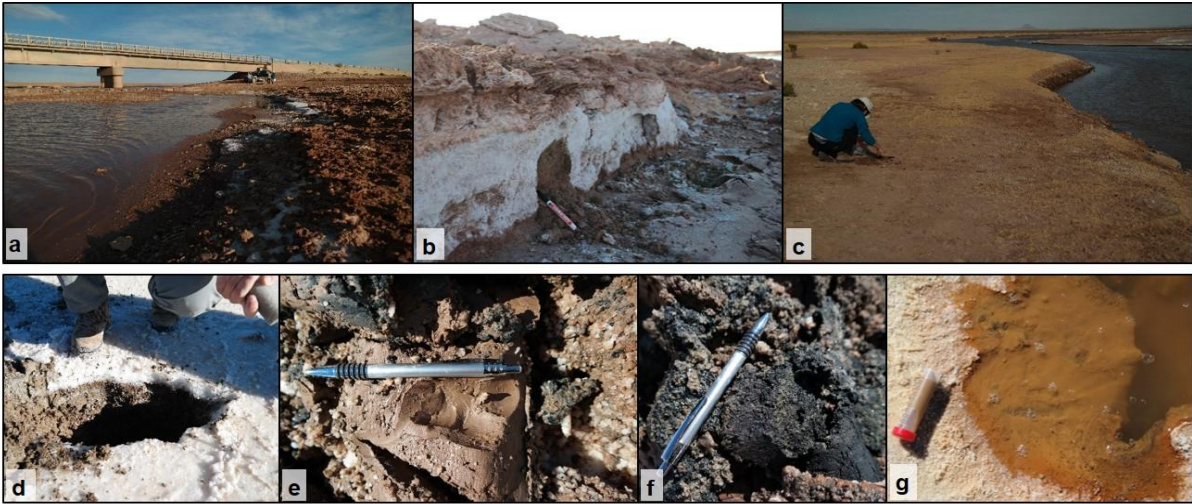
Fig. 18: *Sediment sampling sites: (a) Río Colorado, (b) sampling of shore sediment at Río Colorado, (c) Río Grande, (d) sampling from auger drill hole at SLT-NOR-T3, (e) lacustrine brownish layer at SLT-RIO-01, (f) lacustrine black coloured layer at SLT-RIO-01, (g) sampling of reddish sediment at the "Ojos del Salar"*

Salt crust

During the field campaign in 2014 two types of samples were taken from the Salar's upper salt crust: the uppermost 1 – 5 mm salt precipitate within the salt polygons, and the salt efflorescences at the polygon border (Fig. 19). Samples were taken at 23 spots of the Salar de Uyuni and Coipasa, whereby the locations coincided with drilling and auger drill sites (see Fig. 15). At most locations, the salt surface was covered with a fine layer of dust, which was especially distinct in the dry season of 2014, compared to the years before. Salt efflorescences further indicated the main wind direction, as they accumulate the windblown dust on the windward site.
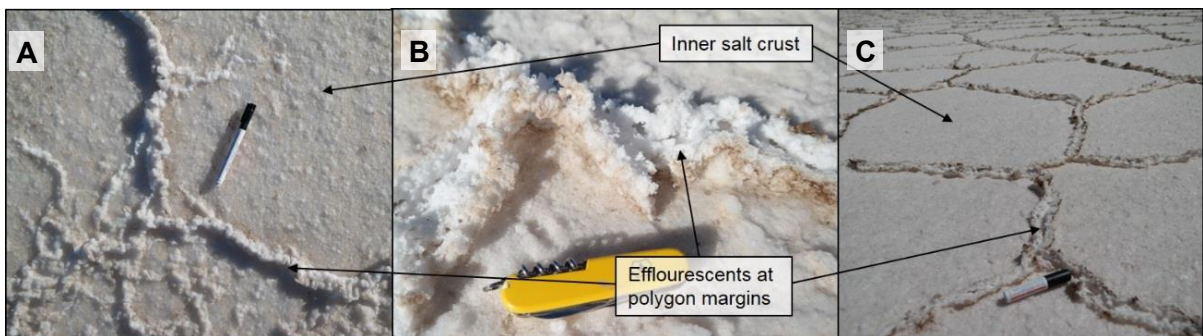
Fig. 19: *Sampling of the uppermost salt crust at the Salar de Uyuni; A: at a transect point in the north (STL-NOR-T3); B and C: at SLT-01-COL*

4.2 Laboratory methods

The processes of lithium enrichment in the salt lake brine were investigated using different analytical methods. Laboratory methods included the preparation of solid samples by means of various types of chemical digestion, the analysis of isotopes and finally the element analysis by ion chromatography and ICP-MS.

4.2.1 Chemical digestion

In order to determine the chemical composition of lacustrine and fluvial sediments, the salt crust and rocks, a chemical digestion was indispensable. In dependence of the specific characteristics, for each sample type an adjusted procedure routine was developed. An overview of applied methods is given in Fig. 20.

Sediments and rocks

First, sediment samples were homogenized. In order to minimize the influence of secondary salts that precipitated from the interstitial brine after sampling, an equivalent of the sample was washed several times with DI (deionized water) and filtrated. Afterwards, washed and unwashed sediments were dried overnight in a drying oven at 40°C. Rock samples were prepared by coarse grinding with rock splitter and hammer. Then, both rocks and sediments were grinded with a planetary ball mill using agate vessels and balls (*Pulverisette 5, Fritsch GmbH*) down to a size of < 63 µm. The samples were milled 60 min at a rotational speed of 280 rpm. Lithium is bound in soil components and minerals in different ways, leading to a difference in leaching effectivity by weathering in different rock types and sediments. In dependency of the integration of lithium in the crystal lattice of silicates two types of digestions were performed. For the quantitative investigation of the easily available lithium fraction (bound for example in clay minerals), a modified aqua regia digestion was performed: in the environment of a closed microwave, concentrated HNO_3 reacted with the 3-fold amount of HCl (Zeien 1995):

$$HNO_3 + 3\ HCl \rightarrow NOCl + 2\ Cl + 2H_2O \tag{1}$$
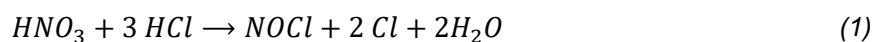
The microwave *ETHOS.lab* from *MLS GmbH* was used. The procedure was following a certain temperature time schedule consisting of:

10. Constant heating of 8 min until a temperature of 190°C,

11. Maintaining temperature for 6 minutes,

12. Cooling down for 20 minutes.

The hermetically closed system ensures leakage prevention of lithium or other volatile elements. The Teflon sample containers were filled with 100 µg grounded sample, then 200 µL DI, 900 µL 65% HNO_3 and 300 µL 37% HCl were added. A blank for every series was used for correction of background values. After digestion, samples were filled up with DI to a dilution factor of 10, and centrifuged prior to ICP-MS measurement.
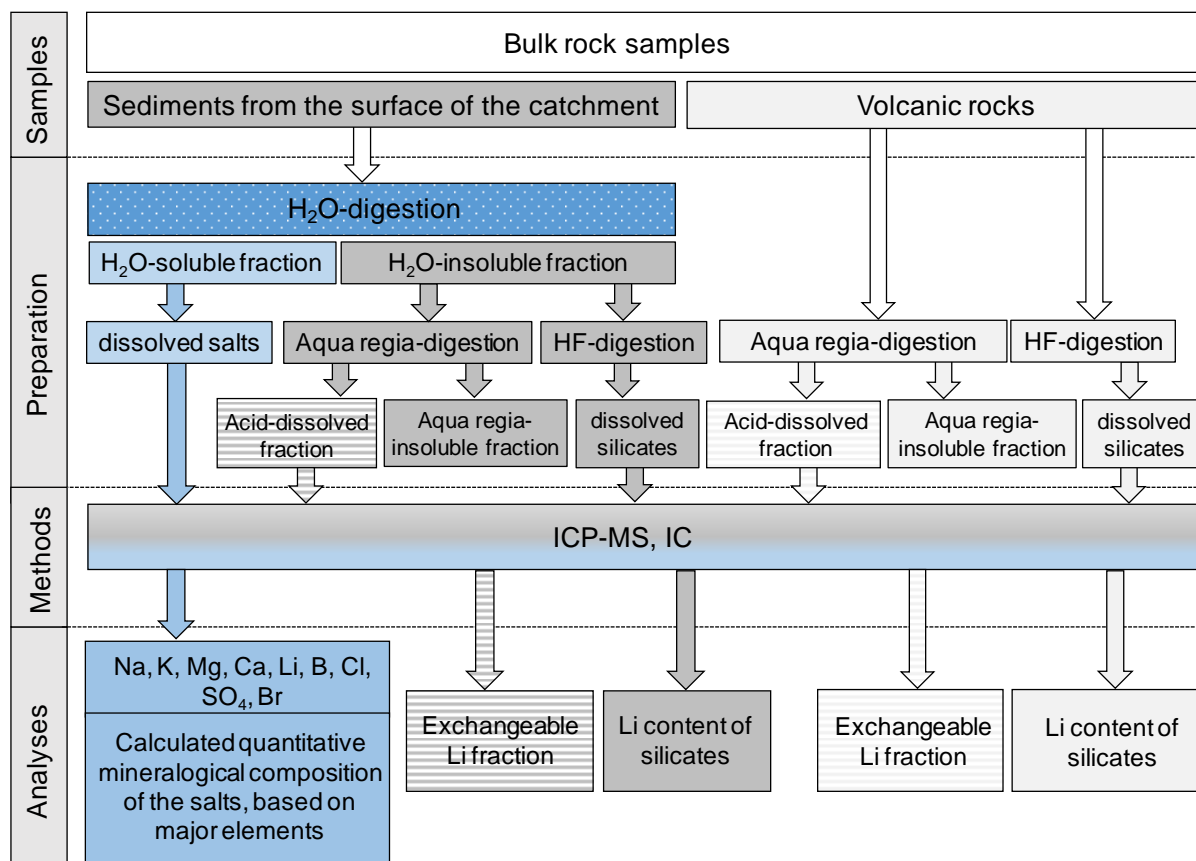
Fig. 20: Flow chart of preparation and analysis of rock and sediment samples for the determination of different lithium fractions

The lithium fraction bound in a siliceous matrix was determined by a total digestion with hydrofluoric acid. Therefore, 100 µg grounded sample was mixed with 3 mL of 48% HF, 2.5 mL of HNO_3 and 0.5 mL DI in a capped Teflon container. Equipped with an agitator, the reaction fluid was stirred and heated up to 60°C in a water bath when needed. In case that the sample was not decomposed completely, more HF was added and reaction time was increased. For every series, a blank was measured concurrently. After digestion 5 mL reaction fluid was mixed with 40 mL DI to prevent reaction with the material of the centrifuge tubes, which were used for storage. For ICP-MS measurements, samples were further diluted to final dilution factors of 350-500, in order to prevent the ICP-MS from damage by high HF concentrations.

Salt crust

Samples were homogenized and pulverized in a mortar, dried for 24 h at 80°C in a drying oven and weighed to portions of 3 g into 50 mL centrifuge tubes. Immediately after weighing, 30 mL DI was added and the complete salt dissolution was awaited. After centrifugation and determination of pH a small part was put aside for ion chromatographic determination. The rest was subject of vacuum filtration and the weight of the residue was determined after drying of the filter. Filtrates were analyzed by IC and ICP-MS with dilution factors of 100 and 1000, respectively.

4.2.2 Element analysis

IC

Ion chromatography (IC) enables the determination of the main cations Li^+, Na^+, K^+ and Mg^{2+} and the anions Cl^- and SO_4^{2-}. The detection of Ca^{2+}, NO_3^-, F^- and Br^- in the brines was not possible by this method due to their low concentrations in the diluted samples. Values were below detection limit or peak overlap occurred. Ca and Br concentrations were thus taken from ICP-MS results. Cation detection was performed with the device *850 Professional IC Cation* (*Metrohm*) using a *Metrosep C4* (150x4mm) separation column. The eluent was composed of 2 mM HNO_3 and 0.7 mM Dipicolinic acid, the flow rate amounted to 0.9 mL/min. Anions were detected using a *881 Compact IC Pro* (*Metrohm*). Here, a mixture of 3.0 mM $NaHCO_3$ and 3.5 mM Na_2CO_3 served as eluent with a flow rate of 1.0 mL/min. Eluents of both cation and anion chromatography were aerated with nitrogen prior to usage to remove dissolved gases and other disturbing substances. For the evaluation of peaks, the software MagIC Net *2.2* by *Metrohm* was used. In dependence of the ion to be measured, brines were diluted with factors of 500 to 2000, because the maximum electrical conductivity of the device is 900 µS/cm. For anion analysis, deionized water (DI) was used for dilution; for the measurement of cations 2 mmolar HNO_3 served as dilution fluid. Due to the high dilution brines were not filtrated before analysis. Stream waters were measured with dilution factors up to 10, and were filtrated with 0.2 µm cellulose-acetate filters.

ICP-MS

ICP-MS (inductively coupled plasma mass spectrometry) measurements were performed for the determination of a broad range of elements, whereat low concentrated components in the samples are typically analyzed best with this method. An *X Series 2* (*Thermo Scientific*) was used for this purpose. Elements were measured either in standard or KED mode (kinetic energy discrimination), whereby latter uses a different carrier gas mixture of 93% He and 7% H_2 instead of Ar. An overview of the 65 obtained elements and detection limits is summarized

in Table A - 9. A standard calibration was performed for quantification using a multi element standard in different dilutions. The recovery rate was determined by the 1:100 addition of an internal standard composed of 50 ppb Ge, 10 ppb Re and 10 ppb Rh. Brine samples (filtrated and acidified in the field) and the dissolved salt crust samples were diluted with factors of 100 to 1000, in order to cover the broad concentration range of elements, and to prevent an instruments' damage by electrical conductivities exceeding 2 mS/cm. Streams were measured undiluted to 1:10, depending on the expected concentrations. Digested rock samples were diluted with dilution factors of 300 to 400 in order to reduce the HF concentration to < 0.01%, as required for the ICP-MS procedure.

Total inorganic content

For the analysis of total inorganic content the elemental analyzer *LiquiTOC* (*Elementaranalysen Systeme GmbH*) was utilized. A dilution factor of 10 was used. The infrared channel 1 (IR-1) and an injection volume of 10 mL was applied. Prior to analysis, samples were acidified with H_3PO_4 in order to transform all carbonate species into CO_2. The resulting TIC values were converted into HCO_3^- by using PhreeqC (Parkhurst and Appelo 1999). Due to high concentrations (up to 92 mmol/L) of boric acid (H_3BO_3) the classical determination of alkalinity by titration with an acid results in a massive overestimation of alkalinity.

4.2.3 Mineralogic composition

Rocks, sediments and salts were analyzed by digestion and determination of the elemental composition by ICS-MS. The mineralogical composition was calculated by means of geochemical calculation rules. For rocks and sediments, results from ICP-MS were transformed to weight proportions c_{sed} [mg/kg] by the following formula:

$$c_{sed} = \frac{c * V}{m}$$

(2)

where *c* [ppm] is the element concentration in the sample, and *V* [mL] and *m* [g] are the initial volume and sample weight. For rocks, element concentrations were converted to corresponding oxides (e.g. Si → SiO₂, Al → Al₂O₃) by multiplying with a factor *f*, which is calculated for different oxides according to the following relation:

$$f = \frac{M_{oxide}}{M_{element}}$$

(3)

where M_{oxide} [g/mol] defines the molar mass of the oxide and $M_{element}$ [g/mol] the molar mass of the contained element. For calculation the results of HF digestion were used, as the extraction includes the siliceous species. Then, the normative mineralogical composition was calculated from the chemical rock analysis using the CIPW norm. This norm uses the bulk composition of a rock for the calculation of typically occurring mineral phases that could theoretically have formed during the complete crystallization of a magma at low temperature. It is therefore especially suitable for the differentiation of volcanic rocks. The calculation was done in an excel spreadsheet[6]. The results were then used for the classification of sampled rocks in a Streckeisen diagram. This double ternary diagram is used for the differentiation of igneous rocks, in this case volcanic rocks, according to their modal mineralogical composition. Thereby, only the four mineral groups quartz, alkali feldspars, plagioclase and feldspathoid (Foid) are included in the calculation.

4.2.4 Isotope analysis

The use of environmental isotopes helps to find answers for numerous questions regarding catchment hydrogeology. This includes the analysis of weathering processes mobilizing solutes along the flow path, the identification of sources of solutes, the characterization of water flow paths from the time of precipitation until discharge at streams, and the analysis of the role

---

[6] The excel file was downloaded from *https://www.geologynet.com/programs/cipwnormexcel.xls* (22.05.2017)

of atmospheric deposition in final water chemistry (Kendall & Caldwell 1998). Stable isotopes of water and dissolved sulphate as well as instable isotopes of carbon were investigated during the work.

Stable isotopes

δ^2H and $\delta^{18}O$ in water, and $\delta^{34}S$ and $\delta^{18}O$ in dissolved sulphate were determined for brine and river water samples from the 2009 and 2010 field campaigns. Water isotopes were analyzed by cavity ring-down spectroscopy (CRDS) at the UFZ in Halle. As the instrument requires EC values of less than 4 mS/cm in the analyte, samples had to be preprocessed with vacuum distillation. The measurement itself was done with a Picarro *L1102-I Isotopic Liquid Water Analyser*. Two reference standards, PES (polar ice shavings) and MAST (mid-atlantic ocean water), were used for calibration. The procedure of sample preparation, distillation and final analysis is described in detail in Heinrich (2012). For the determination of $\delta^{34}S$ and $\delta^{18}O$ in dissolved sulphate $BaSO_4$ was precipitated from the water sample after acidification and addition of $BaCl_2$. The analysis was done with an isotope ratio mass spectrometer (IRMS) *DeltaS* from *Thermo Finnigan*, which is based on the continuous-flow technique. Results of $\delta^{34}S$ were reported in relation to the reference standard VCDT. For $\delta^{18}O$ measurements, values were calculated according to the standard VSMOW (Vienna Standard Mean Ocean Water). Standard deviations were ± 0.3% for $\delta^{34}S$ and ± 0.5% for $\delta^{18}O$, respectively. A detailed description of analytical procedure is found in Heinrich (2012).

Radiocarbon dating

Brine samples from wells representing different depths and locations on the Salar de Uyuni were prepared for radiocarbon dating by means of vacuum extraction. For that, 10-15 mL of 65% H_3PO_4 was added to about 1 L of sample, and dissolved carbon species were extracted and transferred into CO_2. The gas was trapped in special glass vials, which were previously flushed with ultra-pure N_2 and evacuated to -980 mbar with a vacuum pump. Ampules were closed by a valve when a final pressure of -250 mbar was reached, and sealed by a glassmelt within few hours after extraction. Prepared samples were analyzed for $^{14}C/^{12}C$ and $^{13}C/^{12}C$ at the Poznań Radiocarbon Laboratory in Poland. An accelerator mass spectrometer of type 1.5 SDH-Pelletron Model Compact Carbon AMS (*National Electrostatics Corporation*) was used for determination. For calibration, the international standard ^{14}C Oxalic Acid II was used. The ^{14}C activity is determined by the decay of radiocarbon over time. Besides that, it is also affected by natural isotopic fractionation, i.e. the preferential uptake of ^{12}C over ^{13}C and ^{13}C over ^{14}C in biological processes. This fractionation is accounted for by using the $\delta^{13}C$ results of AMS measurements. The correction is based on the following formula (Stuiver & Polach 1977):

$$a_{\delta^{13}C} = a \cdot \left[\frac{1 - 25/1000}{1 + \delta^{13}C/1000} \right]^2 \qquad (4)$$

Here, a defines the raw ^{14}C activity and $a_{\delta^{13}C}$ the fractionation-corrected activity. Corrected values were used for age determination of the brines in the upper meters of the salt crust according to the equation:

$$t = -8{,}267 \cdot ln\left(\frac{a_t{}^{14}C}{a_0{}^{14}C}\right) \qquad (5)$$

Here, $a_t{}^{14}C$ corresponds to the $a_{\delta^{13}C}$ and a_0 to the initial ^{14}C activity, which is generally assumed to be 100 pmC. However, the ^{14}C activity was not constant at 100 pmC during Pleistocene and Holocene, but steadily decreased with time, due to variations in solar output. Results were corrected using adapted values for the initial activity.

4.3   Application of GIS

Remote sensing data are a precious source of information, especially in extremely remote areas with limited possibilities for field observations. Elevation models and satellite data were used for watershed delineation and the spatial demarcation of solute contributions to the Salar de Uyuni. Further, a possible connection between the Salars of Uyuni and Coipasa was investigated by the identification of a former stream bed. Furthermore, the seasonal variability in water coverage was analyzed. For the evaluation of satellite data, the program ArcGIS (*ESRI*) was used. The program also provided the statistical tools for the interpolation of lithium concentrations in the brine.

4.3.1   Watershed delineation

Watershed delineation and terrain analysis were done using the *ArcGIS* extension tool *ArcHydro 9* as topic of a bachelor thesis (Jackisch 2014). The first step comprised the choice of an appropriate DEM (Digital Elevation Model) dataset. 12 tiles of an SRTM (Shuttle Radar Topography Mission) dataset covering the southern part of the Bolivian Altiplano were obtained from the USGS EarthExplorer database[7]. Characteristics of the dataset are comprised in Table 3. Tiles were connected to one file with the mosaic tool in ArcMap and re-projected to the coordinate system WGS 1984 world Mercator. A shapefile comprising streams and river networks of Bolivia and Chile was obtained from *DIVA-GIS*[8], an open-source GIS project providing as well free spatial data for the whole world. The shapefile was matched with Landsat

---

[7] Access online via https://earthexplorer.usgs.gov/

[8] Access online via http://www.diva-gis.org/Data

8 images with a resolution of 30 m, in order to verify the precision and completeness of stream lines in the vector shape.

Table 3: Characteristics of the applied DEM dataset

	SRTM dataset		**SRTM dataset**
Coordinate system	WGS 84	Pixel type and depth	Signed integer, 16 bit
Tile size	1 arc-second	Uncompressed size	593 MB
Cell resolution	28 m	Format	GeoTiff
Number of cells	$1.55*10^8$		

Proceeding of watershed delineation using ArcHydro is shown in Fig. B - 3. Prior to catchment delineation, several steps were necessary in order to enhance the quality of data. The first step, DEM reconditioning, is the process of forcing a linear drainage pattern vector to a DEM surface, creating an enhanced elevation model with a higher agreement of stream networks delineated from the DEM and the input stream vector (Dixon 2016). The next step is the fill sinks tool, which locates depressions and no-data cells in a raster. It fills local sinks in a grid by modifying the elevation value, eliminating the error of water being trapped in a cell and thus being hindered from flow.

For handling the partly extremely flat terrain on the particulary large area, two approaches were tested. The *fill sinks plus* tool, developed by the *Lago Consulting group*, promises to produce more realistic stream paths in flat terrain, but to keep the primary stream paths in steep terrain. Another approach is the *optimized pit removal* tool (Center for Research in Water Resources, University of Texas). By combining the methods of cut and fill, undesired pits are removed while the corresponding changes to the landscape are minimized. The next step builds up a flow direction dataset by calculating the direction to which water would flow out of a cell, based on the slope gradient in the cell (Jenson & Domingue 1988). Thereby, each cell is classified to a number, according to the direction of flow (Fig. 21). The simulation of flow direction from the 8 directly neighbouring pixels is referred to as the D8 algorithm.
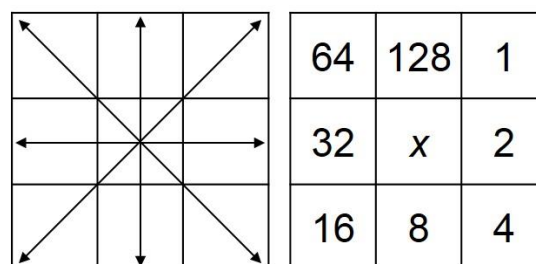
Fig. 21:   *D8 algorithm for the encoding of flow direction to numbers according to the orientation of cell x*

The following flow accumulation step calculates for each cell in the input grid the sum of surrounding cells that flow towards it. The resulting flow accumulation grid serves for the computation of a stream grid by stream definition. Thereby, each cell is compared to a threshold, and either assigned to 1, when having a value greater than the threshold, or to no data, when being below the threshold. Then, catchments are delineated by assigning a value to each cell indicating to which catchment it belongs. The resulting grid is then converted to a catchment polygon feature class. Further steps of terrain pre-processing contain the generation of aggregated upstream catchments out of the catchment feature class and the creation of drainage points (ESRI 2011). Pre-processed spatial data can then be used for watershed delineation.

4.3.2　Interpolation maps

The distribution of lithium and other elements along the salars was done with ArcMap using the method of ordinary kriging. As data source, 92 points with lithium concentrations distributed all over the salar were used. Own analytical results were supplemented by brine analyses of Risacher (1991b), in order to add data to regions with low sampling density and locations which could not be accessed during sampling. Certain preconditions should be fulfilled for the application of kriging, as the normal distribution of data, the existence of stationarity and the absence of trends (Schafmeister 1999). The histogram of Li concentration data shows an asymmetric left skewed distribution. The check for normal distribution was done by means of the Shapiro-Wilk-Test using *OriginPro*. At the significance level $\alpha = 0.5$, the null hypothesis of having normally distributed data was rejected. Hence, a logarithmic transformation was performed in order to reach normal distribution (p-value = 0.3 > α = 0.5, null hypothesis was not rejected). The analysis of the variogram showed, that a spherical semi-variogram best fitted the empirical variogram, and was therefore chosen for the kriging procedure.

4.3.3　Seasonal variability

The existence of an ephemeral or all-season superficial hydrological connection between the salars of Uyuni and Coipasa was investigated with the help of satellite and elevation data. First, meteorological data from the region were screened for years with precipitation-rich summers. Second, satellite data from the beforehand selected years were sighted for high-quality images without cloud coverage and errors. Band combinations were applied to the selected satellite images in ArcMap in order to improve the visibility of a superficial connection of the salt pans during the rainy season. The tool *band composite* in the data management tab served for that purpose.

The relation between the occurrence of all-season humid or water-covered areas of salt crust and the concentration of Li in brine was investigated by the evaluation of satellite images and interpolation maps. For that purpose, the Li distribution map as a result of kriging was used for drawing contour lines of Li concentration. This contour map was then plotted on a satellite image from the dry season in order to compare the overlay of humid areas and regions of high Li concentrations in brine.

Another approach of using GIS was the analysis of lake water coverage during the rainy season. Due to strong winds, water is rapidly transported along the surface of the salt pan. This effects the distribution of solutes from the river deltas to distant regions, as the surface waters are exposed to evaporation and associated precipitation of salts.

The growth or shrinkage of salt pan volume in recent times was analyzed by comparing the oldest available Landsat data from Jan. 1985 (Landsat 5) to new data from Jan. 2015 (Landsat 8). The outlines were drawn in ArcMap, added as layers and compared in size.

4.4 Quality control

The results of hydrochemical analyses were evaluated by means of common procedures. For the chemical analysis of waters and dissolved salt samples the analytical error (comparing sum of anions and sum of cations) was calculated by PhreeqC (Parkhurst & Appelo 1999). Detection limits for ICP-MS and IC were determined by the detection limit of the devices multiplied by the dilution factor. Negative values and values below the threshold were excluded from any further evaluation.

A number of elements (i.e. Li, K, Mg) were measured with IC as well as with ICP-MS. Results of both methods were compared regarding accuracy, detection limit and dilution factor, in order to select the most appropriate method for the analysis of these brines with a high excess of Na and Cl.

Special emphasis was put on the analytical challenges regarding the investigation of extreme brines and the associated adaption of sample preparation and analytical devices. The electrical conductivity of the salar brines usually exceeded 200 mS/cm, which is the upper limit of the used *Hach HQ40D* EC-meter. To check the reliability of values > 200 mS/cm displayed by the instrument, three brine samples from the Salar de Uyuni were diluted stepwise with distilled water. Results were compared with the dilution curve of a saturated NaCl solution provided by Lide (1994). With increasing salinity, the oxygen solubility decreases. For correction, salinity correction factors f_{corr} were obtained from the USGS salinity factor table (Rounds et al. 2013), which was extended to the point of salt saturation based on Nishri & Ben-Yaakov (1990). Measured O_2 concentrations were then transformed according to the following formula:

$$O_{2_{corrected}}[\frac{mg}{L}] = f_{corr} \cdot O_{2_{measured}}[\frac{mg}{L}] \qquad\qquad (6)$$

Piston-stroke pipettes, which were used for the dilution of brine samples, are adjusted to pipetting solutions with a density of 1 g/cm³. For the evaluation of pipette precision, a pipette test according to DIN EN ISO 8655-6 with the brine having a density of ~1.2 g/cm³ was performed.

The correctness of analytical data produced by IC and ICP-MS instruments was checked by the determination of precision and accuracy. Precision was calculated by the repetitive measurement of a single sample under the same analytical conditions; results are shown as standard deviation. Accuracy was tested by the measurement of a lithium standard in the concentration range, which was expected for the samples. The standard was repeatedly measured during the analytical series. Furthermore, samples from the 2010 field trip were determined as duplicates by the laboratory of the hydrogeology department at TU Bergakademie Freiberg and the analytical department of the BGR in order to prove the comparability of different analytical approaches.

The calculation of saturation conditions and the modelling of evaporation processes were performed using the program PhreeqC (Parkhurst & Appelo 1999) using the database PHRQPITZ, which includes PITZER parameters based on the ion-interaction theory and is suitable for ionic strengths from 1 to 6 mol/L (Plummer et al. 1988).

5 Results and interpretation

In order to obtain an extensive and widespread insight to the hydrochemical and hydrogeological conditions of the Salar de Uyuni and its vicinity, a broad range of methodical approaches and analytical techniques was applied. Brine, freshwater, rock, sediment and salt sampling and the chemical analysis of samples regarding element and isotopic composition was complemented by the evaluation of satellite and elevation data using GIS. Subsequently, results from all fields of investigation are presented and supplemented by literature data when needed.

5.1 Hydrochemical characterization

Altogether 112 brine samples from screened wells and 45 brine samples from the shallow drillings were taken during the field campaigns between 2009 and 2015 at the Salars of Uyuni and Coipasa. Further, 22 water samples from tributaries and springs in the catchment of the Salar de Uyuni complement the hydrogeological characterization of the region and the investigation of lithium entry paths. Results of chemical analyses are given in tabular form in Table A - 4 to Table A - 9. For evaluation, small streams were separated from the main inflowing rivers (Río Grande and Río Colorado), due to extensive hydrochemical differences. An overview of brine sampling sites is shown in Fig. 15, the locations of freshwater samples from the catchment are illustrated in Fig. 43.

According to the classification of Drever (1997), streams and rivers contributing to the Salar are fresh to brackish, showing TDS values between 60 ppm in small streams near the spring up to 5.000 ppm in the Río Grande and Río Colorado near their outlet to the Salar. Interstitial brines have dissolved loads between 260 and 360 g/L. Values in the brines taken from wells (well brines) are slightly higher than in the transect brines, which is probably caused by the dilution effect by surficial and subsurface inflow of lower mineralized waters due to the low distance to the shore. Brines are invariably NaCl types with the relative abundance in the quantity of constituents in the following order: $Na^+ \gg K^+ = Mg^{2+} > Li^+ > Ca^{2+}$ and $Cl^- \gg SO_4^{2-} > HCO_3^-$. Between 70 and 95% of dissolved solids is NaCl, so that the brines are in the range of saturation for halite (solubility of halite in demineralized water = 358 g/L at 20°C). No correlation exists between TDS and brine temperature, because the solubility of NaCl is not appreciably affected by a change in temperature.

5.1.1 Field parameters

Fluid temperature, electric conductivity, redox potential and dissolved oxygen content were obtained in the field during the sampling procedure. The TDS was calculated as the sum of all inorganic substances in solution, as determined by IC and ICP-MS. The values for the well and transect brines are comprised in Table A - 7, values for water samples from the catchment are comprised in Table A - 4. Statistics are shown in Table 4.

*Table 4: Number of observations (n), minimum, mean and maximum values of field parameters and TDS from the obtained pore brines of the Salar de Uyuni, and the water samples from the catchment (n may account for multiple sampling in different years; *salinity-adjusted values)*

	Temp.	pH	EC	Eh	O$_2$*	TDS
	°C		mS/cm	mV	mg/L	g/L
		(25°C)	(25°C)	(25°C)		
wells						
n	105	105	105	99	105	112
min	4.6	6.7	184	-171	0.028	289
max	20.7	7.8	245	160	1.68	362
mean	10.7	7.0	221	-49.2	0.28	328
transects						
n	44	44	43	44	20	45
min	5.5	6.4	176	-137	0.042	262
max	22.0	7.3	240	354	0.85	349
mean	14.9	6.9	222	15.6	0.35	318
rivers						
n	6	7	7	5	6	7
min	7.0	8.1	3.0	213	6.2	1.73
max	18.8	8.6	7.5	411	8.2	4.39
mean	12.6	8.4	4.3	293	7.2	2.65
streams						
n	6	10	10	6	6	11
min	0.6	7.4	0.09	177	6.09	0.06
max	23.9	8.98	2.9	374	8.82	1.73
mean	12.8	8.2	0.98	256	7.30	0.77
springs						
n	4	4	4	4	4	4
min	16.2	5.5	1.57	137	1.23	1.13
max	40.1	7.7	10.4	295	4.94	5.31
mean	23.0	6.2	6.18	194	3.31	3.39

Brine temperature generally shows a large range of about 16°C. During spring and summer months the brine temperature follows the trend of the mean air temperature (Fig. 22). However, at the beginning of the dry season and the austral autumn the brine temperature is significantly

higher than the temperature of the air. This can be explained by the heat absorbance capacity of the salt crust and the pore filling fluid storing the heat and cooling down during night. The brine temperature range in spring and summer months is much higher compared to winter, which is due to daily temperature fluctuations. In the dry season, the higher solar radiation with almost no cloud cover leads to an elevated heating of the salt crust during day time, resulting in increasing brine temperatures especially in the upper meters of the evaporates. A significant trend with depth could not be observed at different drillings within one location. However, Sieland (2014) measured brine temperature profiles in single wells during the spring season and found a decreasing trend with depth. Thereby, the temperature decreases down to a depth of about 4 m, and then either stagnates, or slightly increases again. The brines taken at transects from shallow depths (transect brines) generally show a high temperature range, although they all derive from a similar, very shallow depth between 0.1 and 0.5 m. Here, the time of day strongly influences the measured temperature, due to the strong heating of the uppermost salt crust in the course of the day. Therefore, temperatures of the transect brines are averaged 40% higher than of the deeper well brines, and rather in the range of mean maximum air temperature at the Salar de Uyuni (Fig. 22).
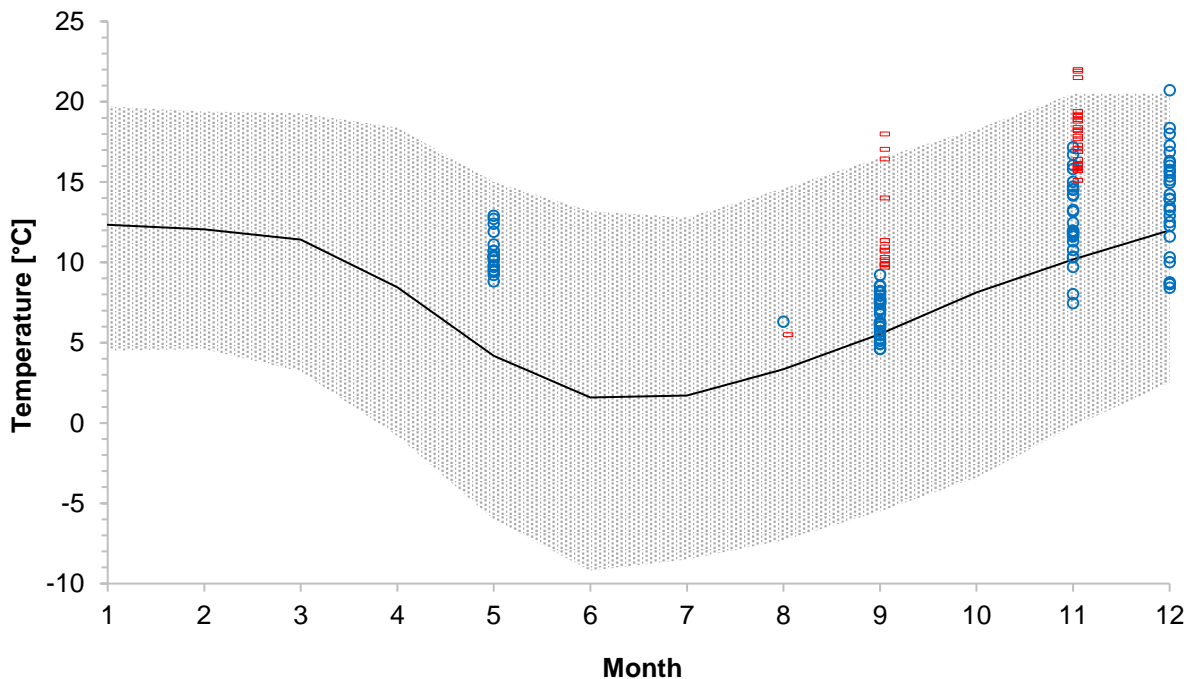
Fig. 22: Annual trend of brine temperature (blue circles: wells, red symbols: shallow transect boreholes) and air temperature (continuous line: mean, shaded area: range between max. and min. mean temperature) at the Salar de Uyuni; air temperatures show data from the Uyuni meteorological station provided by the Bolivian Meteorological Service SENAMHI

Water temperature in tributaries strongly depends on the daytime of sampling. The strong solar insolation leads to a high air temperature variation between day and night and a rapid heating of the surface water. Hence, the lowest temperature of 0.6°C at UTU-RIO-01, a tributary of Río

Quetena, was measured in the morning during the austral winter. Sampled spring waters show temperatures between 16 and 40°C. A spring is defined a thermal spring, when its temperature is 2 K above the yearly mean air temperature (Heath 1983). According to this definition, in the southern Altiplano a thermal spring has a temperature > 10°C. Thus, all sampled springs are thermal springs.

The oxygen content in the brines is low, due to the low solubility of oxygen in the highly saline waters. The solubility of oxygen decreases significantly with increasing salinity, from 9.1 mg/L (0 ppt salinity) to 2.58 mg/L (200 ppt salinity) at 20°C. As the instrument for oxygen analysis did not provide an adjustion for such high salt concentrations, the measured values were corrected manually (see chapter 5.4.3). At some samples, high O_2 values in the range of saturation were measured in deep wells, which may be the result of air drawing by the pump. Hence, the oxygen content strongly depended on the correct functioning of the suction pump, and must be regarded with caution. Especially in the deep well brines, high O_2 saturations of 40% in a depth of 4.50 – 5.50 m (SLT-08-CEN-D-1212) are rather unlikely. In contrast, rivers and streams are generally saturated with respect to oxygen (Table 4), due to the contact with atmosphere and the turbulent flow induced mixing of the water. Springs show a larger variation in oxygen content. The high value of 126% O_2 in the thermal spring OLC-CAL-01 is probably attributed to a high photosynthetic activity by algae, which could be identified as orange and green coatings on the rocks forming at the basement of the spring pools.

pH values in the brines are in the neutral range, showing little variation between deep and shallow brines. The effect of basification due to evaporation applies for the fluid samples from the Uyuni catchment. pH increases steadily from groundwater along springs, streams and finally larger tributaries shortly before entering the salt lake (Fig. 23). The rise can be explained by the degassing of CO_2 from alkaline and neutral waters according to the following reaction (Eugster & Jones 1979):

$$2HCO_3^- = CO_3^{2-} + CO_2 + H_2O \qquad (7)$$
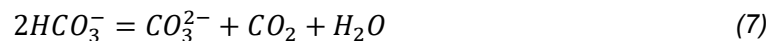
The characteristic of high pH in streams of (semi)-arid hydrological systems is a common phenomenon (Parnachev et al. 1999). CO_2 degassing as a result of groundwater surfacing due to low pCO_2 pressure in ambient air is followed by the precipitation of calcite. In fact, Río Grande and Río Colorado waters are oversaturated with respect to carbonates such as dolomite and calcite according to PHREEQC calculations. In the brines pH is significantly lower compared to the surface waters, which could be explained by sulphate reduction and acidification due to H_2S formation. Indeed, a significant sulphurous odour occurred at several drilling locations, especially, when the sampled salt aquifer was located next to a lacustrine layer.
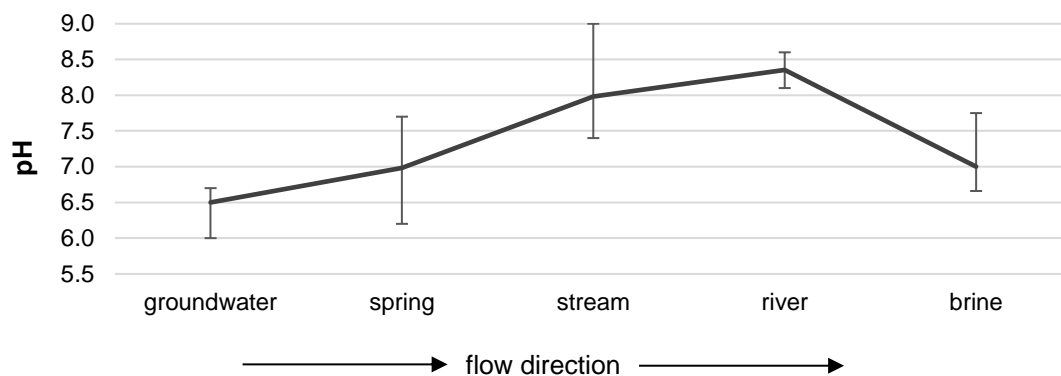
Fig. 23: *Trend of pH in the catchment of the Salar de Uyuni (groundwater, spring and stream values were complemented by samples from an unpublished report of Nittetsu Mining Consultants (2011) to increase reliability)*

Well brines are mainly in the range of euxinic waters, which are anoxic and sulfidic (Fig. 24). Requirements for euxinic conditions are the availability of sulphate ions, organic matter and sulphate reducing bacteria, and the concurrent absence of oxygen (Meyer & Kump 2008). Under these conditions, the following reaction takes place:

$$2CH_2O + SO_4^{2-} \rightarrow H_2S + 2HCO_3^- \qquad (8)$$
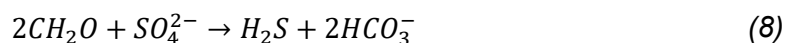
The reduction of S^{+VI} to S^{-2} is by far more complex and includes the formation of intermediate species. The lacustrine sediments that separate the salt layers are composed, amongst others, of organic material resulting from the sedimentation and decomposition of dead plants and animals to the lake bed during a phase of flash floods. These sediments were compacted and isolated from the atmosphere when the ground was covered by halite layers caused by the complete evaporation of lake water during a warm climate period. Transect brines are rather oxidizing compared to the deeper brines, as they were sampled in a maximum depth of 50 cm, thus diffusive controlled contact with the oxygen of the atmosphere is rather likely.
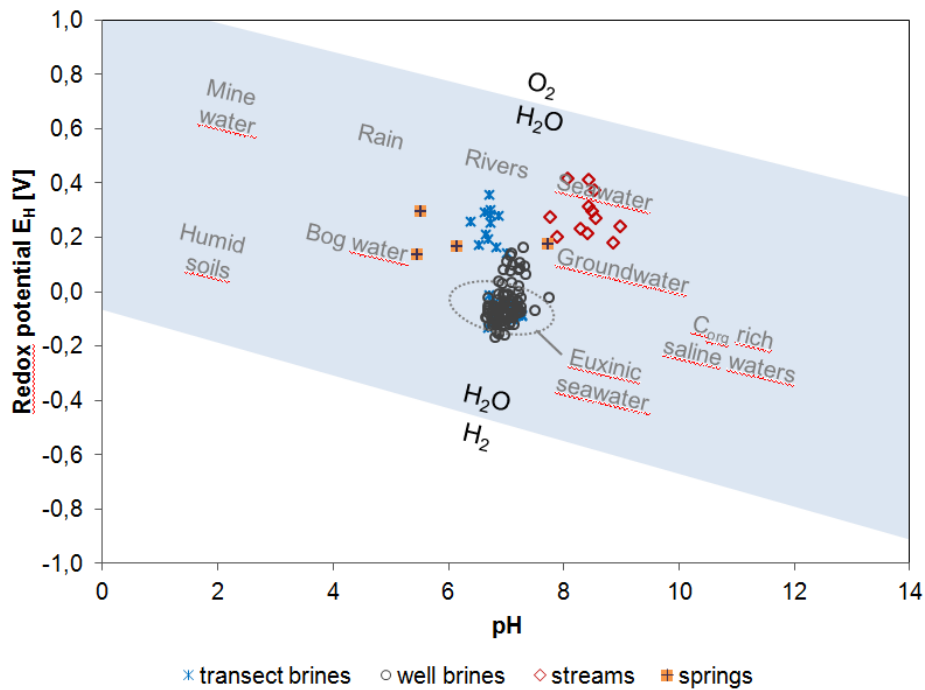
Fig. 24: *Location of different sample types in the E_H – pH diagram in comparison to frequently occurring E_H – pH conditions of natural waters (according to Hölting & Coldewey (2013))*

The electrical conductivity of brines is generally high in the range of 220 mS/cm. The upper limit of the measuring device *HACH HQ40d* is reported with 200 mS/cm by the manufacturer. However, brines of the Salar de Uyuni mostly exceeded this threshold. Dilution experiments (see chapter 5.4.3) proved, that measured values conform well to literature values of pure NaCl, and are thus usable for evaluation. The rivers Río Grande and Río Colorado show a much higher EC than contributing streams, due to evaporation of river water during the flow path, which is intensified by a reduced flow velocity as a result of the low gradient in the lower catchment.

Brines of the Salar de Coipasa have similar values for pH, temperature, oxygen, and redox potential. The only difference was observed in the electrical conductivity, which is in average 15% lower compared to Uyuni brines.

5.1.2 Lithium distribution

The distribution of lithium in the brine of the upper crust was interpolated using ordinary kriging and a spherical variogram. As data source, 92 points with lithium concentrations distributed all over the salar were used. Own analyses were supplemented by Li concentration data from older studies (Risacher & Fritz 1991b) in order to increase information in regions with low data density, for example in the western part of the salt lake. A logarithmic transformation was performed in order to reach normal distribution (see chapter 4.3.2). Fig. 25 shows the resulting

model of Li interpolation. Two zones of Li enrichment can be identified: at the southern margin near the delta of the Río Grande, and in the northernmost part. These zones show significant differences regarding overall concentrations and spreading.
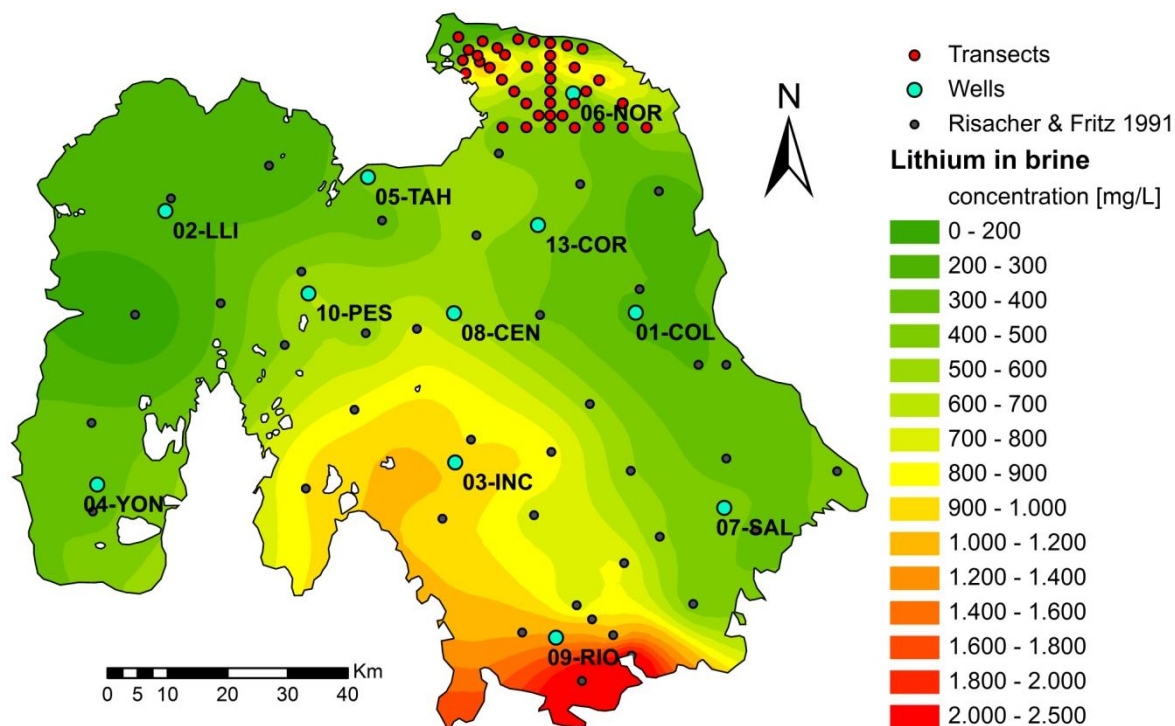
Fig. 25: *Distribution of lithium in the brine of the Salar de Uyuni's upper crust created by kriging in ArcGIS using spherical semivariogram; data stem from own analyses (transects, wells) and Risacher & Fritz (1991b), and were log transformed prior to interpolation*

Risacher & Fritz (1991b) measured Li concentrations up to 2.5 g/L in the brine in the Río Grande delta region. These high values could not be verified by own investigations, caused by the impossibility of accessing the southernmost area due to a high moistness of the salt layer and the demarcation of the region as military area. However, the comparison of selected own sampling locations and proximal data points of Risacher & Fritz (1991b), i.e. at 02-LLI, 09-RIO and 06-NOR, shows a good accordance in Li concentrations, so that it can be trusted in the accuracy of the literature data. The Li distribution in the south is characterized by high concentrations at the margin, which are rapidly decreasing towards the east and slowly decreasing towards the northwest. Besides the Río Grande, the Río Colorado delivers significant amounts of Li with the all-season inflowing water. Fig. 26 shows the Li interpolation in the southern part including the delta plains of the inflowing rivers. Surprisingly, the input of the element by this river is not reflected in the Li distribution pattern in the delta region, as would be expected similar to the Río Grande delta. Hence, the evaporation of river water containing high contents of Li cannot be the only mechanism for the enrichment of the element.
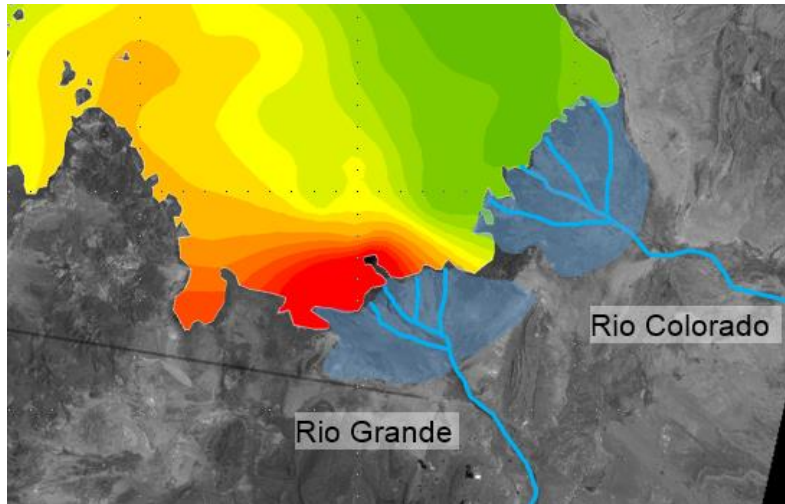
Fig. 26: Distribution of Li in the southeastern part of the Salar de Uyuni; blue shaded are the delta regions of the inflows Río Grande and Río Colorado (legend as in Fig. 25)

A possible explanation could be the transport of inflowing water (and contained solutes) on the surface of the salar towards the west and northwest by winds. However, a check of the SENAMHI database (station Uyuni) reveals, that wind direction is almost constantly W and NW and has remained constant since beginning of record in the 1940s. The same wind direction was estimated in the field by the accumulation of wind-blown dust at the windward side of the salt efflorescence along polygon borders. Hence, the transport of concentrated, lithium enriched solutions which developed from the evaporation of inflows and the dissolution of salts from the surface crust, cannot be responsible for the high Li concentration at the southern border. The distribution of Li in the northern part is described by significantly enlarged Li concentrations in a strip-shaped, about 10 km wide zone running parallel to the 2-3 km distant shore (Fig. 25). Unfortunately, the kriging interpolation underestimated the maximum concentrations in the brines from that region, which were in the range of 1,500 mg/L, comparable to values near the Río Grande delta. Multiple indicator kriging with raw data or simple linear triangulation with raw data would probably provide a more realistic result. In contrast to the Río Grande delta, concentrations are not highest at the shore, but are limited to the described zone. Hence, a different delivery and enrichment mechanism for Li than the input from inflowing streams must be considered.

5.1.3 Variation with depth and seasonal effects

Wells at several locations on the salar were constructed with screens in different depths in order to investigate the brine composition in dependency of the depth. The sampling depth reached from 0.2 m, located right beneath the brine table, until 9 m. A significant change in brine composition over the depth of the upper salt aquifer could not be observed (Fig. 27). Slightly increasing lithium concentrations with depth could be observed only at locations, where the range in sampling depth was higher (SLT-01-COL, SLT-02-LLI, SLT-08-CEN). At most locations, differences in concentrations between samples from different depths were within 10% without a statistically significant trend.
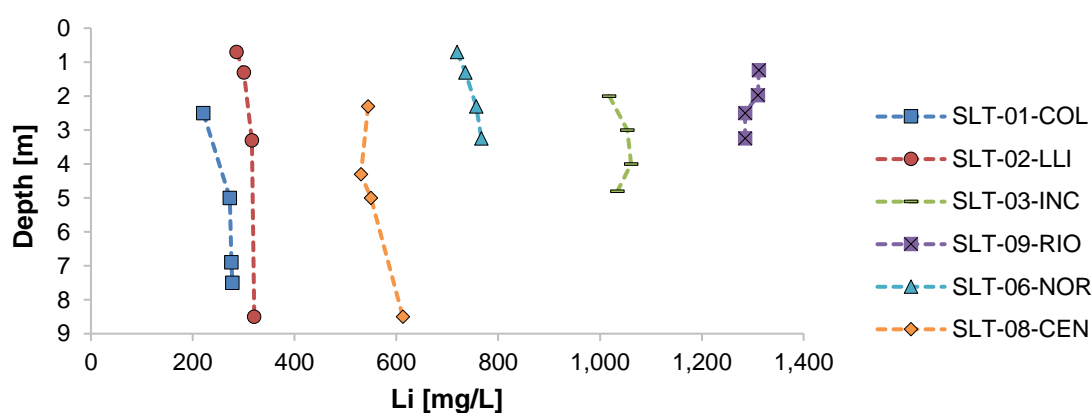
Fig. 27:   *Trend with depth for lithium in brines from locations, where multiple wells in different depths existed*

At drilling location SLT-LLI, it succeeded to install a screen in the second salt layer (LLI-B). Here, the mud layer started in 4 m depth and had a thickness of only 3.8 m, which enabled the drilling beyond that depth and the sampling from the second halite aquifer (8-9 m). The lacustrine layer forms the remnant of paleolake Tauca, and separates the salt crust formed during an earlier and the present dry climatic phase. Due to the low permeability of the separating lacustrine layer, the comparison of brine composition between the two aquifers could give indications for changes in solute input processes during the two different climatic periods. All elements, including Li, show a deviation between the two brine horizons below 5%, which is surprisingly low. A significant change exists only for borone (25% higher in greater depth), Ca and SO_4, which is illustrated in Fig. 28.
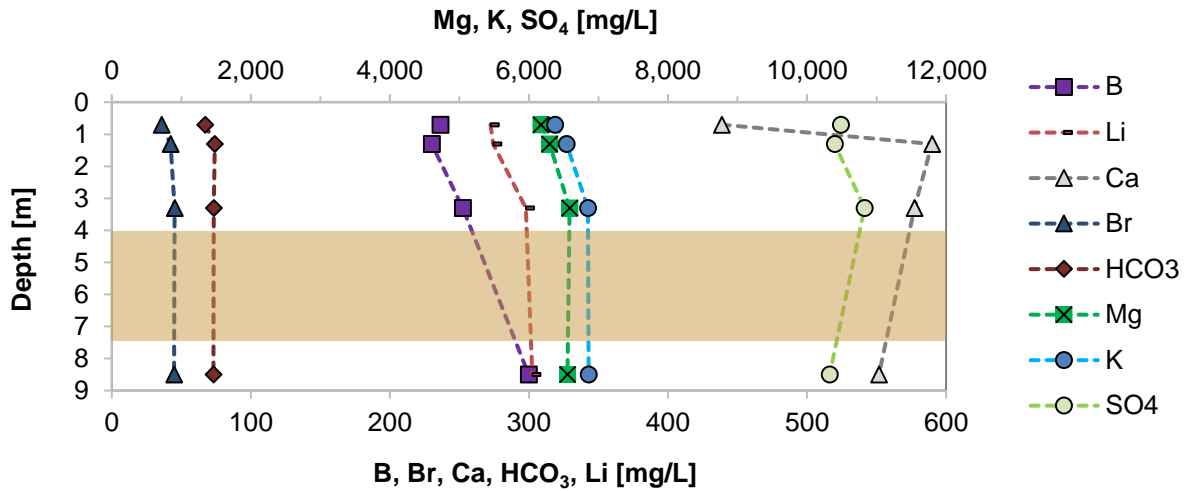
Fig. 28: Variation with depth of selected elements in screened wells of location SLT-LLI (brown shaped area marks position of lacustrine layer)

In Mai 2011, brines from screened wells were sampled right after the rainy season, when rainwater still covered parts of the salt lake. A comparison of chemical composition between these brines and samples from the dry months was performed. The shallowest screened wells with data from Mai 2011 are SLT-06-NOR-A (0.2 – 0.9 m) and SLT-08-CEN-C (1.8 – 2.8 m), and show that the composition does not change significantly. This is plausible because rain water and water from surrounding inflows do not interact readily with the brine. Hence, a dilution effect could not be observed. This fosters the assumption that the upper part of the salt crust, a very compact, cemented layer, is serving as barrier between diluted meteoric waters and concentrated brine underneath. Research regarding porosity and permeability of the Salar de Uyuni salt crust showed that the upper 5-10 cm salt cap is formed by cemented salt with an extremely low share of pores, which are additionally not connected to each other, followed by a friable layer with a high total and effective porosity (Sieland 2014). The stratification is visualized in Fig. 29, showing the upper 50 cm of a drill core from location SLT-08-CEN.

A clear trend over time could not be observed. Brines from screened wells were sampled between 2009 and 2014, and during this time the composition, irrespective of depth and season, did not change significantly. Only at site SLT-02-LLI, the concentration of Br constantly decreases over the years of sampling from ~55 mg/L to 25 mg/L. Although this trend was observed in all four wells of SLT-02-LLI covering a total depth range of 0.3 to 9 m, could not be confirmed at any other sampling site of the Salar de Uyuni.
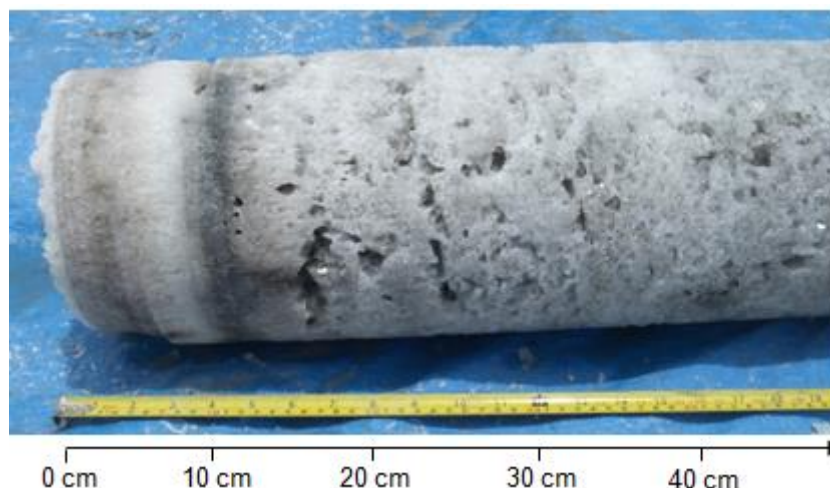
Fig. 29: Image of a drilled salt core (diameter: 8 inch) from the upper salt crust at site SLT-08-CEN-A; the upper 10 cm are composed of a compact, dense layer, followed by a friable zone with a high amount of visible, irregularly shaped pores (image by Ariane Schön)

5.1.4 Isotopic contribution

The stable isotopes deuterium (δ^2H) and $\delta^{18}O$ were determined in the brines of the Salar de Uyuni and the Río Grande river water (Table A - 10: Results of isotopic analyses of brine and river samples, including sampling depth and estimated distance from the Río Grande delta (n.d. - not determined). Results compared to analyses of groundwater, Altiplano streams, lakes and pore brines from former studies are illustrated in Fig. 30. Within the brine, δ^2H values range between -54 and -21‰ SMOW, the river water is significantly lighter with -78‰ SMOW. According to Clark & Fritz (1997), the deuterium signature of the river points to the typical contents in magmatic, meteoric and geothermal waters, hence, a single source cannot be identified. $\delta^{18}O$ values range from -2.5 to 4.8‰ SMOW in the brines, the river water is again distinctly lighter with -8.8‰ SMOW. The comparison to values from Clark & Fritz (1997) shows, that the river water exhibits a $\delta^{18}O$ signature typical for geothermal and meteoric waters.

The local meteoric water line (LMWL) was calculated from δ^2H and $\delta^{18}O$ values, which were collected over several years from monthly precipitation samples of the San Juan meteorological station, which is located at the southern shore of the Salar de Uyuni (Fiorella et al. 2015). The resulting LMWL is:

$$\delta^2H = 8.11 * \delta^{18}O + 16‰ \tag{9}$$

Local meteoric water lines usually show a deviation in slope and deuterium excess compared to the global meteoric water line, which results from local climatic conditions including the annual rainfall regime and the source of the vapour mass (Clark & Fritz 1997). Groundwaters in the catchment of the Salar plot along the GMWL and near the LMWL. This indicates that

their origin is mainly precipitation in form of rainfall and snow. Waters, no matter of which type and source, are exposed to specific local conditions: arid climate and high altitude. The distribution of δ^2H and $\delta^{18}O$ at the Salar de Uyuni are strongly affected by both climate and altitude.
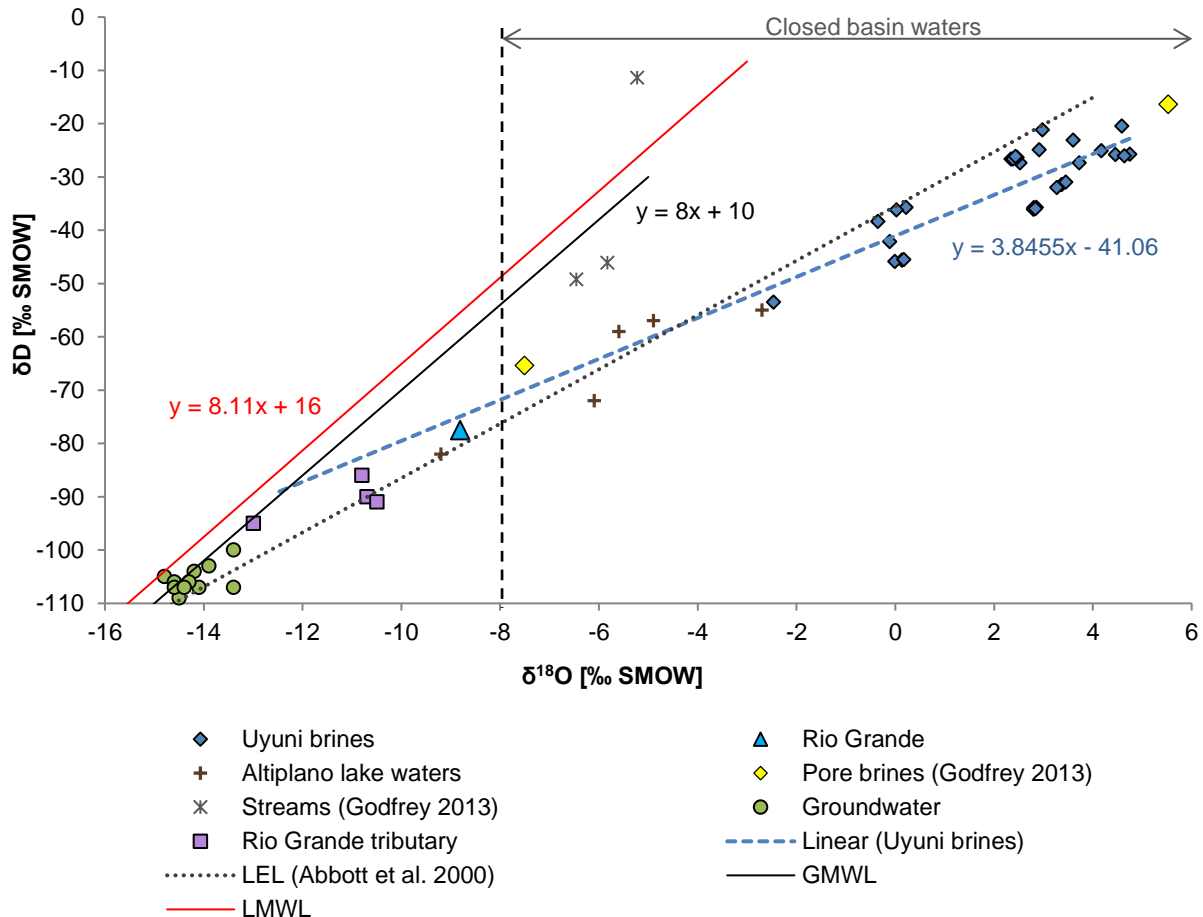
Fig. 30:   *Stable isotopic composition of the Salar de Uyuni basin; Uyuni brines and Río Grande are from own analyses, local evaporation line (LEL) and Altiplano lake waters from Abbott et al. (2000), groundwater from a Bolivian-Japan joint study (Nittetsu Mining Consultants CO. 2011); stream and pore brine values are from the Salar del Hombre Muerto basin (Godfrey et al. 2013); local meteoric water line was calculated from the San Juan river, which is located in the southern Altiplano (Fiorella et al. 2015)*

The brines clearly deviate from the LMWL, which is the result of evaporative enrichment of δ^2H and $\delta^{18}O$. However, brines also show a deviation from the LEL determined by Abbott et al. (2000). The reason is, that Abbott determined the LEL from open lakes on the Altiplano, including lakes directly and indirectly fed by glacial meltwater. In contrast, brines from the Salar de Uyuni are located in a closed basin fed only by precipitation and small inflows, and thus show a strong enrichment in heavy isotopes due to intensive evaporation. The evaporation effect is also visible in the isotopic composition of tributaries to the Río Grande and the Río Grande itself. Streams and rivers are strongly influenced by evaporation on the pathway, caused by solar insolation and a low humidity. Thus, the Río Grande sample, which was taken

near the outlet to the salar, is clearly enriched in δ^2H and $\delta^{18}O$ compared to its tributaries, and plots along the evaporation line of Uyuni brines rather than along the LMWL.

The variation between different depths within one sampling site is much lower than the variation between different sampling sites. This is expressed in a standard deviation of 1.8 between the sampling locations and a mean standard deviation of 0.16 for different depths at one location. Hence, a depth depending trend in δ^2H and $\delta^{18}O$ could not be observed. The high range of 30‰ for $\delta^{18}O$ and 7‰ for δ^2H in the brines indicate, that these waters are situated in differing hydrological settings, depending on their location on the salar. Samples from SLT-01-COL, SLT-02-LLI and SLT-07-SAL are clustered near a $\delta^{18}O$ value of 0‰ (Fig. 30). These sites, which are located not too far from the shore (see Fig. 15), could be influenced by locally feeding groundwater flowing towards the salt layers and mixing with the interstitial brine. This explanation could also apply for site SLT-04-YON, where $\delta^{18}O$ and δ^2H show the lowest values of all sampled brines (-2.5 and -54‰, respectively). The sample stems from the second salt aquifer, located in between a 4 m thick lacustrine layer above and a > 1.3 m thick mud layer underneath (see Fig. B - 1 for visualization). Feeding groundwater from freshwater aquifers at the shore zone could accumulate in the evaporate aquifer and mix with heavy brines, leading to a measurable decline of $\delta^{18}O$ and δ^2H.

In order to investigate the relation of $\delta^{18}O$ and δ^2H to brine evolution, isotopes were compared to a conservative constituent. As Li behaves conservative during the evolutionary path of the brines, it was used as a tracer for brine concentration in the relation to stable isotopes of water.
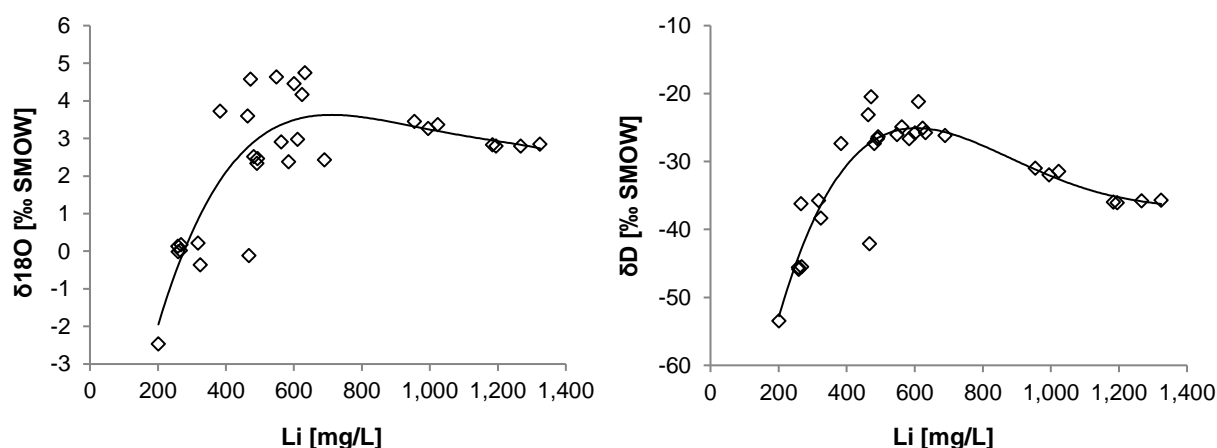
Fig. 31: Relation of stable isotopes of water with Li in the brines of the Salar de Uyuni

Fig. 31 demonstrates that heavy isotopes first increase in the brines with further concentration, but then describe a reverse trend with further brine concentration, reaching a steady-state after a while. This effect has been described in earlier works and is common for solutions with high

salt concentrations (Lloyd 1966). Sofer & Gat (1975) explain reaching stationary isotopic composition with the exceedance of the point of saturation, beyond which the salt concentration does not further increase due to the precipitation of salts.

The isotopic composition of sulphate in water depends on the sources of sulfur and on the fractionation processes occurring during the pathway through the catchment. Fig. 32 shows the distribution of $\delta^{34}S_{SO4}$, $\delta^{18}O_{SO4}$, and corresponding SO_4^{2-} concentration in brines and river water. A striking observation is the high deviation of $\delta^{34}S$ in the inflow compared to the brines. A possible explanation could be the process of dissimilatory sulfate reduction, where anaerobic bacteria form H_2S using SO_4^{2-} as electron acceptor:

$$2CH_2O + SO_4^{2-} \rightarrow 2HCO_3^- + H_2S \qquad (10)$$
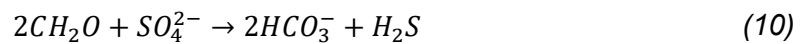
Due to the fact that sulphide has lighter $\delta^{34}S$ values, residual SO_4^{2-} becomes progressively enriched in $\delta^{34}S$. This effect has been previously described for groundwater and pore brines in environments containing an organic carbon source and lacking oxygen (Böttcher et al. 1998, Fritz et al. 1989, Krouse et al. 1970). The formation of H_2S indeed plays a role in the salar brine, which is supported by the characteristic rotten egg smell of some brine samples. Microbiological investigations on the Uyuni salt crust showed the occurrence of sulphate reducing species as *Desulfovibrio*, *Desulfuromonas* and *Desulfotomaculum* (Perez-Fernandez et al. 2016). However, such a process cannot account for the whole extent of $\delta^{34}S$ deviation in river and brine. As the dissolution of gypsum does not go along with a measurable isotopic fractionation, the isotopic composition of SO_4^{2-} in water can be used as tracer for the origin of sulphate (Clark & Fritz 1997). Various gypsum diapirs of marine origin were formed during the Cenozoic northeast of the Salar (Rettig et al. 1980, Risacher 1991b). According to Moser & Rauert (1980), $\delta^{34}S$ in brines conform to marine evaporate sulphates, leading to the assumption, that sulphate in brines partly stem from the dissolution of these diapirs. The detection of highest $\delta^{34}S$ in brines of the sampling site SLT-NOR-06, located in northeastern part of the salar, supports this assumption. A permanent connection of the Salars of Uyuni and Coipasa via the Serrania Intersalar during ancient times could be responsible for the entry of $\delta^{34}S$ rich waters to the Salar de Uyuni from the north.
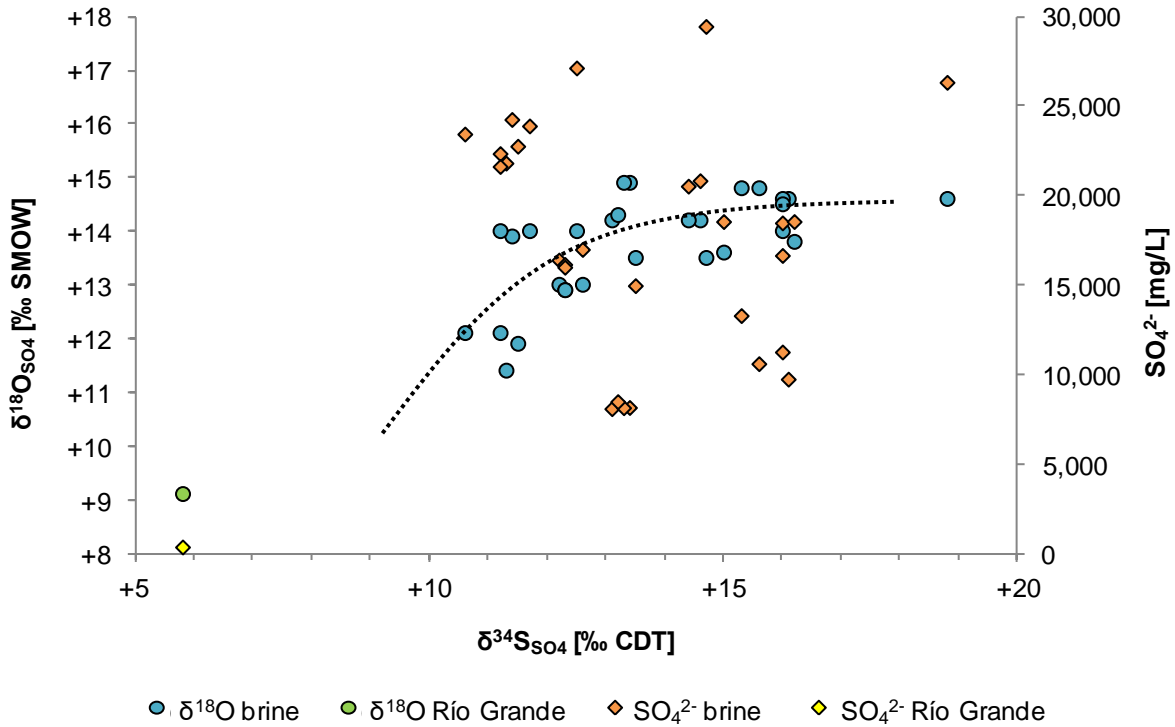
Fig. 32: *Plot of δ³⁴S to δ¹⁸O in SO₄ and SO₄²⁻ concentration in dissolved sulphate of the Salar de Uyuni brines and Río Grande water; dotted line signifies the trend of δ³⁴S/ δ¹⁸O in the brines approaching a constant value*

A correlation of δ³⁴S with the SO_4^{2-} concentration is not visible (Fig. 32). This could occur due to fractionation processes during the precipitation of gypsum from the brines, which are oversaturated with respect to gypsum. This leads to a removal of SO_4^{2-} and the enrichment of ³⁴S in the residual brine, as ³²S is preferentially incorporated in precipitates.

The age of brines was determined on four brine samples from different regions of the Salar by means of radiocarbon dating. Raw ¹⁴C activities (*a*) were corrected for natural isotopic fractionation by using the δ¹³C results of AMS measurements (see chapter 4.2.4). Corrected values were used for age determination of the brines in the upper meters of the salt crust according to the equation:

$$t = -8,267 \cdot ln\left(\frac{a_t{}^{14}C}{a_0{}^{14}C}\right) \qquad (11)$$

Where $a_t{}^{14}C$ corresponds to the $a_{\delta^{13}C}$ and a_0 to the initial ¹⁴C activity, which is generally assumed to be 100 pmC. However, the ¹⁴C activity was not constant at 100 pmC during the Pleistocene and Holocene, but steadily decreased with time (Fig. 33), due to variations in solar output. Results were corrected using adapted values for the initial activity. The results of ¹⁴C analyses are comprised in Table 5. By correcting the value of a_0 for each time span, the age

can be expressed in calender years, rather than radiocarbon years for non-corrected ages (Clark & Fritz 1997).

Table 5: Corrected ^{14}C activities in the samples with $\delta^{13}C$ values used for fractionation correction; and final ages (Age$_{cal}$) of the brines calculated from adjusted a_0 values.

Sample	Depth [m]	a [pmC]	$\delta^{13}C$ [‰PDB]	$a_{\delta^{13}C}$ [pmC]	Age [yr BP]	a_0 [pmC]	Age$_{cal}$ [yr BP]
06-NOR-B	2.8 - 3.8	52.2	-13.5 ± 2.6	51.0 ± 0.41	5,570 ± 65	108	6,200 ± 65
03-INC-C	4.3 - 5.3	41.8	-21.6 ± 1.5	41.5 ± 0.54	7,270 ± 110	109	7,980 ± 110
10-PES	5.0 - 6.0	40.8	-19.3 ± 1.5	40.3 ± 0.41	7,510 ± 85	110	8,300 ± 85
07-SAL	7.1 - 8.1	24.6	-3.4 ± 0.3	23.5 ± 0.16	11,970 ± 55	118	13,340 ± 55

Investigated brines have ages determined from radiocarbon between 6,200 and 13,340 years. A significant linear correlation exists with depth, the brine ages steadily increase downwards (Fig. 34). According to the results of radiocarbon dating, a significant mixture of the brine in the investigated depth range of 3 to 8 m does not occur. This might be due to the existence of thin, dense clayey layers in the salt crust, which impede the rise of brine from deeper strata. Sieland (2014) found, that gypsum layers show a very low gas permeability. The linear correlation with depth is evidence, that the inflow of groundwater from surrounding aquifers into the salt layers and the subsequent mixing with brine is negligible. This is plausible considering the different densities (1.2 g/cm^3 of brine versus 1.0 g/cm^3 of freshwater).
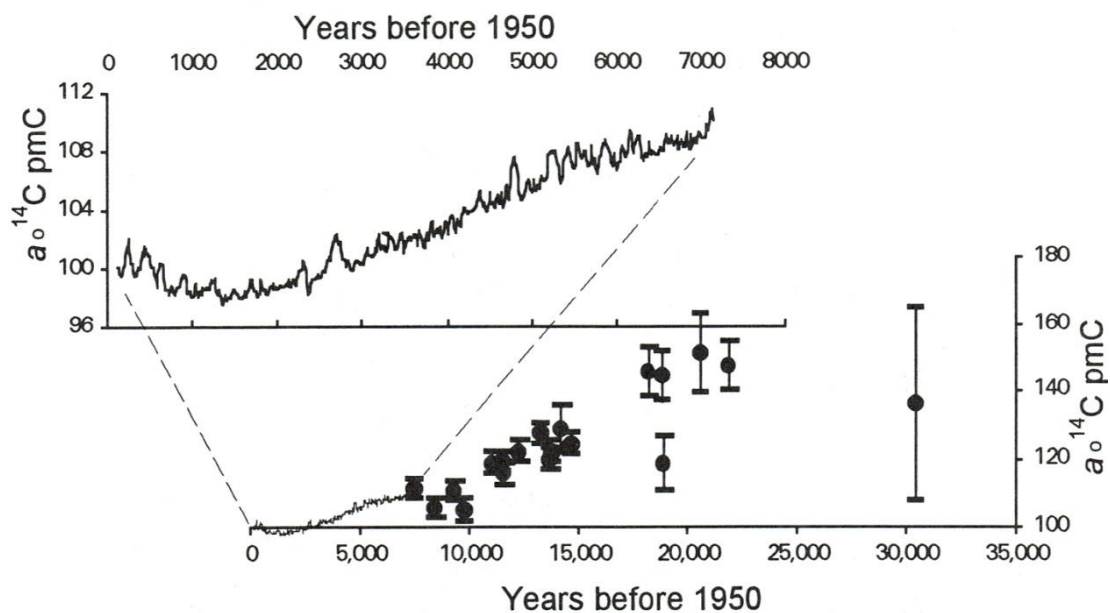
Fig. 33: Development of atmospheric ^{14}C activity during the Holocene, determined from the dendrochronological age of tree rings and the U/Th age of shallow marine corals (Clark & Fritz 1997)

SLT-06-NOR and SLT-07-SAL are located near the shore, in about 10 km distance to the northern and south-eastern salar border, respectively. However, radiocarbon dating showed no measurable mixing of brine with river waters infiltrating in the shore zone and flowing as groundwater along the lacustrine layers. These waters should significantly decrease in measured ages, which is not the case. It must be admitted, that samples stem from different regions of the Salar. In order to verify the assumptions concerning brine stratification, a repetition with samples from different depths at one location having multiple wells would be necessary. Unfortunately, this was not possible due to the low overall content of carbon in the brines and the difficulties in extracting enough carbon for the dating procedure. Mostly, contents of extracted CO_2 were tightly above the minimum amount required for analysis. Further, four samples are not enough to be representative for the whole salar.
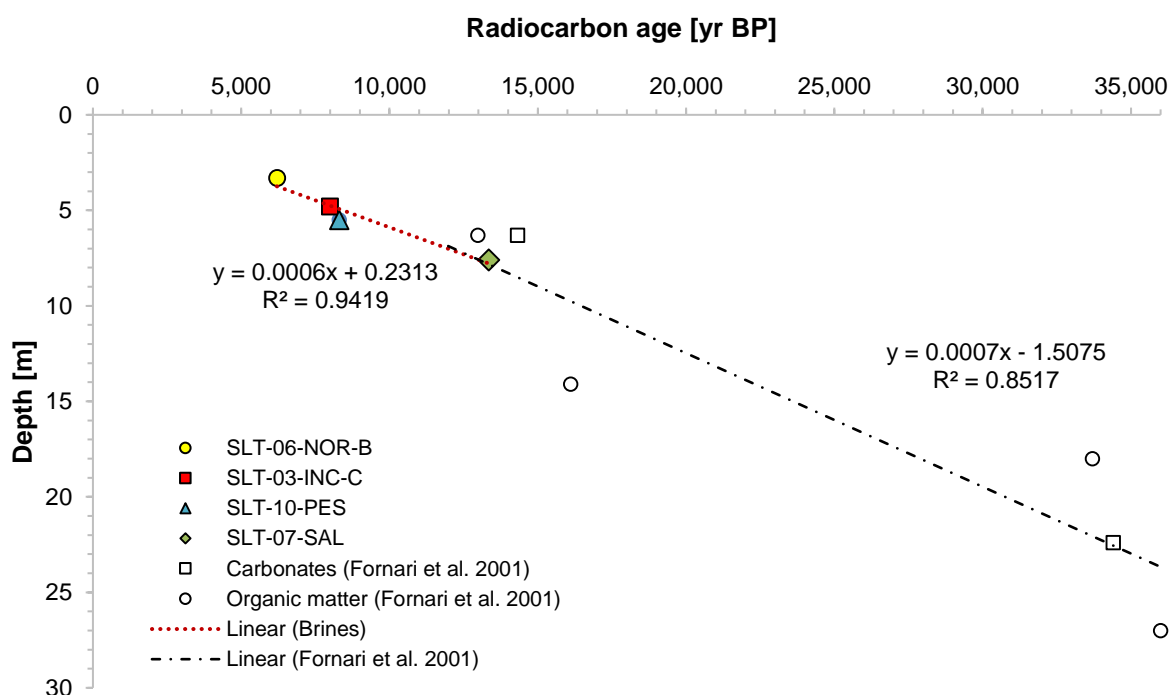
Fig. 34: *Fractionation-corrected, a_0 adjusted radiocarbon ages of brine samples in dependence of depth; and radiocarbon ages from Fornari et al. (2001) for comparison, obtained from carbonates and organic matter in the Salar de Uyuni (for measurement uncertainties see Table 5)*

Literature values for comparison of brine ages in the Salar de Uyuni, and generally in salt lakes, are not existent. However, few sediments were analyzed in the past. Ericksen et al. (1977) reported a radiocarbon age of 3,520 ± 600 years for an organic-rich mud from a depth of 15 cm in the Salar de Uyuni, about 35 km west of Colchani (small village at the middle of the eastern shore). Sylvestre et al. (1999) determined ^{14}C ages from mollusc shells, calcareous crusts and bioherms sampled at the volcanic flanks of Mt. Thunupa to an age of 14,000 – 16,000 yr BP. In the course of a deep drilling in the center of the Salar de Uyuni, Fornari et al.

(2001) measured radiocarbon ages from carbonates and organic matter in lacustrine layers. The comparison to obtained brine ages shows a very good accordance, the ascent is in a similar range (Fig. 34). Thus, it can be assumed, that the interstitial brine in a certain depth corresponds in age to the surrounding evaporates leading to the conclusion that the uppermost brines were formed concurrently with the salt crust. Apparently, a significant mixture of brine with infiltrating rainwater in the upper salt crust during the rainy season does not take place, at least not in depths of > 5m. Also, the increasing brine age with depth contradicts the existence of significant vertical brine flow and supports the theory of a stable stratification. According to Sieland (2014), fine gypsum layers separating the porous upper salt crust in varying depths, show a very low permeability, which might be responsible for the prevention of brine mixing.

Table 6: Locations of radiocarbon dating with particular thickness of the upper salt crust and estimated age

Location	thickness [m]	Calculated age [cal yr BP]
06-NOR-B	5.2	9,770 ± 1,520
03-INC-C	5.8	9,650 ± 1,020
10-PES	8.0	12,070 ± 1,100
07-SAL	9.0	15,800 ± 1,040

The regression equation from calculated radiocarbon ages (Fig. 34) and the maximum depth of the upper salt layer at each ^{14}C sampling site, estimated during core analyses in the field (see Fig. B - 1), served for the determination of the age of the uppermost salt crust (Table 6):

$$Age_{crust} = \frac{m - 0.2313}{0.0006} \qquad (12)$$

Calculated ages between 9,770 and 15,800 years for the formation of the crust are in concordance with results from Fornari (2001), who dated the end of lake Tauca phase to 12,980 cal yr BP, estimated from organic matter in a depth of 6.3 m at the bottom of the upper salt layer. From the ages and brine sampling depths, the annual growth of salt crust since the drying of paleolake Tauca can be estimated, amounting to 0.6 mm per year (Fornari et al. (2001): 0.7 mm/a). The same order of magnitude shows the resulting deposition rate calculated from data of the mud sample from Ericksen et al. (1978) explained above, which would account for 4 mm in 100 years. However, these calculations do not include the initial thickness of the salt crust, which was formed from the complete precipitation of dissolved solutes contained in lake Tauca in the course of total lake evaporation.

5.2   Solute input from the catchment

In a first step, the outline of the catchment of the Salar de Uyuni was determined by means of remote sensing methods, followed by a detailed evaluation of watershed borders and extensions. This included the investigation of a possible recent or ancient superficial connection of the Salars of Uyuni and Coipasa, which would have a considerable impact to the mass balance of lithium and other solutes' input to the Salar de Uyuni. Then, rock and sediments sampled from the southern catchment were evaluated regarding the geological map of the investigation area, and set in relationship to streams and springs in the watershed.

5.2.1   Outline of the catchment

The catchment of the Salar de Uyuni, calculated with ArcMap using the ArcHydro extension, amounts to 63,000 km² (Fig. 35). It contains the subcatchments of the main inflows Río Grande and Río Colorado, and various all-season and ephemeral streams contributing to the rivers. To the north, the Salar de Uyuni catchment is sharply limited by the Serrania Intersalar. To the west, several intermontane sinks extend the catchment far across the Chilean border to only 30 km distance from the Pacific. In these sinks, smaller salt pans have formed which can be identified from satellite images. The input of solutes by streams to the Salar de Uyuni from these regions is probably limited to intensive rain events in summer months. In dryer years, the transport of water masses from surrounding mountains results in the accumulation of salts and sediments, and leads to the formation of smaller salt pans.

Several steps of the catchment delineation procedure using ArcHydro, as the calculation of flow accumulation and the final drawing of watersheds are time consuming and hardware intensive. Thus, the underlying SRTM file should have the minimum necessary extension for covering the complete watershed. The layer of flow accumulation showed unnaturally running parallel horizontal lines in the region of the alt lake and the southern deltas, caused by the flat terrain of the salt flat and the extended floodplains upstream of the delta region. Approaches to avoid such a problem are the *fill sinks plus* tool and the *optimized pit removal* tool. Unfortunately, the *optimized pit removal* tool is limited to a maximum grid size of approximately $5 \cdot 10^7$ cells, which is about the half of the utilized SRTM grid. Hence, the application of the tool resulted in an error. The *fill sinks plus* tool did not provide satisfying results or an improvement compared to the normal fill sinks tool implemented in ArcHydro. However, final watershed delineation was not influenced by the falsified course of subcatchment borders resulting from unnatural parallel lines in the flow accumulation layer.
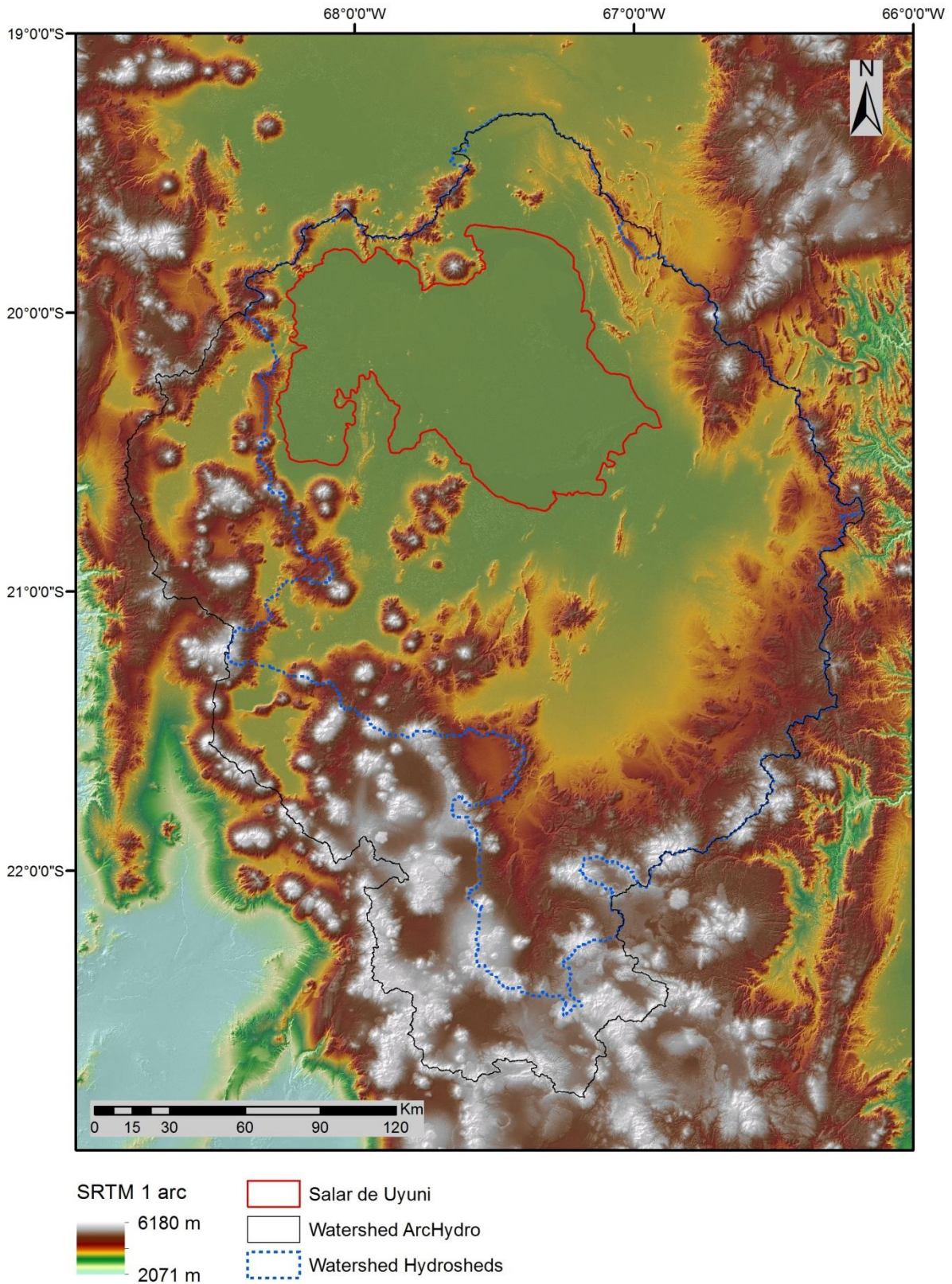
Fig. 35:   *Comparison of Salar de Uyuni watershed derived from own analyses using the ArcHydro extension and Hydrosheds*

Two types of digital elevation models were used for watershed delineation: ASTER and SRTM. Although the used SRTM and ASTER data showed the same spatial resolution, differences in the resulting catchment occurred. Former studies show, that especially in flat terrain, SRTM elevation models better represent the actual conditions and produce less artefacts. Kanoua & Merkel (2016) come to the conclusion, that SRTM data show a more detailed morphology and a slope better reflecting the reality. Furthermore, the active radar based system SRTM shows advantages in penetrating a cloud cover and is thus less affected by atmospheric conditions, compared to passive ASTER using available light. *Table 7* shows the result of watershed estimation compared to literature values. Hydrosheds (Hydrological data and maps based on shuttle elevation derivatives at multiple scales) provides a vector file with watershed boundaries containing the drainage basins of whole South America[9]. The difference in size of about 30% is probably due to the resolution difference of the underlying elevation model. Former studies using the higher resolution could not be found in literature. However, own delineations using a 90 m SRTM did not provide satisfying results, as the shapes were fragmented and incomplete (Jackisch 2014). In order to verify the results obtained by the ArcHydro extension, the procedure was repeated using the tools for watershed delineation provided by the Spatial Analyst tools of ArcGIS. The resulting catchment roughly coincides with the catchment received by ArcHydro, confirming the results of own estimations compared to literature data, and supporting the thesis, that differences arise from different resolutions of the raw data.

Table 7: Watershed area of own analyses compared to different sources

Source	Data source	tool	Catchment size [km²]
Own analysis	SRTM, 30 m	ArcHydro	63,000
Own analysis	SRTM, 30 m	Spatial Analyst	63,031
Hydrosheds	SRTM, 90 m	-	47,220
Guyot et al. 1990	-	-	46,600
Bradley et al. 2013 (USGS)	SRTM, 90 m	-	47,000

The map was used for the assignment of water, rock and sediment sampling sites to the underlying geological unit. The southeastern part of the Salar de Uyuni catchment is mainly characterized by surficial deposits and sediments dating back to Holocene and Pleistocene, including unconsolidated alluvial, eolian and colluvial material, locally supplemented by

[9] Access via https://hydrosheds.cr.usgs.gov/hydro.php in June 2017

shallow lacustrine and salt deposits (Fig. 7). The region west of the salar mostly consists of stratovolcano deposits with lava flows and flow breccias of andesitic to dacitic composition, complemented by extensive outflow sheets of ignimbrites and ash-flow tuffs (Fig. 7). Tributaries to the Río Grande and Río Colorado have their source in partly thermal springs located in elevated mountain regions and volcanic flanks, which are rich in ignimbrites and pyroclastic rocks of volcanic origin. The main course of the rivers and their tributaries is characterized by unconsolidated surficial deposits resulting from the alternating processes of weathering, associated mineral dissolution, and the deposition of silts in the extended floodplains. The dominance of these deposits is reflected in Fig. 36, which illustrates the distribution of geological units in the catchment of the Salar de Uyuni. The evaluation of SKYLAB and LANDSAT images by Francis & Baker (1978) showed that ignimbrite shields in the Southern Bolivian Altiplano have their source in large calderas which erupted during the Miocene and Pliocene.

Fig. 36: Distribution of geological units in the catchment of the Salar de Uyuni (volcanic rocks: undifferentiated, but mainly lava flows)

5.2.2 Hydrological connection between Salars of Uyuni and Coipasa

A superficial hydrological connection between the Salars of Uyuni and Coipasa has not been investigated so far. However, a potential connection would have a high influence on the ionic balance of the salars, the mass balance of input and output to and from the salars, and the existing theories about the sources of solutes to the Salar de Uyuni. A hydrological connection is supported by the observation, that the highest lithium values in the Coipasa brine are located in the south-eastern part, which would be the outflow to the Salar de Uyuni. The Uyuni brine shows a high enrichment of lithium in the north-eastern part, the inflow region of assumed superficial and/or subsurface waters originating from the Salar de Coipasa.

The modelling of watersheds with ArcGIS showed, that the drainage line at the NE side is situated about 30 km north from the northern shore of the Salar de Uyuni (Fig. 35), excluding the Coipasa salt lake. This is due to the fact, that the Salar de Coipasa is located 6 m higher than the Salar de Uyuni. However, a desiccated ancient stream bed called the Quebrada Negrojahuira with a width of approximately 1-2 km can be clearly identified from satellite pictures (Fig. 37). To verify a superficial connection, satellite data of the region of interest were investigated. First, the meteorological data from Uyuni was checked for austral summer months with an especially high amount of precipitation. Second, satellite data from the chosen time interval were selected from the Glovis database. Unfortunately, Landsat data from the rainy season are mostly of poor quality due to the usually high cloud coverage. For example, during the wet months of 2000/2001, 2002/2003 and 2013/2014 a hydrological connection is visible on satellite images, but cannot be evaluated due to the high lack of information by the cloud cover. A further problem is, that Landsat 7 files from the Enhanced Thematic Mapper after May 2003 are not usable because of distracting black stripes without data, caused by the failure of the Landsat 7's Scan Line Corrector in May 2003[10]. As each stripe represents a width of ~400 m, data loss is too high for evaluation of the existence of a water flow in the stream network between the Salars. Between December 1986 and January 1987, the rainfall of 250 mm was the 2.5 fold of average precipitation during that time span.
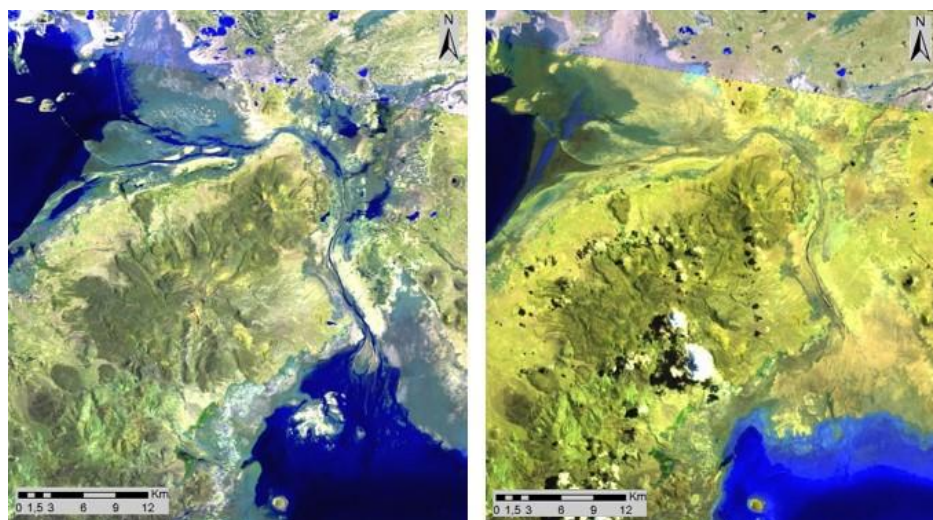
Fig. 37:   Satellite images from January 1987 (left) and March 1987 (right): in January, the hydrological connection is clearly visible; the line results from the sequence of different satellite images

Thus, satellite images from Jan. 1987 were used for several band combinations in order to find the best composition for the visualization of water flooded areas and the detection of streams and river channels. The band combination 7-5-3 emerged to be suitable for the differentiation

---

[10] Information source: https://landsat.usgs.gov/slc-products-background

of water flooded areas and small streams from the surrounding sediments and rocks. Fig. 37 shows the Landsat image from Jan. and March 1987 with bands 7-5-3 combined. A connection of the salars is obvious.

Due to the lack of elevation information in satellite data, the evaluation was extended by taking a look at SRTM data in the concerning region. Fig. 38 shows the elevation model of the Salars of Coipasa and Uyuni. In order to focus the analysis of a superficial hydrological connection to the area of interest, the visualization of the elevation model was limited to the range between 3,665 and 3,670 m a.s.l. Altitudes below and above were set to the colors white and black, respectively.
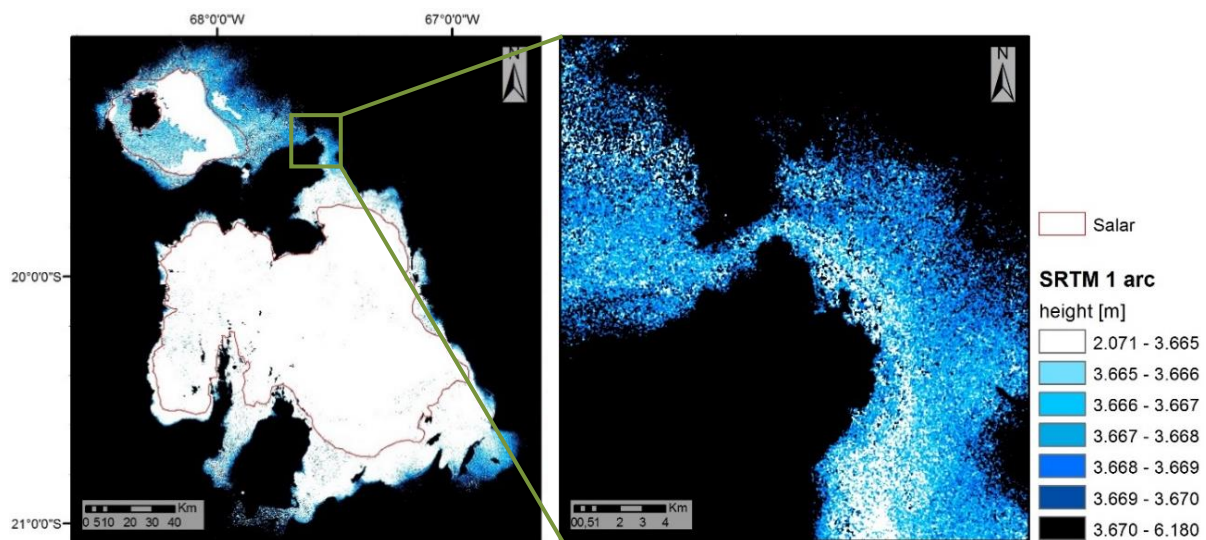
Fig. 38:   Elevation model of Salar de Uyuni and Salar de Coipasa illustrating the possible connection by limiting the shown heights to the range between 3,665 and 3,670 m a.s.l.

However, elevation data of SRTM and ASTER products should be considered critically during the investigation of flat terrain, where minor changes in elevation determine flow directions and flow accumulations. The absolute vertical error was estimated in a couple of studies to 6 – 7 m (Elkhrachy 2017), whereby low-vegetated land and bare soils as occurring in the salt lake environment generally show higher accuracies than dense vegetation and cultivated areas. A closer look to the investigation of a hydraulic connection should be performed by field observations, the detection of streams during the rainy season, which is limited by the hindered access to the regions of interest. A subterrestrial connection could be as well possible. Wolf (2010) suggests the existence of an aquifer consisting of older sedimentary units, covered by the younger volcanic layers of the Serrania Intersalar.

Another approach for solving the question of connectivity between Salar de Coipasa and Salar de Uyuni is a geochemical balance calculation. Therefor, the amount of Li in the brine of the upper salt crust was compared with the input by tributaries during the last 10,000 years since drying of paleolake Tauca at the Salars of Uyuni and Coipasa. Annual discharge of Río Lauca

near its mouth towards Coipasa salt lake is estimated to a minimum of 200 x 10^6 m³ (Grove et al. 2003), Risacher and Fritz (1991b) give a value of 140 x 10^6 m³, provided by the SENAMHI of Bolivia in 1985. Ballivian (1981) roughly measured the flow rate of Río Grande with 1 m³/s during low-level times and 4 m³/s during rainy season months. Assuming an average amount of 4 low-level and 8 high-level months, the overall flow rate of Río Grande would be 2 m³/s and 63 Mio m³/a, respectively. Similar results showed episodic measurements during field trips by Risacher (1991), who estimated an annual discharge of 60 ± 30 x 10^6 m³ (width = 30-70 m; mean depth = 0.15-0.20 m; surface water velocity = 0.3 m/s). Reliable information about lithium resources in the Salar de Coipasa could not be found in literature and thus were calculated from the limited data available. A rough estimation was made with the following equation:

$$R = V \cdot n_p \cdot c_{brine} \qquad (13)$$

Here, R is the lithium resource in Mio t, n_p defines the porosity of the salt crust, and c_{brine} is the lithium concentration in brine in g/L. The volume of the salt lake V is calculated as the product of area and mean depth of the uppermost brine-filled salt crust. The resource estimation covers only the uppermost salt layer, as they form the result of the last 10,000 years' input of solutes mainly from Río Lauca. Smaller streams were negotiated, due to the minor influence on the ionic balance and the lacking of chemical and discharge data. Input parameters and results of calculation are combined in Table 8. The amount of total Li resources in the Salar de Uyuni was adopted from Sieland (2014), because his estimation is based on a resource model taking into account the variations in crust thickness, porosity and Li concentrations in brine, and thus represents the most precise information available.

Table 8: Input parameters for the estimation of Li contribution during the last 10,000 years and present resources in the Salars of Uyuni and Coipasa

Salar	Discharge of main inflow	Li in inflow	Li input in 10,000 yrs	Size	Depth[1]	Porosity	Avg. Li conc. [1]	Li resources[1]
	10^6 m³/a	mg/L	10^6 t	km²	m	%	mg/L	10^6 t
Coipasa	140 - 200	1	1.4-2.0	2,500	1-2	35	300	0.2-0.5
Uyuni	60	3	1.6-1.8	10,000	1-10	14-35[2]	500	6.99[2]

[1]data apply for the upper salt crust
[2]estimation is based on exact calculation in Sieland (2014)

The comparison of lithium input by Río Lauca during the last 10,000 years and the existing lithium accumulated in the upper salt crust shows that the river transported more than the 5-fold of lithium obtained in the salar brine. Hence, a depletion of lithium must have taken place. Possible explanations could be the sorption by clay minerals as illite and smectite, but

lacustrine sediments underlying the salt crust are poor in smectite (Lebrun et al. 2002). Another explanation could be the overflow of brackish, lithium enriched waters during the rainy season and the transport of waters in underlying aquifers towards the Salar de Uyuni. Discharge of Río Lauca is significantly higher compared to Río Grande and, considering the smaller size of the Salar de Coipasa, the surface is consequentially covered by water most time of the year. Thus, a hydraulic gradient is likely to exist towards the Salar de Uyuni, where the surficial water quickly dries up with beginning of the dry season. This could be a possible explanation for the existence of all-season humid areas in the northeastern part of the Salar de Uyuni, and elevated concentrations of lithium in brine, although a visible input of river water is missing. This theory fits to the lithium balance of the Salar de Uyuni, where estimated lithium resources in the upper crust exceed the Li input during the last 10,000 years, calculated from discharge and concentrations in the Río Grande (Table 8).

Other inflows, as the Río Colorado, were disregarded for calculation, because estimations of discharge are missing, and Li concentrations are significantly lower. The large difference between input and resources could be due to the transport of Li with suspended matter. Chemical analyses of river water comprise the dissolved load of elements. Especially during the rainy season large masses of suspended sediments, removed by rainfall from the weathered surface in the southern catchment, are carried towards the salt lake. Elements with a strong affinity for ion-exchange sites on clay minerals like Mg, K and Li are then carried in the clay fraction of suspended load, and accumulated in a relatively concentrated area in the river delta, where flow velocity rapidly decreases allowing the suspended matter to sediment. Considering the results of calculation, it should be admitted, that input parameters for estimation are afflicted with large uncertainties due to the lack of precise information.

5.2.3 Chemical composition of inflows

The relative abundance of major ions in samples from inflows to the Salar de Uyuni is illustrated in a Piper diagram (Fig. 39, values are given in Table A - 5). Streams show no clear trend in composition, but are spread over the area. Springs are mainly of NaCl type with low concentrations of Ca and HCO_3.
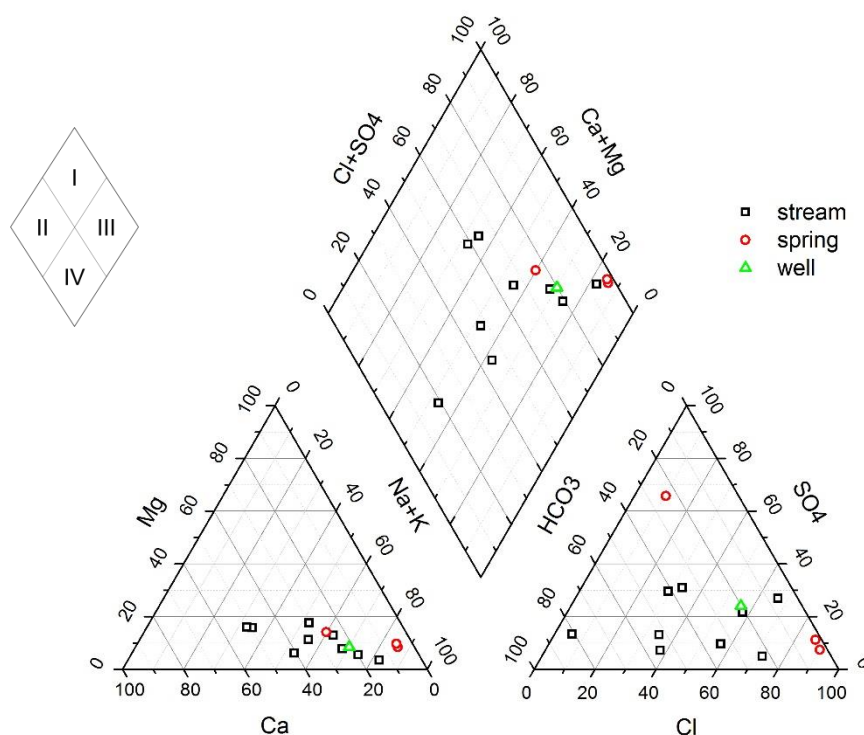
Fig. 39: Piper plot of stream, spring and well waters in the catchment of the Salar de Uyuni (classification of the zones: I – calcium sulfate waters, II – calcium bicarbonate waters, III – sodium chloride waters, IV – sodium bicarbonate waters)

Two of three sampled springs contain high lithium concentrations of 4.9 and 7.2 mg/L (SLT-SPEC-JIR, SLT-SPEC-COA). It is conspicuous, that all sampled streams and springs from the surrounding of volcano Thunupa are remarkably enriched in lithium. High Li contents in springs in the catchment of the Salar de Uyuni have also been measured during former investigations. Ericksen et al. (1978) found 4-6 ppm Li in thermal springs at the margins of Salar de Empexa, located only about 15 km west of the Salar de Uyuni. A thermal spring near Challapata contained 17 ppm Li. Risacher & Fritz (1991) measured significantly increased Li concentrations up to 14 mg/L in rivers and springs contributing to various smaller salars in the Southern Bolivian Altiplano. According to Tan et al. (2012), the content of Li in rivers and streams is a hint for the existence hydrothermal systems in their catchment. Huh et al. (1998) published a compilation of lithium contents in major world rivers, together representing about one third of world river flow and covering different climatic regions. The mean amounted to 215

nM, or 1.5 µg/L. Compared to that value, the sampled streams and rivers from the Uyuni catchment showed enrichment factors between 6 and 3500, with a mean factor of 670, which is visualized in Fig. 40. The graphic shows the plot of Na and Li in the catchment water samples, compared to major world river waters. As the access to streams and hydrothermal springs in the Salar de Uyuni region is impeded by scarce infrastructure, literature data from Risacher & Fritz (1991a) for the Southern Altiplano was included in the evelution. The correlation between Li and Na in water flowing to the salar points to the main source of Li: leaching of volcanic rocks in the catchment.
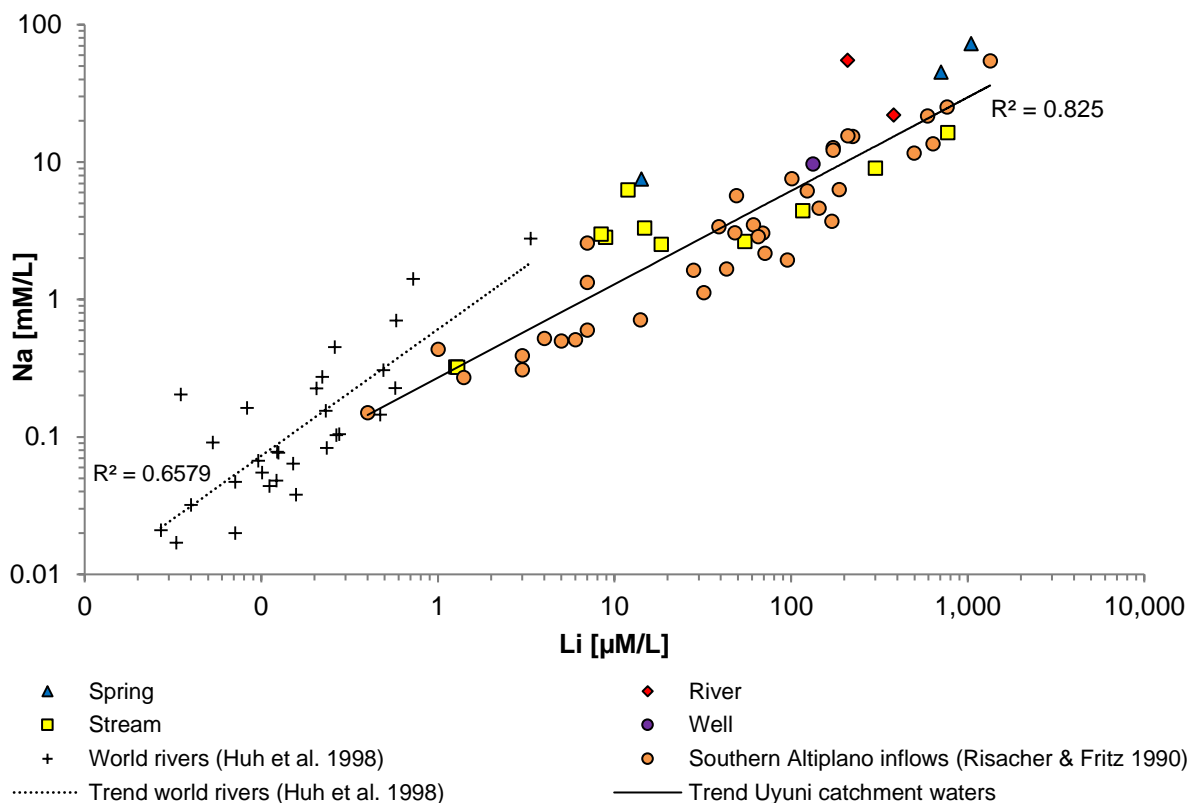
Fig. 40: *Logarithmic scatter plot of Na and Li concentrations in the catchment water samples in comparison to world river waters collected by Huh et al. (1998)*

According to Gibbs (1970), the chemistry of surface waters is controlled by three major mechanisms: evaporation-crystallization, atmospheric precipitation, and rock dominance. The classification of waters is visualized with the help of a Gibbs diagram, which shows two diagonal branches representing the composition of world rivers, lakes and seas regarding the ratios of Na-Ca and Cl-HCO_3 to salinity. Water samples from the Salar de Uyuni basin show the typical pattern of surface waters in arid environments (Fig. 41). Smaller streams plot in the field of rock dominance, meaning that dissolved salts in their waters derive from the weathering of rocks and soils in their basins, whereby the composition depends on the relief and characteristics of the basins bedrock. Clearly, the influence of evaporation is visible in the

mainstreams Río Grande and Río Colorado, as they plot in the evaporation field of the Gibbs diagram (Fig. 41). Here, samples were taken in the final part of the inflows shortly before entering the salar. The arrow in the Gibbs diagram for the inflows to the Salar de Uyuni shows their evolutionary path from the rock-dominated, medium-saline and Ca-rich endmember towards the highly-saline, Na-rich endmember during their flow from the mountain flanks to the evaporites-filled deepest part of the basin. The change in composition is caused by i) evaporation and accompanied increase in salinity, and ii) precipitation of $CaCO_3$ from solution and the relative decrease in Ca and HCO_3 (Gibbs 1970). Fig. 41 highlights, that the contribution of ions from precipitation is neglectible, due to the low annual amount of rainfall. Nonetheless its limited occurrence, rainfall plays a major role in the accumulation of ions in the salt lake, caused by its function as a solvent for salts accumulated at the surface in the catchment, and the transport of dissolved ions towards the tributaries.
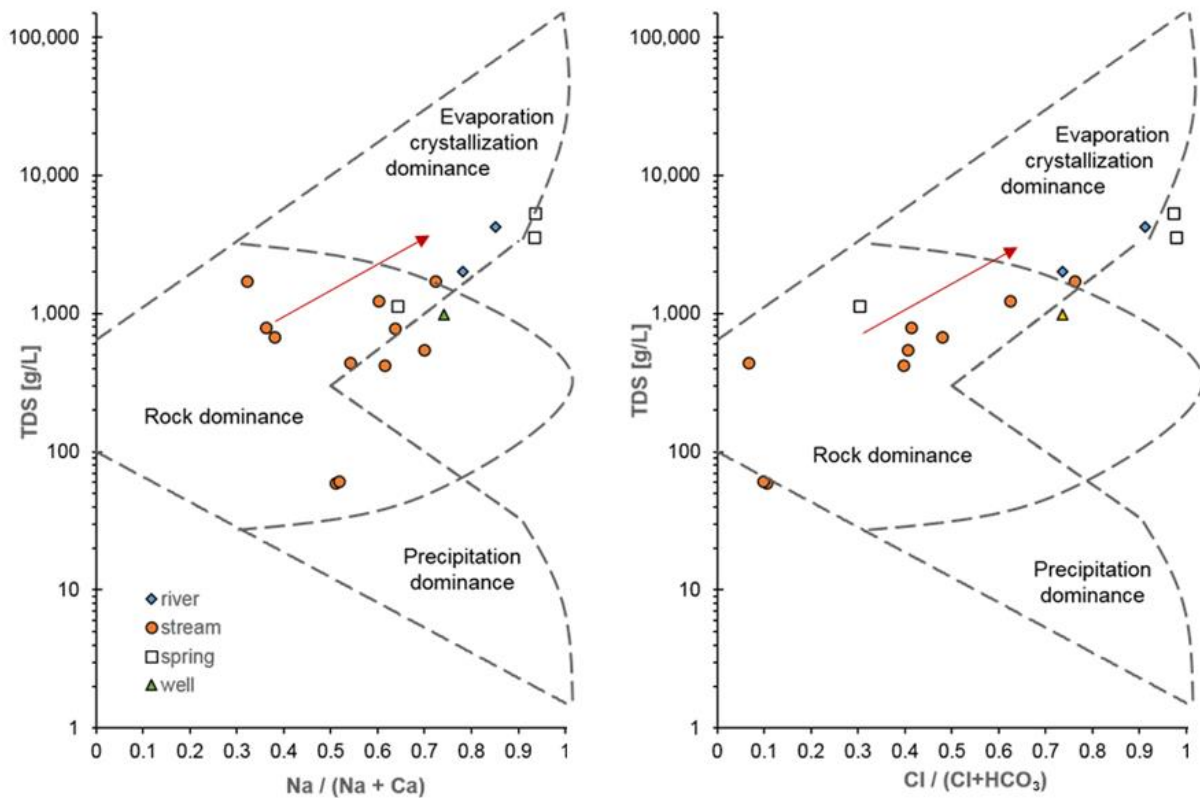
Fig. 41:   Gibbs diagram of inflow waters showing major processes responsible for water chemistry; the red arrow indicates the evolutionary path of surface waters in the Salar de Uyuni basin

Another hint for the sources and enrichment of solutes in waters discharging in the catchment of the Salar de Uyuni is given by the distribution of sodium and chloride in the streams and springs. Spring waters with Cl < 2 mmol/L are plotting above the line of equimolarity and show a fairly scattered distribution (Fig. 42), indicating the absence of extensive contact time with older evaporates in the underground. Their composition must be affected mainly by the alteration of volcanic rocks due to intensive weathering processes. In contrast, spring waters

with Cl > 2 mmol/L show a balanced Na-Cl proportion and generally high concentrations of NaCl, which is typical for waters leaching halite. These waters must be fed from groundwaters, which are influenced by the contact with subsurface halite layers. The classification of spring and stream waters to the groups of (1) volcanic alternation and (2) leaching of evaporites was also observed by Risacher & Fritz (1991a), who extensively studied the geochemistry of salars in the southern Bolivian Altiplano. Streams during sampling campaigns were not dried up, although sampling took place during the dry season. Hence, the streams cannot be exclusively fed by rain and surface runoff, but also by springs discharging from the flanks of the volcanic mountains. This explains the enrichment of Na and Cl in these waters.
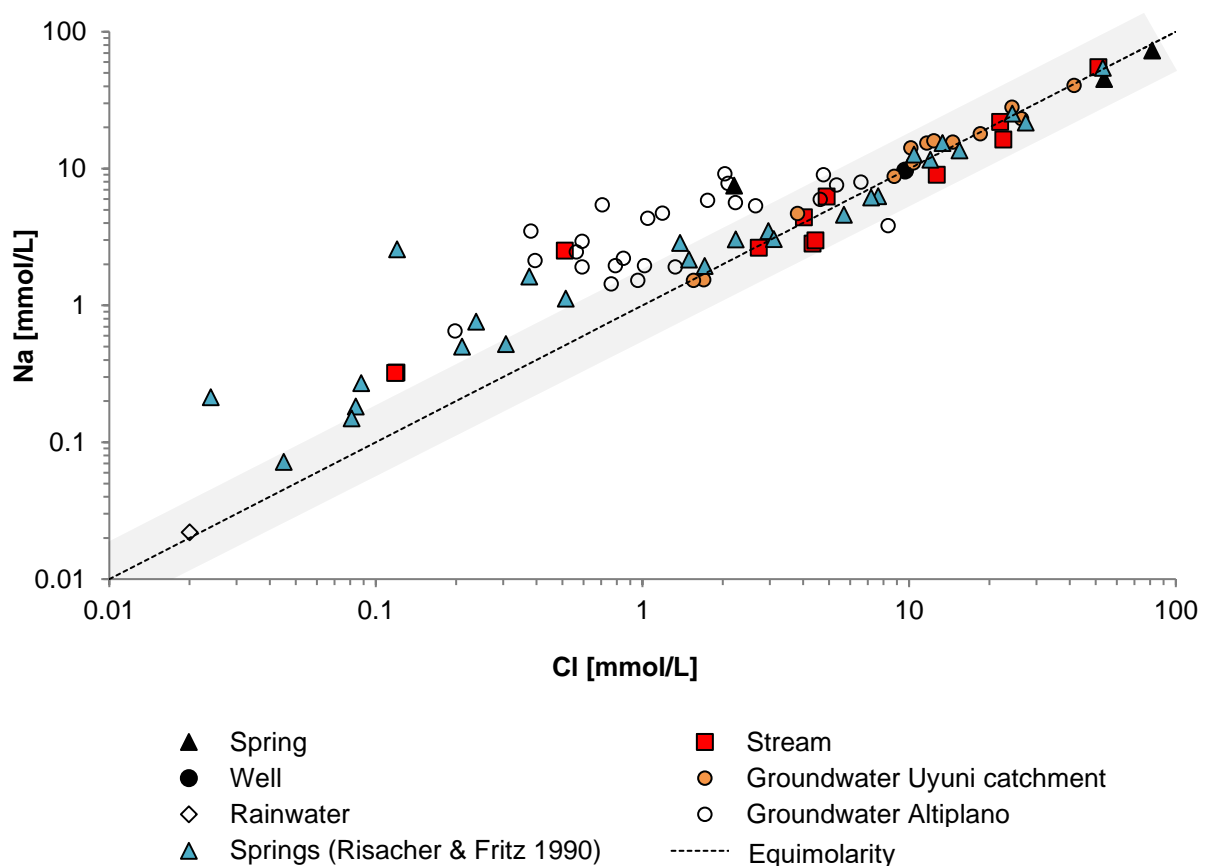
Fig. 42:   *Logarithmic scatter plot of Na versus Cl in the catchment samples supplemented by analyses from former studies (Rainwater: Risacher (1991b), groundwater Uyuni catchment: Nittetsu Mining CO. (2011), groundwater central Altiplano: Ramos Ramos et al. (2012)); waters plotting inside the grey shaded area were affected by the leaching of halite, water plotting above were affected by the alteration of volcanic rocks*

The distribution of Na and Cl in waters leaching halite layers was also found in inflows to the Salar de Atacama (Boschetti et al. 2007). Rainwater from the southern Altiplano region is significantly lower mineralized regarding Na and Cl, showing the absent influence of seawater but rather the origin of southern Altiplano rainwater in the Amazon basin. Groundwaters in the Uyuni catchment are strongly affected by the dissolution of ancient evaporates in the

underground, as they plot on the line of Na-Cl equimolarity. For comparison, groundwaters from a study of the catchment of Lake Poopo in the central part of the Altiplano basin were plotted (Ramos Ramos et al. 2012). These waters, which stem from aquifers located in a volcanic environment, seem to contain generally less NaCl, and furthermore deviate from the line of equimolarity towards an excess of sodium. Another effect leading to the increase of Na and Cl in groundwater compared to precipitation, is the evaporation of rainwater prior to infiltration to the ground and the corresponding enrichment of solutes, as well as the dissolution of salt efflorescences in the rainwater. These thin salt crusts form at the end of the rainy season and occur on the surface in large areas of the catchment, especially in the floodplains.

5.2.4 Geochemical aspects

Altogether 12 rock samples were taken in the catchment of the Salar de Uyuni. Samples stem from the flanks of the volcanoes Iruputuncu, Olca and Uturuncu, which represent the geochemical signature of the region and are of stratovolcanic nature (Fig. 43). The integration of rock samples into the QAPF (Streckeisen) diagram is shown in Fig. B - 4. All analyzed rocks are classified as rhyolites and dacites (Table 9). This is in accordance to literature data, where they are described as the major rock types in the volcanic region of southern Bolivia (Fernández et al. 1973, Rettig et al. 1980). According to the chemical composition, all sampled rocks are siliceous volcanics. SiO_2 contents are between 50 and 70 wt%, but mostly in the range of 60 wt%. Hence, most rocks are of acidic nature, belonging to one of the rock types rhyodacite, dacite or rhyolite. The least acidic rock, found at volcano Olca, is classified as a calc-alcaline andesite (field 9* in the Streckeisen diagram). In comparison to lavas from the adjoining Argentinian Puna and the northern Chile strato-volcano complexes, the rocks of the SW Bolivian strato-volcanoes are significantly more siliceous. This is assumed to be the result of magma generation occurring in different crustal levels (Fernández et al. 1973). Geophysical investigations have shown that magma generation in the southwestern Bolivian Altiplano takes part in the upper crust, in an estimated depth of 9 to 26 km (Ocola et al. 1971). Presumably, the magma in this region stems from the (partial) melting of the upper crust rather than having its origin in basaltic magma (Fernández et al 1973). Analyzed rocks were apparently in a low stage of alteration, as they do not show typical chemical characteristics of altered rocks, where K_2O or Na_2O are >6%, and SiO_2 is >80% (U.S. Geological Survey & Servicio Geológico de Bolivia 1992).

Table 9: Overview of rock samples with source region and rock types according to the QAPF diagram (see Fig. B - 4)

Sample	Location	Description	Rock type
IRU-ROC-01	Volcano Iruputuncu	Pyroclastic	Dacite
IRU-ROC-02	Volcano Iruputuncu	Pyroclastic	Rhyodacite
IRU-ROC-03	Volcano Iruputuncu	Pyroclastic	Rhyolite
IRU-ROC-04	Volcano Iruputuncu	Pyroclastic	Dacite
OLC-ROC-01	Volcano Olca	Pyroclastic	Andesite
OLC-ROC-02	Salar de la Laguna	Lava	Rhyodacite
UTU-ROC-01	Volcano Uturuncu	Pyroclastic	Rhyolite
UTU-ROC-02	Volcano Uturuncu	Pyroclastic	Rhyolite
UTU-ROC-03	Volcano Uturuncu	Lava	Rhyolite
P-1A	Laguna Colorada	Pyroclastic	Dacite - Andesite
P-1B	Laguna Colorada	Pyroclastic	Dacite - Andesite
R-02	Vicinity of stream Río Quetena	Pyroclastic	Rhyolite

According to Fernandez (1973), the volcanic rocks of Cenozoic age in the SW of Bolivia can be divided into four units:

1) Lavas and pyroclastics of the Rondal and Julaca formation (Miocene)
2) Ignimbrites of the Quechua Formation (Miocene to Pliocene)
3) Ignimbrites of the Ignimbrite Formation (Pliocene to Pleistocene)
4) Lavas and pyroclastics of the Strato-volcano Formation (Pleistocene to Holocene)

Lithium concentrations in the rocks range from 4 to 37 mg/kg (Fig. 44). In acidic igneous rocks, the element is contained in silicates and aluminosilicates replacing magnesium, aluminium or iron (Cannon et al. 1975). Parker (1967) reports average values from 22 to 65 ppm Li in igneous rocks. Hence, the samples from the SW Altiplano are not significantly enriched in Li, but are in accordance to Li concentrations of 16 – 65 ppm obtained by Davis & Howard (1982) from ignimbrites of the Ignimbrite and Los Friales Formations in SW Bolivia. Sampled rocks from volcano Iruputuncu and Olca show decreased concentrations of Li. Both volcanoes are located in the southwestern vicinity of the Salar, in a distance of about 50 km. In contrast, Li in rock samples from the southern catchment is about twice as high. Thus, the assumption of rhyolitic rocks in the southern catchment being the main contributor to lithium in the salt lake is confirmed by the rock analyses.
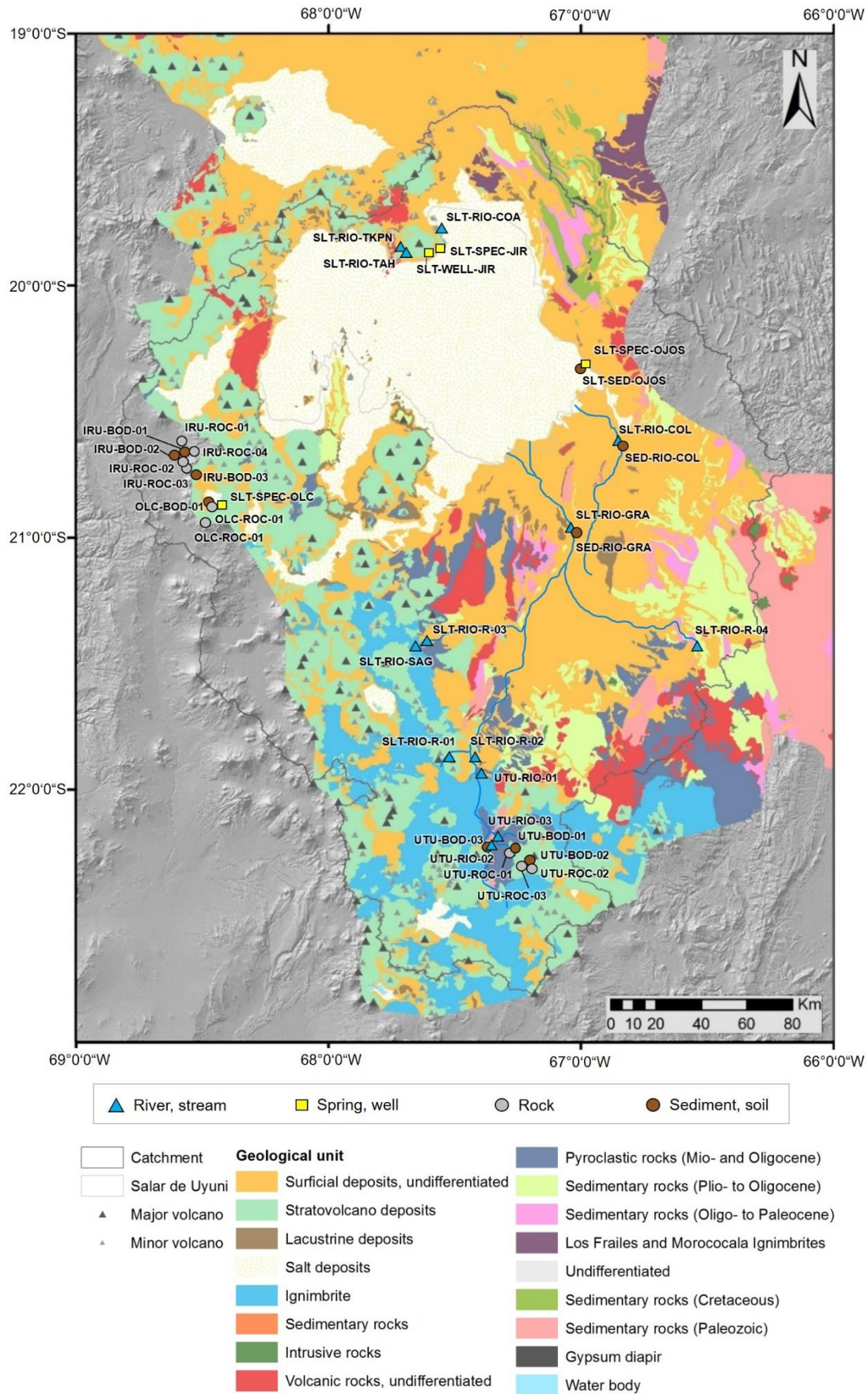
Fig. 43: *Overview of freshwater, rock and sediment sampling sites in the catchment of the Salar de Uyuni, with geological units illustrated in the background*

Rock samples were treated by different digestion methods in order to gain information about the fixation of lithium to the mineral structure and its tendency to be leached. Thereby, the total digestion by HF serves for the analysis of the insoluble fraction, whereas the aqua regia digestion determines the acid-soluble fraction. Results show that a significant part of the lithium contained in rocks is susceptible to leaching by the weathering of surface rocks in the long term.
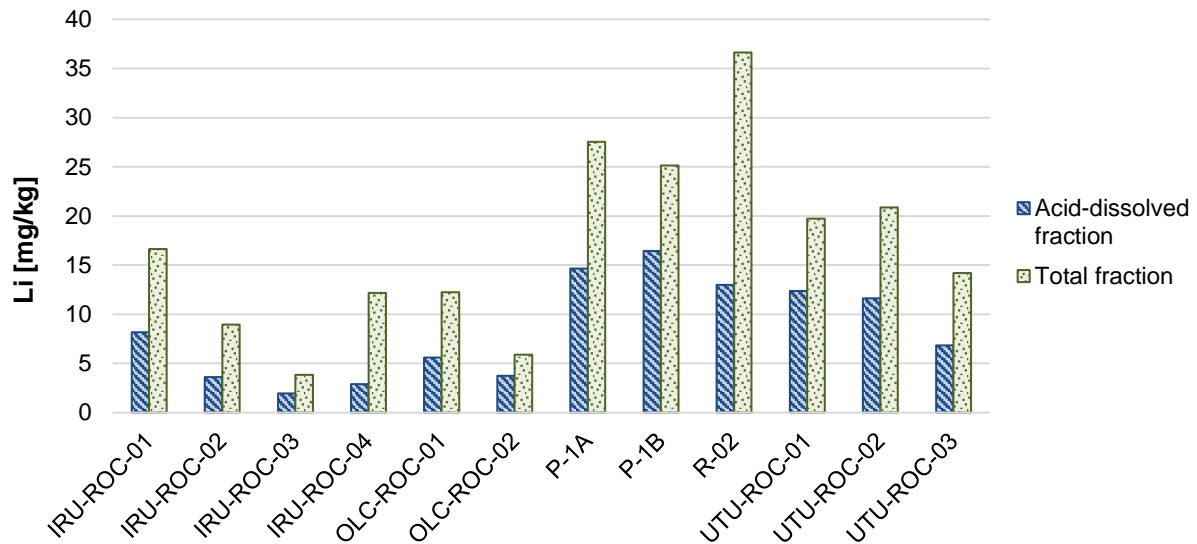
Fig. 44: *Li concentration in rock samples in the catchment of the Salar de Uyuni (acid-dissolved fraction determines the lithium dissolved by aqua regia, total fraction was obtained by HF digestion)*

Unconsolidated material analyzed for chemical composition consisted of soils and surface sediments sampled in the catchment, mainly from a volcanic environment, lacustrine sediments from the mud layer underneath the uppermost salt crust in the Salars of Uyuni and Coipasa, and river bed sands sampled from the shore of the Río Grande and Río Colorado (Table 10).

Lacustrine sediments were eluted with deionized water (DI) prior to digestion in order to obtain the fraction of Li contained in salts and secondary precipitates formed after sampling. HF digestion served for the determination of the acid-insoluble Li fraction in sediments, whereas aqua regia digestion was used for determining the acid-soluble Li content. Generally, the content of acid-soluble components in sediments and river bed sands represents the exchangeable fraction, whereas the acid-insoluble components represent the general mixed source rocks (Tan et al. 2012). Total Li contents in sediments from volcano flanks in the Salar de Uyuni catchment are in the range of 5-28 mg/kg. Sediments from volcanoes Iruputuncu and Olca show minor concentrations, which is consistent with results from rock analyses explained above.

Table 10: Overview of soil and sediment samples for element analysis from the Salar de Uyuni and its catchment, and the Salar de Coipasa

Sample	Location	description
Lacustrine sediments		
COI-SED-A2	Shallow drill hole at Salar de Coipasa	20-25 cm depth
COI-SED-SHORE	Southern shore of Salar de Coipasa	Black muddy sediment from 10 cm depth
SLT-SED-RIO-01-1	Shallow drill hole at site RIO-01	brownish layer in 10-20 cm depth
SLT-SED-RIO-01-2	Shallow drill hole at site RIO-01	black coloured layer in 30 cm depth
SLT-SED-OJOS	Gas emanation spot "Ojos del Salar"	Reddish coloured muddy sediment
SLT-SED-NOR-T3-1	shallow drilling in the northern transect of Uyuni	Grey coloured layer, depth of 8-9 cm
SLT-SED-NOR-T3-2	shallow drilling in the northern transect of Uyuni	Brownish sediment, depth of 25 cm
River sediments		
SED-RIO-GRA-1	Río Grande	shore sediment
SED-RIO-GRA-2	Río Grande	5 m distance from shore, depth 2-5 cm
SED-RIO-COL-1	Río Colorado	shore sediment
SED-RIO-COL-2	Río Colorado	5 m distance from shore, depth 2-5 cm
Soils from catchment		
IRU-BOD-01	Iruputuncu	Fumarole flank; yellow, fine grained
IRU-BOD-02	Iruputuncu	Edge of volcano crater; white, fine grained
IRU-BOD-03	Iruputuncu	Base of volcano; reddish
OLC-BOD-01	Olca	Base of volcano; black / grey, coarse grained
UTU-BOD-01	Uturuncu	Base of volcano; brown, coarse grained
UTU-BOD-02	Uturuncu	Volcano flank; reddish, coarse grained
UTU-BOD-03	Stream close to village Quetena Chico	Light brown, fine grained
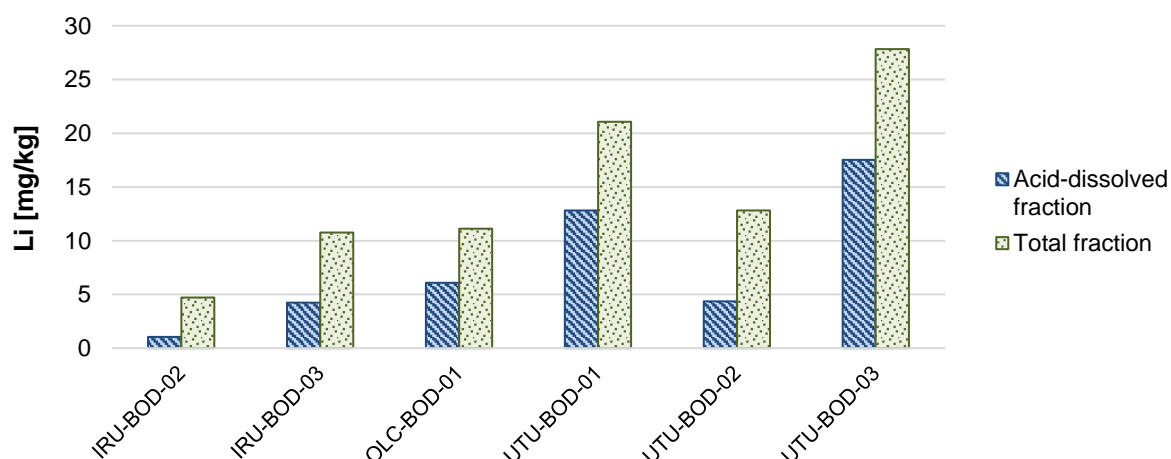
Fig. 45: Lithium in unconsolidated sediments from the surface in the catchment of the Salar de Uyuni (acid-dissolved fraction determines the lithium leached by aqua regia, total fraction was obtained by HF digestion)

Based on the different variations of digestion (DI elution, aqua regia, HF; for details see Fig. 20), Li concentration in different fractions of the sediment was calculated according to the following equations (all units are in mg/kg):

$$c(Li_{salt}) = c(Li_{AR}) - c(Li_{AR-DI}) \tag{14}$$

$$c(Li_{exchange}) = c(Li_{AR-DI}) \tag{15}$$

$$c(Li_{silicates}) = c(Li_{HF-DI}) - c(Li_{AR-DI}) \tag{16}$$

Here, $c(Li_{salt})$ defines the fraction of Li in salts precipitating secondarily from the brine that is contained in the sediment pores. $c(Li_{salt})$ is calculated from the difference of Li concentration obtained by aqua regia digestion $c(Li_{AR})$ and the Li concentration in samples which were eluted with DI prior to aqua regia digestion ($c(Li_{AR-DI})$). The concentration of this fraction is expected to reflect the Li concentration in the interstitial brine $c(Li_{brine})$ occurring at the sediment sampling site and depth. In fact, a positive correlation exists between $c(Li_{salt})$ and $c(Li_{brine})$ at all locations (R^2=0.84). The concentration of Li in the exchangeable fraction $c(Li_{exchange})$ corresponds to the Li fraction obtained by samples eluted with DI prior to aqua regia digestion ($c(Li_{AR-DI})$). According to Martin et al. (1991), leaching using HCl presumably determines easily leached ions from cation exchange sites in clay minerals, carbonates and soluble metal oxides. In contrast, HF/HClO$_4$ dissolution contains more resistant fractions as silicates and organic matter (Martin et al. 1991). The Li fraction contained in silicates $c(Li_{silicates})$ was calculated as the difference of the Li concentration in samples which were eluted with DI prior to HF ($c(Li_{HF-DI})$) and aqua regia digestion, respectively. The distribution of Li in lacustrine sediments of the Salars of Uyuni and Coipasa is shown in Fig. 46.
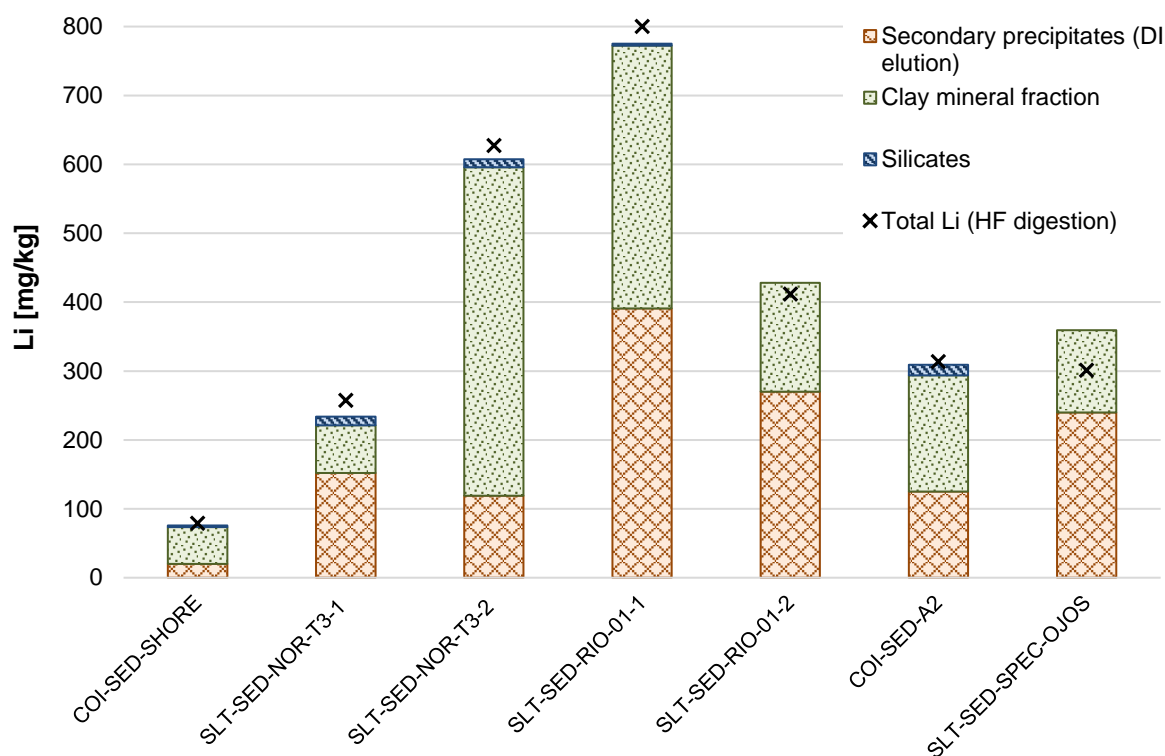
Fig. 46: *Concentration of Li in different fractions of sediments of the Salars of Uyuni (SLT) and Coipasa (COI) resulting from chemical analysis after DI, aqua regia and HF extraction*

The high concentration of Li in sediments from the northeastern part (SLT-SED-NOR) and the delta region of the Río Grande (SLT-SED-RIO) reflects the brine chemistry at these locations. Not only the Li content in secondary precipitates is high, but also the exchangeable Li fraction. The low fraction of acid-insoluble Li shows, that the element is readily released from sediments, accumulating in the surrounding brine. In the delta region of the Río Grande, fluviodeltaic sediments permanently transported within the river load are interbedded with lacustrine layers steming from the sedimentation of both organic and inorganic material during the last lake phase. Both sedimentary units are covered by a thin salt crust, whose thickness increases and moisture decreases with further distance from the shore.

5.2.5   Recent annual salt and sediment input to the salar

The Río Grande de Lipez and the Río Colorado are the main rivers reaching the Salar de Uyuni, feeding the salt lake from the southern and southeastern side. They drain the cordilleras of Chocaya and Lipez, which host numerous up to 6,000 m high snow-capped mountains. During the rainy season, they mainly carry water from intense precipitation events occurring in the catchment. In the dry season, river flow mainly consists of spring waters carried by various tributaries from geothermal springs located at the mountain flanks, occasionally supported by snow melts. In December 2011, a diver (water level recorder) was installed in the Río Grande

river, about 30 km upstream from its mouth. Details about installation are contained in Sieland (2014). The original water level data were corrected for air pressure, which was simultaneously recorded on the island Incahuasi located in the Salar de Uyuni. Results are shown in Fig. 47.
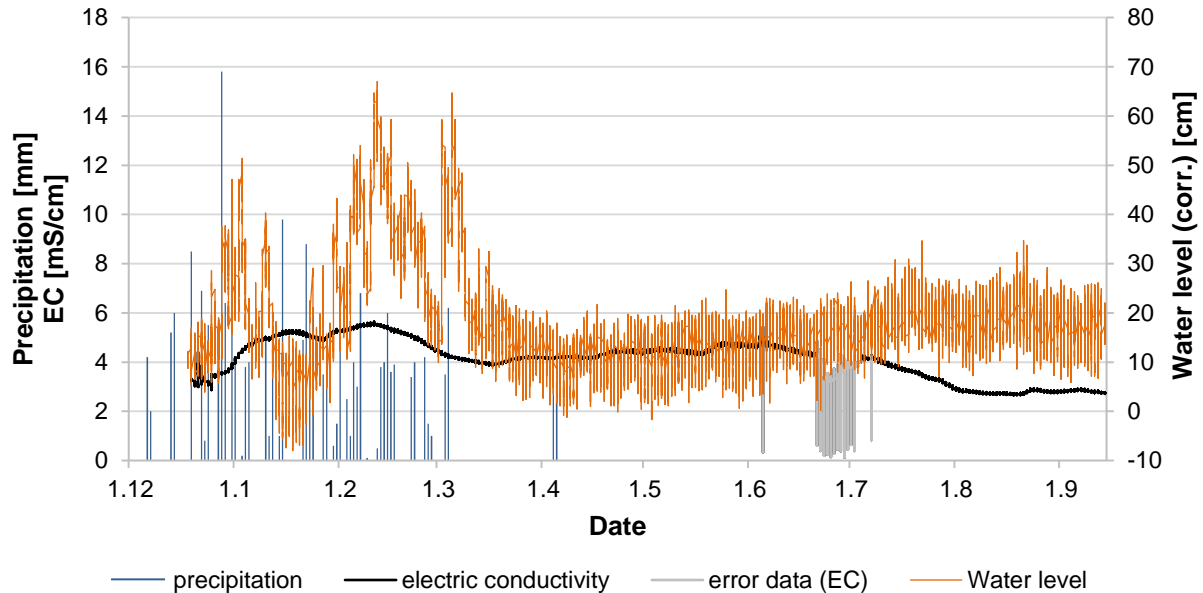
Fig. 47:   *Recorded data (EC and water level) in the Río Grande river obtained by Sieland (2014). Precipitation data were obtained from a nearby meteorological station (San Pablo de Lipez). Baro-compensated river level measurements run from 18.12.2011 to 14.09.2012.*

Precipitation data stem from a meteorological station in the catchment of the Río Grande, thus representing the amount of rainfall that is typically reaching the river. Error values occured for water level and electric conductivity values, when the measured water temperature dropped below the value of -0.5°C. In Fig. 47, the water level and the EC were corrected for implausible values by excluding data measured at a temperature < 0.5°C. The grey curve of electric conductivity shows defective values between June and July. Taking a look at air temperature data during the implied time span shows indeed, that minimal temperatures dropped below -15°C at a high number of days. The graphic shows, that the water level of the river strongly reacts on the occurrence of rainfall events. Also, a relatively small time shift from rainfall events to the increase in water level is visible. With the onset of heavy rainfall at the beginning of the austral summer, the salinity of the water distinctly increases (Fig. 47). This is due to superficial salt efflourescences (salt coatings) formed by chemical and physical weathering during and after the former rainy season. These efflourescences occur in wide parts of the river catchment and are dissolved in the rainwater, which does not immediately infiltrate due to the dry cemented surface. Instead, it flows towards drainage channels and finally to the streams, carrying the solved material as well as suspended detritus. The maximum of water salinity, and thus the maximum load of dissolved solutes, peaked in the mid of February 2012. At the end

81

of the rainy season, when rainfalls decline in volume and intensity, the EC values decrease until a steady value is reached. Generally, the salinity is characterized by a low range especially during the dry season, indicating homogeneous conditions throughout the austral winter months.

The calculation of the recent amount of solutes and especially lithium transported towards the salar is rather complicated. The amount of water as well as the composition of dissolved and suspended matter in the tributary waters reaching the salar are strongly season depended variables. Ballivian (1981) roughly measured the flow rate with 1 m³/s during low-level times and 4 m³/s during the rainy season. Assuming an average amount of 4 low-level and 8 high-level months, the overall flow rate of Río Grande would be 2 m³/s and 63 Mio m³/a, respectively. Risacher (1991) estimated an annual discharge of 60 ± 30 x 10⁶ m³, which corresponds to 1 - 2 m³/s. Table 11 gives an overview of Río Grande discharges mentioned in different references. Based on own field observations, the flow rate of Río Colorado could be conservatively estimated with 1 m³/s, whereby literature data for comparison is lacking.

Table 11: Estimation of Río Grande discharge according to different references

Reference	Low-level months [m³/s]	High-level months [m³/s]	Annual discharge [10⁶ m³/a]
Montes de Octa (1997)			400
Ballivian & Risacher (1981)	1	4	63
Risacher & Fritz (1991)	-	-	60 ± 30
Knight Piésold Consulting (2000)	0,381 (Nov. 1997)	1,55 (Feb. 1998)	24

The total amount of components W transported in dissolved form to the salt lake by the Río Grande within one year is estimated according to the following equation:

$$\sum W = Q \cdot C_{dissolved} \cdot 10^{-6} \qquad (17)$$

Assuming an annual discharge Q of $60 \pm 30 \cdot 10^6$ m³ with a TDS of 2 g/L and a Li concentration $C_{dissolved}$ of 2.7 mg/L in the Río Grande, an amount of 120,000 ± 60,000 t dissolved components including 160 ± 80 t Li is added to the brine of the upper crust per year. For the accumulation of ~7 Mio t of Li, it would have needed between 29,000 and 87,000 years (under the assumption of steady conditions), which is significantly more than the estimated 10,000 years which has elapsed since drying of paleolake Tauca. Not considered here is the input of Li by other tributaries as the Río Colorado. With a Li concentration of 1.5 mg/L and a discharge about the half of Río Grande, its Li input to the Salar de Uyuni should not be more than ⅕ – ¼

of Río Grande input. Still, the range between 10,000 years, estimated from ^{14}C in the brine, organic matter and carbonates, and at least 29,000 years determined from the salt-water balance of the main inflow is large. The difference is probably due to the input of Li by suspended sediments, which are transported especially during the wet season towards the Salar.

Fig. 48: Surface of the Salar de Uyuni in August 2014 (left) and at the end of the rainy season in May 2011 (right); note the layer of dusty particles consisting of weathered material from the vicinity of the Salar as a result of wind transport

A parameter that cannot be estimated quantitatively due to missing data is the input of material by windblown dust. Strong winds occurred regularly during the field trips, especially in the evening hours and during storm events. In August 2014, the salt surface was covered with a thin dusty layer, consisting of clayey material from the surrounding floodplains and bare soil (Fig. 48). In contrast, the sediment layer is covered by a few mm thick, newly crystallized salt crust at the end of the rainy season. The chemical analysis of salt from the upper mm of the crust at polygons and efflorescences included the determination of the content of insoluble material. It showed that the percentage of insoluble matter in the uppermost salt crust is relatively low with 0.1 – 1 wt% in the polygon surface and 0.3 – 2.3 wt% in the efflorescence. Unfortunately, the mass of each sample was not sufficient for a chemical digestion and could thus not be analyzed for the content of e.g. Li. The sediment mainly consists of accumulated salts and clay, which originates from the surrounding mountains subject to weathering processes, and was transported to the floodplains with rivers and streams. Thus, the lithium content is supposed to be elevated as is the case for analyzed sediment from the delta region (see chapter 5.2.4). Nevertheless, though the percentage of sediment in the upper salt crust seems to be small, the influence of windblown dust should not be neglected in the overall lithium balance. The annually recurring process during geological time scales in combination with the large surface of the salt lake leads to a significant accumulation of lithium enriched material in the salt crust.

The annual growth of the salt crust was estimated using the following equation:

$$G_{10,000a} = \frac{TDS_{inflow} \cdot Q_{inflow} \cdot 10^{-6}}{\rho_{salt}} \cdot \frac{1}{A_{salt\ lake}} \cdot 10,000 \qquad (18)$$

Where $G_{10,000a}$ is the growth of the salt crust in mm in 10,000 years, TDS_{inflow} and Q_{inflow} the dissolved load and discharge in g/L and m³/a, ρ_{salt} the density of the salt crust in g/cm³ and $A_{salt\ lake}$ the surface area of the salt lake in km². The growth of the salt crust, under consideration of only the Río Grande input, would amount to 80±40 mm/10,000 a. However, the total input must be much larger than that due to countless streams and channels transporting dissolved and suspended material towards the salt lake during the rainy season.

5.3 Evolution of brine

The enrichment of Li and other elements in the brine by sorption and precipitation reactions has been previously discussed. Following, the role of evaporation will be examined in more detail. The climatic and geomorphologic conditions resulting from the geographic position of the Altiplano and the catchment of the Salar de Uyuni explain the high significance of evaporational processes on the enrichment of elements in surface waters. The potential evaporation of 1,500 mm in this region strongly exceeds the average amount of annual precipitation (180 mm). This high evaporation is due to high solar insolation resulting from low cloud coverage most time of the year, extremely low air humidity at daytime and strong winds. These so-called lake - sea breezes form by differences in air pressure between salt surface and the surrounding land, resulting from different heat capacities of salt and soil. The following consideration of evaporational concentration is divided into the enrichment of Li along its flow path from source to sink, and the final accumulation in the pores of the salt crust.

5.3.1 Enrichment of lithium along the flow path

The progress of Li concentration in different compartments of the geologic and hydrologic cycle is shown in Fig. 49. The first stage is mechanical rock weathering, by which solid rocks are decomposed and made vulnerable to the processes of chemical weathering. As a result of chemical weathering, soils and sediments form, which cover large parts of the catchment of the Salar de Uyuni. At this stage, the Li concentration remains more or less constant, meaning that lithium is not liberated into dissolved form by the processes of physical and chemical weathering. A important result of weathering is the formation of secondary minerals as clay minerals, oxides and hydroxides. A significant enrichment of Li occurs, when surficial

sediments are swept away by heavy rainfalls during the wet season, carried by small streams and transported along the main rivers towards the Salar de Uyuni (Fig. 49). It is thinkable that Li, contained in dissolved form in the river water, is sorbed to the surface of the clay fraction in fluviatile sediments. This material is then sedimented at the shores of the river bed when flow velocity decreases in the widespread delta regions shortly before entering the salt lake. Lacustrine sediments occurring underneath the uppermost salt crust, show elevated concentrations of Li compared to fluviatile sediments, due to the higher content of clay and the equilibrium, which is established between Li sorbed to the clay fraction of lacustrine sediments and the surrounding brine, which shows Li concentrations of more than 1,000 mg/L in the areas of existing and former inflows.
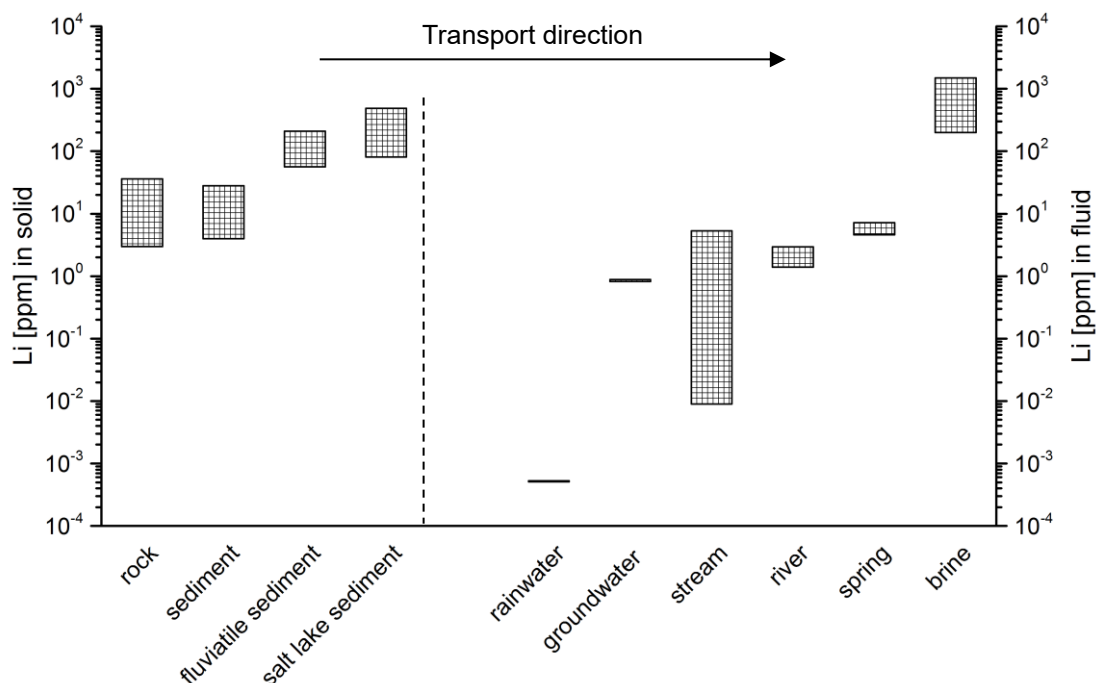
Fig. 49:   Trend of lithium concentrations in the Salar de Uyuni catchment along the path from source (= rock) to final sink (= brine)

As expected, rainwater shows an extremely low Li concentration. Hence, a large difference exists between Li in rainwater and groundwaters in the southern part of the Bolivian Altiplano. These groundwaters are already enriched in Li, because they are in contact with 1) Li-enriched volcanic rocks as rhyolites, ignimbrites and ash flow tuffs; and 2) hydrothermal waters of volcanic origin. The largest range in Li concentration (9 µg/L – 5 mg/L) occurs in the small streams and tributaries feeding the larger rivers flowing towards the Salar de Uyuni, which is due to their different origins. Some of the streams are fed by springs containing mainly rainwater, whereas others have a hydrothermal source and are therefore enriched in elements as Li and B, or have their source in local groundwater, which is naturally enriched in Li as

explained above. Sampled springs, especially thermal springs, contain Li up to 7 mg/L, resulting from their hydrothermal nature in a volcanic environment. Concentrations are in the same range as hot springs (T = 70 – 100°C) in the Yellowstone Park, USA, or in the Wairakai region, New Zealand (White 1957).

Evaporation of river water along the course from the mountains to the deepest part of the basin contributes to the enrichment of Li in solution, because no limiting Li-minerals exist. This is intensified by the extremely gentle gradient in the lower part of the catchment, i.e. in the region of extended floodplains before entering the salar. Fig. 50 shows the profile of Río Colorado with a length of almost 90 km, whereby the lacustrine coastal plain extends over ¾ of the distance. Donselaar et al. (2013) measured a difference of only 3 m over 36 km at the Río Colorado, which is a gradient of 0.083‰. Further, a wide river channel goes along with a low water depth of about 0.5 – 1 m in average, resulting in a high water surface and thus an increased evaporation surface (Fig. 50). During the rainy season, this surface is even increased by the reactivation of abandoned river channels (braided river systems).
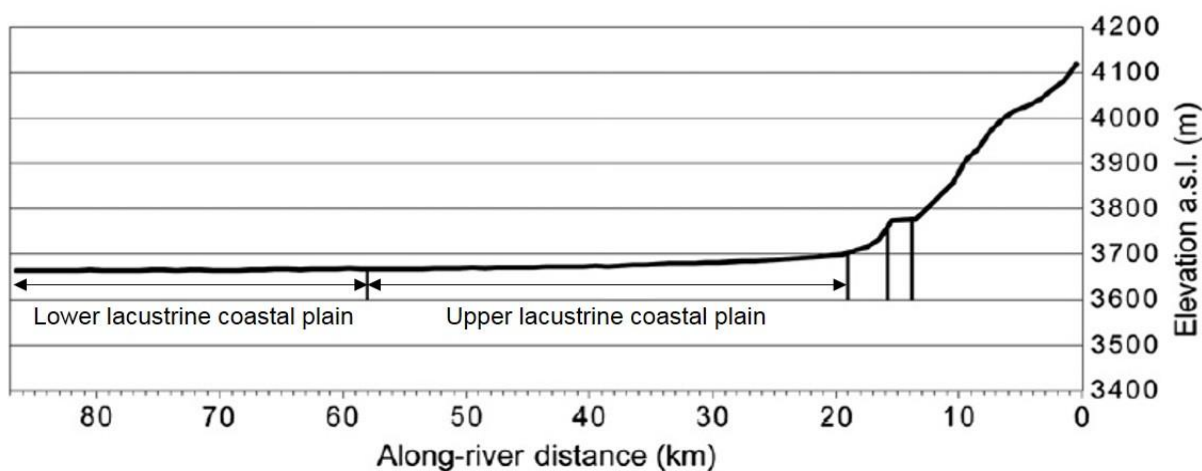
Fig. 50: Present-day down-stream profile of the Río Colorado (adapted from Donselaar et al. (2013))

However, two orders of magnitude in Li concentration are between surficial catchment waters and the interstitial brines of the Salar de Uyuni, which cannot be the result of evaporative enrichment along the flow path.

5.3.2 Concentration during evaporation

For the investigation of enrichment and depletion processes of main ions in the brine in the course of evaporative concentration the comparison to a conservative ion is helpful. Chloride, which is usually used for that purpose, is not suitable due to the dominance of halite in the salar system. Bromine is incorporated into halite only in very small quantities, and overall concentrations in brine are lower than for lithium. Thus, it is suitable for the analysis of the behaviour of other brine components with further brine concentration. Element proportions were compared to the curve of simple evaporative concentration. The calculation of this line was based on the ratio of an ion to bromine in the main inflow Río Grande and its trend according to a simple evaporative concentration, disregarding precipitation, sorption or other enrichment and depletion processes. Ratios were calculated as mean values from 4 samples taken in winter and summer seasons of different years and showed deviations between 3 and 6.0%, implying a high stability of main ion composition over time. Ratios of Mg, K, Li and SO_4 to Br in Río Grande water were 50, 40, 4, and 400. The trends of main ions in brine compared to Br are shown in Fig. 51, divided in well and transect brines, from Uyuni and Coipasa. Sampling in the Río Grande delta area is, since several years, impossible due to the status of the region as military restricted area and the all-season humidity leading to the impossibility of an access by car. That's why, values from Rettig et al. (1980) for the Río Grande delta were included in the evaluation.

Sodium concentrations constantly decrease with increasing bromine, due to the precipitation of halite in the saturated solutions (Fig. 51). The decrease of sodium goes along with nearly stable chloride contents with further brine concentration, caused by the strong predominance of chloride over sodium at the onset of halite precipitation. The slope of sodium decrease is shallower for the Coipasa brines, which could be due to higher sodium and lower chloride concentrations in Coipasa inflows. In fact, when comparing the molar ratio of Cl to Na in the main inflow to the salars, the value of 0.8 for Río Lauca (calculated from river analyses in Lebrun et al. (2002)) is lower than 1.0 for Río Grande. Waters sampled in the Río Grande delta show an opposite trend of increasing bromine with increasing sodium. These brackish to salty waters, deriving from the inflow of the major river, lack significant contact time with the halite layers of the salar crust further north, so that these waters are not yet saturated with respect to halite. The sharp rise reflects the dissolution of the halite when reaching the surface of the salt crust. With further brine concentration, Na concentrations in the delta brines approximate to the concentrations in pore brines.
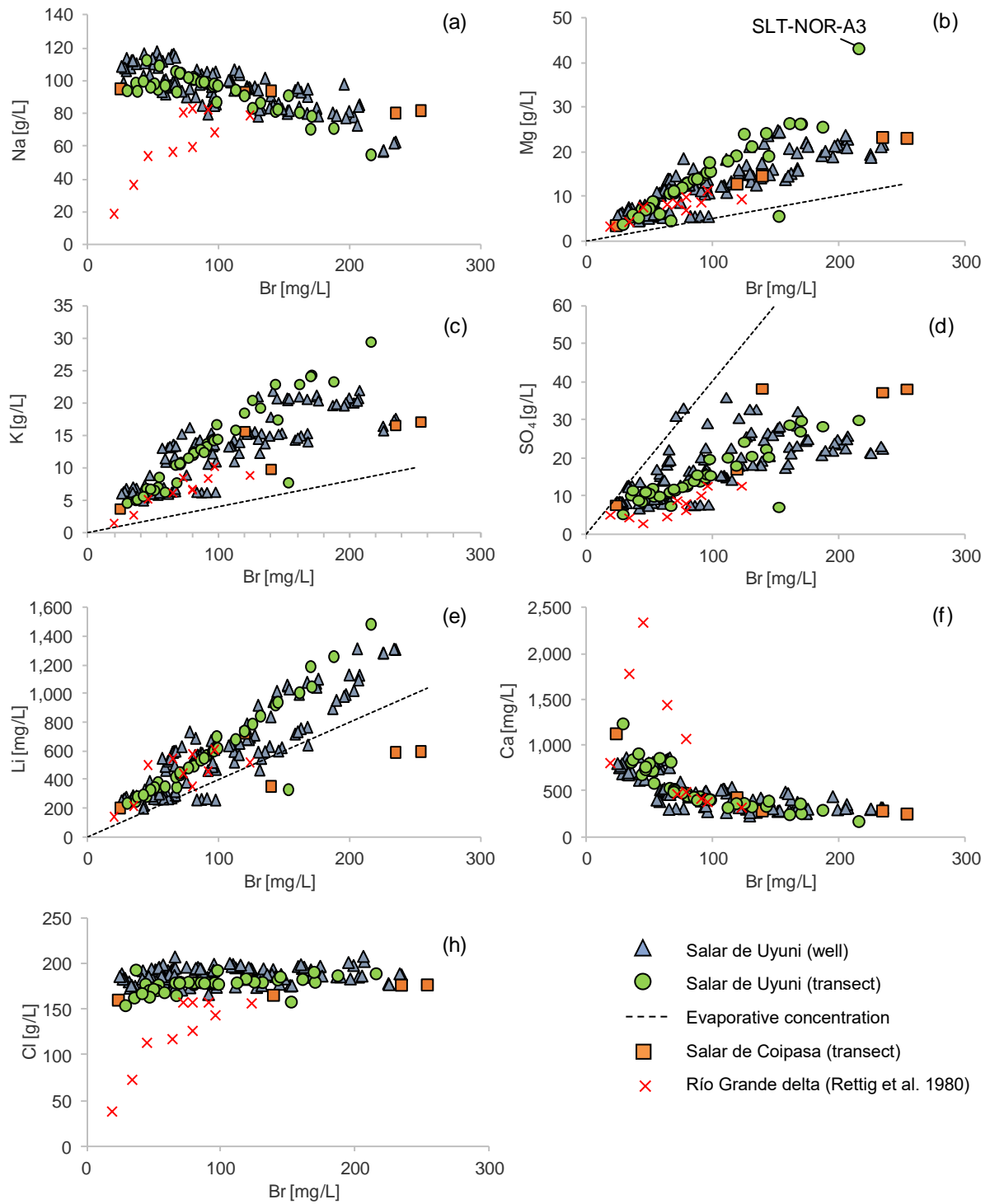
Fig. 51: *Bromine concentration in well brines and transect brines of the Salars of Uyuni and Coipasa plotted against the content of major ions in solution; values from the Río Grande delta were added for comparison*

The evaporation line in Fig. 51 is the calculated enrichment of the perspective element or species under the assumption that the Br concentration has not changed over time. On contrary to Na, Ca and SO_4 the elements Mg, K and Li plot significantly above the evaporation

line, giving evidence that these elements are enriched by means of evaporation and an additional process (e.g. via sorption on clay minerals).

Magnesium is correlated to bromine with increasing concentration ($R^2 = 0.7$) indicating that the element is not removed from solution by the formation of precipitates. Compared to the evaporation line, Mg is as said before additionally enriched in the pore brines. The concentrations of Uyuni transect brines plot above those of well brines indicating that the additional source of Mg delivers more Mg in the transect brines. Rettig et al. (1980) found a significant loss of magnesium compared to evaporative concentration in the Uyuni brines and even more in the Coipasa brines, and speculated about the uptake of Mg by silicates and carbonates. This could not be confirmed at all by these investigations.

Potassium concentrations plot as well above the evaporation line. This is especially the case for the transect brines. Thus, one can state that K and Mg behave similar. This could be due to the release of K and Mg from clay minerals, which are transported as suspended matter in the inflows and which are not included in the analytical procedure of river water due to filtration of samples. Two processes of K release are conceivable: the release of exchangeable K from clay mineral layers, and the dissolution of the clay mineral itself.

Lithium behaves partly similar to Mg and K regarding the enrichment in the brine compared to Br. However, in the first stages of brine concentration, Li plots on the evaporation line indicating the conservative behaviour of Li due to evaporation. At about 150 mg/L Br, Li plots above the evaporation line indicating an additional Li source. In the Salar de Coipasa transect, this effect is contrary and the curve of Li/Br is significantly flattened, pointing to the removal of Li from brine. On contrary, transect brines of the Salar de Uyuni plot above the evaporation line over the entire enrichment path pointing to the role of clay sediments in the enrichment of Li in surface-near parts of the brine-filled layers. This is supported by the fact that fluid samples were continuously taken from mud-dominated layers in about 50 cm depth. The trend of Li/Br in the delta brines above the slope of evaporative concentration shows, that the enrichment of Li apart from evaporative concentration takes place at the entry of the river water to the all-season flooded regions at the southern margin of the salar.

Especially the delta brines are depleted in **sulphate** compared to the inflow, which is due to the precipitation of gypsum. This theory is supported by the plot of Ca/Br, which shows a strong decrease of Ca with evaporative concentration (Fig. 51-f), especially in the first stages of enrichment. According to Jones et al. (1977), part of the observed sulphate loss can be explained by bacterial sulphate reduction. The process is evidenced in the H_2S-rich, lacustrine mud accumulations separating the halite layers and in the characteristic smell of the pumped brines. The removal of sulphate takes place as H_2S or by the formation of iron sulphides (Eugster et al. 1979). The precipitation of sulphate bearing minerals should play a minor role

in the removal of the ion, as PhreeqC modelling shows that most sulphate minerals are undersaturated in the brines. Saturation indices for epsomite, mirabilite and kieserite are in the range of -1.6 to -0.5, -0.9 to -0.4, and -2.6 to -1.3, respectively.

The sharp decrease of **calcium** in the delta brines is the result of gypsum precipitation due to oversaturation with respect to gypsum in the brine. Indeed, pore brines of the salar show slightly positive saturation indices for gypsum. Flattening and converging of the curve with increasing bromine reach equilibrium with approximately 300 mg/L Ca in the brine. The formation of gypsum is accompanied by the precipitation of calcite, which explains the significant removal of HCO_3 from the delta brines.

The Río Grande transports large amounts of suspended particles, which is intensified especially during and after the rainy season caused by the extended flooding of the upstream plains at the southern shore of the Salar de Uyuni. Suspended particles are not considered in the analysis of dissolved ions by IC and ICP-MS. Thus, suspended matter is not included in the overall balance. During the flow of the Río Grande a separation of suspended sediments takes place, depending on the size of particles and flow velocity of the river. Larger particles are deposited near the shore of the salt flat, where flow velocity is strongly reduced, whereas small particles are transported towards the center of the salt lake. When being in contact with brine, chemical weathering goes along with the constant decomposition of clay particles and the release of incorporated ions as Mg, K and Li. The specific conditions like the high salinity of the pore brines, combined with the high duration of reaction time, extreme day / night temperature variations are effective weathering factors. The dissolution of the clay mineral lattice could be a mechanism of K and Li release from clay minerals. Lithium shows a similar behaviour as K and Mg regarding the ratio to Br in brine, though to a minor extent. This might be explained by the minor amount of Li sorbed to clay minerals in comparison to K and Mg, and the preferential exchange of K and Mg.

A possible source of error could be, that the line of evaporative concentration does not exactly represent the K / Br ratio in the main inflow. Sampling in the Río Grande took place about 40 km upstream of the delta to the Salar de Uyuni. In the course of waterflow until that sampling spot K in the water could be subject to sorption reactions with clay particles contained in the river water. Hence, the K / Br ratio changes significantly along the river course from source to sink. Tributaries, which were sampled as far as 100 km upstream from the Río Grande sampling site, should therefore show higher K / Br ratios. Indeed, this is the case for most streams, where ratios up to 200 were measured, compared to 40 in Río Grande.

SLT-NOR-A1 marks a location, which differs significantly regarding chemical composition compared to other transect samples. Not only main ions as Mg, K, Li, Br and B are significantly

higher, but also minor elements like Rb, V, and Cs. A systematic error by means of a constant relative deviation does not occur, hence a dilution error can be excluded.

Generally, well brines show a larger variation in ion / bromine ratios and are wider spread than transect brines, which have higher correlation coefficients. This may be due to the facts, that the transect samples stem from a relatively limited area, and were taken from a similar depth, compared to well brines, which origin from widespread locations on the salar and from depths differing between 0.5 and 12 meters.

Coipasa pore brines show differences in the ratio of Br to Na, K, Li and SO_4 with increasing brine concentration. Ca concentrations are generally lower, leading to the assumption, that the major amount of Ca has been removed from solution by the precipitation of gypsum, leaving a brine becoming more concentrated in sulphate due to evaporation. A similar origin of the transect brines in the northern part of Uyuni and the eastern part of Coipasa could not be confirmed by the chemical analyses. K and Li concentrations deviate, especially with increasing brine concentration (Fig. 51).

Gas emanation spots, locally called "Ojos del Salar" (= eyes of the Salar) occur in the salt crust at the eastern margin, about 1 km from the shore. These spots are characterized by open brine pools, where a crystallization and formation of a salt crust is inhibited by permanent flow of gas bubbles from the subsurface (Fig. 52). The open pools are filled with a brine comparable to the interstitial brine in the salt crust. Analyses showed that the TDS is about 15% lower than in the salt crust brine, indicating a freshwater source from the underground. Brine temperature is twice as high as brine from a near well (SLT-COL), which is due to the influence of solar insolation. CO_2 is the major component in the emerging gas bubbles according to the lab of the mineralogical department of TUBAF (oral communication). The low pH of 5.8 supports this observation. The hypothesis that groundwater rich in volcanic gases (CO_2) is forced to the surface at the interface between fresh groundwater and the brine of the salar is based on the Ghyben-Herzberg theory. However, due to the high density of the brine the interface is rather flat (approximately with a ratio of 1 to 4). The lithium content of 340 mg/L is significantly lower than in the nearby analyzed brine ($Li_{SLT-07-SAL}$ = 560 mg/L), which supports the mixture of brine with feeding freshwater sources. Water in the pools is strongly enriched in iron, values reach 40 mg/L compared to less than 200 µg/L in the well brines.

Fig. 52: "Ojos del Salar" – gas emanation spot located at the eastern margin of the Salar de Uyuni

5.3.3 Evaporation on the salt crust

In order to investigate the correlation of high Li concentrations in the brine with the occurrence of all-season wet regions on the salar, a Landsat image (December 2001, band 5) highlighting moist and water-covered areas was overlapped with the map of lithium distribution (Fig. 53). It is remarkable, that both the southern and the northern regions, where Li concentrations are highest, are characterized by a wet surface, which exists throughout the year (December is the final month of dry season). It is obvious, that the enrichment of Li in the brine correlates to the moistness of the upper salt crust and the duration of water coverage on the salt surface.
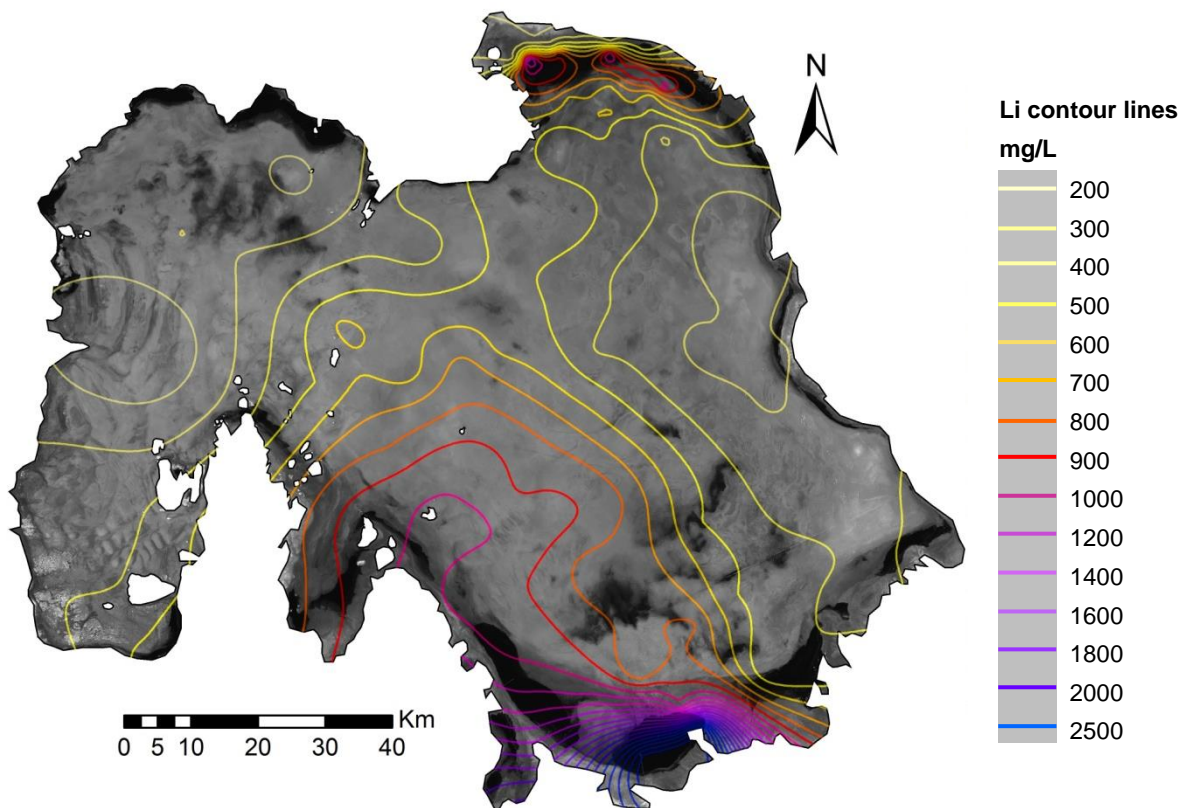
Fig. 53: Lithium contour lines as result of kriging plotted on a Landsat TM image (band 5) from December 2001 highlighting moist areas of the salar surface as dark shades

Altogether 23 spots on the Salar de Uyuni and Coipasa were sampled for the uppermost cm of the salt crust, whereby at 13 locations the salt efflorescences at polygon borders could also be sampled. Especially in the northern part of Uyuni the brine table is very shallow, in only a few cm depths. Hence, the salt surface is all-season wet due to capillary rise of interstitial water which impedes the formation of polygons and the associated building of salt efflorescences. At most locations the salt surface was covered with a fine layer of dust, which was especially distinct in the dry season of 2014, compared to the years before. In order to diminish the error when analyzing the salt composition, the percentage of the insoluble residue was determined and included in the mass balance. The pH value of the dissolved salt solutions showed little variation and was in the range of 8.3 – 8.8. The sum of dissolved elements and insoluble residues amounted to 91 – 98% of the initial weight, implying an analytical error between 2 and 9%. Thereby, the error inversely correlated with the percentage of NaCl in the sample. Thus, it is assumed that the missing amount to 100% is due to measurement uncertainties of the Na and Cl concentrations. As Na and Cl sum up to more than 95 wt% of the sample, already small analytical deviations in the range of 5% have a high influence on overall balance. A further source of error could be crystallization water contained in the mineral polyhalite, which is not removed by drying at 100°C and results in a falsified balance. The content of a specific ion in the salt was calculated according to the following equation:

$$content_{ion} \left[\frac{mg}{kg}\right] = \frac{c * V * 1,000}{m} \qquad (19)$$

Here, c is the concentration of an ion [mg/L] as measured with IC, V the volume of solvent [L] and m the initial weight [g]. The composition of crust and salt efflorescences is comprised in Table A - 11. The content of water-insoluble residues was in the range of 0.1 to 2.3 wt%, and mainly consisted of fine-grained wind-blown dust particles. Compared to the salt crust, efflorescences are strongly enriched in elements as Li, Mg and K, which is illustrated in Fig. 54.
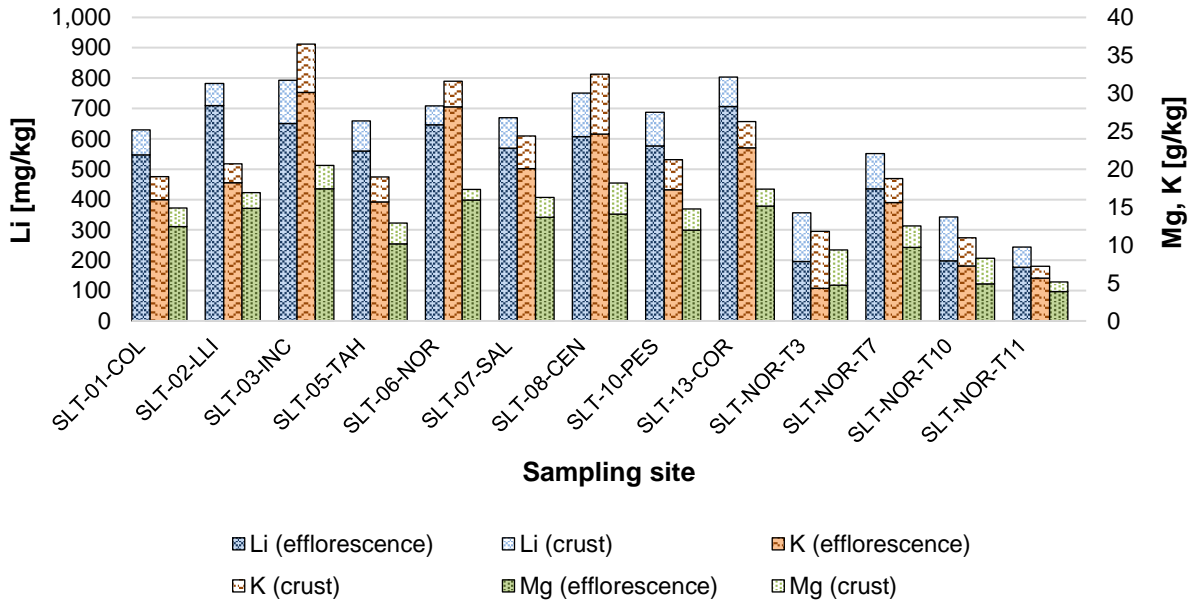
Fig. 54: Contents of Li, Mg and K in the upper cm of salt crust and salt efflorescences at polygon borders of the Salar de Uyuni

Literature values for the composition of the upper crust, which is located above the brine table, are not existent. Ericksen (1977) reported lithium concentrations between 1 and 60 ppm for 35 salt core samples from all over the Salar de Uyuni, but these samples stem from layers which are saturated with brine, and the distribution of elements, including lithium, probably reflects the composition of the circumjacent brine.

During the rainy season the surface of the salar is flooded by rain water to a depth between 10 and 50 cm. Thereby the water body behaves dynamic, meaning that it moves in dependence of wind direction and speed. Field observations showed that the system reacts very quickly to an increasing occurrence of wind, leading to a rapidly varying thickness of water cover. During this time, the uppermost centimeters of the salt crust are dissolved.

Fig. 55: Shallow, but closed water coverage on the surface at the Salar de Uyuni in May 2011 (left), and advanced stage of desiccation: collection of residual water along the polygon borders (right)

Field observations showed, that the polygons themselves with their specific shape and size persist during the time of water coverage (Fig. 55, left). Only the salt efflorescences at the polygon borders are completely dissolved. At the end of the rainy season the surface water quickly evaporates due to intense solar insolation which is supported by strong winds. Remaining water, which is now strongly enriched in lithium, potassium and magnesium due to the precipitation of halite, is collected at the polygon borders (Fig. 55, right) and infiltrates because of the high porosity along these lines. Hence, the brine table is filled up with a strongly enriched solution, leading to the accumulation of Li and other solutes in the brine over large time scales.

When the salt surface completely dried out, it turns into a very compact cemented crust of 10 – 20 cm thickness, which impedes the underlying brine from capillary rise to the surface. The ascent of brine is now restricted to the margins of the polygons, which do not completely close in the course of crystallisation and hardening of the uppermost crust at the beginning of the dry season. Capillary rise forces the brine to ascent along the polygon borders, until the final brine table is reached. Attaining the surface the water quickly evaporates, and the included salts completely precipitate according to their solubility coefficients. Hence, lithium and other solutes as Mg and K should be strongly enriched compared to the surficial salt crust within the polygons, which was confirmed by the analyses performed (Fig. 54).
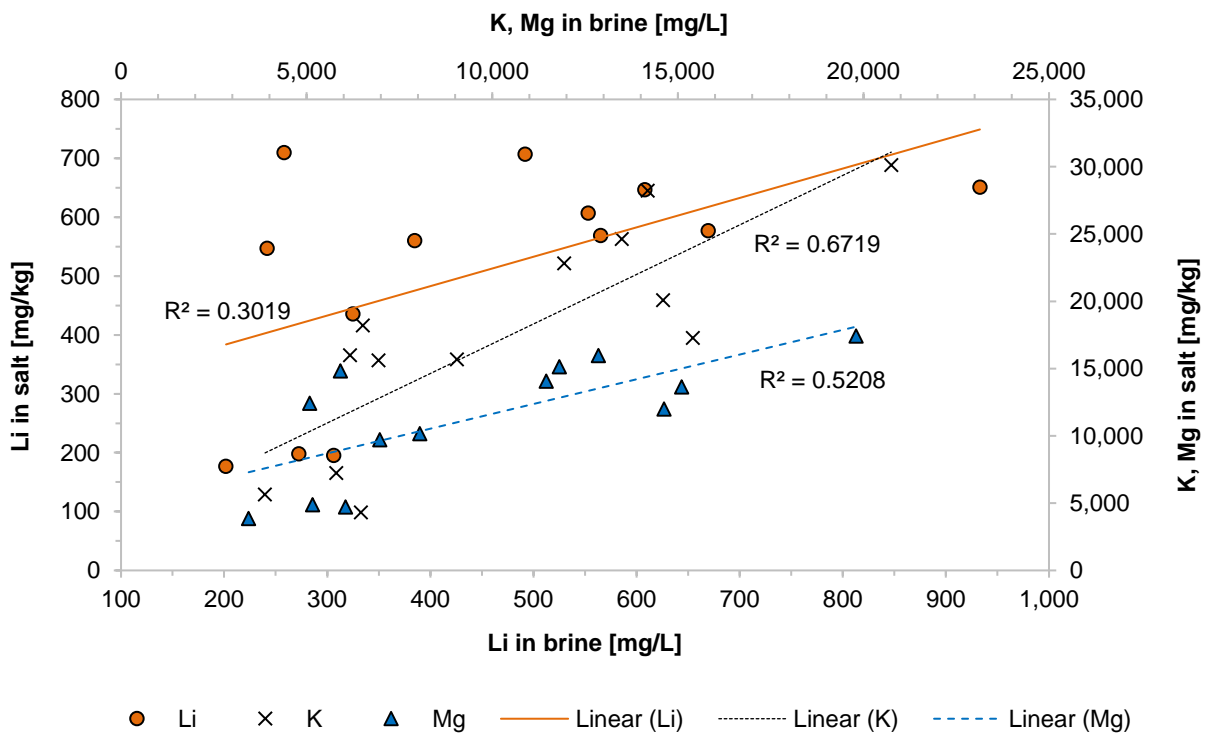
Fig. 56: *Li and K concentrations in the salt efflorescence in relation to the underlying brine*

It could be assumed as well, that the composition of the salt efflorescences reflect the underlying brine composition. In order to investigate a possible correlation, the concentrations of Li and K in the salt efflorescences were compared to the underlying brine, taken from the shallowest well of the particular location. However, a significant correlation could not be observed (Fig. 56).

The quantitative mineralogical composition of the uppermost crust and salt efflorescence was determined by a calculation rule, which is also implemented in the software *ZECHMIN-7* (Bornemann et al. 2008). The composition of main geochemical components Na, Mg, K, Ca, Cl and SO_4 in the sample is the basis for the calculation of the main mineral phases halite, carnallite, sylvite, polyhalite, gypsum and kieserite. Based on a second chemical extraction with pure ethanol, only carnallite is desolved and the Mg (alk. ex.) content of this extraction solution is used for calculating the carnallite content. The analysis of a salt core from the drilling location SLT-01-A by the BGR in 2010 showed that the concentration of Mg (alk. ex.) in the salt approximates the content of total Mg (Mg_{ges}) in the upper cm's of the salt crust (Schmidt 2010). Thus, the extraction step was left out and the content of carnallite was calculated using Mg_{ges}. The calculation template, which was implemented in an excel file, is illustrated in Fig. 57. When the value for the rest of a component was negative, it was set to 0, in order to avoid negative values for resulting minerals. In the samples, the minerals calculated by that procedure summed up to between 97 and 102%, with an average of 99%. Hence, residues of components, which could not be assigned to a mineral phase, are rather small and negligible. The mineralogical composition of the salts is shown in Table A - 12. Decimal places are software based and were not used for interpretation.

Na	halite	NaCl
Mg (alk. ex.)	carnallite	$KMgCl_3 \cdot 6H_2O$
rest of Cl	sylvite	KCl
rest of K	polyhalite	$K_2Ca_2Mg(SO_4)_4 \cdot 2\,H_2O$
rest of Ca	gypsum	$CaSO_4 \cdot 2\,H_2O$
rest of SO_4	kieserite	$MgSO_4 \cdot H_2O$

Fig. 57:   *Calculation template for the quantification of the mineralogical composition of sampled salts (modified after Bornemann et al. 2008)*

In average, halite makes up 94 wt% of the salt surface, but only 83 wt% of the efflorescences. Efflorescences show significant contents of carnallite (5 - 20 wt%), sylvite (0 - 8 wt%) and kieserite (0.6 – 3 wt%), and minor amounts of gypsum (~0.8 wt%).This is the result of the processes happening during the drying of the salt crust at the end of the wet season and the capillary rise of brine described above.

The distribution of halite, carnallite and kieserite correlates significantly to the concentration of lithium in the evaporite samples (Fig. 58). A possible explanation of the relationship between Li, K and Mg may be based on fluid inclusions that frequently occur in precipitating salt minerals during evaporation, reflecting probable increased Li, K and Mg concentration in the brine. Another possibility could be the precipitation of lithium as lithium carnallite ($LiCl \cdot MgCl_2 \cdot 7H_2O$) with increasing concentration. In Schmidt et al. (2009) is mentioned that the formation of lithium carnallite occurs during evaporation of brines from salt lakes in South America, however without further information or citations. On the other hand, the formation of lithium carnallite from crystallization experiments in the laboratory, whereat lithium carnallite precipitates by cooling down an artificial $MgCl_2 \cdot 6H_2O$- and LiCl-solution (Schmidt et al. 2009) and under evaporation conditions embedded in Li production processes (An et al. 2012). It is questionable whether these laboratory/technical conditions are transferable to the conditions of the Salar de Uyuni. The precipitation of Mg in form of kieserite from the brine is accompanied by a very probable precipitation of Li_2SO_4, explaining the correlation of Li and kieserite contents in the salt. The concurrent precipitation of Li and Mg as sulphates was also observed at evaporation studies of Salar de Uyuni and Salar de Atacama brines (Ogawa et al. 2014). This process is one of the complicating factors of Li recovery from Mg rich brines.
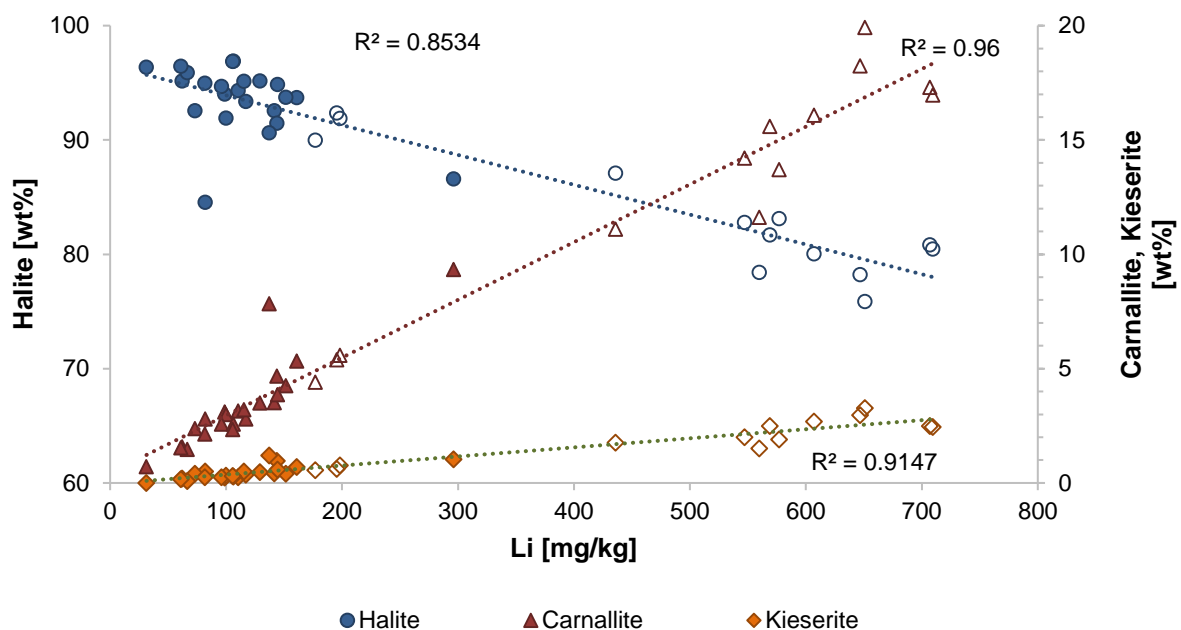
Fig. 58:   Distribution of halite, carnallite and kieserite in the evaporite samples with lithium concentration (closed symbols: polygon surface; open symbols: salt efflorescences)

5.4   Quality assessment

The results of chemical analyses using different methods must be evaluated critically using common quality control standards. A special emphasis must be put on the analytical challenge of highly saline brines and the associated adaptions of sample preparation and instrumental devices.

5.4.1   Correction of field parameters

The electrical conductivity of the salar brines usually exceeded 200 mS/cm, which is the upper limit of the used measuring device (*Hach HQ40D*). Although the device displayed values above the upper threshold, the reliability of these data must be doubted. Thus, laboratory tests with dilution series of three brines with varying chemical composition were performed. TDS values were transformed from g/L to g/kg by the use of the density, which was measured simultaneously by a portable *DMA density meter* at each dilution step. Data for measured EC, density and calculated corresponding TDS of a dilution experiment with saturated NaCl solution and 3 brines are comprised in Table A - 13.
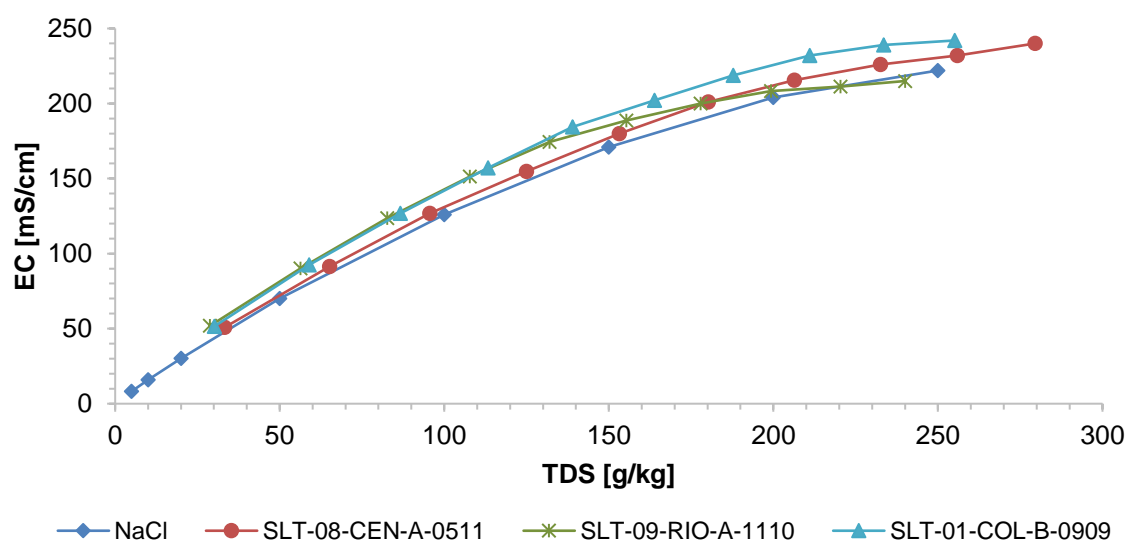
Fig. 59:   *Measured EC values over the brine concentration range of 10 to 100% (values of NaCl at 20°C are from Lide (1994))*

The resulting Uyuni brine dilution curves show a similar trend to the curve of pure NaCl (Fig. 59). Generally, EC values in the brines are up to 10% higher. Differences between the sample brines and in comparison to NaCl are the result of a varying chemical composition by means of main ions in solution. Dilution series show, that the *HACH HQ40* device for measuring the EC of water can be used for brines extending the upper limit of the instrument, at least to a value of ~240 mS/cm, without producing random numbers. The dilution of sample prior to

determining the EC, in order to stay below the upper range, is not recommended, as the trend of TDS with EC is not linear at higher salinities (Fig. 59).

Oxygen solubility decreases with increasing salinity. For the correction of oxygen values measured in the field, salinity correction factors f_{corr} were applied (see chapter 4.4). Correction factors were in the range of 0.055 to 0.32, and thus lowered the measured O_2 contents significantly.

5.4.2   Quality of analytical data

The standard deviation as a measure for the precision of determinations using the ICP-MS device at a dilution of 1:200 was 0.49% (Li), 0.43% (B), 0.75% (Mg), 0.70% (Ca), 0.32% (Br) and 0.35% (Rb). Thereby, the standard deviation of an ion increased with its concentration in the brine. The accuracy for Li, determined by the difference of the theoretical and measured value of a pure 1 ppm Li standard, is 3.9% for the ICP-MS.

The ionic balance as a measure for the analytical error of an analysis was calculated from the deviation of the summed equivalent concentrations of cations and anions. Errors in the brine samples were mainly in the range of ± 5%, which is acceptable regarding the required high dilutions. It is conspicuous, that brine analyses from 2010 are generally lacking cations in solution, leading to a negative error. A closer look to the chemical composition reveals, that Na concentrations are ~15% lower than in samples from the other years, buther other ions do not differ significantly. Presumably, Na determined by IC in brine samples from 2010 were subject to analytical inaccuracies. The error in stream and spring waters is between ± 4%. Samples with errors exceeding that range do mostly lack a complete chemical analysis, with missing values for e.g. HCO_3^- or SO_4^{2-} leading to the falsification of the ionic balance.

5.4.3   Analysis of saturated brines

For sampling, in-situ and laboratory analysis of brines with salinities in the range of 250 – 350 g/L, adaptations to the specific conditions of the fluid must be performed. For the low-flow pumping of brines from wells for sampling, submersible pumps are more convenient than classical suction pumps, which are susceptible to the aspiration of air due to the high density of the brine. This in turn leads to the falsification of oxygen concentrations, being significantly higher than expected. The preparation and chemical analysis of saturated brines requires adaptations in the procedure. This comprises the pipetting step, the choice of an appropriate dilution and the specific parameters of the analytical device. Piston-stroke pipettes, as used for dilution of the samples, are usually adjusted by using distilled water as medium. When

pipetting solutions with a higher density, the volume of liquid aspirated into the tip is lower than the set volume. In this case, the density of the brines amounts to ~ 1.2 g/cm³, which results in a deviation of -0.2% compared to the set volume (Ewald 2005). The high viscosity of brines enhances the remaining of a small droplet in the pipette tip, especially when pipetting small volumes. For the evaluation of pipette precision a pipette test according to DIN EN ISO 8655-6 with the brine was performed. The systematic error for the 20 µL piston stroke pipette was -0.69%, which varies within the acceptable range of ± 1%, according to DIN 8655.

Dilution factors (DF) of 200 and 1,000 were chosen for the ICP-MS. The factor of 200 was the smallest possible to prevent the instrument from damage by high sodium and chloride concentrations. Unfortunately, numerous elements in lower concentrations (i.e. rare earth elements) fell below the detection limit at this minimum dilution. The dilution of 1000 was necessary to stay in the calibration range for major ions as K, Mg and Li. The relative deviation increases with decreasing pipetting volume, thus it seemed reasonable to work with intermediate dilutions in order to reach a DF of 1,000.

5.4.4   Comparison of IC and ICP-MS

The concentrations of Li, Ca, K, Mg and Br in water were determined with both IC and ICP-MS. The results were compared regarding accuracy and precision, in order to select the appropriate method for the analysis of solutions with a high excess of Na and Cl over other ions. K and Mg exceeded the upper calibration range for ICP-MS even at the higher dilution of 1:1000, so that values of IC had to be used for evaluation. The bromine peak at IC measurements was mostly covered by the high sodium peak, so that a reliable calculation of Br concentrations could not be performed. The same applied for Ca, whose peak could not clearly be distinguished from the subsequent Mg peak. Thus, values of ICP-MS were used for the evaluation of Br and Ca. Lithium seemed to be determinable by the use of both methods, in the concentration range that prevailed in the 1:200 – 1:1,000 diluted brine samples. However, deviations in Li between both methods were in the range of 0.5 to 12%, in the SLT-09-RIO samples even up to 20%. It is known, that the measurement of lithium by ICP-MS is affected by the concentrations of other ions in solution as Na, Mg, Cl and K (Misra & Froelich 2009). Previous investigations showed, that Na and K can strongly enhance the signal due to spectral overlapping, while Cl depresses it (Dai et al. 2015, Bond & Canterford 1971). The high deviation in the SLT-09-RIO samples could be the result of the specific brine composition at this location, characterized by higher Mg and K concentrations compared to other sampling locations at the Salar de Uyuni. IC measurement of Li runs the risk of peak overlap between the Li and the Na peak, as retention times are close together (Li: 3.9 min, Na: 4.9 min). The ratio of Na/Li is up to 400 in brine samples, leading to the possible coverage of the Li peak and

the consequent underestimation of Li concentrations in the brine. A strategy to overcome spectral interferences and peak overlaps could be the addition of a similar ionic composition as in the samples to the standard solutions used for calibration. However, a whole series of standard solutions with differing compositions would be required in order to serve the high ionic variations in the brine samples.
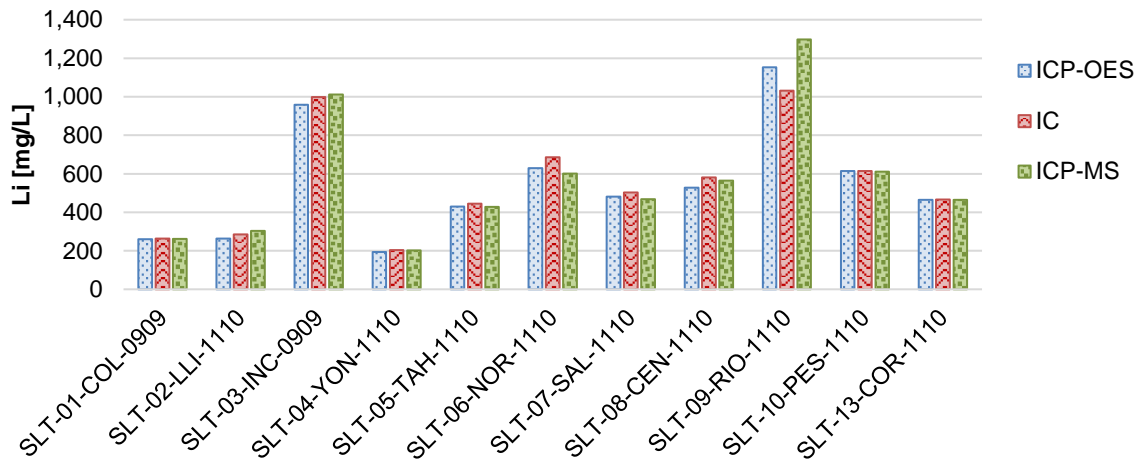
Fig. 60: *Comparison of different methods for lithium determination in the brine (ICP-OES analysis was performed at the BGR Hannover, IC and ICP-MS analysis at TU Freiberg)*

Parallel to own measurements, brine samples were analyzed for main chemical composition at the Bundesanstalt für Geowissenschaften und Rohstoffe, Hannover. The applied method was ICP-OES for Li concentrations. The comparison shows, that results from this method are comparable to own analyses, and often the result is located in between the values of IC and ICP-MS, as is the case for SLT-09-RIO and SLT-06-NOR (Fig. 60). Thus, for the evaluation of Li concentrations, the average of obtained IC and ICP-MS results were used.

6   Summary, discussion and outlook

The Salar de Uyuni became a matter of public interest in the course of developing new deposits for the demand of lithium in the electric mobility sector. This industrial branch is increasing rapidly, and present suppliers will not be able to serve the market sufficiently in future. The Salar de Uyuni contains reserves of about 7.0 Mio tonnes of lithium (Sieland 2014) in the uppermost crust, which is more than one third of worldwide deposits in salt lake brines. However, the processes leading to the enrichment of lithium in the salt crust and its specific spatial distribution in the Salar de Uyuni are not yet completely understood. The present work should help improving the knowledge about potential sources, pathways and accumulation mechanisms of lithium and other solutes in the pore brine of this salt lake.

Environmental samples, which form the analytical base of this work, comprise fresh waters from streams, rivers and springs in the catchment of the Salar de Uyuni, brines from varying places and depths of the salt lake, rocks mostly of volcanic origin, sediments and soils formed by weathering of the bedrock, lacustrine sediments from mud layers within the salt crust, and salt material from the surface of the crust. The large amount of samples was subject to various methods of chemical analyses, depending on the particular purpose of investigation. In order to localize the spatial extent of Li and other solutes' supply to the Salar de Uyuni, the superficial catchment was determined using spatial remote sensing data in form of SRTM datasets. The size of the catchment as a result of delineation with ArcHydro is 63,000 km² in total, and encompasses several subcatchments where smaller salt pans and playas exist. The geologic nature of the catchment is characterized by volcanic deposits as ignimbrites, pyroclastics and lava sheets at the higher situated borders and flanks of volcanoes, and merges into surficial unconsolidated sediments, salt deposits and lacustrine material in widespread flood plains, which attend the main tributaries and rivers feeding the salar. The question of a hydraulic connection between the Salar de Uyuni and the Salar de Coipasa could not be entirely solved, but certainly existed during past times and obviously still exists during precipitation intensive years. The transport of Li-enriched waters from the Salar de Coipasa to the Salar de Uyuni is likely, as balance calculations regarding the total superficial input of elements and their actual occurrence in the pore brine showed.

Brines from the Salars of Uyuni and Coipasa are of NaCl type, with a total mineralization between 260 and 360 g/L. For the investigation of brine evolution, element to bromine ratios were compared to progression of simple evaporation of the average Río Grande water. K and Mg behave similar, as both elements' concentration plot above the line of simple evaporation with further brine concentration. Probably, K and Mg are not removed from solution by the formation of precipitates, but are rather released from clay minerals by ion exchange leading

to their enrichment in the pore brine. Lithium behaves similar to K and Mg, whereby the enrichment in relation to bromine is even higher in the transect brines compared to the well brines. The fact, that fluid samples in transects were taken from muddy and clayey layers in about 50 cm depth, supports the theory of clay minerals having an important role in the enrichment of Li in surface-near parts of the brine-filled layers. The distribution of lithium in the Salar de Uyuni was interpolated using ordinary kriging with a spherical semi-variogram. In the south, high concentrations occur in the Río Grande delta region directly at the margin of salt crust and fluviatile sediments. To the east, concentrations decrease rapidly, because the transport direction of lithium containing surface waters and suspended load is rather to the northwest. The delivery of lithium by the Río Colorado does not lead to the enrichment of lithium in the pore brine of the delta region. In the northern site, lithium shows contents in the range of 1.5 g/L along a strip-shaped, about 10 km wide zone parallel to the 2-3 km distant shore. Obviously, the accumulation of lithium does not happen only by the input of lithium enriched waters of tributaries, but also by the enrichment of the element directly inside the salt crust. A significant brine composition change with depth is not observed in most wells, which points to the existence of stable environmental conditions over the last 10,000 years since drying of paleolake Tauca and the formation of the uppermost salt crust.

The investigation of ^{14}C in brine shows a stable stratification of brine without significant density and temperature driven flow within the salt crust. The brines in the uppermost salt layer are between 6,200 and 13,340 years old and correspond in age to the surrounding evaporites, leading to the assumption that the uppermost brines are formed concurrently with the salt crust. However, a local mixing of the brine with freshwater feeding from groundwater aquifers especially near the shore of the salar was observed by the analysis of $\delta^2 H$ and $\delta^{18}O$ in the brines. The distribution of stable isotopes also show the strong influence of evaporation, even smaller tributaries feeding the Río Grande are enriched in heavy isotopes of H and O. The effect of evaporational concentration leading to the enrichment of lithium in the brines could also be observed by the analysis of superficial salts from the upper crust. Salt efflorescences are significantly enriched regarding Li, K, Mg and other ions compared to the surface within the polygons. The enrichment of Li in brine occurs all-season along shrinkage cracks at polygon borders, where brine rises up, water evaporates and NaCl precipitates, leaving a solution even more concentrated in Li and other solutes as Br, B, K and Mg. This process is more intensively taking place in regions, where the water stays longest at the end of the rainy season, leading to an all-season humid surface and a shallow brine table, where capillary rise of brine is facilitated. Thus, lithium concentrations are highest in the northern and southeastern areas of the salt pan, where the salt is moist throughout the whole year (Fig. 53).

Analyzed rocks, mostly of rhyolitic and dacitic type, show moderate lithium concentrations in the range of 4 to 37 mg/kg. SiO_2 contents of ~60 wt% point to a low stage of alteration. In

average, more than 50% of contained lithium was released from the mineral structure by the digestion with aqua regia. It can be concluded, that rock types occurring in the Salar de Uyuni catchment are a substantial supplier of lithium by the intensive physical and chemical weathering due to the specific environmental conditions. Increased lithium concentrations in rock and sediment samples from the volcano flanks south of the salar indicate, that the southern catchment is the main supplier of lithium to the salt lake. In lacustrine sediments, the high lithium contents in the northeastern and southern parts reflect the brine chemistry in these regions. Here, significant amounts of the element were released by the aqua regia digestion, indicating that lithium could be incorporated in the clay mineral fraction of lacustrine sediments. Clay minerals (smektites) do not tend to dissolve under neutral pH and moderate temperature conditions (Hofmann et al. 2004). Hence, the release of lithium does not mainly occur by weathering and associated dissolution of clay minerals, but by exchange of ions with the surrounding brine.

The high concentrations of dissolved Li in the main tributaries Río Grande and Río Colorado as well as some streams feeding them have their source in weathered rhyolites and ignimbrites occurring in the catchment, combined with a significant contribution from hydrothermal systems existing in the subsurface of the volcanically marked region. The last-mentioned factor is confirmed by extraordinary high Li contents in sampled (thermal) springs in direct vicinity of the Salar. However, estimated Li resources in the uppermost salt crust are too high to be only the result of river input in dissolved form. Presumably, a part of lithium input happens by the transport of particulate matter in the river load, which is strongly intensified during the rainy season, where river discharge and content of suspended sediments increase significantly. This is due to the annual hydrological and geochemical cycle in the catchment of the Salar de Uyuni. During austral winter, surficial rocks are subject to intensive physical and chemical weathering resulting from the combination of high temperature differences and strong solar insolation. The generated detritus and unconsolidated material are then transported along the drainage system towards the main tributaries. Extended floodplains upstream of the southern shore serve for the slowdown of water masses and sedimentation of detrital material with associated separation according to particle size. The release of lithium is thought to be the result of ion exchange, when sediments are compacted and get in contact with the shallow brine table. This process, working together with the enrichment by capillary rise of brine described above, explains the extraordinary enrichment of lithium in a limited spatial extension in the southern part of the Salar de Uyuni, in relation to its total size.

In summary, the following conditions and processes happen at the Salar de Uyuni, resulting in the occurrence of Li enriched brines:

1. Occurrence of rhyolitic bedrock and ignimbrites typical for volcanic environments with moderate to elevated contents of Li.

2. Hydrothermal activity in the catchment with discharge of hydrothermal, Li enriched waters to the surface by means of springs; associated to that is the mixture with groundwater and thus, elevated Li concentrations in groundwater of the region.

3. The occurrence of an endorheic basin, where drainage from a large catchment is collected during the rainy season.

4. The occurrence of intensive physical and chemical weathering, which is triggered by the specific climatic conditions of the region (heavy rainfalls during wet season, high day/night shifts in temperature, strong solar insolation, low air humidity); this leads to the transport and accumulation of sediments and solutes into the salar.

5. The properties of the salt surface, where brine rises up by capillary forces along the shrinkage cracks between polygons and is concentrated in Li by evaporation and precipitation of salt efflorescences.

6. The occurrence of fault systems underneath the salt pan and the catchment, which enable hydrothermal fluids to rise from deeper strata and provide a possible migration path for lithium enriched waters.

7. The occurrence of Li-enriched clay minerals by weathering of the bedrock, their transport with the tributaries towards the salt lake and the release of Li by ion exchange reactions.

8. The existence of a similar salt lake in the vicinity, from where the supply of Li-enriched waters by overflow or a subterraneous connection is likely.

6.1 Comparison to other salt lakes

The question, why some salt lakes are strongly enriched in lithium, whereas others show no considerable concentrations, must be regarded by the comparison of major site characteristics. Table 12 summarizes the main geographic, climatic, geological, and chemical conditions of selected salt lakes, playas and salt pans all over the world. They all share the characteristic of being the deepest part of a closed basin, where evaporation strongly exceeds precipitation, which is reflected in the generally high aridity index in these regions. The relation of basin area to lake area is generally high, so that large masses of tributary waters, dissolved ions and suspended matter are transported towards the lakes. Most basins are located in volcanically active regions, where volcanic rocks are commonly occurring and, by weathering processes, provide the minerals for the accumulation of large evaporate beds. Also, hydrothermal springs or geothermal activity are characteristics, which are shared by most salt lakes considered. However, differences can be observed as well. Most salt lakes with significantly enriched lithium brines are located at altitudes above 1,000 m. This is especially the case for salars in the lithium triangle, as they are part of the Altiplano between the Andean cordilleras. It is conspicuous, that several salt lakes are located above fault systems. Faults provide the path for hydrothermal, in solutes enriched fluids to rise along cracks from deeper strata, and thus are a possibility for the migration of Li to the surface.

Table 12: Hydrological, chemical, geological and geochemical characteristics of selected salt lakes with brines containing significant amounts of lithium

	Lake area	Basin area	Elevation	T (Ø)	Köppen[1]	Rainfall	Evaporation	Brine type	Source[2]
	km²	km²	m	°C		mm/a	mm/a		
Great Salt Lake	4,400	86,896	1,280	10.5	Csa	186	1,800	Na-Mg-Cl	7
Clayton Valley	72	1,342	1,298	13	BWk	90-130	760-1,370	Na-Cl	7; 12
Salar de Coipasa	2,218	145,279	3,661	8	BWk	320	1,316	Na-Cl	5, 9
Salar de Uyuni	10,000	60,000	3,656	9.3	BWk	180	1,500	Na-Cl	6
Hombre Muerto	600	4,000	3,968	6.7	ET	55-70	1,100	Na-Cl	4; 7
Zabuye	243	16,768	4,400	0.2	ET	200	2,300	Na-Cl-CO$_3$	8
Salar de Atacama	3,000	18,100	2,300	13.9	BWk	39	2,600-3,200	Na-Cl	1; 7
Tuz Gölü	1,600	16,000	925	11	Csb	350	1,175-1,390	Na-Cl-SO$_4$	3; 11
Dead Sea	1,023	44,000	-415	24	BSh	90	2,000-3,000	Mg-Na-Cl	2; 7; 10

	Li in brine ppm	Bedrock / Basement	Li sources	Characteristics of basin
Great Salt Lake	30-60	Volcanic	unknown	Fault system underneath salt lake
Clayton Valley	100-300	Volcanic, sedimentary (clays: smectite, illite; halite, gypsum), carbonates and clastics	Weathering, leaching of volcaniclastics and ash-fall tuffs, geothermal	Interbedded fine grained sediments and halite, ash layer, clays (hectorite), fault systems
Salar de Coipasa	320	Volcanic	Weathering, leaching of volcanic rocks	Volcanic features, evaporitic sediments, Gypsum diapirs
Salar de Uyuni	100-1,500	Volcanic	Weathering, leaching of volcanic rocks, hydrothermal springs	Extended floodplains with clayey sediments, Gypsum diapirs, intrabasinal faulting
Salar de Hombre Muerto	100-700	Ignimbrites, tuffs from volcanic eruptions of Cerro Galán	Leaching of volcanic deposits (ash-flow tuffs), geothermal waters	Volcanic features, Fault system underneath salar, ulexite, clay minerals (smectites)
Zabuye	700-1,000	-	Mainly geothermal waters; volcanic, lacustrine, sedimentary rocks	$LiCO_3$ as natural salt precipitate
Salar de Atacama	1,000-7,000	Volcanic, evaporites (Cordillera de la Sal)	Weathering of volcanic rocks	Clastic and evaporitic sediments; domes of gypsum and rock salts; Fault system underneath salar
Tuz Gölü	200	Rhyolitic tuffs, ignimbrites, metamorphic rocks	unknown	Major fault zone east of lake; alluvial deposits (lacustrine, clays), gypsum outcrops
Dead Sea	17-21	Neogene to quaternary sediments, thick evaporate fillings	Hypersaline thermal springs, remnant of earlier brine body, enrichment by interaction with clay minerals	Laminates of aragonite, halite and detritus; basin is situated in the offset of longitudinal faults; halite karst, sinkholes

[1]Aw – tropical wet savanna; BWk – arid, cold desert; BWh – arid, hot desert; ET – polar tundra; Csa – temperate, dry, hot summer; Csb – temperate, dry, warm summer; BSh – semi-arid, hot steppe

[2]1 - Boschetti et al. (2007), 2 – Nissenbaum (1977), 3 - Camur & Mutlu (1996), 4 - Godfrey et al. (2013), 5 - Lebrun et al. (2002), 6 - Risacher & Fritz (1991b), 7 - Warren (2016), 8 - Zheng & Liu (2009), 9 - Munk et al. (2016), 10 – Salameh & Al-Saber (1999), 11 - Voigt (2014), 12 – Munk et al. (2011)

Geophysical investigations showed that also the quaternary lake deposits of the Salar de Uyuni are offset by various faults, which are particularly distinct at the eastern side of the salar (McGeary et al. 2003). Also, the brine-filled basins of the Clayton Valley and the Salar de Atacama are located along active intra-basin faults (Warren 2016).

6.2 Environmental issues

Since several years, the national mining corporation Comibol (Corporación Minera de Bolivia) is planning and constructing a pilot plant for the production of lithium carbonate and potassium chloride from the interstitial brine. The complex consists of various evaporation pans, to where the brine is pumped from wells (Fig. 61). These pans serve for the sun-powered precipitation of halite, silvinite, carnallite and bischofite, before the Li- enriched brine is transported to the plant to be undertaken to several steps of purification. For the connection of the producing plant on the salt lake to the shore a 17 km long dam for the purpose of a road was constructed. The absence of breaktroughs impedes the transport of inflowing water masses from the Río Grande during and after the rainy season, which leads to the accumulation of water to the east of the road (Fig. 61).

Fig. 61:   *System of evaporation pans near the Río Grande delta for the extraction of elements from the brine by the national mining corporation Comibol (image taken by the Copernicus Sentinel- 2B satellite on 17 May 2017 and provided by ESA[1])*

In August 2017, an area of approximately 170 km² of the Salar de Uyuni was covered by evaporation pans and buildings for production and processing, which is the 14-fold extent of the size in 2014.Several factors give raise to strong doubts in the project's success. First, unfavourable climatological conditions with an intensive rainy season and a comparably short dry season lead to the incomplete evaporation of the brine and its re-dilution by rainwater. Second, the high Mg/Li ratio results in tremendously higher material and cost efforts, compared to other locations of Li extracting facilities like the Salar de Atacama. The sparse infrastructure and missing possibilities for the further processing of the lithium carbonate are other factors driving up costs and increasing environmental impacts. The onsite production of Li_2CO_3 needs water and this can only be supplied by groundwater. Fossil groundwater resources are decreasing rapidly, and recharge is slow due to the arid climate. The water consumption of the plant competes with regional agriculture and the open-pit mining of silver, zinc and lead in San Cristóbal (50,000 m³ H_2O / day). Massive groundwater pumping from freshwater aquifers near the Salar would result in the lowering of the waterlevel and a shift of the saltwater / freshwater interface towards the surrounding, leading to the salinization of potable water. Lagunas at the shore and in the floodplains of the delta regions inhibit various animal and plant species, which would suffer from the drying of the lagunas due to the lowering of the groundwater table. The floodplains in the delta region, serving as breeding area for the rare Andean flamingo, are considered a Ramsar site, which is a convention for the protection and conservation of wetlands (UNESCO 1971). The sensitivity of the region to interventions brought up by economic interests must lead to the development of mining techniques minimizing the negative consequences for nature and inhabitants. Modern approaches, as the cone technology developed in collaboration of scientists from the TU Bergakademie Freiberg and the University of Potosí, could be an option for economic and environmental friendly pre-enrichment of lithium and other valuable elements considering as well local population and tourism.

6.3 Recommendations for future research

The present thesis comprises a large volume of sampling material and a variety of analytical methods in order to investigate the sources of lithium and processes of its enrichment in the salt lake brine. Nevertheless, the processes linked together for the accumulation of lithium are widespread, feasible analytical methods are numerous and the area of investigation is large. During the work and evaluation of results, several ideas for the improvement of analytical work and topics for future research arose. First, deeper drillings (>10 m depth) in the salt crust together with depth-dependent brine sampling should be performed in order to gain information about deeper salt layers and the chemical composition, especially lithium, of the interstitial solution.

The determination of stable isotopes proved to be an appropriate method for investigating the water cycle in arid regions with intensive weathering. Here, the analysis should be extended to surface waters as streams and springs as well as groundwater in the catchment of the Salar de Uyuni, in order to gain a comprehensive database compared to the small amount of published data that is available for this region. The analysis of lithium isotopes is an appropriate method for the investigation of the lithium cycle. A change in the $^6Li/^7Li$ ratio points to the sources of lithium (as leaching from rocks, rise of magmatic fluids and hydrothermal waters) and processes affecting its accumulation. As evaporation does not affect the isotopic composition of lithium, and sorption only to a small extent, the method is useful for the investigation of weathering processes and associated leaching of the element from source rocks.

Literature data for the Río Grande discharge show a large range; information for other inflows as the Río Colorado are lacking. Thus, frequent or continuous readings of discharge and chemical composition of inflows would give hints for the input of solutes throughout the year, putting a special emphasis on the difference between the dry winter and wet summer season. In this regard, the analysis of suspended matter transported towards the salar would help improving the balance of past and present lithium input and existing resources in the brine.

The intensification of research in the region of a possible hydraulic connection of the salars of Uyuni and Coipasa, for example by taking water and particulate matter samples during rain intensive years, could help to make more precise assumptions about the past and present exchange of solutes.

7   Literature

ABBOTT, M.B.; WOLFE, B.B.; ARAVENA, R.; WOLFE, A.P.; SELTZER, G.O. (2000) Holocene hydrological reconstructions from stable isotopes and paleolimnology, Cordillera Real, Bolivia. *Quaternary Science Reviews* 19 (17-18), pp. 1801–1820.

AHLFELD, F., BRANISA, L. (1960) Geologia de Bolivia. La Paz: Don Bosco.

ALLMENDINGER, R.W., JORDAN, T.E., KAY, S.M., ISACKS, B.L. (1997) The evolution of the Altiplano-Puna plateau of the Central Andes. *Annual Review of Earth and Planetary Sciences* 25, pp. 139–174.

AN, J.W.; KANG, D.J.; TRAN, K.T.; KIM, M.J.; LIM, T.; TRAN, T. (2012) Recovery of lithium from Uyuni salar brine. *Hydrometallurgy* 117-118, pp. 64-70.

ANDERSON, M.; BERTSCH, P.M.; MILLER, W.P. (1989) Exchange and Apparent Fixation of Lithium in Selected Soils and Clay Minerals. *Soil Science Society of America Journal* 148, pp. 46–52.

ANGERER, G.; MARSCHEIDER-WEIDEMANN, F.; WENDL, M.; WIETSCHEL, M. (2009) Lithium für Zukunftstechnologien - Nachfrage und Angebot unter besonderer Berücksichtigung der Elektromobilität. Fraunhofer ISI Karlsruhe, 69 pp.

ANGHEL, I.; TURIN, H.J.; REIMUS, P.W. (2002): Lithium sorption to Yucca Mountain tuffs. *Applied Geochemistry* 17 (6), pp. 819–824.

ARAVENA, D.; MUÑOZ, M.; MORATA, D.; LAHSEN, A.; PARADA, M.Á.; DOBSON, P. (2016) Assessment of high enthalpy geothermal resources and promising areas of Chile. *Geothermics* 59, pp. 1–13.

ARGOLLO, J.; MOURGUIART, P. (2000) Late Quaternary climate history of the Bolivian Altiplano. *Quaternary International* 72 (1), pp. 37–51.

BACH, R.O.; KAMIENSKI, C.W.; ELLESTAD, R.B. (1967) Lithium and lithium compounds. In: Kirk-Othmer Encyclopedia of Chemical Technology, Vol. 12, pp. 529–554.

BAKER, P. A.; RIGSBY, C. A.; SELTZER, G.O.; FRITZ, S.C.; LOWENSTEIN, T.K.; BACHER, N.P.; VELIZ, C. (2001) Tropical climate changes at millennial and orbital timescales on the Bolivian Altiplano. *Nature* 409 (6821), p. 698.

BALLIVIAN, O. & RISACHER, F. (1981) Los Salares del Altiplano boliviano - Metodos de Estudio y Estimación economica. *O.R.S.T.O.M.* Paris, 253 pp.

BANKS, D.; FRENGSTAD, B.; MIDTGÅRD, A.K.; KROG, J.R.; STRAND, T. (1998) The chemistry of Norwegian groundwaters: I. The distribution of radon, major and minor elements in 1604 crystalline bedrock groundwaters. *Science of The Total Environment* 222 (1), pp. 71–91.

BANKS, D.; MARKLAND, H.; SMITH, P.V.; MENDEZ, C.; RODRIGUEZ, J.; HUERTA, A.; SAETHER, O.M. (2004) Distribution, salinity and pH dependence of elements in surface waters of the catchment areas of the Salars of Coipasa and Uyuni, Bolivian Altiplano. *Journal of Geochemical Exploration* (84), pp. 141–166.

BARROW, C.J. (1992) World atlas of desertification (United nations environment programme), Vol. 3, John Wiley & Sons, London, 69 pp.

BENGTSSON, L. (2012) Poopó Lake, Bolivia. In: BENGTSSON, L.; HERSCHY, R.W.; FAIRBRIDGE, R.W. (Eds.) Encyclopedia of Lakes and Reservoirs. Springer Netherlands, pp. 616–618.

BERTHOLD, C.E.; BAKER, D.H. (1976) Lithium recovery from geothermal fluids. In: VINE, J.D. (Ed.) Lithium Resources and Requirements by the Year 2000. *US Geological Survey* Prof. Paper 1005, pp. 61–66.

BILLS, B.G.; BORSA, A. A.; COMSTOCK, R.L. (2007) MISR-based passive optical bathymetry from orbit with few-cm level of accuracy on the Salar de Uyuni, Bolivia. *Remote Sensing of Environment* 107 (1-2), pp. 240–255.

BIRKLE, P.; ARAGÓN, J.J. ROSILLO; PORTUGAL, E. (2002): Evolution and origin of deep reservoir water at the Activo Luna oil field, Gulf of Mexico, Mexico. *AAPG Bulletin* 86, pp. 457–484.

BLODGETT, T.A.; ISACKS, B.L.; LENTERS, J.D. (1997) Constraints on the Origin of Paleolake Expansions in the Central Andes. *Earth Interact* 1 (1), pp. 1–28.

BOND, A.M.; CANTERFORD, D.R. (1971) Interference of lithium in atomic absorption spectrometry. *Analytical Chemistry* 43 (1), pp. 134–135.

BORNEMANN, O.; BEHLAU, J.; FISCHBECK, R.; HAMMER, J.; JARITZ, W.; KELLER, S. ET AL. (2008) Description of the Gorleben Site Part 3: Results of the geological surface and underground exploration of the salt formation. *Geologisches Jahrbuch* Reihe C, Schweizerbart Science Publishers, Stuttgart, 73 pp.

BORSA, A.A.; BILLS, B.G.; MINSTER, J.-B. (2008a) Modeling the topography of the salar de Uyuni, Bolivia, as an equipotential surface of Earth's gravity field. *Journal of Geophysical Research* 113, pp. 1–21.

BORSA, A.A.; FRICKER, H.A.; BILLS, B.G.; MINSTER, J.-B.; CARABAJAL, C.C.; QUINN, K.J. (2008b) Topography of the salar de Uyuni, Bolivia from kinematic GPS. *Geophysical Journal International* (172), pp. 31–40.

BOSCHETTI, T.; CORTECCI, G.; BARBIERI, M.; MUSSI, M. (2007): New and past geochemical data on fresh to brine waters of the Salar de Atacama and Andean Altiplano, northern Chile. *Geofluids* (7), pp. 33–50.

BÖTTCHER, M.E.; BRUMSACK, H.-J.; LANGE, G.J. DE (1998) Sulfate reduction and related stable isotope (34S, 18O) variations in interstitial waters from the Eastern Mediterranean. *Proceedings of the Ocean Drilling Program,* Scientific Results 160, pp. 365–373.

BRADLEY, D.; MUNK L.A.; JOCHENS, H.; HYNEK, S.; LABAY, K. (2013) A Preliminary Deposit Model for Lithium Brines. *US Geological Survey Open-File Report* 2013-1006, pp. 1–6.

BUNDESREGIERUNG (2009) Nationaler Entwicklungsplan Elektromobilität der Bundesregierung. Edited by Bundesministerium für Bildung und Forschung.

CAMPBELL, M.G. (2009) Battery lithium could come from geothermal waters. *New Scientist* 204 (2738), p. 23.

CAMUR, M.Z.; MUTLU, H. (1996) Major-ion geochemistry and mineralogy of the Salt Lake (Tuz Gölü) basin, Turkey. *Chemical Geology* 127, pp. 313–329.

CANNON, H.L.; HARMS, T.F.; HAMILTON, J.C. (1975) Lithium in unconsolidated sediments and plants of the Basin and Range Province, southern California and Nevada. *Geological Survey Prof. Paper* 918, 23 pp.

CARROLL, D. (1959) Ion exchange in clays and other minerals. *Geological Society of America Bulletin* 70 (6), pp. 749–779.

CHEPSTOW-LUSTY, A.; BUSH, M.B.; FROGLEY, M.R.; BAKER, P.A.; FRITZ, S.C.; ARONSON, J. (2005) Vegetation and climate change on the Bolivian Altiplano between 108,000 and 18,000 yr ago. *Quaternary Research* 63 (1), pp. 90–98.

CLARK, I.D.; FRITZ, P. (1997): Environmental Isotopes in Hydrogeology. Boca Raton New York.

COLLINS, A.G. (1978) Geochemistry of anomalous lithium in oil-field brines. *Oklahoma Geological Survey Circular* 79, pp. 95–98.

DAI, L.; WIGMAN, L.; ZHANG, K. (2015) Sensitive and direct determination of lithium by mixed-mode chromatography and charged aerosol detection. *Journal of Chromatography* A 1408, pp. 87–92.

DAN, L.(2015) Untersuchung der Lithiumanreicherung im Salar de Uyuni mittels Batch-Versuchen. Master thesis. TU Bergakademie Freiberg, Freiberg.

DAVIS, J.R.; HOWARD, K.A.; RETTIG, S.L.; SMITH, R.L.; ERICKSEN, G.E.; RISACHER, F.; ALARCON, H.; MORALES, R. (1982): Progress report on lithium-related geologic investigations in Bolivia. *US Geological Survey Open-File Report* 82-782. 18 pp.

DEBERITZ, J. (1993) Lithium. Verlag Moderne Industrie Landsberg/Lech, 70 pp.

DIBBLE, W.E.; DICKSON, F.W. (1976) The behavior of lithium in experimental rock-water interaction studies. In: James D. Vine (Ed.) Lithium Resources and Requirements by the Year 2000. *U.S. Geological Survey Prof. Paper* 1005, pp. 142–147.

DIXON, B.; UDDAMERI, V. (2016) GIS and Geocomputation for Water Resource Science and Engineering, John Wiley & Sons, West Sussex, 545 pp.

DOHRMANN, R. (2006) Cation exchange capacity methodology II: A modified silver–thiourea method. *Applied Clay Science* 34 (1-4), pp. 38–46.

DONSELAAR, M.E.; CUEVAS GOZALO, M.C.; MOYANO, S. (2013) Avulsion processes at the terminus of low-gradient semi-arid fluvial systems: Lessons from the Río Colorado, Altiplano endorheic basin, Bolivia. *Sedimentary Geology* 283, pp. 1–14.

DREVER, J.I. (1997) The Geochemistry of natural waters. Surface and groundwater environments. 3rd ed., Prentice-Hall New Jersey. 436 pp.

ELKHRACHY, I. (2017) Vertical accuracy assessment for SRTM and ASTER Digital Elevation Models: A case study of Najran city, Saudi Arabia. *Ain Shams Engineering Journal.*11 pp.

ERICKSEN, G.E. (1961) Rhyolite tuff, a source of the salts of northern Chile. *U.S. Geological Survey Prof. Paper* 424.

ERICKSEN, G.E.; CHONG, D.G.; VILA, T.G. (1976) Lithium resources of salars in the central Andes. In: James D. Vine (Ed.) Lithium Resources and Requirements by the Year 2000. *U.S. Geological Survey Prof. Paper* 1005, pp. 66–75.

ERICKSEN, G.E.; VINE, J.D.; BALLÓN, R. (1977) Lithium-rich brines at Salar de Uyuni and nearby Salars in southwestern Bolivia. *U.S. Geological Survey Open-File Report* 77-615.

ERICKSEN, G.E.; VINE, J.D.; RAUL BALLÓN, A. (1978) Chemical composition and distribution of lithium-rich brines in salar de Uyuni and nearby salars in southwestern Bolivia. *Energy* 3 (3), pp. 355–363.

ESRI (2011) Arc Hydro Tools 2.0 - Tutorial. New York.

EUGSTER, H.P; JONES, B.F (1979) Behavior of major solutes during closed-basin brine evolution. *American Journal of Science* 279, pp. 609–631.

EVANS, K. (2008) An Abundance of Lithium. Unpublished paper. Available at {http://lithiumabundance.blogspot.com/}

EWALD, K. (2005) Influence of physical parameters on the dispensed volume of air-cushion pipette. No. 21. Edited by Eppendorf (Userguide).

FERNÁNDEZ, A.C.; HÖRMANN, P.K.; KUSSMAUL, S.; MEAVE, J.; PICHLER, H.; SUBIETA, T. (1973) First petrologic data on young volcanic rocks of SW-Bolivia. *Tschermaks mineralogische und petrographische Mitteilungen* 19 (3), pp. 149–172.

FIORELLA, RICHARD .P.; POULSEN, C.J.; PILLCO ZOLÁ, R.S.; BARNES, J.B.; TABOR, C.R.; EHLERS, T. A. (2015) Spatiotemporal variability of modern precipitation δ18O in the central Andes and implications for paleoclimate and paleoaltimetry estimates. *Journal of Geophysical Research: Atmospheres* 120 (10), pp. 4630–4656.

FONTES, J.-CH.; BOULANGE, B.; CARMOUZE, J. P.; FLORKOWSKI, T. (1979) Preliminary oxygen-18 and deuterium study of the dynamics of Lake Titicaca. In: Isotopes in Lake Studies: Proceedings of an Advisory Group Meeting on the Application of Nuclear Techniques to the Study of Lake Dynamics (International Atomic Energy Agency) Unipub, New York, pp. 145–150.

FORNARI, M.; RISACHER, F.; FÉRAUD, G. (2001) Dating of paleolakes in the central Altiplano of Bolivia. *Palaeogeography, Palaeoclimatology, Palaeoecology* 172, pp. 269–282.

FRANCIS, P.W.; BAKER, M.C.W. (1978) Sources of two large ignimbrites in the central andes: Some landsat evidence. *Journal of Volcanology and Geothermal Research* 4, pp. 81-84

FRICKER, H.A.; BORSA, A.A.; MINSTER, J.-B.; CARABAJAL, C.C.; QUINN, K.J.; BILLS, B.G. (2005) Assessment of ICESat performance at the salar de Uyuni, Bolivia. *Geophysical Research Letters* 32, 5 pp.

FRITZ, P.; BASHARMAL, G.M.; DRIMMIE, R.J.; IBSEN, J.; QURESHI, R.M. (1989) Oxygen isotope exchange between sulphate and water during bacterial reduction of sulphate. *Chemical Geology: Isotope Geoscience section* 79 (2), pp. 99–105.

FRITZ, S.C.; BAKER, P.A.; LOWENSTEIN, T.K.; SELTZER, G.O.; RIGSBY, C.A.; DWYER, G.S.; TAPIA, P.M.; ARNOLD, K.K.; KU, T.-L.; LUO, S. (2004) Hydrologic variation during the last 170,000 years in the southern hemisphere tropics of South America. *Quaternary Research* 61, pp. 95–104.

FRITZ, S.C.; BAKER, P.A.; SELTZER, G.O.; BALLANTYNE, A.; TAPIA, P.; CHENG, H.; EDWARDS, R. L. (2007) Quaternary glaciation and hydrologic variation in the South American tropics as reconstructed from the Lake Titicaca drilling project. *Quaternary Research* 68 (3), pp. 410–420.

GARREAUD, R.; VUILLE, M.; CLEMENT, A.C. (2003) The climate of the Altiplano: observed current conditions and mechanisms of past changes. *Palaeogeography, Palaeoclimatology, Palaeoecology* 194, pp. 5–22.

GARRETT, D.E. (2004) Handbook of Lithium and Natural Calcium Chloride - Their Deposits, Processing, Uses and Properties: Elsevier.

GIBBS, R.J. (1970) Mechanisms Controlling World Water Chemistry. *Science* 170 (3962), pp. 1088.

GLANZMAN, R.K.; MCCARTHY, J.H.; RYTUBA, J.J. (1978) Lithium in the McDermitt caldera, Nevada and Oregon. *Energy* 3 (3), pp. 347–353.

GODFREY, L.V.; CHAN, L.-H.; ALONSO, R.N.; LOWENSTEIN, T.K.; MCDONOUGH, W.F.; HOUSTON, J.; LI, J.; BOBST, A.; JORDAN, T.E. (2013) The role of climate in the accumulation of lithium-rich brine in the Central Andes. *Applied Geochemistry* 38, pp. 92–102.

GRIMAUD, D.; HUANG, S.; MICHARD, G.; ZHENG, K. (1985) Chemical study of geothermal waters of Central Tibet (China). *Geothermics* 14 (1), pp. 35–48.

GROSJEAN, C.; MIRANDA, P.H.; PERRIN, M.; POGGI, P. (2012) Assessment of world lithium resources and consequences of their geographic distribution on the expected development of the electric vehicle industry. *Renewable and Sustainable Energy Reviews* 16 (3), pp. 1735–1744.

GROVE, M.J.; BAKER, P. A.; CROSS, S.L.; RIGSBY, C.A.; SELTZER, G.O. (2003) Application of strontium isotopes to understanding the hydrology and paleohydrology of the Altiplano, Bolivia-Peru. *Palaeogeography, Palaeoclimatology, Palaeoecology* 194 (1-3), pp. 281–297.

GRUBER, P.; MEDINA, P. (2010) Global lithium availability: A constraint for electric vehicles? Master thesis. University of Michigan.

GRUBER, P.W.; MEDINA, P.A.; KEOLEIAN, G.A.; KESLER, S.E.; EVERSON, M. P.; WALLINGTON, T.J. (2011) Global Lithium Availability. A Constraint for Electric Vehicles? *Journal of Industrial Ecology* 15 (5), pp. 760–775.

GUYOT, J.L.; ROCHE, M.A.; NORIEGA, L.; CALLE, H.; QUINTANILLA, J. (1990) Salinities and Sediment Transport in the Bolivian Highlands. *Journal of Hydrology* (113), pp. 147–162.

HASTENRATH, S.; KUTZBACH, J. (1985) Late Pleistocene climate and water budget of the south American Altiplano. *Quaternary Research* 24 (3), pp. 249–256.

HEATH, R.C. (1983) Basic Ground-Water Hydrology. *U.S. Geological Survey Water-Supply Paper* 2220. 86 pp.

HEINRICH, J. (2012) Chemical and isotopic investigation of lithium-rich brine from the Salar de Uyuni (Bolivia). Diplomarbeit. TU Freiberg, Freiberg.

HITCHON, B.; BILLINGS, G.K.; KLOVAN, J.E. (1971) Geochemistry and origin of formation waters in the western Canada sedimentary basin - III. Factors controlling chemical composition. *Geochimica et Cosmochimica Acta* 35 (6), pp. 567–598.

HOELZGEN, J. (2009) Lithium-Mangel bedroht die Auto-Revolution. *Spiegel Online* article, Hamburg Germany.

HOFMANN, H.; BAUER, A.; LAURENCE, N. (2004) Behavior of Smectite In Strong Salt Brines Under Conditions Relevant to the Disposal of Low- to Medium-grade Nuclear Waste. *Clays and Clay Minerals* 52 (1), pp. 14-24.

HÖLTING, B.; COLDEWEY, W.G. (2013) Hydrogeologie - Einführung in die Allgemeine und Angewandte Hydrogeologie. 8th ed., Springer-Verlag Berlin, Heidelberg.

HORSTMAN, E.L. (1957) The distribution of lithium, rubidium and caesium in igneous and sedimentary rocks. *Geochimica et Cosmochimica Acta* 12 (1-2), pp. 1–28.

HOSSEINI ARIA, S.E.; DONSELAAR, M.E.; LINDENBERGH, R.; KOENDERS, R.; LI, J.; OYEN, A. (2012) Monitoring a river channel network at Salar de Uyuni using Landsat ETM+ images. *Proceedings of SPIE - The International Society for Optical Engineering* 8531:85310A, 9 pp.

HUH, Y.; CHAN, L.-H.; ZHANG, L.; EDMOND, J.M. (1998) Lithium and its isotopes in major world rivers: Implications for weathering and the oceanic budget. *Geochimica et Cosmochimica Acta* 62 (12), pp. 2039–2051.

JACKISCH, R. (2014) Estimation of the surface catchment area of the Salar de Uyuni, in order to investigate the sources of minerals accumulated in the salt lake. Bachelor thesis. TU Bergakademie Freiberg, Freiberg.

JENSON, S.K.; DOMINGUE, J.O. (1988) Extracting Topographic Structure from Digital Elevation Data for Geographic Information System Analysis. *Photogrammetic Engineering & Remote Sensing* 54 (11), pp. 1593–1600.

JONES, B.F.; EUGSTER, H.P.; RETTIG, S.L. (1977) Hydrochemistry of the Lake Magadi Basin, Kenya. *Geochimica et Cosmochimica Acta* 41, pp. 53–72.

KAMPF, S.K.; TYLER, S.W.; ORTIZ, C.A.; Munoz, J.F.; ADKINS, P.L. (2005) Evaporation and land surface energy budget at the Salar de Atacama, Northern Chile. *Journal of Hydrology* 310, pp. 236–252

KANOUA, W.; MERKEL, B.J. (2016) Modification of a digital elevation model (DEM) in a flat topographic area with respect to manmade features. *Geosciences Journal* 20 (1), pp. 101–115.

KENDALL, C.; CALDWELL, E.A. (1998) Fundamentals of Isotope Geochemistry. In: KENDALL, C; MCDONNELL, J.J. (Eds.) Isotope Tracers in Catchment Hydrology. 1st volume, Elsevier Amsterdam, pp. 51–86.

KESLER, S.E.; GRUBER, P.W.; MEDINA, P.A.; KEOLEIAN, G.A.; EVERSON, M.P.; WALLINGTON, T.J. (2012) Global lithium resources: Relative importance of pegmatite, brine and other deposits. *Ore Geology Reviews* 48, pp. 55–69.

KING, M. (2010) Amended inferred resource estimation of Lithium and Potassium at the Cauchari and Olaroz Salars, Jujuy province, Argentina. Report, 126 pp.

KNIGHT PIÉSOLD CONSULTING (2000) Proyecto San Cristóbal, Provincia de Nor Lípez, República de Bolivia. Estudio de Evaluación de Impacto Ambiental. Unpublished report

KROUSE, H.R.; COOK, F.D.; SASAKI, A.; SMEJKAL, V. (1970) Microbial isotope fractionation in springs in western Canada. In: OGATA, K.; HAYAKAWA, T. (Eds.) Recent Developments in Mass Spectroskopy. *Proceedings International Conference on Mass Spectroskopy* Kyoto, Japan, pp. 629–639.

LARRONDO, P., SIMON, A., ETIENNE, M. (2011) Salar de Diablillos Project, Salta Province, Argentina, Technical Report on Brine Resource Estimate 43-101.

LEBRUN, V.; PACOSILLO, P.; GUTIERREZ, J.; CACERES, F.; POOL, E.; PIRARD, E. (2002) Geochemistry of bitter brines in the Salar de Coipasa – Bolivia. *Aardkundige Mededelingen* (12), pp. 185–188.

LI, J. (2014) Terminal Fluvial Systems in a Semi-arid Endorheic Basin, Salar de Uyuni (Bolivia). Dissertation, TU Delft, 164 pp.

LI, J.; MENENTI, M.; MOUSIVAND, A.; LUTHI, S.M. (2014) Non-Vegetated Playa Morphodynamics Using Multi-Temporal Landsat Imagery in a Semi-Arid Endorheic Basin: Salar de Uyuni, Bolivia. *Remote Sensing* 6, pp. 10131–10151.

LIDE, D. (1994) CRC Handbook of Chemistry and Physics. 75th ed., CRC Press.

LLOYD, R.M. (1966) Oxygen isotope enrichment of sea water by evaporation. *Geochimica et Cosmochimica Acta* 30 (8), pp. 801–814.

LÜDERS, V.; PLESSEN, B.; ROMER, R.L; WEISE, S.M; BANKS, D.A; HOTH, P.; DULSKI, P.; SCHETTLER, G. (2010) Chemistry and isotopic composition of Rotliegend and Upper Carboniferous formation waters from the North German Basin. *Chemical Geology* 276, pp. 198–208.

MARDONES, L. (1998) Flux et evolution des solutions salines dans les systemes hydrologiques des salars d'Asoctan et d'Atacama. PhD Dissertation, University of Paris, 278 p.

MARSH, S.P.; RICHTER, D.H.; LUDINGTON, S.; SORIA-ESCALANTE, E.; ESCOBAR-DIAZ, A. (1995) Digital Geologic Map of the Altiplano and Cordillera Occidental, Bolivia. *U.S. Geological Survey Open-File Report* 95-454

MARTIN, J.B.; KASTNER, M.; ELDERFIELD, H. (1991) Lithium: sources in pore fluids of Peru slope sediments and implications for oceanic fluxes. Marine Geology 102, pp. 281–292.

MARTIN, G.; RENTSCH, L.; HÖCK, M.; BERTAU, M. (2017): Lithium market research – global supply, future demand and price development. *Energy Storage Materials* 6, pp. 171–179.

MCGEARY, S.; BILLS, B.G.; JIMENEZ, G. (2003) Shallow Seismic Reflection Imaging of the Salar de Uyuni, Bolivia: Quaternary Neotectonics and Stratigraphy. *American Geophysical Union*, Fall Meeting 2003, 1 p.

MEIER, L.P.; KAHR, G. (1999) Determination of the Cation Exchange Capacity (CEC) of Clay Minerals Using the Complexes of Copper(II) Ion with Triethylenetetramine and Tetraethylenepentamine. *Clays and Clay Minerals* 47 (3), pp. 386–388.

MEYER, K.M.; KUMP, L.R. (2008) Oceanic Euxinia in Earth History: Causes and Consequences. *Annal Reviews in Earth and Planetary Science* 36 (1), pp. 251–288.

MIANPING, Z. (1997) An Introduction to Saline Lakes on the Qinghai—Tibet Plateau. *Monographiae Biologicae* 76, Springer Netherlands, 295 pp.

MISRA, S.; FROELICH, P.N. (2009): Measurement of lithium isotope ratios by quadrupole-ICP-MS: application to seawater and natural carbonates. *Journal of Analytical Atomic Spectrometry* 24 (11), pp. 1524–1533.

MOHR, S.H.; MUDD, G.M.; GIURCO, D. (2012) Lithium Resources and Production: Critical Assessment and Global Projections. *Minerals* 2, pp. 65–84.

MOSER, H.; RAUERT, W. (1980) Isotopenmethoden in der Hydrologie. Lehrbuch der Hydrogeologie 8, Borntraeger.

MÜLLER, E.P.; PAPENDIECK, G. (1975) Zur Verteilung, Genese und Dynamik von Tiefenwässern unter besonderer Berücksichtigung des Zechsteins. *Zeitschrift für geologische Wissenschaften* 3 (2), pp. 167–196.

MUNK, L.A.; BRADLEY, D.C.; HYNEK, S.A.; CHAMBERLAIN, C.P. (2011) Origin and Evolution of Li-rich Brines at Clayton Valley, Nevada, USA. *11th SGA Biennial Meeting*, Antofagasta, Chile. pp. 217-219.

MUNK, L.A.; HYNEK, S.A.; BRADLEY, D.C.; BOUTT, D.; LABAY, K.; JOCHENS, H. (2016) Lithium Brines: A Global Perspective. *Reviews in Economic Geology* 18, pp. 339–365.

NEWMAN, B.D.; FUENTES, H.R.; POLZER, W.L. (1991) An Evaluation of Lithium Sorption Isotherms and Their Application to Ground-Water Transport. *Ground Water* 29 (6), pp. 818–824.

NISHRI, A.; BEN-YAAKOV, S. (1990) Solubility of oxygen in the Dead Sea brine. *Hydrobiologia* 197 (1), pp. 99–104.

NISSENBAUM, A. (1977) Minor and trace elements in Dead Sea water. *Chemical Geology* 19, pp. 99–111.

NITTETSU MINING CONSULTANTS CO., LTD (2011) Bolivia-Japan Joint Study on the Groundwater Resources in San Cristobal Mine. Unpublished report, 86 pp.

NORTON, J. J. (1973): Lithium, Cesium, and Rubidium - The rare alkali metals. In: D. A. BROBST, W. P. PRATT (Eds.) United States Mineral Resources. *Geological Survey Prof. Paper* 820, pp. 365–378.

OCOLA, L.C., MEYER, R.P., ALDRICH, L.T. (1971) Gross crustal structure under Peru-Bolivia altiplano. *Earthquake Notes* 42, pp.33–48

OGAWA, Y.; KOIBUCHI, H.; SUTO, K.; INOUE, C. (2014) Effects of the Chemical Compositions of Salars de Uyuni and Atacama Brines on Lithium Concentration during Evaporation. *Resource Geology* 64 (2), pp. 91–101

PARKER, R.L. (1967) Composition of the Earth's crust, Chap. D. In: Data of geochemistry, 6th edition. *U.S. Geological Survey Prof. Paper* 440-D, 19 p.

PARKHURST, D.L; APPELO, C.A.J. (1999): PHREEQC for Windows. A Computer Program for Speciation, Batch-reaction, One-dimensional Transport and Inverse Geochemical Calculations. *U.S. Geological Survey Water Resources Investigations Report* (99-4259) Denver, Colorado.

PARNACHEV, V.P.; BANKS, D.; BEREZOVSKY, A.Y.; GARBE-SCHÖNBERG, D. (1999) Hydrochemical evolution of Na-SO4-Cl groundwaters in a cold, semi-arid region of southern Siberia. *Hydrogeology Journal* 7 (6), pp. 546–560.

PAVLOVIC, P., FOWLER, J. (2004) Evaluation of the potential of Salar del Rincon brine deposit as a source of lithium, potash, boron and other mineral resources. Edited by Admiralty Resources NL. Melbourne, Australia.

PEREZ-FERNANDEZ, C.A.; IRIARTE, M.; HINOJOSA-DELGADILLO, W.; VEIZAGA-SALINAS, A.; CANO, R.J.; RIVERA-PEREZ, J.; TORANZOS, G.A. (2016) First insight into microbial diversity and ion concentration in the Uyuni salt flat, Bolivia. *Caribbean Journal of Science* 49 (1), pp. 57–75.

PLUMMER, L.N.; PARKHURST, D.L; FLEMING, G.W.; DUNKLE, S.A. (1988) A computer program incorporating Pitzer's equations for calculation of geochemical reactions in brines. *U.S. Geological Survey Water-Resources Investigations Report* 88-4153.

RAMOS RAMOS, O.E.; CÁCERES, L.F.; ORMACHEA MUÑOZ, M.R.; BHATTACHARYA, P.; QUINO, I.; QUINTANILLA, J.; SRACEK, O.; THUNVIK, R.; BUNDSCHUH, J.; GARCÍA, M.E. (2012) Sources and behavior of arsenic and trace elements in groundwater and surface water in the Poopó Lake Basin, Bolivian Altiplano. *Environmental Earth Sciences* 66 (3), pp. 793–807.

RETTIG, S. L.; JONES, B.F.; RISACHER, F. (1980) Geochemical Evolution of Brines in the Salar of Uyuni, Bolivia. *Chemical Geology* (30), pp. 57–79.

REYES, N.; VIDAL, A.; RAMIREZ, E.; ARNASON, K.; RICHTER, B.; STEINGRIMSSON, B.; ACOSTA, O.; CAMACHO, J. (2011) Geothermal Exploration at Irruputuncu and Olca Volcanoes: Pursuing a Sustainable Mining Development in Chile. *GRC Transactions* 35, pp. 983–986.

RISACHER, F.; FRITZ, B. (1992) Paleoclimatic Significance of the Occurrence of Polyhalite in the Salar of Uyuni (Bolivia) - Detection of an Extremely Severe Drought in the Central Altiplano. *Comptes Rendus De L'Academie Des Sciences Serie Ii* 314 (12), pp. 1371–1377.

RISACHER, F.; FRITZ, B. (2009) Origin of Salts and Brine Evolution of Bolivian and Chilean Salars. *Aquatic Geochemistry* 15, pp. 123–157.

RISACHER, F.; MIRANDA, J. (1977) High lithium and boron concentrations in the evaporitic ponds of the Bolivian Altiplano. *O.R.S.T.O.M. Paris* (Prelim. Note).

RISACHER, F.; FRITZ, B. (1991a) Geochemistry of Bolivian salars, Lipez, southern Altiplano: Origin of solutes and brine evolution. *Geochimica et Cosmochimica Acta* (55), pp. 687–705.

RISACHER, F.; FRITZ, B. (1991b) Quaternary geochemical evolution of the salars of Uyuni and Coipasa, Central Altiplano, Bolivia. *Chemical Geology* 90, pp. 211–231.

RISACHER, F.; FRITZ, B. (2000): Bromine geochemistry of salar de Uyuni and deeper salt crusts, Central Altiplano, Bolivia. .*Chemical Geology* 167 (3-4), pp. 373–392.

RISACHER, F.; FRITZ, B.; ALONSO, H. (2006) Non-conservative behavior of bromide in surface waters and brines of Central Andes: A release into the atmosphere? G*eochimica et Cosmochimica Acta* 70 (9), pp. 2143–2152.

ROCHE, M. A., BOURGES, J., CORTES, J., MATTOS, R. (1992): Climatology and hydrology of the Lake Titicaca basin. In C. Dejoux, A. Iltis (Eds.): Lake Titicaca. A Synthesis of Limnological Knowledge. Dordrecht: Kluwer Academic, pp. 63–88.

RODRÍGUEZ, I.; ROCHE, O.; MOUNE, S.; AGUILERA, F.; CAMPOS, E.; PIZARRO, M. (2015) Evolution of Irruputuncu volcano, Central Andes, northern Chile. *Journal of South American Earth Sciences* 63, pp. 385–399.

RONOV, A.B; MIGDISOV, A.A; VOSKRESENSKAYA, N.T; KORZINA, G.A (1970) Geochemistry of Lithium in the sedimentary Cycle. *Geochemistry International* 7 (1), pp. 75–102.

ROUNDS, S.A., WILDE, F.D., AND RITZ, G.F. (2013) National field manual for the collection of water-quality data, 6.2 Dissolved oxygen. chapter A6: field measurements. In: USGS (Ed.) U.S. Geological Survey Techniques of Water-Resources Investigations, book 9.

SALAMEH, E.; EL-NASER, H. (1999) Does the Actual Drop in Dead Sea Level Reflect the Development of Water Sources Within its Drainage Basin? *Acta hydrochim. hydrobiol.* 27, pp. 5–11.

SCHAFMEISTER, M.TH. (1999) Geostatistik für die hydrogeologische Praxis. Springer Berlin, Heidelberg.

SCHMIDT, H.; EULER, B.; VOIGT, W.; HEIDE, G. (2009) Lithium carnallite, $LiCl \cdot MgCl_2 \cdot 7H_2O$. *Acta Crystallographica* C65, pp. i57-i59.

SCHMIDT, N. (2010) Hydrogeological and hydrochemical investigations at the Salar de Uyuni, Bolivia, with regard to the extraction of lithium. *Freiberg Online Geology* 26, 142 pp.

SCHULER, M., BLANC-VALLERON, M.M., RISACHER, F. (1995) La matière organique des alternances sel-Marne du salar d'Uyuni (Altiplano, Bolivie): études géochimiques et palynologiques. *Sciences Géologiques Bulletin* 48 (4), pp. 211–247.

SERVANT, M., FONTES, J.C. (1978) Les lacs quaternaires des hauts plateaux des Andes boliviennes: premières interprétations paléoclimatiques. *Cahiers ORSTO Série Géologie* 10 (1), pp. 9–23.

SHCHERBAKOV, A.V.; DVOROV, V.I. (1970) Thermal waters as a source for extraction of chemicals. *Proceedings of the United Nations symposium on the development and utilization of geothermal resources* 2 (Part 2), pp. 1636–1639.

SHOUAKAR-STASH, O.; ALEXEEV, S.V.; FRAPE, S.K.; ALEXEEVA, L.P.; DRIMMIE, R.J. (2007) Geochemistry and stable isotopic signatures, including chlorine and bromine isotopes, of the deep groundwaters of the Siberian Platform, Russia. *Applied Geochemistry* 22 (3), pp. 589–605.

SIELAND, R. (2014): Hydraulic investigations of the Salar de Uyuni, Bolivia. Dissertation. TU Freiberg, Freiberg. Geologie.

SOFER, Z.; GAT, J. R. (1975) The isotope composition of evaporating brines: Effect of the isotopic activity ratio in saline solutions. *Earth and Planetary Science Letters* 26, pp. 179–186.

SPARKS, R.S.J.; FOLKES, C..; HUMPHREYS, M.C.S.; BARFOD, D.N.; CLAVERO, J.; SUNAGUA, M.C.; MCNUTT, S.R.; PRITCHARD, M.E. (2006) Uturuncu Volcano, Bolivia; volcanic unrest due to mid-crustal magma intrusion. *American Journal of Science* 308 (6), pp. 727–769.

STANLEY, C.J.; JONES, GARY C.; RUMSEY, M.S.; BLAKE, C.; ROBERTS, A.C.; STIRLING, J.A.R.; CARPENTER, G.J.C.; WHITFIELD, P.S.; GRICE, J.D.; LEPAGE, Y. (2007) Jadarite, $LiNaSiB_3O_7(OH)$, a new mineral species from the Jadar Basin, Serbia. *European Journal of Mineralogy* 19 (4), pp. 575–580.

STARKEY, H.C. (1982) The Role of Clays in Fixing Lithium. *U.S. Geological Survey Bulletin* 1278-F.

STRECKEISEN, A. (1979): Classification and nomenclature of volcanic rocks, lamprophyres, carbonatites, and melilitic rocks: Recommendations and suggestions of the IUGS Subcommission on the Systematics of Igneous Rocks. *Geology* 7 (7), pp. 331–335.

STUIVER, M.; POLACH, H.A. (1977) Discussion - Reporting of 14C Data. *Radiocarbon* 19 (3), pp. 355–363.

SVENDSEN, J.B. (2003) Parabolic halite dunes on the Salar de Uyuni, Bolivia. *Sedimentary Geology* (155), pp. 147–156.

SYLVESTRE, F.; SERVANT, M.; SERVANT-VILDARY, S.; CAUSSE, C.; FOURNIER, M.; YBERT, J. P. (1999) Lake-level chronology on the southern Bolivian Altiplano (18 degrees-23 degrees S) during late-glacial time and the early Holocene. *Quaternary Research* 51 (1), pp. 54–66.

TAN, H.; CHEN, J.; RAO, W.; ZHANG, W.; ZHOU, H. (2012) Geothermal constraints on enrichment of boron and lithium in salt lakes: An example from a river-salt lake system on the northern slope of the eastern Kunlun Mountains, China. *Journal of Asian Earth Sciences* 51, pp. 21–29.

TAN, H.; RAO, W.; MA, H.; CHEN, J.; LI, T. (2011) Hydrogen, oxygen, helium and strontium isotopic constraints on the formation of oilfield waters in the western Qaidam Basin, China. *Journal of Asian Earth Sciences* 40 (2), pp. 651–660.

TARDY, Y.; KREMPP, G.; TRAUTH, N. (1972) Le lithium dans les minéraux argileux des sédiments et des sols. *Geochimica et Cosmochimica Acta* 36 (4), pp. 397–412.

THORBURN, P.J.; WALKER, G.R.; WOODS, P.H. (1992) Comparison of diffuse discharge from shallow water tables in soils and salt flats. *Journal of Hydrology* 136, pp. 253–274.

UNESCO (1971) Convention on Wetlands of International Importance especially as Waterfowl Habitat. Ramsar, Iran, 3 pp.

U.S. GEOLOGICAL SURVEY (2017) Mineral commodity summaries.

U.S. GEOLOGICAL SURVEY; SERVICIO GEOLOGICO DE BOLIVIA (1992) Geology and mineral resources of the Altiplano and Cordillera Occidental, Bolivia. *U.S. Geological Survey Bulletin* 1975.

VENGOSH, A.; STARINSKY, A.; KOLODNY, Y.; CHIVAS, A.R. (1991) Boron isotope geochemistry as a tracer for the evolution of brines and associated hot springs from the Dead Sea, Israel. *Geochimica et Cosmochimica Acta* 55 (6), pp. 1689–1695.

VINANTE, D.; ALONSO, R.N. (2006) Evapofacies del Salar de Hombre Muerto, Puna Argentina: Distribucion y Genesis. *Revista de la Asociación Geológica Argentina* 61 (2), pp. 286–297.

VINE, J.D. (1975) Lithium in sediments and brines - how, why, and where to search. *Journal of Research of the U.S. Geological Survey* 3 (4), pp. 479-485.

VINE, J.D. (1980) Where on earth is all the lithium? *U.S. Geological Survey Open-File Report* 80-1234.

VINE, J.D.; TOURTELOT, E.B.; GLANZMAN, R.K.; BOHANNON, R.G.; DAVIS, J.R.; MEIER, A.L. (1975) Are lithium-rich sedimentary rocks and brines related to tectonic activity. *9th International Congress of Sedimentology, Nice,* pp. 105–110.

VOIGT, W.; HEIDE, G.; SCHMITT, J.; BELTZ, C.; HERTAM, A.; JIMENEZ, C.J.T.; MORALES, H.R.; MORALES, G.M.; TERCEROS, L.F. (2010a) Verfahren und Vorrichtung zur solaren Eindampfung von Salzlösungen. Patent WO 2010/086375 A1. Technische Universität Bergakademie Freiberg and Universidad Autónoma Tomas Frias (Potosí, Bolivia).

VOIGT, W.; JIMENEZ, C.J.T.; MORALES, H.R.; TERCEROS, L.F. (2010b) Verfahren zur Abreicherung von Magnesium und Anreicherung von Lithium in chloridisch geprägten Salzlösungen. German patent DE102010019554. Technische Universität Bergakademie Freiberg and Universidad Autónoma Tomas Frias (Potosí, Bolivia).

VOIGT, W. (2014) Lithiumgewinnung aus Primärrohstoffen - Stand und Perspektiven. In: KAUSCH, P.; BERTAU, M.; GUTZMER, J.; MATSCHULLAT, J. (Eds.) Strategische Rohstoffe - Risikovorsorge. Springer Berlin Heidelberg, pp. 75-95.

VUILLE, M. (1999) Atmospheric circulation over the Bolivian Altiplano during dry and wet periods and extreme phases of the Southern Oscillation. *International Journal of Climatology* 19 (14), pp. 1579–1600.

WANG, L.; MENG, C.G.; HAN, M.; MA, W. (2008) Lithium uptake in fixed-pH solution by ion sieves. *Journal of Colloid and Interface Science* 325 (1), pp. 31–40.

WARREN, J.K. (2016) Evaporites. A geological compendium. 2nd ed., Springer.

WHITE, D.E. (1957) Thermal waters of volcanic origin. *Bulletin of the Geological Society of America* 68 (12), pp. 1637-1658.

WIETELMANN, U.; STEINBILD, M. (2000) Lithium and Lithium Compounds. Ullmann's Encyclopedia of Industrial Chemistry: Wiley-VCH Verlag.

WILLIAMS, W. D. (1996) The largest, highest and lowest lakes of the world: Saline Lakes. *Verhandlungen des Internationalen Verein Limnologie* 26, pp. 61–79.

WOLF, M. (1988) Salare des Altiplanos: Ihre Entstehung und wirtschaftliche Bedeutung. Veröffentlichung Nr. 2305 der Sektion Geowissenschaften. TU Bergakademie Freiberg.

WOLF, M. (2010) Salar des Altiplano - ihre Entstehung und wirtschaftliche Bedeutung. *Bodenökologie und Bodengenese* 41, 80 p.

YAKSIC, A.; TILTON, J.E. (2009) Using the cumulative availability curve to assess the threat of mineral depletion: The case of lithium. *Resources Policy* 34, pp. 185–194.

ZEIEN, H. (1995) Chemische Extraktionen zur Bestimmung der Bindungsformen von Schwermetallen in Böden. *Bonner Bodenkundliche Abhandlungen* 17, Bonn.

ZHENG, M.; LIU, X. (2009) Hydrochemistry of Salt Lakes of the Qinghai-Tibet Plateau, China. *Aquat Geochem* 15 (1-2), pp. 293–320.

Appendix

Appendix A: Tables

Table A - 1: *Estimated world lithium resources according to source type (max. Li-contents are in ppm (brines) and % (rocks)*

Type	Country	Name	Li-content max.	Approximate Li resources [kt]	Sources
Oilfield brines	China	Qaidam Basin	1,890	3,000	Tan et al. (2011)
	USA	Smackover Formation	692	1,000	Collins (1978)
Geothermal brines	USA	Salton Sea	194	316	Berthold & Baker (1976)
		Brawley	219	1,000	Gruber et al. (2011)
Formation brines	Canada	Beaverhill Lake	32	515	Hitchon et al. (1971)
Pegmatite / Spodumene	Australia	Greenbushes	1.6	560	Gruber et al. (2011)
	USA	North Carolina	-	2,600	Yaksic & Tilton (2009)
	Congo	Manono	0.6	2,300	Yaksic & Tilton (2009)
	Canada	-	-	250	Evans (2008)
	Russia	various	-	1,000	Evans (2008)
	China	various	-	750	Evans (2008)
Hectorite / Jadarite	Usa	King's Valley	-	2,000	Gruber et al. (2011)
	Serbia	Jadar Valley	-	1,000	Gruber et al. (2011)
Salt lake brines	Argentina	Diablillos	1,000	530	Larrondo et al. (2011)
		Hombre Muerto	2,000	2,500	Vinante et al. (2006)
		Salar de Olaroz	825	1,200	King (2010)
		Salar del Rincon	2,400	5,500	Pavlovic & Fowler (2004)
	Bolivia	Salar de Uyuni	1,500	7,000	Sieland (2014)
	Chile	Salar de Atacama	4,000	7,000	Boschetti et al. (2007)
		Maricunga	-	220	Gruber et al. (2011)
	China	Zabuye	1,500	2,600	Kesler et al. (2012)
		DXC	430	181	Gruber & Medina (2010)

Given the large amount of brine, fresh water, rock and sediment samples, a distinct sample notation was essential. In the following table abbreviations are explained.

Table A - 2: Abbreviations used for the notation of solid samples from rocks, sediments, and salt crust; and fluid samples from brines, streams, springs, and wells

Notation	Explanation	Notation	Explanation
SLT	Salar de Uyuni	RÍO	River, stream
COI	Salar de Coipasa	SED	sediment
01-COL	Colchani	ROC	rock
02-LLI	Llica	SPEC	Spring / well
03-INC	Incahuasi	GRA	Río Grande
04-YON	Yonsa	COL	Río Colorado
05-TAH	Tahua	COA	Río Colcaja
06-NOR	Norte	OJO	Ojos del Salar – gas emanations
07-SAL	Sal	JIR	Jirira
08-CEN	Centro	TAH	Tahua
09-RÍO	Río Grande delta	UTU	Volcano Uturuncu
10-PES	Pescado	OLC	Volcano Olca
13-COR	Corazon	IRU	Volcano Irruputuncu

Table A - 3: Description of water sampling locations, including brine and freshwater samples (DL = drilling location; multiple sampling = more than one sample from different years)

Sample ID	Description	Coordinates (UTM, WGS 84)		Multiple sampling
		longitude	latitude	
Screened wells				
SLT-01-COL	DL "Colchani"	679816	7774574	x
SLT-02-LLI	DL "Llica"	601596	7791495	x
SLT-03-INC	DL "Incahuasi", ~ 8 km from island Incahuasi	649792	7749641	x
SLT-04-YON	DL "Yonsa"	590267	7745962	x
SLT-05-TAH	DL "Tahua", ~ 5 km from northern coast	635275	7797122	x
SLT-06-NOR	DL "Norte", northeastern part of salar	669422	7811071	x
SLT-07_SAL	DL "Hotel de Sal", ~ 10 km distance from salt hotel	694556	7742079	x
SLT-08-CEN	DL "Centro",central part of salt flat	649590	7774480	x
SLT-09-RÍO	DL "Río Grande", near to delta of Río Grande	666568	7720469	x
SLT-10-PES	DL "Pescado", near island "Isla Pescado"	625383	7777770	x
SLT-13-COR	DL "Corazon", central part of salt flat	663551	7788958	x
Shallow drillings				
SLT-NOR-A1	shallow transect drilling	653520	7817354	
SLT-NOR-A2	shallow transect drilling	655544	7815349	
SLT-NOR-A3	shallow transect drilling	657558	7813352	
SLT-NOR-A4	shallow transect drilling	659616	7811374	
SLT-NOR-A5	shallow transect drilling	661613	7809390	
SLT-NOR-A6	shallow transect drilling	663687	7807373	
SLT-NOR-B2	shallow transect drilling	665618	7815387	
SLT-NOR-B3	shallow transect drilling	665624	7813503	
SLT-NOR-B4	shallow transect drilling	665620	7811404	
SLT-NOR-B5	shallow transect drilling	665619	7809428	
SLT-NOR-B6	shallow transect drilling	665600	7807374	
SLT-NOR-C2	shallow transect drilling	673715	7813266	
SLT-NOR-C3	shallow transect drilling	671592	7811398	
SLT-NOR-C4	shallow transect drilling	669631	7809381	
SLT-NOR-C5	shallow transect drilling	667633	7807356	
SLT-NOR-D1	shallow transect drilling	657667	7805419	
SLT-NOR-D2	shallow transect drilling	661643	7805425	
SLT-NOR-D3	shallow transect drilling	665617	7805412	
SLT-NOR-D4	shallow transect drilling	669676	7805371	
SLT-NOR-D5	shallow transect drilling	673666	7805424	
SLT-NOR-D6	shallow transect drilling	677685	7805374	
SLT-NOR-D7	shallow transect drilling	681631	7805374	
SLT-NOR-Z1	shallow transect drilling	661721	7815473	
SLT-NOR-Z2	shallow transect drilling	669663	7815372	
SLT-NOR-Z3	shallow transect drilling	677645	7809397	
SLT-NOR-T2	shallow transect drilling	650317	7820437	
SLT-NOR-T2W	shallow transect drilling	668410	7819016	

Sample ID	Description	Coordinates (UTM, WGS 84)		Multiple sampling
		longitude	latitude	
SLT-NOR-T3	shallow transect drilling	651999	7818299	
SLT-NOR-T3W	shallow transect drilling	662934	7819640	
SLT-NOR-T4	shallow transect drilling	665616	7819429	
SLT-NOR-T4W	shallow transect drilling	656802	7818610	
SLT-NOR-T5	shallow transect drilling	665614	7817347	
SLT-NOR-T5W	shallow transect drilling	653869	7816348	
SLT-NOR-T6W	shallow transect drilling	651528	7814397	
SLT-NOR-T7	shallow transect drilling	670972	7818478	
SLT-NOR-T8	shallow transect drilling	660262	7820080	
SLT-NOR-T9	shallow transect drilling	658075	7817476	
SLT-NOR-T10	shallow transect drilling	651056	7816569	
SLT-NOR-T11	shallow transect drilling	654345	7819732	
SLT-RÍO-01	shallow drilling in southeastern part of salt flat	675614	7720920	
Rivers and streams				
SLT-RÍO-GRA	main inflow to salar (south)	704491	7681573	x
SLT-RÍO-COL	main inflow to salar (southeast)	724248	7719257	x
SLT-RÍO-TKPN	tributary to salar (north)	636432	7799868	
SLT-RÍO-TAH	"Río Tauha", tributary to salar (north)	636282	7800139	
UTU-RÍO-01	tributary, Uturuncu	667304	7574731	
UTU-RÍO-02	tributary, Uturuncu	673890	7546769	
UTU-RÍO-03	tributary "Quetena chico"	672615	7544216	
SLT-RÍO-R-01	tributary to Río Grande	653115	7582178	
SLT-RÍO-R-02	tributary to Río Grande	664044	7589285	
SLT-RÍO-R-03	tributary to Río Grande	641605	7630340	
SLT-RÍO-R-04	tributary to Río Grande	757269	7629465	
SLT-RÍO-SAG	tributary near village "San Agustin"	642576	7629631	
SLT-RÍO-COA	tributary "Río Colcaya"	651603	7811398	
Springs				
SLT-SPEC-JIR	thermal spring at foot of volcano Tunupa (northern coast)	648938	7800792	x
SLT-SPEC-OLC	Hot spring "Olca"	558107	7692772	
Others				
SLT-WELL-JIR	domestic well near village Jirira	649456	7803766	
SLT-SPEC-OJO	gas emanation spot at border area of salar, "Ojos del Salar"	709130	7752722	x
Salar de Coipasa				
COI-01-ENT	coast of Salar de Coipasa	598241	7838736	
COI-WES-A2	shallow transect drilling	615314	7845211	
COI-WES-A3	shallow transect drilling	612786	7844872	
COI-WES-A4	shallow transect drilling	609834	7844449	
COI-WES-A5	shallow transect drilling	606920	7844031	
COI-WES-A6	shallow transect drilling	603887	7843607	

Table A - 4: Field parameters and TDS values of stream, spring and groundwater samples from the Salar de Uyuni catchment

Sample ID	Type	TDS	T	pH	EMF	Eh	EC	O₂	
		g/L	°C		mV	mV	mS/cm	mg/L	%
SLT-RÍO-GRA-1210	stream	2.07	-	8.1	-	-	3.0	-	-
SLT-RÍO-GRA-0511	stream	1.73	7.0	8.4	188	411	3.08	8.21	107
SLT-RÍO-GRA-1211a	stream	2.03	18.8	8.4	101	314	3.38	6.22	107
SLT-RÍO-GRA-1211b	stream	2.29	17.3	8.6	<59,3	-	3.47	6.45	104
SLT-RÍO-GRA-0814	stream	1.99	14.3	8.4	24.5	213	3.1	6.69	104
SLT-RÍO-COL-0511	stream	4.05	7.5	8.5	73	296	6.51	8.18	106
SLT-RÍO-COL-1211a	stream	38.4	-	-	-	-	-	-	-
SLT-RÍO-COL-1211b	stream	61.2	10.7	8.1	194	414	86	6.96	98.4
SLT-RÍO-COL-0814	stream	4.39	10.5	8.3	39	231	7.52	7.41	105
SLT-RÍO-TKPN-1211	stream	0.68	21.3	8.6	164	374	1.06	6.22	112
SLT-RÍO-TAH-0914	stream	0.79	7.7	7.9	6.5	201	1.05	8.08	105
UTU-RÍO-01-0914	stream	0.78	0.6	8.9	12.9	177	0.809	8.82	93.5
UTU-RÍO-02-0914	stream	1.23	5.4	7.8	46.5	274	1.88	7.76	-
UTU-RÍO-03-0914	stream	0.44	17.7	8.6	56	271	479	6.09	106
SLT-R-01-0814	stream	0.06	-	7.4	-	-	91.2	-	-
SLT-R-02-0814	stream	1.72	-	8.1	-	-	2940	-	-
SLT-R-03-0814	stream	0.42	-	7.9	-	-	594	-	-
SLT-R-04-0814	stream	1.73	-	-	-	-	-	-	-
SLT-RÍO-SAG-1014	stream	0.55	23.9	9.0	31	240	818	6.82	129
SLT-RÍO-COA-0914	spring	5.31	18.6	6.2	3.6	167	10.4	4.56	75.9
SLT-SPEC-JIR-0511	spring	3.60	16.2	5.5	-78	137	6.62	1.23	16.3
SLT-SPEC-JIR-1211	spring	3.52	17.1	5.5	80.8	295	6.12	2.51	40.6
SLT-SPEC-OLC-0914	spring	1.13	40.1	7.7	33	176	1.57	4.94	126
SLT-WELL-JIR-0914	groundwater	0.98	-	-	-	-	-	-	-

Table A - 5: Element analysis of catchment water samples derived by IC (all values in mg/L, n.d. = not determined)

Sample ID	Li⁺	Na⁺	K⁺	Ca²⁺	Mg²⁺	Cl⁻	Br⁻	SO₄²⁻	HCO₃⁻
SLT-RÍO-GRA-1210	2.56	504	24.8	133	39.9	773	0.62	312	266
SLT-RÍO-GRA-0511	2.63	485	23.3	151	38.5	739	0.513	279	
SLT-RÍO-GRA-1211a	2.58	514	26.5	136	38.4	755	n.d.	307	237
SLT-RÍO-GRA-1211b	2.85	576	27.2	152	41.6	878		310	286
SLT-RÍO-GRA-0814	2.81	448	24.6	142	36.7	743	0.305	255	330
SLT-RÍO-COL-0511	1.38	1,207	32.8	210	50.7	1,842	0.293	698	
SLT-RÍO-COL-1211a		11,200	272	1149	651	19,239		5,689	
SLT-RÍO-COL-1211b	1.81	19,746	155	1621		35,911		3,580	123
SLT-RÍO-COL-0814	1.38	1,324	38.3	225	58.7	1783	n.d.	766	176
SLT-RÍO-TKPN-1211	0.056	65.2	9.20	97.9	33.9	154		144	167
SLT-RÍO-TAH-0914	0.050	68.6	8.72	128	38.1	157	0.137	160	223
UTU-RÍO-01-0914	0.092	76.2	10.4	57.2	73.7	n.d.	n.d.	78.2	485
UTU-RÍO-02-0914	2.01	207.7	20.8	148	46.3	450	0.486	76.7	270
UTU-RÍO-03-0914	0.134	57.9	6.36	47.3	7.52	18.1	n.d.	42.6	257
SLT-R-01-0814	<DL	7.43	3.96	5.52	1.61	4.23	n.d.		36.2
SLT-R-02-0814	6.67	376	33.8	139	47.4	797	0.629	55.0	250
SLT-R-03-0814	0.384	60.8	5.80	47.7	22.3	96.7	0.041	37.0	147
SLT-R-04-0814	0.135	144	5.54	341	33.0	174	n.d.	1,025	n.d.
SLT-RÍO-SAG-1014	0.838	102	10.7	27.7	23.1	143	0.066	27.3	209
SLT-RÍO-COA-0914	6.63	1,676	142	91.9	177	2,887	0.442	237	79.1
SLT-SPEC-JIR-0511	4.58	1,045	122	77.4	136	1,954	0.838	247	
SLT-SPEC-JIR-1211	4.43	1,030	122	71.4	131	1,865		242	43.8
SLT-SPEC-OLC-0914	0.105	173	48.7	104	52.3	78.1	0.022	493	179
SLT-WELL-JIR-0914	0.832	223	33.3	75.3	31.0	342	0.070	147	123

Table A - 6: Chemical composition of catchment water samples derived by ICP-MS (values with < are below detection limit

Sample ID	Li	B	Al	Si	P	V	Mn	Fe	Ni
	ppb	ppm	ppb	ppm	ppb	ppb	ppb	ppb	ppb
SLT-RÍO-GRA-1210	2,884	12.6	5.31	33.2	77.8	18.2	10.4	7.30	0.38
SLT-RÍO-GRA-0511	2,555	10.8	11.2	28.2	99.1	10.9	31.9	17.1	0.52
SLT-RÍO-GRA-1211a	2,685	13.5	10.8	32.7	85.1	15.9	8.94	12.6	0.53
SLT-RÍO-GRA-1211b	2,946	14.0	13.8	29.5	112	16.0	29.9	13.8	0.76
SLT-RÍO-GRA-0814	2,143	8.92	11.4	20.6	105	10.8	6.01	10.8	0.25
SLT-RÍO-COL-0511	1,373	9.14	3.87	28.6	38.6	14.1	58.1	4.45	0.69
SLT-RÍO-COL-1211a	14,840	108	15.2	20.5	148	40.0	2,818	25.0	6.57
SLT-RÍO-COL-1211b	5,852	20.5	<10	17.1	137	22.7	1,012	121	2.78
SLT-RÍO-COL-0814	1,517	11.5	<11	28.9	<110	15.0	9.97	<11	<1.1
SLT-RÍO-TKPN-1211	61.8	3.70	3.15	40.7	146	6.39	14.1	20.4	0.21
SLT-RÍO-TAH-0914	58.3	3.85	2.00	35.0	130	5.17	3.30	24.7	0.28
UTU-RÍO-01-0914	103	0.62	6.38	41.7	69.7	20.4	3.98	10.6	0.49
UTU-RÍO-02-0914	2,082	5.54	5.76	36.8	70.3	9.40	163	69.5	0.43
UTU-RÍO-03-0914	127	0.73	9.19	19.8	25.1	8.02	5.79	25.2	0.20
SLT-R-01-0814	8.73	0.310	33.2	17.7	47.3	1.85	6.86	162	<0.1
SLT-R-02-0814	5,334	11.1	3.30	35.2	73.5	18.6	87.2	33.3	0.35
SLT-R-03-0814	380	1.70	26.7	28.6	185	17.7	3.32	8.25	<0.1
SLT-R-04-0814	82.5	1.57	3.05	8.6	43.5	5.42	2.72	4.27	<0.2
SLT-RÍO-SAG-1014	806	2.44	6.71	37.3	157	13.24	4.38	17.9	0.13
SLT-RÍO-COA-0914	7,240	11.9	<11	39.5	310	6.36	2.74	<11	6.07
SLT-SPEC-JIR-0511	4,594	8.62	6.27	48.8	393	2.44	1,445	78.1	12.1
SLT-SPEC-JIR-1211	5,178	9.21	5.64	50.0	404	2.86	1,616	50.7	13.1
SLT-SPEC-OLC-0914	98.6	1.66	2.71	60.2	128	46.3	0.123	1.80	<0.1
SLT-WELL-JIR-0914	923	3.02	2.42	42.0	712	7.22	3.02	2.53	4.93

Sample ID	Cu	Zn	As	Br	Rb	Sr	Mo	Cs	Ba	U
	ppb	ppb	ppb	ppb	ppb	ppb	ppb	ppb	ppb	ppb
SLT-RÍO-GRA-1210	1.23	37	265	725	54.2	2,342	4.73	14.9	75.4	3.20
SLT-RÍO-GRA-0511	<2	180	229	634	37.8	2,168	3.77	13.1	74.2	3.15
SLT-RÍO-GRA-1211a	<2	<2	244	716	57.1	2,214	4.39	24.6	71.2	3.20
SLT-RÍO-GRA-1211b	1.21	<2	296	745	49.9	2,584	4.86	22.0	78.3	2.89
SLT-RÍO-GRA-0814	2.19	<2	204	498	36.6	1,498	2.62	8.23	58.1	2.21
SLT-RÍO-COL-0511	<2	111	105	444	8.32	2,628	5.84	0.78	78.9	5.32
SLT-RÍO-COL-1211a	<10	<10	426	6,048	78.2	30,430	87.6	9.04	193	44.9
SLT-RÍO-COL-1211b	<10	<10	190	1,497	55.0	25,680	35.8	7.01	296	8.75
SLT-RÍO-COL-0814	<11	79.2	109	451	12.1	3,213	7.93	0.470	58.0	6.14
SLT-RÍO-TKPN-1211	<2	<2	4.75	367	11.8	714	0.902	0.06	57.6	0.791
SLT-RÍO-TAH-0914	<1	74.7	5.83	389	9.96	615	0.926	0.04	50.3	1.14
UTU-RÍO-01-0914	<1	10.2	46.1	45.3	46.4	648	7.90	4.09	30.4	2.89
UTU-RÍO-02-0914	<1	1.95	360	886	74.5	1,750	2.17	66.3	61.1	0.937
UTU-RÍO-03-0914	9.98	12.6	22.6	56.5	19.4	420	0.529	1.42	8.11	1.71
SLT-R-01-0814	1.01	11.4	5.64	19.8	15.5	45.5	0.400	0.940	11.2	0.03
SLT-R-02-0814	<3	<3	560	1,163	214.90	2,767	2.53	379.60	61.0	1.63
SLT-R-03-0814	<1	9.31	206	196	21.6	287	1.46	12.4	6.64	1.44
SLT-R-04-0814	3.82	3.26	15.1	149	1.29	4,806	0.80	0.132	18.3	3.09
SLT-RÍO-SAG-1014	<1	<1	445	138	41.4	389	2.50	42.7	17.0	1.61
SLT-RÍO-COA-0914	<11	239	<2.2	2,097	379	1,937	0.547	49.8	68.5	2.22
SLT-SPEC-JIR-0511	< 2	208	6.42	1,116	135	403	0.43	8.29	19.5	0.173
SLT-SPEC-JIR-1211	<5	62.2	5.84	1,163	139	439	0.52	7.93	15.7	0.165
SLT-SPEC-OLC-0914	<1	1.72	116	85.0	103	342	22.0	12.2	4.21	0.54
SLT-WELL-JIR-0914	3.39	159	2.58	353	39.39	194	2.30	0.404	38.6	0.03

Table A - 7: Field parameters and TDS values of brine samples from screened wells and shallow transect drillings from the Salar de Uyuni (n.e. – no equilibrium)

Sample ID	TDS	T	pH	EMF	Eh	EC	O₂	
	g/L	°C		mV	mV	mS/cm	mg/L	%
Screened wells								
SLT-01-COL-B-0909	307	5.1	7.1	-115	95.9	242	3.99	49
SLT-01-COL-B-0511	321	10.4	7.3	-277	-56.6	243	0.89	-
SLT-01-COL-B-1211	330	15.1	7.2	-104	-	235	0.96	15.3
SLT-01-COL-B-0914	318	4.9	7.3	-37	160	234	0.65	7.5
SLT-01-COL-C-0909	311	4.6	7.1	-73	138	234	3.19	38.2
SLT-01-COL-C-0511	330	10.3	7.3	-294	-73.7	240	0.38	5.2
SLT-01-COL-C-1211	332	8.7	7.2	<-105	-	228	1.21	15.5
SLT-01-COL-C-0914	317	4.9	7.2	-234	-36.8	235	3.47	43.4
SLT-01-COL-E-0909	300	4.6	7.1	-81	130	238	6.24	75.6
SLT-01-COL-E-0511	332	9.2	7.3	-246	-24.7	238	0.37	4.9
SLT-01-COL-E-1211	331	16.0	7.3	-111	104	232	1.01	15.9
SLT-01-COL-E-0914	308	6.2	7.2	-116	80.4	235	4.63	58.8
SLT-01-COL-F-0909	309	7.4	7.1	-133	77.5	227	3.68	47.7
SLT-01-COL-F-0511	326	8.8	7.3	-157	64.6	245	4.94	66.3
SLT-01-COL-F-1211	326	13.5	7.2	-132	85.4	228	1.23	18.4
SLT-01-COL-F-0914	312	6.0	7.3	-104	91.9	228	4.57	57.5
SLT-02-LLI-A-1211	330	16.3	7.1	-252	-36.9	232	1.07	17
SLT-02-LLI-A-1112	312	11.3	7.2	-298	-78.6	237	1.42	-
SLT-02-LLI-A-0914	309	6.8	7.1	-283	-87.5	234	0.47	5.8
SLT-02-LLI-B-1110	293	12.5	7.0	-336	-81.0	224	0.80	11.8
SLT-02-LLI-B-1211	327	15.8	7.1	<-230	-	233	0.89	13.7
SLT-02-LLI-B-1112	313	7.5	7.2	-292	-68.9	240	4.40	-
SLT-02-LLI-B-0914	311	8.1	7.2	-173	21.0	231	3.01	39.7
SLT-02-LLI-C-1110	333	16.1	7.1	-317	-65.0	228	0.50	7.9
SLT-02-LLI-C-1211	332	14.2	7.1	-244	-27.5	233	<1.19	18.1
SLT-02-LLI-C-1112	317	8.0	7.2	-264	-41.5	238	2.06	-
SLT-02-LLI-C-0914	312	6.0	7.1	-293	-96.5	232	0.44	5.8
SLT-02-LLI-D-1110	324	16.7	7.5	-320	-68.5	227	1.70	27.6
SLT-02-LLI-D-1211	331	14.0	7.2	-220	-3.25	232	0.28	4.1
SLT-02-LLI-D-1112	314	10.3	7.2	-280	-59.6	239	1.64	-
SLT-02-LLI-D-0914	315	6.3	7.2	-277	-80.7	235	0.40	4.9
SLT-03-INC-A-0909	330	7.1	6.9	-276	-65.4	194	6.99	89.5
SLT-03-INC-A-0511	349	11.1	6.9	-370	-150	208	0.73	10.0
SLT-03-INC-A-1211	349	12.5	-	-301	-83.1	207	0.31	4.3
SLT-03-INC-A-1212	331	-	-	-	-	-	-	-
SLT-03-INC-A-0914	336	5.7	6.7	-295	-98.1	206	5.75	71.5
SLT-03-INC-B-0909	328	8.2	6.8	-279	-68.7	203	6.30	83.7
SLT-03-INC-B-0511	351	11.9	6.8	-356	-137	207	1.60	22.8
SLT-03-INC-B-1211	361	12.3	-	-319	-100	206	1.30	18.7
SLT-03-INC-B-1212	332	-	-	-	-	-	-	-
SLT-03-INC-B-0914	334	7.7	6.8	-298	-104	201	2.80	36.1
SLT-03-INC-C-0909	328	9.2	6.9	-270	-59.9	212	6.86	93.6
SLT-03-INC-C-0511	341	9.4	7.0	-329	-108	217	1.13	15.2
SLT-03-INC-C-1211	362	20.7	6.9	n.e.	-	211	1.20	20.3
SLT-03-INC-C-1212	333	-	-	-	-	-	-	-
SLT-03-INC-C-0914	341	6.2	6.7	-325	-129	207	0.25	3.1
SLT-03-INC-E-0909	329	7.0	6.9	-264	-53.4	209	6.94	89.4
SLT-03-INC-E-0511	346	9.8	6.9	-371	-150	210	0.70	9.3
SLT-03-INC-E-1211	361	15.0	6.8	-280	-64	211	0.47	7.5
SLT-03-INC-E-1212	333	-	-	-	-	-	-	-
SLT-03-INC-E-0914	331	5.5	6.8	-312	-115	208	0.48	6.2
SLT-04-YON-1110	305	13.2	6.8	-307	-52.6	226	2.10	31.9

Sample ID	TDS	T	pH	EMF	Eh	EC	O₂	
	g/L	°C		mV	mV	mS/cm	mg/L	%
SLT-05-TAH-A-1110	318	15.0	7.0	-339	-86.1	239	1.10	-
SLT-05-TAH-A-0914	319	7.9	7.0	-117	77.7	225	0.94	12
SLT-05-TAH-B-1112	317	-	-	-	-	-	-	-
SLT-05-TAH-B-0914	322	7.7	7.0	-287	-92.5	228	3.42	44.8
SLT-05-TAH-C-1211	340	16.9	6.9	-323	-108	230	0.84	13.3
SLT-05-TAH-D-1110	304	14.6	6.8	-353	-99.7	226	1.10	-
SLT-05-TAH-D-0914	320	7.6	6.9	-159	35.2	224	2.64	34
SLT-06-NOR-A-1110	320	17.2	6.9	-320	-68.8	216	1.70	28.9
SLT-06-NOR-A-0511	338	9.5	7.0	-	-	220	0.63	8.6
SLT-06-NOR-A-1211	338	18.0	7.0	-250	-36.9	222	0.46	7.5
SLT-06-NOR-A-0914	311	7.6	7.0	-317	-123	223	2.72	35
SLT-06-NOR-B-1110	325	14.2	7.0	-335	-81.4	207	1.20	18.2
SLT-06-NOR-B-0511	330	12.9	6.8	-	-	213	0.98	14.5
SLT-06-NOR-B-1211	345	15.6	6.7	-311	-95.6	211	0.94	14.5
SLT-06-NOR-C-1110	326	14.2	6.8	-312	-58.4	213	1.30	20.1
SLT-06-NOR-C-0511	343	12.4	6.9	-	-	216	0.62	8.9
SLT-06-NOR-C-1211	342	15.4	6.9	-227	-11.4	211	0.28	4.2
SLT-06-NOR-C-0914	333	8.6	6.9	-267	-73.0	216	4.26	56.6
SLT-06-NOR-D-1110	327	14.7	6.9	-314	-60.9	216	1.30	19.2
SLT-06-NOR-D-0511	342	10.3	7.0	-	-	221	0.99	13.6
SLT-06-NOR-D-1211	344	16.2	7.0	-271	-55.8	214	0.32	5
SLT-06-NOR-D-0914	323	7.5	7.0	-292	-97.6	221	1.37	18.3
SLT-07_SAL-1110	312	10.4	6.9	-365	-108	199	1.70	24.1
SLT-07-SAL-0511	351	10.7	6.9	-376	-156	205	0.42	5.7
SLT-07-SAL-1211	344	13.9	6.9	n.e.	-	205	0.69	10.1
SLT-07-SAL-1212	339	-	-	-	-	-	-	-
SLT-07-SAL-0914	339	6.2	6.8	-367	-171	207	0.83	10.3
SLT-08-CEN-A-1110	329	15.8	7.0	-293	-40.8	240	1.50	23.6
SLT-08-CEN-A-0511	340	9.7	7.1	-344	-124	223	0.50	6.7
SLT-08-CEN-A-1211	343	13.3	7.8	-241	-23.4	224	1.22	18.1
SLT-08-CEN-A-1212	321	10.3	7.1	-302	-81.6	228	5.90	-
SLT-08-CEN-A-0914	320	5.7	6.9	-260	-63.7	226	0.44	5.3
SLT-08-CEN-B-1110	320	11.8	7.0	-264	-8.4	240	2.26	32.4
SLT-08-CEN-B-0511	339	10.7	7.1	-343	-124	224	0.43	6.1
SLT-08-CEN-B-1211	341	10.0	7.0	-234	-13.3	226	0.29	3.9
SLT-08-CEN-B-1212	322	8.7	7.1	-299	-77.1	228	6.03	-
SLT-08-CEN-B-0914	321	8.2	7.0	-257	-63.3	225	1.11	14.3
SLT-08-CEN-C-1110	317	12.0	7.0	-272	-16.6	244	1.80	26.4
SLT-08-CEN-C-0511	338	10.1	7.1	-334	-114	224	1.10	15.0
SLT-08-CEN-C-1211	339	11.6	7.1	-268	-48.8	225	0.19	2.6
SLT-08-CEN-C-1212	322	8.4	7.1	-290	-67.8	229	5.94	-
SLT-08-CEN-C-0914	325	5.3	6.9	-231	-33.7	224	0.43	5.2
SLT-08-CEN-D-1110	330	11.6	6.9	-229	26.7	240	4.69	68.7
SLT-08-CEN-D-0511	341	10.4	7.1	-319	-98.5	226	2.63	36.4
SLT-08-CEN-D-1211	343	18.4	7.1	-222	-9.2	226	1.15	19.5
SLT-08-CEN-D-1212	323	8.8	7.1	-189	32.8	225	7.54	-
SLT-08-CEN-D-0914	321	8.5	7.0	-84.5	109	219	2.57	34.9
SLT-09-RÍO-A-1110	295	12.0	6.7	-318	-62.6	186	0.80	12.1
SLT-09-RÍO-A-0814	328	6.3	6.7	-	-	199	1.15	14.3
SLT-09-RÍO-B-1110	315	10.8	6.7	-312	-55.6	186	1.20	16.4
SLT-09-RÍO-C-1110	293	9.7	6.7	-280	-22.7	184	3.20	43.7
SLT-09-RÍO-D-1110	315	11.7	6.7	-326	-70.4	185	1.10	15.3
SLT-10-PES-1110	322	13.3	6.7	-333	-78.7	213	1.80	26.7
SLT-10-PES-1211	354	17.3	6.8	-341	-127	212	0.67	10.8
SLT-10-PES-1212	338	-	-	-	-	-	-	-
SLT-10-PES-0914	327	6.3	6.8	-308	-112	209	0.24	3

Sample ID	TDS	T	pH	EMF	Eh	EC	O$_2$	
	g/L	°C		mV	mV	mS/cm	mg/L	%
SLT-13-COR-1110	289	11.9	6.9	-355	-99.5	215	3.00	43.2
SLT-13-COR-0511	346	12.7	7.0	-	-	219	1.02	14.7
SLT-13-COR-1211	353	12.9	6.9	no	-	220	0.49	7.4
SLT-13-COR-0914	332	7.5	7.0	-355	-160	213	0.60	7.7
Shallow transects								
SLT-NOR-A1-1212	349	-	-	-	-	-	-	-
SLT-NOR-A2-1212	334	18.3	6.9	-276	-63.1	-	-	-
SLT-NOR-A3-1212	328	17.9	7.1	-260	-46.7	219	-	-
SLT-NOR-A4-1212	320	15.7	7.2	-307	-91.7	228	-	-
SLT-NOR-A5-1212	320	15.9	7.2	-273	-57.8	227	-	-
SLT-NOR-A6-1212	320	15.1	7.2	-269	-53.1	225	-	-
SLT-NOR-B2-1212	333	21.5	6.8	-301	-91.1	216	-	-
SLT-NOR-B3-1212	323	19.1	7.1	-318	-106	229	-	-
SLT-NOR-B4-1212	317	16.1	7.1	-319	-104	233	-	-
SLT-NOR-B5-1212	321	18.4	7.1	-312	-99.2	228	-	-
SLT-NOR-B6-1212	318	16.9	7.3	-295	-80.8	234	-	-
SLT-NOR-C2-1212	340	22.0	6.8	-304	-94.6	210	-	-
SLT-NOR-C3-1212	319	18.9	7.2	-304	-91.7	232	-	-
SLT-NOR-C4-1212	320	18.8	7.1	-302	-89.6	232	<3.23	-
SLT-NOR-C5-1212	318	17.3	7.3	-301	-87.2	237	-	-
SLT-NOR-D1-1212	318	16.4	7.2	-297	-82.4	237	2.70	-
SLT-NOR-D2-1212	318	15.9	7.3	-292	-76.9	236	2.33	-
SLT-NOR-D3-1212	318	15.8	7.2	-263	-47.7	232	< 1.9	-
SLT-NOR-D4-1212	318	16.1	7.2	-290	-75.0	234	-	-
SLT-NOR-D5-1212	313	17.1	7.3	-308	-94.0	240	<1.65	-
SLT-NOR-D6-1212	314	18.2	7.2	-298	-85.0	235	-	-
SLT-NOR-D7-1212	321	17.7	6.9	-295	-81.6	230	<1.6	-
SLT-NOR-Z1-1212	331	21.9	7.0	-257	-47.5	217	-	-
SLT-NOR-Z2-1212	343	19.4	6.8	-256	-44.2	204	-	-
SLT-NOR-Z3-1212	328	19.2	6.9	-307	-95.0	222	-	-
SLT-NOR-T2-0914	262	10.3	6.9	105	277	229	2.11	29.5
SLT-NOR-T2W-0914	294	10.2	6.7	109	281	230	0.40	5.2
SLT-NOR-T3-0914	288	9.8	6.7	1.3	194	235	1.57	21.5
SLT-NOR-T3W-0914	293	11.0	6.6	118	289	219	1.28	17.7
SLT-NOR-T4-0914	282	9.9	6.7	125	297	231	2.08	28.7
SLT-NOR-T4W-0914	295	10.7	6.5	-3.3	168	232	0.71	10
SLT-NOR-T5-0914	337	14.0	6.7	-202	-13.7	203	2.31	35.2
SLT-NOR-T5W-0914	340	17.0	6.7	-302	-137	207	3.54	56.8
SLT-NOR-T6W-0914	335	18.0	7.0	-23.9	141	216	3.80	63
SLT-NOR-T7-0914	285	11.4	6.4	86.3	257	225	1.45	19.7
SLT-NOR-T8-0914	309	9.9	6.7	81	253	229	0.35	4.2
SLT-NOR-T9-0914	326	16.4	6.8	-23.8	162	212	3.53	55.9
SLT-NOR-T10-0914	287	10.8	6.7	37.7	209	236	2.18	-
SLT-NOR-T11-0914	270	9.7	6.7	182	354	232	4.26	58.5
SLT-RÍO-01-0814	322	5.5	7.0	-208	17	221	4.50	56.1
others								
SLT-SPEC-OJO-0909	272	12.4	5.8	4	210	230	0.38	-
SLT-SPEC-OJO-0914	279	10.2	5.9	-67.3	125	232	1.96	27.2
Salar de Coipasa								
COI-WES-A2-0814	323	10.2	6.9	-283	-63	200	1.25	21
COI-WES-A3-0814	336	12.1	6.9	-187	32	187	6.00	86.4
COI-WES-A4-0814	339	10.0	6.9	-293	-72	188	2.90	40.3
COI-WES-A5-0814	345	9.4	6.7	-273	-52	176	2.68	35.9
COI-WES-A6-0814	344	11.8	6.8	-243	-24	182	3.03	43.1

Table A - 8: Element analysis of brine samples from the Salars of Uyuni and Coipasa, derived by IC

Sample ID	Li+	Na+	K+	Mg2+	Cl-	SO4 2-	HCO3-	Error
	mg / L	g/L	g/L	g/L	g/L	g/L	mg/L	%
Screened wells								
SLT-01-COL-B-0909	268	104	6.39	5.41	183	7.93	50.7	-1.13
SLT-01-COL-B-0511	276	111	6.47	5.61	188	8.58	-	0.53
SLT-01-COL-B-1211	261	116	6.48	5.57	192	8.81	50.3	1.11
SLT-01-COL-B-0914	291	108	6.01	5.51	187	10.3	-	-1.02
SLT-01-COL-C-0909	272	105	6.41	5.54	184	8.10	49.2	-0.96
SLT-01-COL-C-0511	286	115	6.78	5.81	193	8.63	-	1.04
SLT-01-COL-C-1211	266	116	6.58	5.70	194	8.82	51.8	1.14
SLT-01-COL-C-0914	254	114	6.47	5.23	183	8.09	57.0	2.48
SLT-01-COL-E-0909	257	105	6.45	5.49	174	8.11	46.3	2.00
SLT-01-COL-E-0511	290	118	6.92	6.02	192	8.55	-	2.49
SLT-01-COL-E-1211	261	114	6.55	5.68	195	8.87	61.9	0.18
SLT-01-COL-E-0914	260	108	6.53	5.28	179	8.48	50.6	1.25
SLT-01-COL-F-0909	254	107	6.45	5.50	181	8.05	47.6	0.49
SLT-01-COL-F-0511	227	116	5.58	4.70	192	7.06	-	0.98
SLT-01-COL-F-1211	244	114	6.16	5.27	192	8.30	63.0	0.21
SLT-01-COL-F-0914	242	110	6.18	5.09	182	7.73	106	1.37
SLT-02-LLI-A-1211	264	114	6.18	5.78	194	9.33	62.3	-0.05
SLT-02-LLI-A-1112	278	112	6.43	6.84	173	13.1	71.3	5.02
SLT-02-LLI-A-0914	258	98.8	6.52	5.91	188	9.03	67.9	-4.48
SLT-02-LLI-B-1110	276	91.9	6.49	6.17	177	9.70	54.4	-4.45
SLT-02-LLI-B-1211	286	112	6.85	6.37	191	9.56	67.3	0.66
SLT-02-LLI-B-1112	280	110	7.07	7.32	175	13.1	114	4.23
SLT-02-LLI-B-0914	288	106	7.03	6.35	182	8.92	56.6	0.64
SLT-02-LLI-C-1110	284	100	6.93	6.52	207	11.2	66.0	-8.19
SLT-02-LLI-C-1211	275	113	6.61	6.26	195	9.93	90.8	-0.48
SLT-02-LLI-C-1112	284	112	7.27	7.50	176	13.2	71.0	4.74
SLT-02-LLI-C-0914	266	108	6.58	6.06	182	8.92	65.7	0.94
SLT-02-LLI-D-1110	298	100	7.17	6.66	198	10.6	89.2	-5.81
SLT-02-LLI-D-1211	270	114	6.33	6.00	195	9.50	70.8	-0.07
SLT-02-LLI-D-1112	304	112	6.44	6.89	175	12.7	72.7	4.49
SLT-02-LLI-D-0914	250	109	6.21	5.63	185	8.85	63.7	0.15
SLT-03-INC-A-0909	988	77.9	20.2	21.1	185	23.9	139	0.84
SLT-03-INC-A-0511	1066	82.7	21.1	22.1	196	24.8	-	0.71
SLT-03-INC-A-1211	1005	81.2	21.0	21.7	197	25.2	-	-0.52
SLT-03-INC-A-1212	1003	81.6	20.6	24.4	175	27.4	106	6.32
SLT-03-INC-A-0914	967	78.4	21.2	21.2	187	26.3	-	0.13
SLT-03-INC-B-0909	991	77.3	20.2	21.3	183	24.2	144	1.13
SLT-03-INC-B-0511	1078	83.3	21.4	22.0	196	25.2	-	0.64
SLT-03-INC-B-1211	1061	85.3	22.1	22.9	202	26.1	-	0.81
SLT-03-INC-B-1212	1008	80.0	20.9	24.8	176	28.2	110	5.80
SLT-03-INC-B-0914	989	78.5	20.5	21.2	186	25.2	155	0.77
SLT-03-INC-C-0909	918	80.3	19.8	19.2	185	21.0	145	0.57
SLT-03-INC-C-0511	868	90.8	18.0	17.5	193	19.6	-	1.17
SLT-03-INC-C-1211	893	97.8	19.7	18.9	201	22.2	160	2.82
SLT-03-INC-C-1212	1004	81.7	20.9	24.5	175	28.6	132	6.13
SLT-03-INC-C-0914	1047	84.9	22.0	21.9	185	25.0	189	3.84
SLT-03-INC-E-0909	950	78.7	20.0	20.1	185	22.3	137	0.52
SLT-03-INC-E-0511	1031	83.9	21.1	20.8	194	23.2	-	0.81
SLT-03-INC-E-1211	975	84.3	20.9	20.9	207	25.2	113	-2.21
SLT-03-INC-E-1212	984	82.8	20.8	23.7	177	26.9	88.2	5.89
SLT-03-INC-E-0914	933	80.0	20.7	19.8	185	23.5	139	0.99
SLT-04-YON-1110	203	103	5.13	4.48	183	8.44	62.9	-2.61

Sample ID	Li+	Na+	K+	Mg2+	Cl-	SO4 2-	HCO3-	Error
	mg / L	g/L	g/L	g/L	g/L	g/L	mg/L	%
SLT-05-TAH-A-1110	398	90.1	9.09	8.66	195	13.2	136	-7.84
SLT-05-TAH-A-0914	385	104	9.05	8.05	185	12.0	106	0.08
SLT-05-TAH-B-1112	350	111	7.55	7.92	176	14.1	75.8	4.50
SLT-05-TAH-B-0914	467	101	11.1	10.3	183	15.6	143	1.01
SLT-05-TAH-C-1211	478	107	11.2	10.9	195	15.2	106	0.92
SLT-05-TAH-D-1110	491	85.7	11.1	10.8	178	16.6	148	-3.66
SLT-05-TAH-D-0914	492	97.4	11.6	10.8	183	16.2	125	0.16
SLT-06-NOR-A-1110	672	83.4	15.1	14.2	187	18.4	115	-3.48
SLT-06-NOR-A-0511	706	95.1	15.4	14.9	192	18.4	-	0.57
SLT-06-NOR-A-1211	625	94.0	14.5	13.8	196	17.7	102	-1.59
SLT-06-NOR-A-0914	608	87.8	14.2	12.9	177	17.4	112	-0.10
SLT-06-NOR-B-1110	704	82.9	15.5	16.1	183	26.3	203	-2.46
SLT-06-NOR-B-0511	728	96.3	15.8	17.0	173	26.0	-	5.88
SLT-06-NOR-B-1211	675	90.4	15.5	16.3	193	28.8	157	-2.02
SLT-06-NOR-C-1110	686	86.1	15.4	14.9	188	20.8	128	-2.31
SLT-06-NOR-C-0511	713	95.9	15.6	15.1	194	20.6	-	0.30
SLT-06-NOR-C-1211	660	93.1	15.1	15.1	196	21.5	132	-1.30
SLT-06-NOR-C-0914	676	93.4	15.5	14.6	189	19.9	121	0.37
SLT-06-NOR-D-1110	681	83.1	15.5	14.5	194	18.5	110	-4.95
SLT-06-NOR-D-0511	719	96.5	15.7	15.1	195	18.3	-	0.75
SLT-06-NOR-D-1211	647	95.7	14.8	14.6	198	18.8	120	-0.99
SLT-06-NOR-D-0914	636	90.8	14.9	13.7	185	17.3	103	-0.03
SLT-07_SAL-1110	503	82.3	12.5	13.3	175	27.1	212	-4.14
SLT-07-SAL-0511	606	102	13.9	12.5	187	33.1	-	-0.58
SLT-07-SAL-1211	562	94.9	14.2	15.9	185	32.5	218	0.10
SLT-07-SAL-1212	591	94.2	14.5	18.3	174	36.2	180	3.49
SLT-07-SAL-0914	565	94.3	14.6	15.1	180	33.1	274	0.50
SLT-08-CEN-A-1110	588	86.1	13.7	12.3	199	16.4	97.5	-6.67
SLT-08-CEN-A-0511	608	101	14.0	12.7	195	15.5	-	0.63
SLT-08-CEN-A-1211	594	104	14.1	12.9	196	14.6	127	1.85
SLT-08-CEN-A-1212	529	98.6	13.4	13.4	175	18.5	93.4	4.58
SLT-08-CEN-A-0914	568	96.4	13.5	10.5	183	14.8	95.6	0.46
SLT-08-CEN-B-1110	573	85.0	13.5	12.1	191	16.1	109	-5.50
SLT-08-CEN-B-0511	621	102	14.0	12.7	193	15.3	-	1.31
SLT-08-CEN-B-1211	579	99.4	13.6	12.5	199	15.8	110	-0.98
SLT-08-CEN-B-1212	588	99.8	13.7	13.9	174	19.6	89.4	5.54
SLT-08-CEN-B-0914	542	96.1	13.3	11.2	185	14.3	93.8	0.20
SLT-08-CEN-C-1110	560	84.9	13.1	11.7	190	16.0	102	-5.55
SLT-08-CEN-C-0511	598	102	13.9	12.5	193	15.1	-	1.59
SLT-08-CEN-C-1211	570	99.3	13.5	12.3	196	15.6	111	-0.59
SLT-08-CEN-C-1212	575	99.3	13.8	13.8	174	19.5	96.8	5.29
SLT-08-CEN-C-0914	553	97.0	13.5	11.5	187	14.6	92.3	0.23
SLT-08-CEN-D-1110	600	90.2	14.1	12.6	194	16.9	108	-3.45
SLT-08-CEN-D-0511	596	97.8	14.5	16.2	194	17.2	-	1.99
SLT-08-CEN-D-1211	562	100	13.4	12.3	200	15.8	113	-1.10
SLT-08-CEN-D-1212	562	99.4	13.5	13.9	175	19.8	98.7	5.18
SLT-08-CEN-D-0914	544	93.3	13.2	10.9	185	17.4	100	-1.79
SLT-09-RÍO-A-1110	972	56.8	16.6	19.4	178	21.8	120	-7.61
SLT-09-RÍO-A-0814	1174	72.8	20.5	23.7	186	22.8	118	1.09
SLT-09-RÍO-B-1110	1070	62.5	17.8	21.7	187	22.7	123	-5.40
SLT-09-RÍO-C-1110	1020	57.3	15.9	18.8	176	21.6	123	-7.78
SLT-09-RÍO-D-1110	1063	61.9	17.5	21.2	188	23.4	124	-6.51
SLT-10-PES-1110	615	84.8	13.7	13.8	179	29.4	169	-3.48
SLT-10-PES-1211	676	95.4	15.4	15.9	195	30.8	153	-1.34
SLT-10-PES-1212	749	95.2	16.4	18.5	173	33.5	110	5.31
SLT-10-PES-0914	669	93.6	15.4	14.6	170	31.3	199	2.78

Sample ID	Li⁺	Na⁺	K⁺	Mg²⁺	Cl⁻	SO₄²⁻	HCO₃⁻	Error
	mg / L	g/L	g/L	g/L	g/L	g/L	mg/L	%
SLT-13-COR-1110	467	79.6	10.8	11.3	166	20.5	166	-3.57
SLT-13-COR-0511	548	104	12.4	13.2	192	23.0	-	1.11
SLT-13-COR-1211	527	105	12.4	13.3	198	23.0	178	0.37
SLT-13-COR-0914	492	97.9	11.9	11.8	186	22.5	-	-0.96
Shallow transects								
SLT-NOR-A1-1212	1645	54.7	29.6	43.2	188	30.2	-	7.55
SLT-NOR-A2-1212	1017	81.3	23.0	24.1	182	22.6	74.2	5.61
SLT-NOR-A3-1212	856	86.5	19.4	21.2	179	20.8	89.5	5.68
SLT-NOR-A4-1212	590	98.3	13.9	14.2	178	14.3	123	5.20
SLT-NOR-A5-1212	553	99.0	13.5	13.9	178	14.1	102	5.08
SLT-NOR-A6-1212	610	96.8	14.6	14.9	178	15.1	70.6	5.28
SLT-NOR-B2-1212	939	83.1	20.6	24.0	179	24.5	109	5.74
SLT-NOR-B3-1212	619	98.0	14.4	15.3	178	16.0	123	5.59
SLT-NOR-B4-1212	546	101	12.7	13.1	176	13.3	99.9	5.61
SLT-NOR-B5-1212	634	97.0	14.6	15.6	177	15.7	89.7	5.91
SLT-NOR-B6-1212	521	102	12.1	12.7	177	12.9	110	5.59
SLT-NOR-C2-1212	1068	78.3	24.5	26.2	179	30.0	82.4	5.63
SLT-NOR-C3-1212	531	101	12.5	13.0	178	13.4	92.5	5.05
SLT-NOR-C4-1212	555	99.1	13.0	13.8	179	14.3	97.7	4.88
SLT-NOR-C5-1212	463	106	10.6	10.6	178	11.4	81.5	5.08
SLT-NOR-D1-1212	456	105	10.7	10.8	179	11.9	99.3	4.54
SLT-NOR-D2-1212	459	105	11.1	11.2	179	11.8	102	4.96
SLT-NOR-D3-1212	500	102	11.7	11.9	179	12.7	61.4	4.45
SLT-NOR-D4-1212	474	105	10.9	11.2	178	12.2	72.9	5.03
SLT-NOR-D5-1212	303	112	7.03	7.08	177	8.82	76.2	5.07
SLT-NOR-D6-1212	365	109	8.76	8.73	176	10.1	157	5.34
SLT-NOR-D7-1212	561	99.2	12.6	13.9	178	15.9	83.2	4.76
SLT-NOR-Z1-1212	783	90.8	18.6	19.1	183	18.3	57.5	5.07
SLT-NOR-Z2-1212	1099	80.6	23.0	26.4	182	29.0	101	5.59
SLT-NOR-Z3-1212	706	94.3	16.0	17.9	178	20.4	98.7	5.55
SLT-NOR-T2-0914	238	93.9	4.78	3.69	154	5.59	36.2	1.73
SLT-NOR-T2W-0914	376	94.7	7.24	8.84	170	12.4	117	0.64
SLT-NOR-T3-0914	306	97.0	6.47	6.05	168	10.3	78.9	0.30
SLT-NOR-T3W-0914	326	96.7	6.61	7.27	170	11.6	75.2	0.20
SLT-NOR-T4-0914	260	98.5	5.19	5.33	162	10.5	45.4	1.53
SLT-NOR-T4W-0914	338	98.1	6.75	7.32	171	11.1	89.7	0.63
SLT-NOR-T5-0914	1126	70.9	23.4	25.6	186	28.6	146	1.13
SLT-NOR-T5W-0914	1190	70.4	24.3	26.3	190	27.2	156	0.87
SLT-NOR-T6W-0914	785	87.0	16.9	17.6	192	20.0	71.2	-0.39
SLT-NOR-T7-0914	325	96.0	6.94	6.98	163	11.4	66.7	1.86
SLT-NOR-T8-0914	267	93.5	5.31	5.88	192	11.8	66.1	-8.63
SLT-NOR-T9-0914	856	82.4	17.6	19.0	185	20.6	121	0.97
SLT-NOR-T10-0914	272	99.7	5.80	5.17	167	9.24	60.5	1.06
SLT-NOR-T11-0914	202	95.1	3.88	3.44	160	7.99	48.9	-0.71
SLT-RÍO-01-0814	630	92.8	15.8	12.8	182	17.3	128	1.08
others								
SLT-SPEC-OJO-0909	345	90.8	7.92	5.52	157	7.44	634	0.53
SLT-SPEC-OJO-0914	336	93.1	7.90	4.50	164	7.76	765	-1.03
Salar de Coipasa								
COI-WES-A2-0814	328	93.8	9.98	14.6	165	38.5	221	0.49
COI-WES-A3-0814	532	80.2	16.7	23.3	176	37.5	233	1.30
COI-WES-A4-0814	543	81.7	17.3	23.0	176	38.4	214	1.59
COI-WES-A5-0814	609	77.2	18.5	26.3	174	46.0	274	1.87
COI-WES-A6-0814	600	77.2	19.3	25.9	177	41.0	214	1.99

Table A - 9:   Chemical composition of Salar de Uyuni and Salar de Coipasa brine samples, derived by ICP-MS (values with < are below detection limit)

Sample ID	Li mg/L	B mg/L	Si mg/L	Ca mg/L	V µg/L	Mn µg/L	Fe µg/L	As µg/L	Se µg/L	Br mg/L	Rb µg/L	Sr µg/L	Mo µg/L	Cs µg/L	Ba µg/L
Detection limit (1:1000)	0.1	1	100	20	100	50	1,000	200	500	2	5	20	1	1	50
Detection limit (1:200)	0.02	0.2	20	4	20	10	200	40	100	0.4	1	4	0.2	0.2	10
Screened wells															
SLT-01-COL-B-0909	263	203	<20	-	13.9	1,020	<200	579	351	86.0	5,452	17,180	14.9	176	80.9
SLT-01-COL-B-0511	273	243	<20	726	87.2	1,139	<200	1,187	<100	51.8	5,084	17,350	28.6	223	114
SLT-01-COL-B-1211	273	230	<20	841	33.7	1,119	<200	706	187	63.3	4,997	15,140	13.6	200	44.2
SLT-01-COL-B-0914	265	201	<20	815	25.7	1,273	<200	923	103	52.7	5,425	16,160	11.7	188	46.5
SLT-01-COL-C-0909	268	212	<20	-	12.1	1,047	<200	640	357	90.1	5,548	18,360	21.3	184	91.1
SLT-01-COL-C-0511	278	229	<20	740	78.4	1,131	<200	1,182	115	51.3	5,097	17,450	43.2	230	66.2
SLT-01-COL-C-1211	287	226	<20	851	31.0	1,169	<200	687	305	64.7	5,210	15,770	17.3	213	22.1
SLT-01-COL-C-0914	259	193	<20	690	24.8	1,230	<200	1003	<100	28.7	4,656	14,250	17.4	187	403
SLT-01-COL-E-0909	259	213	<20	-	10.7	1,057	<200	624	409	96.8	5,626	18,160	28.2	182	73.8
SLT-01-COL-E-0511	276	215	<20	738	55.3	1,103	<200	1,140	168	51.9	4,988	16,980	56.4	219	73.3
SLT-01-COL-E-1211	292	223	<20	865	27.0	1,026	<200	664	251	66.1	5,259	15,760	18.0	196	16.9
SLT-01-COL-E-0914	252	219	31.1	866	20.4	1,221	510	1,118	827	31.7	5,048	13,900	21.4	189	181
SLT-01-COL-F-0909	260	208	<20	-	11.1	1,024	<200	613	452	82.4	5,510	17,430	31.9	177	61.5
SLT-01-COL-F-0511	221	171	<20	619	43.0	770	<200	975	267	42.0	4,117	13,650	62.3	175	350
SLT-01-COL-F-1211	267	203	<20	843	47.4	1,268	<200	914	416	60.7	5,072	15,160	33.4	211	46.9
SLT-01-COL-F-0914	268	200	<20	807	36.7	1,188	<200	971	<100	49.3	5,287	15,710	12.4	184	175
SLT-02-LLI-A-1211	286	235	<20	783	25.8	1,789	<200	418	218	48.4	5,472	14,270	13.8	187	25.4
SLT-02-LLI-A-1112	269	225	<20	685	25.4	1,359	<200	873	<100	32.4	5,989	16,480	5.20	209	109
SLT-02-LLI-A-0914	262	249	<20	756	<20	1,217	270	816	398	26.3	5,461	13,060	14.9	168	349
SLT-02-LLI-B-1110	325	302	<20	774	73.2	707	<200	221	527	58.5	6,555	16,700	45.9	265	248
SLT-02-LLI-B-1211	321	301	<20	827	26.0	2,572	<200	158	231	56.2	5,875	14,360	16.6	133	149
SLT-02-LLI-B-1112	286	276	<20	708	27.7	1,193	<200	570	<100	36.2	6,212	16,010	5.48	193	123
SLT-02-LLI-B-0914	278	320	<20	800	<20	922	361	557	<100	28.4	5,653	12,040	7.04	173	306
SLT-02-LLI-C-1110	318	247	<20	757	25.3	1,382	<200	566	607	65.9	6,804	18,560	81.0	257	174
SLT-02-LLI-C-1211	316	261	<20	792	23.7	1,331	<200	254	245	54.1	5,961	15,400	15.1	205	12.0
SLT-02-LLI-C-1112	289	242	<20	678	23.7	1,392	<200	921	<100	33.6	6,253	17,560	6.27	199	111
SLT-02-LLI-C-0914	268	260	27.6	775	<20	1,309	<200	907	562	27.1	5,604	13,540	15.8	173	725
SLT-02-LLI-D-1110	266	214	<20	744	19.1	1,448	<200	555	472	57.1	6,238	16,710	38.1	210	144
SLT-02-LLI-D-1211	300	239	<20	800	23.7	1,502	<200	359	265	53.7	5,642	14,900	14.2	197	73.8
SLT-02-LLI-D-1112	278	229	<20	701	22.3	1,541	<200	944	<100	33.3	5,969	17,090	6.18	203	148
SLT-02-LLI-D-0914	253	239	20.2	802	<20	1,383	386	768	579	24.8	5,249	13,220	16.5	172	482
SLT-03-INC-A-0909	1,023	1,055	<20	-	17.3	1,613	<200	5,441	1,011	203	17,270	1,112	278	514	37.1
SLT-03-INC-A-0511	1,074	992	<20	263	46.3	1,248	<200	4,654	339	174	17,880	505	133	636	11.7
SLT-03-INC-A-1211	1,132	1,040	<20	298	22.3	1,129	207	610	276	199	17,280	488	40.2	629	<10
SLT-03-INC-A-1212	1,054	1,017	<20	283	23.0	1,099	<200	3,842	<100	152	18,070	468	25.6	627	15.0
SLT-03-INC-A-0914	920	897	<20	230	33.1	1,236	<200	4,487	136	129	14,610	516	51.6	612	167
SLT-03-INC-B-0909	995	1,059	<20	-	13.7	1,313	<200	4,526	1,025	197	17,400	552	128	568	29.6
SLT-03-INC-B-0511	1,046	975	<20	255	45.4	1,059	<200	4,212	411	174	17,380	298	156	623	12.7
SLT-03-INC-B-1211	1,130	1,039	<20	316	20.0	1,052	<200	552	389	207	17,200	348	63.4	626	<10
SLT-03-INC-B-1212	1,061	1,027	<20	279	26.0	1,082	<200	3,961	218	152	19,350	695	35.7	681	21.2
SLT-03-INC-B-0914	1,103	1,073	<20	305	31.1	1,170	<200	4,609	1,709	175	17,170	851	365	676	42.6
SLT-03-INC-C-0909	897	856	<20	-	16.1	1,198	<200	4,293	1,039	186	15,920	317	188	554	31.8
SLT-03-INC-C-0511	840	724	<20	403	39.1	1,931	<200	3,497	433	139	13,320	7,321	154	491	108
SLT-03-INC-C-1211	982	846	<20	441	22.4	1,578	<200	1,234	529	195	15,440	5,505	81.5	559	42.9
SLT-03-INC-C-1212	1,034	984	<20	287	29.6	924	<200	3,698	224	153	19,030	930	34.3	672	24.8
SLT-03-INC-C-0914	946	1,011	<20	321	26.0	931	274	4,326	767	141	15,810	927	53.5	575	251
SLT-03-INC-E-0909	955	962	<20	-	16.1	1,845	<200	5,760	957	189	17,590	1,843	233	467	37.6
SLT-03-INC-E-0511	997	903	<20	290	40.4	1,435	<200	5,357	398	161	16,780	901	184	567	11.0
SLT-03-INC-E-1211	1,097	978	<20	355	22.5	1,487	<200	306	606	206	16,810	883	99.3	608	<10
SLT-03-INC-E-1212	1,018	951	<20	315	30.8	1,493	841	5,139	256	144	18,940	999	34.9	648	19.1
SLT-03-INC-E-0914	1,081	1,007	<20	319	31.5	1,494	<200	5,626	1,837	167	16,750	1,015	366	629	44.5
SLT-04-YON-1110	201	186	21.7	874	18.0	250	<200	54.8	256	41.5	4,975	17,990	11.4	249	185

Sample ID	Li mg/L	B mg/L	Si mg/L	Ca mg/L	V µg/L	Mn µg/L	Fe µg/L	As µg/L	Se µg/L	Br µg/L	Rb µg/L	Sr µg/L	Mo µg/L	Cs µg/L	Ba µg/L
Screened wells															
SLT-05-TAH-A-1110	383	244	21.8	600	17.2	1,030	<200	711	423	74.4	8,415	12,870	30.2	287	218
SLT-05-TAH-A-0914	389	309	24.8	628	<20	853	362	1,229	696	46.3	7,595	10,880	26.8	252	66.6
SLT-05-TAH-B-1112	330	215	22.1	692	24.9	1,280	<200	1,177	125	42.5	6,889	16,510	9.0	224	237
SLT-05-TAH-B-0914	465	383	23.4	516	<20	666	235	1,307	1,035	58.6	9,121	8,655	49.8	312	66.9
SLT-05-TAH-C-1211	523	367	<20	480	<20	1,817	<200	1,321	550	111	9,194	7,993	70.4	279	111
SLT-05-TAH-D-1110	472	326	23.4	442	16.9	851	<200	441	496	97.2	10,590	9,208	66.8	330	176
SLT-05-TAH-D-0914	494	363	<20	387	31.5	692	<200	378	138	58.1	8,939	7,871	25.2	298	204
SLT-06-NOR-A-1110	632	376	23.6	425	18.3	1,532	<200	3,436	716	138	15,350	13,040	90.8	546	127
SLT-06-NOR-A-0511	697	448	<20	390	37.8	1,756	<200	3,197	499	123	14,630	10,930	203	504	53.5
SLT-06-NOR-A-1211	719	438	<20	490	20.0	1,679	<200	2,252	540	158	13,420	10,900	68.4	519	47.0
SLT-06-NOR-A-0914	622	461	<20	455	21.0	1,226	303	3,468	1,141	94.3	13,070	8,610	56.8	441	83.1
SLT-06-NOR-B-1110	624	409	27.6	309	21.1	1,303	<200	657	797	148	14,650	4,030	147	514	126
SLT-06-NOR-B-0511	712	493	<20	304	28.2	780	<200	2,750	590	127	13,770	2,703	271	529	65.3
SLT-06-NOR-B-1211	767	499	<20	379	21.3	924	<200	1,884	486	167	13,380	4,387	67.8	505	29.7
SLT-06-NOR-C-1110	601	376	29.5	395	19.8	1,866	<200	1,199	806	145	15,110	9,617	150	503	112
SLT-06-NOR-C-0511	680	446	<20	353	21.6	1,557	<200	3,170	817	123	14,210	7,271	335	459	104
SLT-06-NOR-C-1211	757	481	<20	408	20.3	1,176	<200	1,746	597	162	13,930	6,992	69.3	524	26.3
SLT-06-NOR-C-0914	674	442	<20	330	28.9	1,021	<200	3,514	<100	93.4	12,540	6,610	35.8	445	80.4
SLT-06-NOR-D-1110	549	336	31.5	405	19.7	1,742	<200	2,992	756	132	13,890	11,950	142	483	121
SLT-06-NOR-D-0511	682	430	<20	381	< 20	1,613	<200	3,028	914	121	14,510	11,130	385	478	62.5
SLT-06-NOR-D-1211	736	447	<20	474	21.0	1,583	<200	1,827	709	160	13,490	9,556	70.4	526	23.3
SLT-06-NOR-D-0914	631	471	<20	459	22.0	1,210	575	3,532	1,073	95.3	13,080	8,082	48.5	440	149
SLT-07_SAL-1110	468	690	32.5	331	20.2	1,543	<200	5,751	695	131	10,640	5,202	89	596	191
SLT-07-SAL-0511	597	955	<20	270	21.4	616	<200	6,209	968	135	9,980	1,868	385	610	21.3
SLT-07-SAL-1211	642	1,000	<20	331	23.0	907	<200	220	589	167	10,760	1,875	70.1	656	<10
SLT-07-SAL-1212	598	1,019	<20	267	35.1	1,940	4126	6,467	144	111	11,700	2,169	21.4	637	214
SLT-07-SAL-0914	593	1,070	<20	266	26.2	390	<200	5,565	<100	129	11,060	1,746	35.8	620	<10
SLT-08-CEN-A-1110	493	379	35.1	495	21.7	3,128	<200	1,076	691	94.9	11,470	9,513	118	409	80.0
SLT-08-CEN-A-0511	573	444	<20	450	23.5	3,029	<200	2,773	1,001	83.0	10,050	8,689	408	380	40.0
SLT-08-CEN-A-1211	654	482	<20	543	<20	2,833	<200	708.7	457	115	10,720	8,847	59.7	394	23.8
SLT-08-CEN-A-1212	594	460	<20	489	28.9	3,254	<200	2,668	111	63.8	11,050	10,300	14.3	415	64.4
SLT-08-CEN-A-0914	613	496	<20	486	29.4	3,164	<200	2,824	111	93.7	11,510	9,979	30.4	382	256
SLT-08-CEN-B-1110	491	375	41.0	500	21.2	3,249	<200	1,128	707	94.6	11,440	9,581	120	405	118
SLT-08-CEN-B-0511	588	452	<20	447	< 20	3,066	<200	2,891	1,129	85.4	10,120	9,499	469	379	41.8
SLT-08-CEN-B-1211	647	474	<20	522	<20	2,821	<200	421	509	109	10,580	8,665	61.4	401	<10
SLT-08-CEN-B-1212	599	464	<20	470	28.7	3,275	<200	2892	170	64.9	11,250	9,893	16.1	413	76.4
SLT-08-CEN-B-0914	530	482	20.4	514	23.2	2,907	277	3140	995	60.3	10,050	8,287	42.1	359	172
SLT-08-CEN-C-1110	584	393	218.1	482	29.5	3,306	<200	2,722	228	86.5	11,770	10,410	12.7	437	41.6
SLT-08-CEN-C-0511	569	444	<20	436	20.5	3,048	<200	2,842	1,361	80.9	10,020	8,882	500	365	42.4
SLT-08-CEN-C-1211	650	472	<20	523	<20	2,895	<200	803	540	108	10,560	8,767	55.4	396	<10
SLT-08-CEN-C-1212	591	457	<20	467	27.4	3,275	<200	2,780	168	64.4	11,270	10,060	16.3	421	69.4
SLT-08-CEN-C-0914	545	495	20.6	530	24.2	2,928	669	3,078	969	61.8	10,290	8,656	43.5	359	149
SLT-08-CEN-D-1110	690	496	78.9	453	32.2	3,499	<200	869	205	81.4	11,720	10,970	29.4	420	155
SLT-08-CEN-D-0511	567	446	<20	440	< 20	2,470	<200	2,634	1,508	84.7	9,970	7,663	566	360	40.7
SLT-08-CEN-D-1211	637	461	<20	512	<20	3,034	<200	1,037	664	107	10,280	8,540	49.1	383	27.1
SLT-08-CEN-D-1212	600	466	<20	464	28.6	3,367	264	1,415	183	66.3	11,290	9,642	15.6	398	130
SLT-08-CEN-D-0914	550	429	<20	403	30.5	3,162	341	497	<100	55.9	9,380	8,199	26.2	356	131
SLT-09-RÍO-A-1110	1,285	963	21.9	300	10.6	1,973	<200	8,959	412	225	19,320	962	84.5	581	82.5
SLT-09-RÍO-A-0814	1,315	1,048	26.7	311	36.4	1,448	<200	9,046	962	205	16,950	1,553	279	548	84.0
SLT-09-RÍO-B-1110	1,310	911	23.1	318	11.3	1,998	<200	8,995	548	235	19,440	816	172	563	103
SLT-09-RÍO-C-1110	1,285	877	24.0	306	11.6	1,924	<200	2,145	636	225	18,790	745	201	552	99.0
SLT-09-RÍO-D-1110	1,312	882	29.6	320	14.1	2,685	<200	8,924	651	233	20,090	673	226	561	142
SLT-10-PES-1110	611	447	35.3	277	13.2	1,576	<200	546	519	95.9	13,160	4,612	142	445	66.4
SLT-10-PES-1211	791	573	<20	320	<20	1,595	<200	240	548	121	12,700	4,914	55.4	434	<10
SLT-10-PES-1212	735	568	<20	308	27.7	1,551	<200	2,544	<100	77.0	13,190	5,360	15.1	447	37.1
SLT-10-PES-0914	631	584	25.4	311	21.2	1,378	274	3,894	536	70.9	11,760	3,408	56.9	450	63.7

Sample ID	Li	B	Si	Ca	V	Mn	Fe	As	Se	Br	Rb	Sr	Mo	Cs	Ba
	mg/L	mg/L	mg/L	mg/L	µg/L	µg/L	µg/L	µg/L	µg/L	µg/L	µg/L	µg/L	µg/L	µg/L	µg/L
SLT-13-COR-1110	464	427	34.8	393	14.2	1,228	<200	676	418	90.9	10,730	9,352	85.7	449	105
SLT-13-COR-0511	522	525	<20	338	22.6	1,189	<200	2,744	2,159	94.5	9,816	7,480	868	402	63.6
SLT-13-COR-1211	575	539	<20	397	20.5	1,397	<200	269.2	578	115	9,857	7,181	52.0	412	57.7
SLT-13-COR-0914	499	508	<20	302	27.8	991	<200	5,792	<100	65.4	9,159	6,599	25.3	425	162
transect drillings															
SLT-NOR-A1-1212	1,486	926	<20	169	57.0	2,180	290	6,612	<100	216	26,690	2,909	92.1	1,299	128
SLT-NOR-A2-1212	923	584	<20	335	23.0	2,932	203	4,421	<100	143	18,830	24,000	44.4	876	80.6
SLT-NOR-A3-1212	845	552	<20	330	<20	3,096	<200	3,392	<100	131	16,720	21,190	34.2	720	71.4
SLT-NOR-A4-1212	569	367	<20	439	<20	2,558	<200	1,664	<100	90.2	11,600	18,470	30.3	535	114
SLT-NOR-A5-1212	569	362	<20	437	<20	1,788	<200	1,682	113	90.0	11,540	16,940	33.0	489	105
SLT-NOR-A6-1212	599	391	<20	412	<20	1,522	<200	1,636	173	94.5	11,950	13,080	37.6	494	84.1
SLT-NOR-B2-1212	789	506	<20	366	24.7	1,227	<200	4,753	211	125	15,570	23,730	63.0	629	147
SLT-NOR-B3-1212	602	392	<20	409	<20	1,612	<200	2,909	246	95.4	12,140	18,740	45.8	508	108
SLT-NOR-B4-1212	511	327	<20	442	<20	1,425	<200	1,502	236	79.9	10,450	17,380	47.6	457	94.9
SLT-NOR-B5-1212	619	402	<20	406	<20	1,468	<200	1,968	257	98.4	12,450	15,590	51.2	525	64.5
SLT-NOR-B6-1212	503	321	<20	478	<20	1,382	<200	1,600	272	79.6	10,260	20,610	50.4	419	113
SLT-NOR-C2-1212	1,049	704	<20	256	<20	4,272	<200	3,991	361	170	20,650	7,296	69.7	854	55.4
SLT-NOR-C3-1212	496	323	<20	447	<20	1,103	<200	1,605	449	80.1	10,110	16,700	59.3	443	127
SLT-NOR-C4-1212	537	349	<20	433	<20	1,702	<200	1,497	395	85.3	10,750	16,330	58.4	464	75.4
SLT-NOR-C5-1212	420	269	<20	532	<20	1,135	<200	1,413	462	66.2	8,656	19,490	53.4	378	154
SLT-NOR-D1-1212	434	285	<20	521	<20	1,568	<200	1,170	461	69.6	9,010	20,120	52.1	384	122
SLT-NOR-D2-1212	448	282	<20	506	<20	1,161	<200	1,403	459	70.3	9,091	20,480	51.5	395	168
SLT-NOR-D3-1212	483	308	<20	481	<20	1,117	<200	1,411	473	75.9	9,886	21,220	49.7	414	158
SLT-NOR-D4-1212	450	289	<20	490	<20	1,203	<200	1,352	529	69.3	9,080	19,630	47.9	390	166
SLT-NOR-D5-1212	284	182	<20	679	<20	575	<200	819	556	44.0	5,863	15,930	37.5	254	214
SLT-NOR-D6-1212	351	225	<20	586	<20	1,137	<200	1,198	519	53.6	7,084	17,060	37.6	309	192
SLT-NOR-D7-1212	551	352	<20	400	<20	1,495	<200	1,457	505	87.9	10,320	12,520	45.7	434	76.0
SLT-NOR-Z1-1212	740	473	<20	365	21.7	710	<200	3,675	574	119	15,350	27,320	76.4	667	115
SLT-NOR-Z2-1212	1,008	663	<20	244	<20	2,841	<200	4,130	645	161	19,060	6,529	77.7	810	64.7
SLT-NOR-Z3-1212	681	457	<20	319	<20	1,878	<200	1,975	717	112	13,060	9,113	66.2	567	77.9
SLT-NOR-T2-0914	236	79.1	32.5	1,235	24.1	841	477	308	703	29.1	5,801	24,660	48.1	305	89.8
SLT-NOR-T2W-0914	381	168	32.7	722	24.4	7,414	282	1,400	697	52.6	5,267	12,770	30.4	127	72.1
SLT-NOR-T3-0914	352	125	<20	858	40.4	5,977	<200	211	492	58.1	5,721	22,030	62.7	235	129
SLT-NOR-T3W-0914	328	138	21.0	736	37.9	10,180	603	920	600	47.0	4,610	13,140	27.1	109	72.4
SLT-NOR-T4-0914	249	115	26.0	816	37.3	390	423	718	381	35.7	3,492	13,890	18.9	93.7	152
SLT-NOR-T4W-0914	345	170	25.1	802	<20	6,863	784	619	796	50.0	5,419	14,580	23.6	145	80.9
SLT-NOR-T5-0914	1,260	772	20.7	291	32.3	9,307	443	10,570	1,433	187	20,940	6,343	461	702	49.8
SLT-NOR-T5W-0914	1,190	827	30.5	362	32.4	8,164	461	8,169	669	170	23,010	6,741	51.6	787	80.9
SLT-NOR-T6W-0914	701	453	<20	407	25.0	18,390	433	1,498	1,042	97.6	13,260	12,710	95.1	505	78.1
SLT-NOR-T7-0914	328	128	<20	764	<20	3,764	245	585	577	47.0	4,798	15,590	25.5	145	67.6
SLT-NOR-T8-0914	281	113	27.61	843	29.1	5,009	151	544	529	36.9	3,972	14,940	39.3	105	60.3
SLT-NOR-T9-0914	942	557	<20	392	38.9	5,797	<200	7,062	1,788	144	16,280	18,610	324	571	105
SLT-NOR-T10-0914	294	136	20.9	908	24.6	4,970	572	193	446	41.4	5,718	17,920	24.7	248	191
SLT-NOR-T11-0914	203	85.6	23.4	1,127	20.9	101	<200	297	338	23.7	3,577	20,180	16.7	125	55.7
SLT-RÍO-01-0814	726	607	<20	429	35.2	3,898	<200	3,579	1,564	119	10,460	8,243	229	331	97.8
others															
SLT-SPEC-OJO-0909	331	421	23.6	0	12.4	2,003	40610	339	643	153	8,692	18,700	44.0	1,177	57.9
SLT-SPEC-OJO-0914	347	409	<20	819	26.6	2,030	13590	119	<100	67.0	7,513	11,970	31.9	1,275	307
Salar de Coipasa															
COI-WES-A2-0814	354	771	<20	285	59.6	662	217	10,640	486	139	9,053	6,522	114	298	38.2
COI-WES-A3-0814	591	1,641	<20	284	53.4	2,092	772	14,800	1,103	235	17,290	11,370	369	608	75.4
COI-WES-A4-0814	597	1,624	<20	252	43.3	1,653	<200	12,710	1,623	254	18,700	9,974	346	684	35.3
COI-WES-A5-0814	666	1,851	<20	221	34.6	2,325	<200	17,100	1,645	285	21,020	7,323	350	812	25.9
COI-WES-A6-0814	628	1,783	<20	249	34.9	2,430	<200	11,040	1,708	270	20,110	5,767	334	796	53.3

Table A - 10:   *Results of isotopic analyses of brine and river samples, including sampling depth and estimated distance from the Río Grande delta (n.d. - not determined)*

Sampling point	Year	$\delta^{18}O$	δ^2H	$\delta^{34}S_{sulphate}$	$\delta^{18}O_{sulphate}$	depth	distance
		[‰VSMOW]	[‰VSMOW]	[‰VCDT]	[‰VSMOW]	m	km
SLT-01-COL-E	2009	0.13	-45.6	13.4	14.9	7.5	75
SLT-01-COL-F	2009	-0.01	-45.9	13.1	14.2	2.5	75
SLT-01-COL-C	2009	0.17	-45.5	13.3	14.9	6.9	75
SLT-02-LLI-B	2010	-0.36	-38.3	16.1	14.6	8.5	110
SLT-02-LLI-C	2010	0.21	-35.7	16.0	14.6	3.3	110
SLT-02-LLI-D	2010	0.02	-36.2	15.6	14.8	1.3	110
SLT-03-INC-A	2009	3.36	-31.5	11.7	14.0	3	46.5
SLT-03-INC-B	2009	3.27	-32.0	11.4	13.9	4	46.5
SLT-03-INC-E	2009	3.45	-31.0	11.2	14.0	2	46.5
SLT-04-YON	2010	-2.47	-53.5	13.2	14.3	7.4	n.d.
SLT-05-TAH-A	2010	3.72	-27.3	15.3	14.8	0.4	97.5
SLT-05-TAH-D	2010	4.58	-20.5	16.0	14.5	3.2	97.5
SLT-06-NOR-A	2010	4.75	-25.7	16.0	14.0	0.6	115
SLT-06-NOR-B	2010	4.17	-25.1	18.8	14.6	3.2	115
SLT-06-NOR-C	2010	4.45	-25.8	14.6	14.2	2.3	115
SLT-06-NOR-D	2010	4.63	-26.1	16.2	13.8	1.3	115
SLT-07-SAL	2010	-0.11	-42.1	12.5	14.0	7.6	60
SLT-08-CEN-L	2010	2.52	-27.3	13.5	13.5		71
SLT-08-CEN-A	2010	2.46	-26.4	12.2	13.0	8.5	71
SLT-08-CEN-B	2010	2.34	-26.6	12.3	12.9	4.3	71
SLT-08-CEN-C	2010	2.38	-26.6	12.3	12.9	2.3	71
SLT-08-CEN-D	2010	2.43	-26.2	12.6	13.0	5	71
SLT-09-RÍO-A	2010	2.85	-35.7	11.3	11.4	2.5	11.25
SLT-09-RÍO-B	2010	2.80	-35.8	11.5	11.9	2	11.25
SLT-09-RÍO-C	2010	2.79	-36.1	11.2	12.1	3.3	11.25
SLT-09-RÍO-D	2010	2.83	-36.0	10.6	12.1	1.3	11.25
SLT-10-PES	2010	2.97	-21.2	14.7	13.5	1.3	82.5
SLT-13-COR	2010	3.60	-23.1	14.4	14.2	5.5	86
SLT-RÍO-GRA	2010	-8.81	-77.5	5.8	9.1	0.1	0

Table A - 11: *Composition of Salar de Uyuni evaporate samples from the upper cm of the salt crust, samples with * are from salt efflorescences; IR = insoluble rest; boron values from ICP-MS analysis, rest from IC*

Sampling point	Na$^+$	K$^+$	Mg^{2+}	Cl$^-$	SO$_4$$^{2-}$	Ca$^+$	Li$^+$	B	Sr	IR	error
	g/kg	g/kg	g/kg	g/kg	g/kg	g/kg	mg/kg	mg/kg	mg/kg	wt%	%
SLT-01-COL	333	3.03	2.44	570	6.50	1.25	82.1	56.9	19.2	0.17	8.2
SLT-01-COL*	326	16.0	12.4	555	18.2	1.84	547	327	39.4	0.35	6.7
SLT-02-LLI	364	2.50	2.08	577	5.85	1.26	73.2	29.2	17.6	0.30	4.4
SLT-02-LLI*	317	18.2	14.8	556	21.4	1.88	709	275	45.1	0.32	6.5
SLT-03-INC	364	6.38	3.07	580	5.25	0.97	142	94.3	16.1	0.22	3.7
SLT-03-INC*	298	30.1	17.4	530	25.3	1.27	651	640	28.4	0.76	8.5
SLT-05-TAH	370	3.28	2.72	581	6.27	1.94	99.0	48.4	19.5	0.23	3.2
SLT-05-TAH*	308	15.7	10.2	558	14.6	1.70	560	234	39.2	0.41	8.2
SLT-06-NOR	374	3.36	1.38	581	2.73	0.82	62.1	23.0	7.28	0.29	3.5
SLT-06-NOR*	308	28.2	16.0	536	23.7	1.75	647	320	46.6	1.07	7.2
SLT-07-SAL	362	4.28	2.62	579	6.11	1.60	100	57.6	25.4	0.27	4.1
SLT-07-SAL*	321	20.1	13.6	538	21.7	1.85	569	313	39.7	0.69	7.5
SLT-08-CEN	360	7.91	4.09	573	8.30	1.56	144	109	28.9	0.32	4.2
SLT-08-CEN*	315	24.6	14.1	541	21.0	1.35	607	426	32.1	0.57	7.5
SLT-10-PES	371	3.97	2.75	576	5.91	1.73	110	52.0	24.1	0.31	3.5
SLT-10-PES*	327	17.3	12.0	552	17.4	1.76	577	273	43.2	0.32	6.7
SLT-13-COR	372	3.44	2.25	578	6.33	1.91	96.1	41.7	15.9	0.28	3.3
SLT-13-COR*	318	22.8	15.1	540	21.5	1.77	707	390	38.0	0.52	7.3
SLT-NOR-T3	369	7.48	4.66	578	6.61	0.72	161	61.2	32.6	0.32	3.1
SLT-NOR-T3*	363	4.31	4.71	574	7.33	1.27	196	69.6	44.9	0.32	4.2
SLT-NOR-T5	367	3.15	2.45	583	3.01	0.22	117	51.9	6.12	0.15	3.9
SLT-RÍO-01	341	23.1	8.17	565	13.5	1.00	296	315	77.5	0.15	4.4
COI-WES-A2	356	7.44	6.85	573	10.2	0.78	137	528	31.0	0.14	4.3
SLT-NOR-T2	379	0.96	0.62	590	2.88	1.25	31.3	1.2	19.1	0.28	2.3
SLT-NOR-T4	374	1.82	1.87	576	7.39	2.36	81.9	16.6	24.7	0.98	2.7
SLT-NOR-T7	374	3.17	2.80	579	7.25	1.59	115	28.9	26.3	0.31	2.9
SLT-NOR-T7*	343	15.6	9.71	555	15.8	1.72	436	110	68.6	0.87	5.0
SLT-NOR-T8	369	3.88	3.72	573	8.38	2.34	152	42.4	40.4	0.39	3.6
SLT-NOR-T11	377	1.55	1.28	576	8.23	3.20	66.5	8.93	29.0	0.51	2.8
SLT-NOR-T11*	354	5.65	3.86	566	9.01	2.14	177	29.2	46.3	2.31	3.6
SLT-NOR-T2W	379	1.60	1.34	583	5.11	1.64	61.0	12.9	18.5	0.40	2.3
SLT-NOR-T3W	374	2.82	3.06	575	9.27	2.49	129	36.9	23.5	0.22	3.0
SLT-NOR-T5W	381	2.97	2.25	581	3.03	0.44	106	42.4	10.5	0.19	2.7
SLT-NOR-T6W	381	2.40	2.04	591	2.88	0.32	106	34.5	7.78	0.13	1.9
SLT-NOR-T10	373	3.72	3.38	577	7.30	1.34	144	54.6	27.2	0.22	3.2
SLT-NOR-T10*	361	7.24	4.88	567	8.36	1.26	198	86.2	62.2	1.46	3.5

Table A - 12:   *Mineralogical composition of evaporates from the upper cm of the salt crust, samples with * are from salt efflorescences; values in wt%*

Sampling point	Halite	Carnallite	Sylvite	Polyhalite	Gypsum	Kieserite	Sum [%]
SLT-01-COL	84.6	2.79	9.65	0	0.53	0.51	98.0
SLT-01-COL*	82.8	14.2	0	0	0.79	1.99	99.8
SLT-02-LLI	92.6	2.38	1.27	0	0.54	0.41	97.2
SLT-02-LLI*	80.5	17.0	0.57	0	0.81	2.44	101.3
SLT-03-INC	92.6	3.51	1.00	0	0.42	0.42	97.9
SLT-03-INC*	75.9	19.9	0	1.60	0	3.28	100.7
SLT-05-TAH	94.0	3.11	0	0	0.83	0.23	98.2
SLT-05-TAH*	78.4	11.6	7.96	0	0.73	1.51	100.2
SLT-06-NOR	95.2	1.58	0	0.88	0	0.19	97.8
SLT-06-NOR*	78.2	18.2	0	1.97	0	2.97	101.4
SLT-07-SAL	91.9	2.99	2.18	0	0.69	0.33	98.1
SLT-07-SAL*	81.7	15.6	0	0	0.79	2.49	100.6
SLT-08-CEN	91.5	4.68	0	1.02	0	0.96	98.1
SLT-08-CEN*	80.0	16.1	0	1.53	0	2.68	100.3
SLT-10-PES	94.3	3.14	0	0	0.74	0.26	98.5
SLT-10-PES*	83.1	13.7	0	0	0.75	1.89	99.5
SLT-13-COR	94.7	2.57	0	0	0.82	0.25	98.3
SLT-13-COR*	80.8	17.3	0	0	0.76	2.48	101.4
SLT-NOR-T3	93.7	5.33	0	0	0.31	0.70	100.1
SLT-NOR-T3*	92.4	5.39	0	0	0.54	0.62	98.9
SLT-NOR-T5	93.4	2.80	1.30	0	0.10	0.36	97.9
SLT-RÍO-01	86.6	9.34	0.91	4.01	0	1.03	101.9
COI-WES-A2	90.6	7.84	0	0	0.33	1.21	100.0
SLT-NOR-T2	96.4	0.71	0.47	0	0.54	0	98.1
SLT-NOR-T4	95.0	2.14	0	0	1.02	0.25	98.4
SLT-NOR-T7	95.1	3.21	0	0	0.68	0.50	99.5
SLT-NOR-T7*	87.1	11.1	0	0.0028	0.65	1.76	100.6
SLT-NOR-T8	93.7	4.25	0	0	1.00	0.40	99.4
SLT-NOR-T11	95.9	1.46	0	0	1.37	0.08	98.8
SLT-NOR-T11*	90.0	4.41	0.73	0	0.92	0.56	96.6
SLT-NOR-T2W	96.5	1.53	0	0	0.70	0.17	98.9
SLT-NOR-T3W	95.2	3.50	0	0	1.07	0.47	100.2
SLT-NOR-T5W	96.9	2.57	0	0	0.19	0.28	99.9
SLT-NOR-T6W	96.9	2.33	0	0	0.14	0.30	99.6
SLT-NOR-T10	94.9	3.86	0	0	0.57	0.59	99.9
SLT-NOR-T10*	91.9	5.58	0	0	0.54	0.77	98.8

Table A - 13:   Measured electric conductivity and density, and calculated TDS values of three brine samples, underlined values are above the instruments' treshold

Brine/ DI	SLT-08-CEN-A-0511			SLT-09-RÍO-A-1110			SLT-01-COL-B-0909		
	EC mS/cm	ρ g/cm³	TDS g/L	EC mS/cm	ρ g/cm³	TDS g/L	EC mS/cm	ρ g/cm³	TDS g/L
10/0	<u>240</u>	1.216	340	<u>215</u>	1.229	295	<u>250</u>	1.205	307
9/1	<u>232</u>	1.196	306	<u>211</u>	1.205	266	<u>239</u>	1.184	277
8/2	<u>226</u>	1.170	272	<u>208</u>	1.184	236	<u>232</u>	1.165	246
7/3	<u>216</u>	1.153	238	200	1.161	207	<u>219</u>	1.145	215
6/4	<u>201</u>	1.132	204	189	1.140	177	<u>202</u>	1.125	184
5/5	180	1.110	170	174	1.118	148	184	1.105	154
4/6	155	1.088	136	151	1.095	118	157	1.085	123
3/7	127	1.067	102	124	1.071	88.5	127	1.064	92.2
2/8	91.4	1.044	68	90.1	1.047	59	92.4	1.043	61.5
1/9	50.9	1.021	34	51.9	1.023	29.5	51.5	1.020	30.7

Table A - 14:   Explanation of geological units occurring in the geological map of the Altiplano (modified after Marsh et al. 1995)

Definition	Description
Surficial deposits, undifferentiated (Holocene and Pleistocene)	Includes unconsolidated alluvial, eolian, colluvial, and glacial deposits. Locally may include lacustrine and salt deposits that are not shown separately
Stratovolcano deposits (Holocene to Miocene)	Lava flows, flow breccias, lahars, and minor pyroclastic deposits chiefly of andesitic to dacitic composition. May include domes and shallow intrusive bodies mostly in vent complexes
Lacustrine deposits (Holocene and Pleistocene)	Chiefly calcareous tufa in ancient lake shorelines and lacustrine mud and silt deposits. Includes deposits mapped as Minchin Limestone
Salt deposits (Holocene and Pleistocene)	Playa-lake evaporites. May include interbedded fine-grained lacustrine deposits. Locally may be seasonally covered with water
Ignimbrite (Pleistocene to Miocene)	Welded and nonwelded ash-flow tuffs, chiefly in extensive outflow sheets. Mostly of dacitic composition. Sources probably large caldera complexes, only a few of which are identified. Locally, may include basinal lacustrine sediments. Includes deposits mapped as Ignimbrite Formation and Perez Tuff
Sedimentary rocks (Pleistocene and Pliocene)	Nonmarine sandstone, conglomerate, and shale. May include minor interlayered volcanic rocks
Intrusive rocks (Pliocene to Oligocene)	Chiefly subvolcanic stocks, plugs, and dikes of dacitic composition in vent complex of eroded volcanic eruptive centers. Not all intrusive rocks mapped; many are included in unit of undifferentiated volcanic rocks. Important host rock for Bolivian polymetallic vein deposits
Volcanic rocks, undifferentiated (Miocene and Oligocene)	Chiefly lava flows, but includes extensive pyroclastic deposits and intrusive rocks, and locally may include interbedded nonmarine sedimentary rocks. Mostly of andesitic and dacitic composition. Sources are poorly defined volcanic eruptive centers, now deeply eroded
Pyroclastic rocks (Miocene and Oligocene)	Chiefly welded to nonwelded ash-flow tuffs, but includes air-fall tuffs and thin, volcaniclastic beds. Mostly dacitic in composition. Source same as undifferentiated volcanic rocks, but generally occur more distant from eruptive center
Sedimentary rocks (Pliocene to Oligocene)	Nonmarine sandstone, conglomerate, shale, marl, and evaporites
Sedimentary rocks (Oligocene to Paleocene)	Nonmarine, mostly reddish colored conglomerate, sandstone, shale, and mudstone. Primary host for sedimentary-hosted copper deposits
Los Frailes and Morococala Ignimbrites (Miocene)	Ash-flow tuffs of dacitic composition in extensive ignimbrite field exposed primarily east of map area
Sedimentary rocks (Cretaceous)	Marine and nonmarine sandstone, shale, marl, and limestone
Sedimentary rocks (Paleozoic)	Chiefly marine sandstone and shale of Devonian to Ordovician age. Rocks are generally highly folded and locally penetratively deformed
Gypsum diapirs (Miocene to Eocene)	May include halite and other evaporite minerals

Table A - 15:   Coordinates of rock and sediment samples analyzed for chemical composition

Sample ID	Coordinates (UTM, WGS 84)	
	Longitude	Latitude
Lacustrine sediments		
COI-SED-A2	615314	7845211
SLT-SED-RÍO-01 -1	675616	7720922
SLT-SED-RÍO-01-2	675616	7720922
SLT-SED-OJOS	709130	7752722
SLT-SED-NOR-T3-1	651999	7818299
SLT-SED-NOR-T3-2	651999	7818299
River sediments		
SED-RÍO-GRA-1	704490	7681574
SED-RÍO-GRA-2	704490	7681574
SED-RÍO-COL-1	724248	7719257
SED-RÍO-COL-2	724248	7719257
Soils from catchment		
IRU-BOD-01	546119	7706969
IRU-BOD-02	546128	7706939
IRU-BOD-03	549543	7704771
OLC-BOD-01	557995	7692599
UTU-BOD-01	679451	7541735
UTU-BOD-02	686435	7537282
UTU-BOD-03	672615	7544216
Rocks		
UTU-ROC-01	679451	7541735
UTU-ROC-02	686435	7537282
UTU-ROC-03	685812	7537393
OLC-ROC-01	557995	7692599
OLC-ROC-02	553826	7686293
IRU-ROC-01	546105	7707156
IRU-ROC-02	546186	7706967
IRU-ROC-03	546115	7706860
IRU-ROC-04	546112	7706791

Table A - 16: *Chemical analysis of rocks and sediments measured by ICP-MS after HF digestion (DL – detection limit; w – washed; uw – unwashed)*

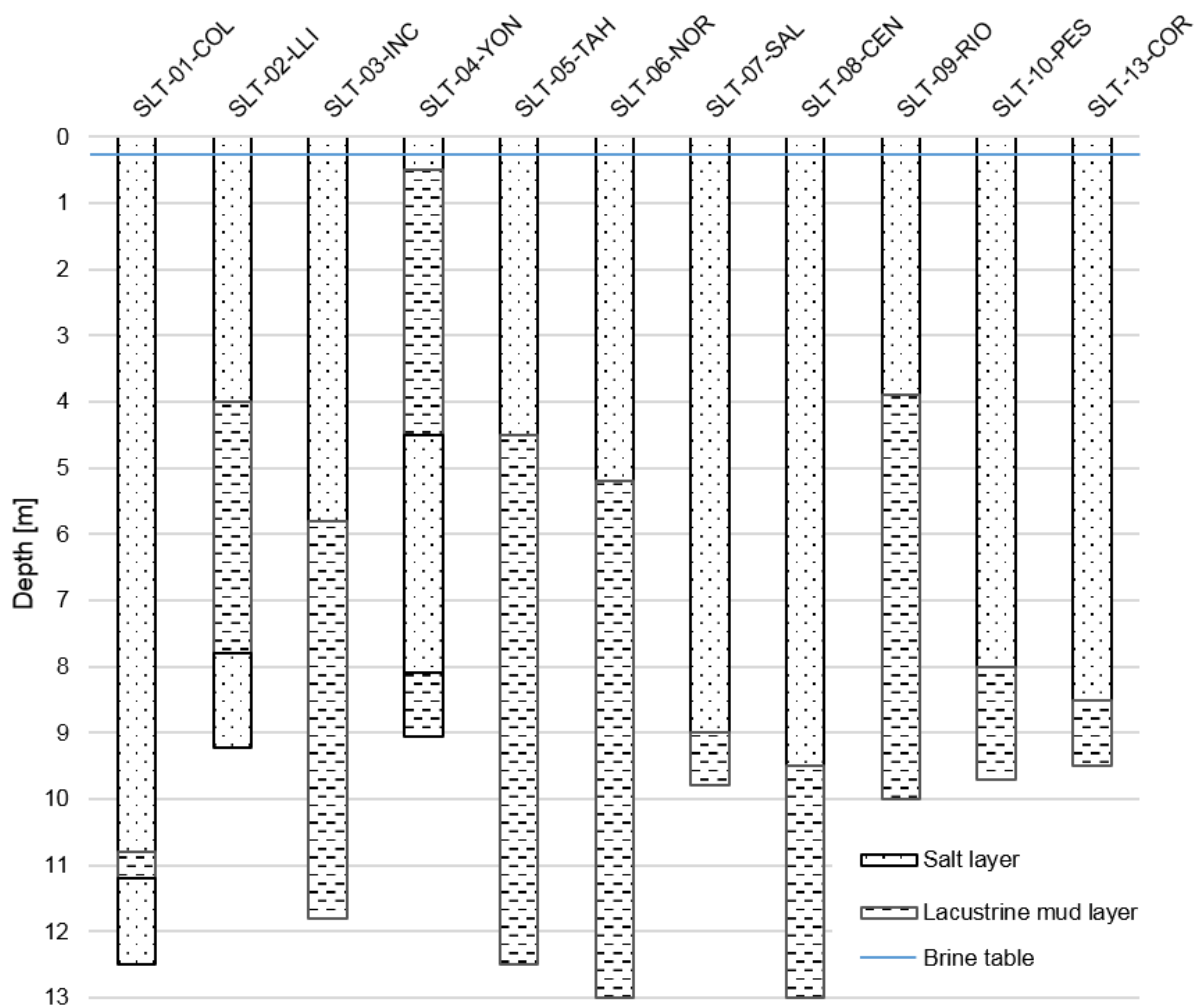|	Li	B	Na	Mg	Al	Si	P	S	K	Ca	Mn	Fe	Rb	Sr	Ba
	ppm	ppm	‰	‰	‰	‰	ppm	‰	‰	‰	ppm	‰	ppm	ppm	ppm
rocks															
IRU-ROC-01	16.6	633	20.8	7.24	60.3	276	1124	<DL	20.6	13.8	356	42.7	81.4	397	665
IRU-ROC-02	8.97	615	20.9	5.44	59.1	273	1109	<DL	19.9	6.74	383	36.0	75.2	164	393
IRU-ROC-03	3.83	666	8.21	0.499	67.5	239	1509	23.1	23.8	1.74	134	90.1	67.1	471	613
IRU-ROC-04	12.2	842	22.0	8.18	57.7	307	1222	<DL	20.1	15.8	445	37.6	70.1	309	467
OLC-ROC-01	12.2	832	18.6	8.79	64.0	255	1506	<DL	16.9	31.2	576	50.6	42.1	461	522
OLC-ROC-02	5.90	878	18.7	4.84	56.1	273	1374	<DL	22.0	11.3	421	42.7	86.7	219	410
UTU-ROC-01	19.7	219	16.0	6.05	77.6	319	1054	<DL	22.6	14.7	305	30.8	86.2	206	424
UTU-ROC-02	20.9	395	12.5	10.8	69.8	303	1643	<DL	27.5	22.9	463	39.5	136	302	555
UTU-ROC-03	14.2	422	8.69	8.41	53.8	276	1494	<DL	26.2	11.8	463	41.7	96.6	171	284
P-1A	27.5	942	20.6	6.16	73.1	267	1459	<DL	21.0	25.6	522	35.4	101	287	509
P-1B	25.1	929	23.7	6.60	79.5	291	1479	<DL	21.8	36.0	461	36.6	110	380	962
R-02	36.6	940	20.1	3.95	60.8	282	1140	<DL	29.0	21.5	374	23.2	175	222	419
lacustrine sediments															
COI-SED-A2_uw	314	2417	89.0	37.3	21.2	85.4	454	32.3	14.1	86.1	336	9.08	53.1	4553	409
COI-SED-A2_w	184	1991	16.7	42.5	32.6	137	696	25.9	12.8	99.2	487	13.8	71.2	5536	602
SLT-SED-RÍO-01-1_uw	800	3124	53.6	47.0	38.7	153	789	<DL	28.8	3.51	323	28.9	137	267	369
SLT-SED-RÍO-01-1_w	384	2336	7.39	54.4	54.1	215	1079	<DL	22.7	4.74	431	44.1	170	314	469
SLT-SED-RÍO-01-2_uw	412	2026	26.8	14.8	9.7	122	589	57.1	15.9	34.6	186	11.3	59.7	755	61.0
SLT-SED-RÍO-01-2_w	157	1483	5.07	24.1	22.9	76.8	472	67.5	8.64	121	177	14.4	55.9	3653	264
SLT-SED-SPEC-OJOS_uw	301	1777	56.8	7.76	6.41	5.17	1277	<DL	8.01	148	155	27.8	25.3	2814	70
SLT-SED-SPEC-OJOS_w	109	1425	10.5	5.58	7.14	17.8	1863	<DL	4.60	203	192	42.8	25.4	4022	80
SLT-SED-NOR-T3-1_uw	258	676	37.3	7.82	48.8	252	588	<DL	29.6	5.99	458	8.65	95.3	209	966
SLT-SED-NOR-T3-1_w	81.8	840	23.1	6.63	58.9	296	673	<DL	30.5	7.18	560	10.3	112	244	1311
SLT-SED-NOR-T3-2_uw	627	1265	53.2	54.3	44.4	200	929	<DL	20.5	11.1	1170	19.6	125	365	588
SLT-SED-NOR-T3-2_w	488	1030	15.1	63.5	54.0	245	1099	<DL	19.2	9.29	1289	23.7	146	349	653
River sediments															
SLT-SED-GRA-1	56.6	908	15.3	6.96	56.2	278	1147	<DL	15.4	30.0	587	29.1	75.9	472	580
SLT-SED-GRA-2	135	880	24.0	8.77	59.9	258	1144	<DL	16.9	33.7	653	28.9	85.8	521	798
SLT-SED-COL-1	209	997	11.5	8.64	33.0	199	1016	<DL	21.0	38.8	443	23.1	67.3	1011	339
SLT-SED-COL-2	195	682	17.9	18.3	49.5	228	1010	<DL	17.7	76.9	836	24.7	109	853	749
Soils from catchment															
IRU-BOD-01	<DL	645	<DL	0.07	0.85	<DL	<DL	<DL	<DL	0.39	4.54	0.13	1.54	5.96	36.8
IRU-BOD-02	4.71	864	4.05	1.07	30.7	301	799	28.7	11.6	3.27	143	5.02	72.8	120	946
IRU-BOD-03	10.7	746	20.5	4.25	69.1	255	913	<DL	14.4	16.5	292	31.0	42.0	566	502
OLC-BOD-01	11.1	810	18.5	4.94	63.6	236	1102	<DL	17.0	24.8	389	32.8	55.3	545	286
UTU-BOD-01	21.1	518	14.5	5.50	63.2	246	842	<DL	15.6	22.6	408	37.4	58.8	277	215
UTU-BOD-02	12.8	573	7.60	6.48	53.2	253	1251	<DL	23.4	8.09	275	30.1	145	277	513
UTU-BOD-03	27.8	514	18.4	5.93	61.5	246	748	<DL	17.5	13.5	289	23.9	72.1	281	271

Appendix B: Figures

Fig. B - 1: Depth profile of drilling sites at the Salar de Uyuni; lower end of each profile points to maximum drilling depth at that site, the particular layer continues beyond that depth
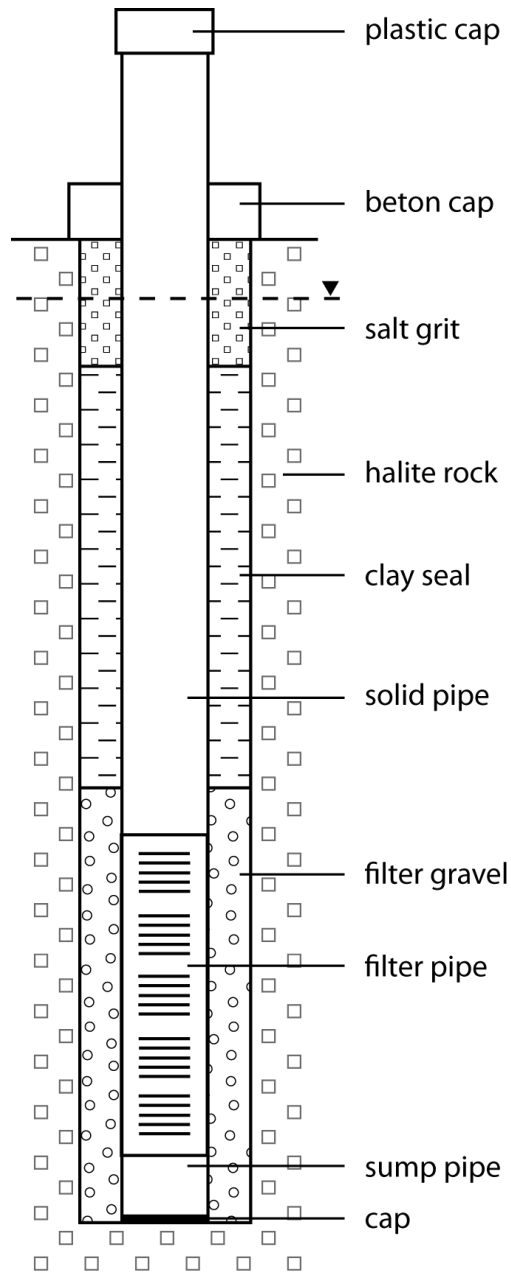
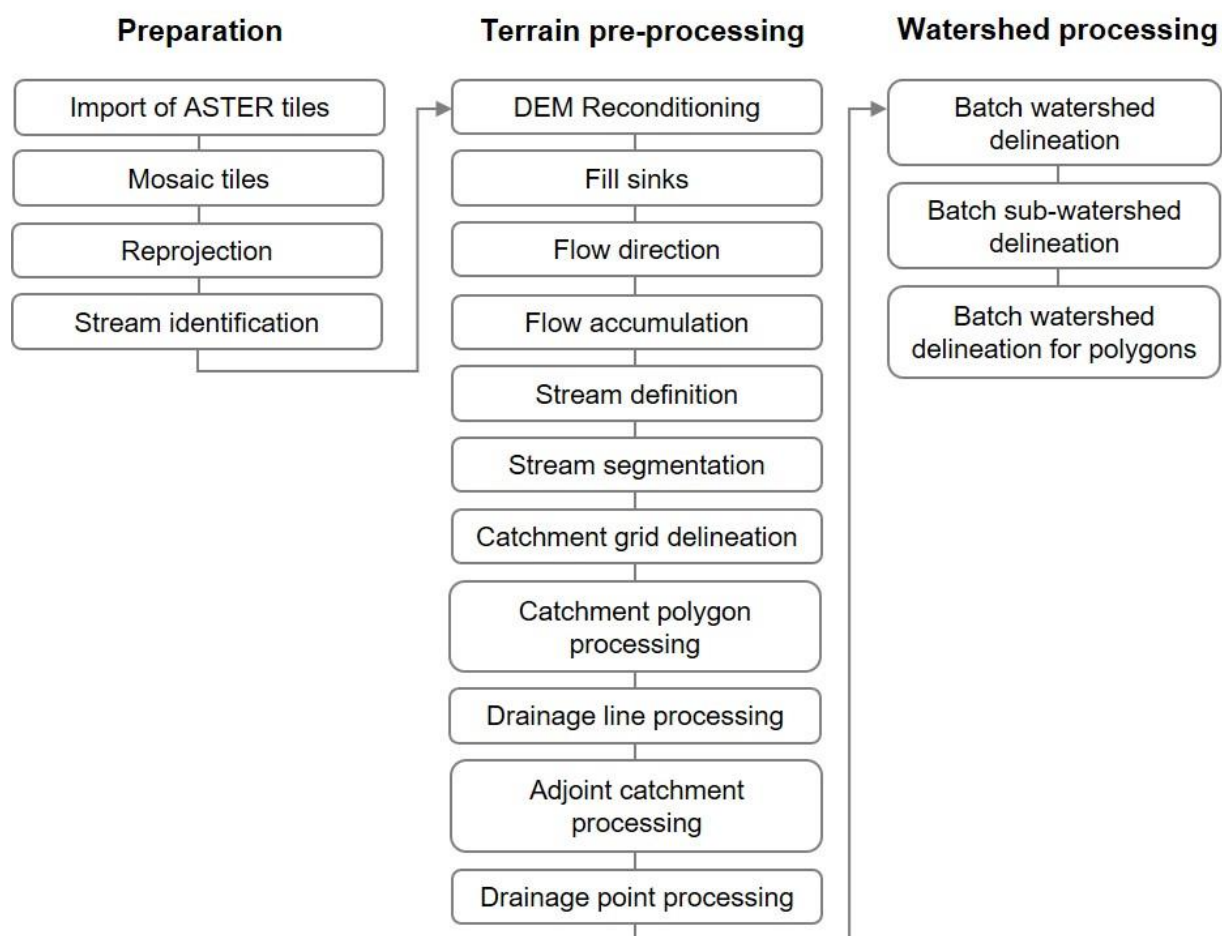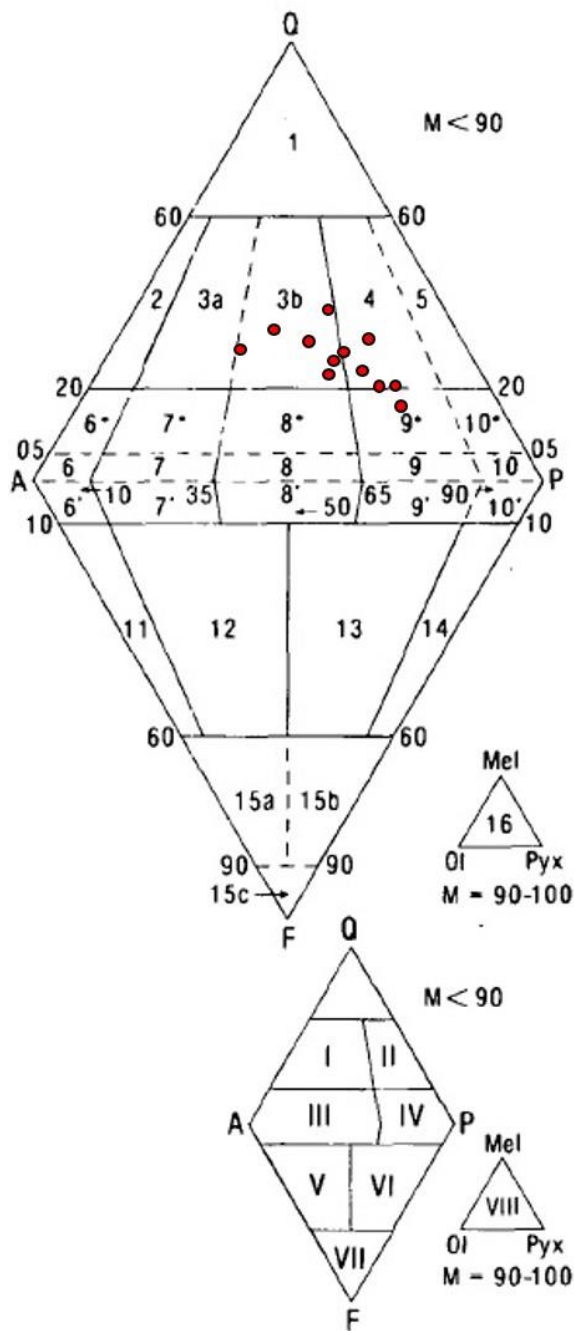*Fig. B - 2: Schema of the well casing, not to scale (after Schmidt (2010))*

Fig. B - 3: Flow chart of watershed delineation using DEM data in ArcMap with the ArcHydro extension

Q

M < 90

1

60 / 60

2 3a 3b 4 5

20 / 20

6* 7* 8* 9* 10*

05 / 05
A / P
6 7 8 9 10
6' 10 7* 35 8* 50 65 9* 90 7* 10*
10 / 10

11 12 13 14

60 60

15a 15b

90 / 90
15c →
F

Mel

16

Ol Pyx

M = 90-100

Q

M < 90

I II

A III IV P

Mel

V VI

VIII

VII

Ol Pyx

M = 90-100

F

ROOT NAMES

2   alkali (-feldspar) rhyolite
     (liparite) (see text)

3a
3b   rhyolite (liparite) (see text)

4
5   dacite (see text)

6*   quartz-alkali (-feldspar) trachyte
6,   alkali (-feldspar) trachyte
6'   foid-bearing alkali (-feldspar) trachyte

7*   quartz trachyte
7,   trachyte
7'   foid-bearing trachyte

8*   quartz latite
8,   latite
8'   foid-bearing latite

9
10   andesite, basalt (see text)

11   phonolite

12   tephritic phonolite

13   phonolitic tephrite (basanite)

14   tephrite, basanite

15a   phonolitic foidite
15b   tephritic foidite
15c   foidite

16   ultramafitite

GROUP NAMES

Fields

2, 3a, 3b	I	rhyolitoids
4, 5	II	dacitoids
6, 7, 8	III	trachytoids
9, 10	IV	andesitoids, basaltoids
11, 12	V	phonolitoids
13, 14	VI	tephritoids
15	VII	foiditoids
16	VIII	ultramafitites

Fig. B - 4: *Classification of volcanic rocks according to their location in the QAPF diagram, and position of rock samples (red dots) from the catchment of the Salar de Uyuni (modified from Streckeisen (1979))*

154

Fig. B - 5: Photo documentation of rock samples (pictures taken by Wolfram Canzler)

UTU-ROC-01 (volcano Uturuncu)

UTU-ROC-02 (volcano Uturuncu)

UTU-ROC-03 (volcano Uturuncu)

OLC-ROC-01 (volcano Olca)

OLC-ROC-02 (volcano Olca)

IRU-ROC-01 (volcano Iruputuncu)

IRU-ROC-02 (volcano Iruputuncu)

IRU-ROC-03 (volcano Iruputuncu)

IRU-ROC-04 (volcano Iruputuncu)

P-1A

P-1B